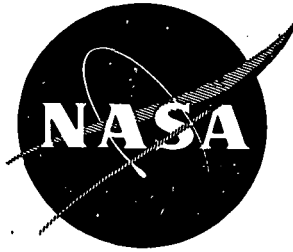


N73-27408

NASA CR-121224



CASE FILE
COPY

DEVELOPMENT OF FORMING AND JOINING TECHNOLOGY FOR TD-NiCr SHEET

by R. T. Torgerson

CONVAIR AEROSPACE DIVISION OF
GENERAL DYNAMICS CORPORATION

prepared for
NATIONAL AERONAUTICS AND SPACE ADMINISTRATION

NASA Lewis Research Center
Contract NAS3-15567

1. Report No. NASA CR-121224		2. Government Accession No.		3. Recipient's Catalog No.	
4. Title and Subtitle DEVELOPMENT OF FORMING AND JOINING TECHNOLOGY FOR TD-NiCr SHEET				5. Report Date April 1973	
				6. Performing Organization Code	
7. Author(s) R. T. Torgerson				8. Performing Organization Report No.	
9. Performing Organization Name and Address Convair Aerospace Division General Dynamics Corporation San Diego, California				10. Work Unit No.	
				11. Contract or Grant No. NAS 3-15567	
12. Sponsoring Agency Name and Address National Aeronautics and Space Administration Washington, D. C. 20546				13. Type of Report and Period Covered Contractor Report 6/71-3/73	
				14. Sponsoring Agency Code	
15. Supplementary Notes Project Managers, C. P. Blankenship and K. H. Holko, Materials and Structures Division, NASA Lewis Research Center, Cleveland, Ohio					
16. Abstract Dispersion-strengthened TD-NiCr alloy has outstanding potential for elevated temperature applications such as thermal protection systems of space shuttle vehicles, but effective utilization requires further development of engineering design data. Forming and joining techniques and properties data were developed for thin-gage TD-NiCr sheet in the recrystallized and unrecrystallized conditions. Theoretical and actual forming limit data are presented for several gages of each type of material for five forming processes: brake forming, corrugation forming, joggling, dimpling and beading. Recrystallized sheet can be best formed at room temperature, but unrecrystallized sheet requires forming at elevated temperature. Formability is satisfactory with most processes for the longitudinal orientation but poor for the transverse orientation. Dimpling techniques require further development for both material conditions. Data on joining techniques and joint properties are presented for four joining processes: resistance seam welding (solid-state), resistance spot welding (solid-state), resistance spot welding (fusion) and brazing. Resistance seam welded (solid-state) joints with 5t overlap were stronger than parent material for both material conditions when tested in tensile-shear and stress-rupture. Brazing studies resulted in development of NASA 18 braze alloy (Ni-16 Cr-15Mo-8Al-4Si) with several properties superior to baseline TD-6 braze alloy, including lower brazing temperature, reduced reaction with TD-NiCr, and higher stress-rupture properties.					
17. Key Words (Suggested by Author(s)) Dispersion-strengthened nickel alloys Forming Theoretical formability Brazing Resistance welding Stress-rupture Solid-state welding Tensile-shear				18. Distribution Statement Unlimited	
19. Security Classif. (of this report) Unclassified		20. Security Classif. (of this page) Unclassified		21. No. of Pages 241	
				22. Price*	

FOREWORD

The program described in this report was conducted by the Convair Aerospace Division of General Dynamics — San Diego Operation with R. T. Torgerson as program manager and principal author. Other Convair Aerospace personnel who participated in the program and contributed to preparation of the report are: J. W. Baer (deputy program manager), J. J. Christiana (forming), D. E. Krantz (forming), W. A. Roden (welding), V. V. Sowinski (welding and hot dimpling) and R. Szabo (welding).

The resistance seam welding (solid-state) and brazing development work was performed under subcontract by Solar Division of International Harvester Company, San Diego, California. Solar personnel who participated in the program and contributed to preparation of the report are Dr. A. G. Metcalfe (Solar program manager), F. G. Rose (resistance seam welding, solid-state), and A. N. Hammer (brazing).

TABLE OF CONTENTS

Section		Page
	SUMMARY	
1	INTRODUCTION	1
2	MATERIALS	5
3	THEORETICAL FORMABILITY	11
4	FORMABILITY OF RECRYSTALLIZED TD-NiCr SHEET	19
	Material Properties	20
	Tensile Properties	20
	Compressive Properties	25
	Theoretical Forming Limit Curves	26
	Brake Forming	33
	Brake Forming Limits	33
	Effect of Die Span	41
	Effect of Part Width	50
	Tensile Properties of Formed Parts	51
	Effect of Annealing	53
	Corrugation Forming	57
	Corrugation Forming Limits	57
	Microstructure	67
	Joggling	67
	Joggle Limits	67
	Microstructure	70
	Dimpling	70
	Dimpling Limits	75
	Microstructure	80
	Beading	85
	Beading Limits	85
	Microstructure	95
5	FORMABILITY OF UNRECRYSTALLIZED TD-NiCr SHEET	97
	Material Properties	98
	Theoretical Forming Limit Curves	99
	Selection of Forming Temperature	108
	Brake Forming	108
	Forming Limits	108

TABLE OF CONTENTS, Contd

Section	Page
Tensile Properties of Formed Parts	112
Microstructure	112
Corrugation Forming	113
Forming Limits	113
Microstructure	118
Dimpling	118
Dimpling Limits	121
Microstructure	125
 6 JOINING OF TD-NiCr SHEET	 127
Parent Material Properties Tests	128
Tensile-Shear Tests	128
Stress-Rupture Tests	129
Resistance Seam Welding (Solid-State)	135
Establishing Weld Parameters - Step A	136
Tensile-Shear Tests	142
Stress-Rupture Tests	144
Metallographic Evaluation	145
Selection of Weld Parameters for Step B	155
Joint Efficiencies - Step B	155
Post-Test Metallographic Examination	163
Resistance Spot Welding (Solid-State)	167
Weld Schedules for Recrystallized Material	167
Weld Schedules for Unrecrystallized Material	170
Corrugation-Stiffened Panel	173
Resistance Spot Welding (Fusion)	175
Materials	177
Test Plan for Weld Parameter Optimization	178
Schedule Development for 0.25 mm (0.010 in.) Sheet	178
Evaluation of Elevated Temperature Spot Weld Properties	184
Schedule Development for 0.08 mm (0.003 in.) Sheet	184
Brazing	185
Development of Braze Alloy Series No. 1	186
Development of Braze Alloy Series No. 2	188
Development of Braze Alloy Series No. 3	190
Development of Braze Alloy Series No. 4	192

TABLE OF CONTENTS, Contd

Section	Page
Remelt Temperature Tests	196
Brazement Properties Evaluation	204
7 CONCLUSIONS	213
Forming of Recrystallized Sheet	213
Forming of Unrecrystallized Sheet	214
Resistance Seam Welding (Solid-State)	214
Resistance Spot Welding (Solid-State)	215
Resistance Spot Welding (Fusion)	215
Brazing	215
Appendix	
A COMPUTER PROGRAM FOR CALCULATIONS OF THEORETICAL FORMABILITY EQUATIONS	217
B TENSILE PROPERTIES OF RECRYSTALLIZED TD-NiCr SHEET	219
C TENSILE PROPERTIES OF UNRECRYSTALLIZED TD-NiCr SHEET	223
D PARENT MATERIAL PROPERTIES OF RECRYSTALLIZED TD-NiCr SHEET	227
E TEST PROCEDURES FOR DETERMINING MECHANICAL PROPERTIES OF RESISTANCE SEAM WELDED AND BRAZED JOINTS	229
Tensile and Tensile-Shear Tests	229
Stress-Rupture Tests	229
REFERENCES	231
DISTRIBUTION LIST	235

LIST OF FIGURES

Figure		Page
1	Typical Microstructure of Recrystallized and Unrecrystallized TD-NiCr Sheet	8
2	Geometric Variables and Formability Envelopes	12
3	Material Breakdown and Test Plan for Recrystallized TD-NiCr Forming Evaluation	19
4	Tensile Specimen	20
5	Fractured Tensile Specimens with 0.63 cm (0.25 in.) and 0.05 cm (0.02 in.) Grid Patterns	22
6	Compression Specimen	26
7	Theoretical Formability Curves for Brake and Corrugation Forming of 0.5 mm (0.020 in.) Recrystallized TD-NiCr Sheet — Heat 3640 (Code B2)	28
8	Theoretical Formability Curves for Jogging of 0.5 mm (0.020 in.) Recrystallized TD-NiCr Sheet — Heat 3640 (Code B2)	29
9	Theoretical Formability Curves for Dimpling of 0.5 mm (0.020 in.) Recrystallized TD-NiCr Sheet — Heat 3640 (Code B2)	30
10	Theoretical Formability Curves for Rubber Press Beading of 0.5 mm (0.020 in.) Recrystallized TD-NiCr Sheet — Heat 3640 (Code B2)	31
11	Theoretical Formability Curves for Drop Hammer Beading of 0.5 mm (0.020 in.) Recrystallized TD-NiCr Sheet — Heat 3640 (Code B2)	32
12	Adjustable Brake-Form Die	34
13	Brake Formed Parts of 0.25 mm (0.010 in.) Recrystallized TD-NiCr Sheet (Heat 3700) Showing Typical Small Cracks Parallel and Transverse to the Rolling Direction — Cold Rolled Surface Finish	38
14	Brake Formed Parts of 1.0 mm (0.040 in.) Recrystallized TD-NiCr Sheet (Heat 3715) Showing Typical Small Cracks Parallel and Transverse to the Rolling Direction — Belt Polished Surface Finish	39
15	Typical Surface Cracks and Deformation Bands in Brake Formed 0.25 mm (0.010 in.) Recrystallized TD-NiCr Sheet	40
16	Theoretical and Actual Brake Forming Limit Curves for 0.25 mm (0.010 in.) Recrystallized TD-NiCr Sheet — Heat 3637 (Code F2)	42
17	Theoretical and Actual Brake Forming Limit Curves for 0.25 mm (0.010 in.) Recrystallized TD-NiCr Sheet — Heat 3700 (Code H1)	43
18	Theoretical and Actual Brake Forming Limit Curves for 0.5 mm (0.020 in.) Recrystallized TD-NiCr Sheet — Heat 3629 (Code A1)	44
19	Theoretical and Actual Brake Forming Limit Curves for 0.5 mm (0.020 in.) Recrystallized TD-NiCr Sheet — Heat 3640 (Code B1)	45

LIST OF FIGURES, Contd

Figure		Page
20	Theoretical and Actual Brake Forming Limit Curves for 1.0 mm (0.040 in.) Recrystallized TD-NiCr Sheet — Heat 3708 (Code D2)	46
21	Theoretical and Actual Brake Forming Limit Curves for 1.0 mm (0.040 in.) Recrystallized TD-NiCr Sheet — Heat 3715 (Code E2)	47
22	Effect of Die Span on Actual Brake Forming Limits of 0.5 mm (0.020 in.) Recrystallized TD-NiCr Sheet — Heat 3640 (Code B6)	49
23	Specimen Configuration for Tensile Testing of Formed Parts	51
24	Microstructure of Brake Formed Part of 1.0 mm (0.040 in.) Recrystallized TD-NiCr Sheet As-Formed and After Annealing at 982C (1800F)	54
25	Microstructure of Brake Formed Part of 1.0 mm (0.040 in.) Recrystallized TD-NiCr Sheet After Annealing at 1093C (2000F) and 117C (2150F)	55
26	Corrugation Forming Cycle	57
27	Corrugation Die Assembly with Replaceable Inserts	59
28	Corrugation Die Mounted in Press Brake	60
29	Corrugation Angles of 45, 60, and 75 Degrees Formed from 0.5 mm (0.020 in.) Recrystallized TD-NiCr Sheet	60
30	Typical Small Cracks in Radius of Corrugation Specimen of Recrystallized Sheet with Strain Longitudinal to the Rolling Direction	62
31	Typical Small Cracks in Radius of Corrugation Specimen of Recrystallized Sheet with Strain Transverse to the Rolling Direction	62
32	Theoretical and Actual Corrugation Forming Limit Curves for 0.25 mm (0.010 in.) Recrystallized TD-NiCr Sheet — Heat 3700 (Code H3)	64
33	Theoretical and Actual Corrugation Forming Limit Curves for 0.5 mm (0.020 in.) Recrystallized TD-NiCr Sheet — Heat 3640 (Code B1)	65
34	Theoretical Corrugation Forming Limit Curves and Actual Forming Data for 0.08 mm (0.003 in.) Recrystallized TD-NiCr Sheet — Heat 3702 (Code M)	66
35	Typical Joggled Parts of Recrystallized TD-NiCr Sheet	69
36	Typical splitting Failure of 1.0 mm (0.040 in.) Recrystallized Sheet Joggled Transverse to Rolling Direction	69
37	Actual Forming Data Superimposed on Theoretical Jogging Limit Curves for 0.25 mm (0.010 in.) Recrystallized TD-NiCr Sheet — Heat 3700 (Code H1)	71

LIST OF FIGURES, Contd

Figure		Page
38	Actual Forming Data Superimposed on Theoretical Jogging Limit Curves for 0.5 mm (0.020 in.) Recrystallized TD-NiCr Sheet - Heat 3640 (Code B2)	72
39	Actual Forming Data Superimposed on Theoretical Jogging Limit Curves for 1.0 mm (0.040 in.) Recrystallized TD-NiCr Sheet - Heat 3715 (Code E)	73
40	Typical Circumferential and Radial Cracks in Dimples in Recrystallized TD-NiCr Sheet Formed with Ram-Coin Dimpling Dies	77
41	Microstructure of a Dimple Containing Circumferential Cracks in 1.0 mm (0.040 in.) Recrystallized Sheet	78
42	Comparison of Dimpling Test Results with Theoretical Dimpling Limits for 0.25 mm (0.010 in.) Recrystallized TD-NiCr Sheet - Heat 3700 (Code H)	81
43	Comparison of Dimpling Test Results with Theoretical Dimpling Limits for 0.5 mm (0.020 in.) Recrystallized TD-NiCr Sheet - Heat 3640 (Code A)	82
44	Comparison of Dimpling Test Results with Theoretical Dimpling Limits for 1.0 mm (0.040 in.) Recrystallized TD-NiCr Sheet - Heat 3714 (Code E)	83
45	Microstructure of As-Formed Dimple in 1.0 mm (0.040 in.) Recrystallized TD-NiCr Sheet	84
46	Microstructure Adjacent to Hole of Annealed Dimple in 0.5 mm (0.020 in.) Recrystallized Sheet	84
47	Verson Wheelon Rubber Press with a TD-NiCr Beaded Panel Shown on the Press Table	86
48	Sketch of Beading Die Configuration	86
49	Set of Beading Tools for Forming 0.76 cm (0.3 in.) Radius Beads	87
50	Partially Formed 0.25 mm (0.010 in.) TD-NiCr Beaded Panels and Stainless Steel Caul Sheets After Preform Operation	89
51	Typical Rubber Press Beaded Test Panels of Recrystallized TD-NiCr Sheet	92
52	Typical Splitting Failure During Beading Test of TD-NiCr Sheet Preformed on Female Die	92
53	Theoretical and Actual Forming Limits for Rubber Press Beading of 0.25 mm (0.010 in.) Recrystallized TD-NiCr Sheet - Heat 3637 (Code F1)	93

LIST OF FIGURES, Contd

Figure		Page
54	Theoretical and Actual Forming Limits for Rubber Press Beading of 0.5 mm (0.020 in.) Recrystallized TD-NiCr Sheet — Heat 3629 (Code A4)	94
55	Material Breakdown and Test Plan for Unrecrystallized TD-NiCr Forming Evaluation	98
56	Tensile Properties of 0.5 mm (0.020 in.) Unrecrystallized TD-NiCr Sheet — Heat 3709 (Code G1)	100
57	Tensile Properties of 0.25 mm (0.010 in.) Unrecrystallized TD-NiCr Sheet — Heat 3714 (Code K5)	101
58	Theoretical Formability Curves for Hot Brake and Corrugation Forming of 0.5 mm (0.020 in.) Unrecrystallized TD-NiCr Sheet — Heat 3709 (Code G1)	103
59	Theoretical Formability Curves for Hot Dimpling of 0.5 mm (0.020 in.) Unrecrystallized TD-NiCr Sheet — Heat 3709 (Code G1)	104
60	Theoretical Formability Curves for Drop Hammer Beading of 0.5 mm (0.020 in.) Unrecrystallized TD-NiCr Sheet at 760C (1400F) — Heat 3709 (Code G1)	105
61	Theoretical Formability Curves for Hot Brake and Corrugation Forming of 0.25 mm (0.010 in.) Unrecrystallized TD-NiCr Sheet — Heat 3714 (Code K5)	106
62	Theoretical Formability Curves for Hot Dimpling of 0.25 mm (0.010 in.) Unrecrystallized TD-NiCr Sheet — Heat 3714 (Code K5)	107
63	Hot Brake Forming Die Assembly	108
64	Actual and Predicted Brake Forming Limits at 760C (1400F) for 0.25 mm (0.010 in.) Unrecrystallized TD-NiCr Sheet — Heat 3714 (Code K7 and K8)	110
65	Actual and Predicted Brake Forming Limits at 760C (1400F) for 0.5 mm (0.020 in.) Unrecrystallized TD-NiCr Sheet — Heat 3709 (Code G1)	111
66	Typical Microstructure of Hot Brake Formed 0.5 mm (0.020 in.) Unrecrystallized Sheet After Recrystallization Anneal	114
67	Hot Corrugation Forming of Unrecrystallized TD-NiCr Sheet	115
68	Theoretical and Actual Corrugation Forming Limit Curves at 760C (1400F) for 0.25 (0.010 in.) Unrecrystallized TD-NiCr Sheet — Heat 3714 (Code K6 and K7)	116
69	Theoretical and Actual Corrugation Forming Limit Curves at 760C (1400F) for 0.5 mm (0.020 in.) Unrecrystallized TD-NiCr Sheet — Heat 3709 (Code G3)	117

LIST OF FIGURES, Contd

Figure		Page
70	Microstructure of Hot Corrugated Parts of 0.25 mm (0.010 in.) Unrecrystallized TD-NiCr Sheet	119
71	Details of Dies and Operational Sequence for Hot Dimpling by Resistance Heating on a Spotwelder	121
72	Actual Forming Data Superimposed on Theoretical Formability Curves for Hot Dimpling of 0.25 mm (0.010 in.) Unrecrystallized TD-NiCr Sheet – Heat 3714 (Code K)	123
73	Actual Forming Data Superimposed on Theoretical Formability Curves for Hot Dimpling of 0.5 mm (0.020 in.) Unrecrystallized TD-NiCr Sheet – Heat 3709 (Code G)	124
74	Microstructure of Hot Formed Dimples in Unrecrystallized TD-NiCr Sheet	126
75	Material Matrix for Joining Development	128
76	Double Shear Specimen Configuration for Parent Material Tensile-Shear Tests	130
77	Typical Fractures in Tensile-Shear Specimens of 0.25 mm (0.010 in.) Recrystallized TD-NiCr – Heat 3691 (Code L6)	130
78	Stress-Rupture Properties of 0.25 mm (0.010 in.) TD-NiCr Sheet at 982C (1800F) – Heat 3691 (Code L6)	131
79	Stress-Rupture Properties of 0.25 mm (0.010 in.) TD-NiCr Sheet at 1093C (2000F) – Heat 3691 (Code L6)	131
80	Stress-Rupture Properties of 0.25 mm (0.010 in.) TD-NiCr Sheet at 1204C (2200F) – Heat 3691 (Code L6)	132
81	Stress-Rupture Properties of 0.25 mm (0.010 in.) TD-NiCr Sheet at 982C (1800F) – Heat 3689 (Code J1)	132
82	Stress-Rupture Properties of 0.25 mm (0.010 in.) TD-NiCr Sheet at 1093C (2000F) – Heat 3689 (Code J1)	133
83	Stress-Rupture Properties of 0.25 mm (0.010 in.) TD-NiCr Sheet at 1204C (2200F) – Heat 3689 (Code J1)	133
84	Stress-Rupture Properties of 0.08 mm (0.003 in.) TD-NiCr Sheet at 982C (1800F) – Heat 3702	134
85	Stress-Rupture Properties of 0.08 mm (0.003 in.) TD-NiCr Sheet at 1093C (2000F) – Heat 3702 (Code M)	134
86	Stress-Rupture Properties of 0.08 mm (0.003 in.) TD-NiCr Sheet at 1204C (2200F) – Heat 3702 (Code M)	135
87	Lap Joints of 0.25 mm (0.010 in.) Recrystallized TD-NiCr Showing Effects of Various Pre-weld Surface Treatments	138

LIST OF FIGURES, Contd

Figure		Page
88	Microstructure of Joint Interface of Lap Joint Made in 0.25 mm (0.010 in.) Recrystallized TD-NiCr Sheet by Resistance Seam Welding	140
89	Tensile Stress as a Function of Time to Rupture for Resistance Seam Welded Lap Joints in 0.25 mm (0.010 in.) Recrystallized TD-NiCr Sheet	140
90	TD-NiCr Tensile-Shear Specimens After Testing at 1093C (2000F)	144
91	Transverse Section Through Lap Seam Weld in Unrecrystallized 0.25 mm (0.010 in.) TD-NiCr Sheet with L/L Orientation Showing Effect of Surface Preparation on Structure of Weld Line	146
92	Microstructure of Welded Lap Joint in 0.25 mm (0.010 in.) Recrystallized TD-NiCr After Stress-Rupture Testing at 1204C (2200F)	147
93	Microstructure of Welded Lap Joint in 0.25 mm (0.010 in.) Recrystallized TD-NiCr After Stress-Rupture Testing at 1204C (2200F)	148
94	Microstructure of Welded Lap Joint 0.25 mm (0.010 in.) Recrystallized TD-NiCr After Stress-Rupture Testing at 1204C (2200F)	150
95	Microstructure of Welded Lap Joint in 0.25 mm (0.010 in.) Recrystallized TD-NiCr After Stress-Rupture Testing at 1204C (2200F)	151
96	Microstructure of Welded Lap Joint in 0.25 mm (0.010 in.) Recrystallized TD-NiCr After Stress-Rupture Testing at 1204C (2200F)	152
97	Cross Section of U-L/T-B Type Lap Joints Showing Recrystallization at Joint Edges	153
98	982C (1800F) Stress-Rupture Properties of Longitudinal Resistance Seam Welded Joints of Unrecrystallized 0.25 mm (0.010 in.) TD-NiCr Sheet - Heat 3689	159
99	982C (1800F) Stress-Rupture Properties of Longitudinal Resistance Seam Welded Joints of Unrecrystallized 0.25 mm (0.010 in.) TD-NiCr Sheet - Heat 3691	159
100	1093C (2000F) Stress-Rupture Properties of Longitudinal Resistance Seam Welded Joints of Unrecrystallized 0.25 mm (0.010 in.) TD-NiCr Sheet - Heat 3689	160

LIST OF FIGURES, Contd

Figure		Page
101	1093C (2000F) Stress-Rupture Properties of Transverse Resistance Seam Welded Joints of Unrecrystallized 0.25 mm (0.010 in.) TD-NiCr Sheet - Heat 3689	160
102	1093C (2000F) Stress-Rupture Properties of Longitudinal Resistance Seam Welded Joints of Recrystallized 0.25 mm (0.010 in.) TD-NiCr Sheet - Heat 3691	161
103	1204C (2200F) Stress-Rupture Properties of Longitudinal Resistance Seam Welded Joints of Unrecrystallized 0.25 mm (0.010 in.) TD-NiCr - Heat 3689	161
104	1204C (2200F) Stress-Rupture Properties of Transverse Resistance Seam Welded Joints of Unrecrystallized 0.25 mm (0.010 in.) TD-NiCr Sheet - Heat 3689	162
105	1204C (2200F) Stress-Rupture Properties of Longitudinal Resistance Seam Welded Joints of Recrystallized 0.25 mm (0.010 in.) TD-NiCr Sheet - Heat 3691	162
106	Microstructure of Welded Lap Joint in 0.25 mm (0.010 in.) Unrecrystallized TD-NiCr Sheet After Stress-Rupture Testing at 1093C (2000F)	164
107	Grain Boundary Sliding in Transverse Leg of Stress-Rupture Specimen of Figure 106, which was Exposed 118.1 Hours at 1093C (2000F) with a Uniaxial Stress of 62.1 MN/m ² (9.0 ksi)	165
108	Microstructure of Welded Lap Joint in 0.25 mm (0.010 in.) Unrecrystallized TD-NiCr Sheet After Stress-Rupture Testing at 1093C (2000F)	165
109	Microstructure of Welded Lap Joint in 0.25 mm (0.010 in.) Unrecrystallized TD-NiCr Sheet After Stress-Rupture Testing at 1204C (2200F)	166
110	Microstructure of Solid-State Spotweld of 0.25 mm (0.010 in.) Recrystallized TD-NiCr with Surface Preparation A	169
111	Microstructure of Solid-State Spotweld of 0.25 mm (0.010 in.) Recrystallized TD-NiCr Sheet With Surface Preparation B	171
112	Microstructure of Solid-State Spot Weld of 0.25 mm (0.010 in.) Unrecrystallized TD-NiCr with Surface Preparation A	174
113	Microstructure of Solid-State Spot Welded Joint in Corrugation-Stiffened Panel Fabricated from 0.25 mm (0.010 in.) Unrecrystallized TD-NiCr Sheet	174
114	In-Process Control Unit	176

LIST OF FIGURES, Contd

Figure		Page
115	Control Panel of Convair Weld Energy Monitor/Limiter	177
116	Diagram of Spotweld Schedule 3 for Resistance Spotwelding of 0.25 mm (0.010 in.) Recrystallized TD-NiCr	180
117	Typical Resistance Spotweld Microstructure for 0.25 mm (0.010 in.) Recrystallized TD-NiCr - Weld Schedule 3	183
118	Alloy NASA 17 - Button Ingot	193
119	Alloy NASA 18 - Button Ingot	193
120	Alloy NASA 19 - Button Ingot	194
121	Alloy NASA 20 - Button Ingot	194
122	T-Joint Brazement - NASA 17 Loaded Side - 2 mm (10 U.S.S. Mesh) Chunk	197
123	T-Joint Brazement - NASA 18 Loaded Side - 2 mm (10 U.S.S. Mesh) Chunk	197
124	T-Joint Brazement - NASA 19 Loaded Side - 2mm (10 U.S.S. Mesh) Chunk	197
125	T-Joint Brazement - NASA 20 Loaded Side - 2 mm (10 U.S.S. Mesh) Chunk	198
126	T-Joint Brazement, TD-6 Powder, Loaded Side	198
127	NASA 17 Alloy Brazement - As-Brazed	198
128	NASA 18 Alloy Brazement - As-Brazed	199
129	NASA 19 Alloy Brazement - As-Brazed	199
130	NASA 20 Alloy Brazement - As-Brazed	200
131	NASA 17 Alloy Brazement - Diffusion Annealed	200
132	NASA 18 Alloy Brazement - Diffusion Annealed	201
133	NASA 19 Alloy Brazement - Diffusion Annealed	201
134	NASA 20 Alloy Brazement - Diffusion Annealed	202
135	TD-6 Alloy T-Joint Brazement	202
136	Microstructure of TD-6 Brazement	203
137	Microstructure of B-2 Alloy Brazement - Diffusion Annealed	205
138	TD-6 Alloy Brazement - As-Brazed	206
139	TD-6 Alloy Brazement - Diffusion Annealed	206
140	1093C (2000F) Stress-Rupture Properties of NASA 18 Alloy Brazements	210
141	1093C (2000F) Stress-Rupture Properties of NASA B-2 Alloy Brazements	210
142	1093C (2000F) Stress-Rupture Properties of TD-6 Alloy Brazements	211

LIST OF TABLES

Table		Page
1	List of Sheet Material Used for Forming and Joining Development	6
2	Tensile and Compressive Properties Data Required for Forming Predictability Equations (Room or Elevated Temperature)	17
3	Summary of Tensile Properties of Recrystallized TD-NiCr Sheet	21
4	Transverse Mechanical Properties of TD-NiCr Sheet from Fan-steel Certifications	24
5	Compressive Properties of Recrystallized TD-NiCr Sheet	25
6	Experimental Press Brake Forming Limits of Recrystallized TD-NiCr Sheet for 45° Bend Angle	35
7	Experimental Press Brake Forming Limits of Recrystallized TD-NiCr Sheet for 90° Bend Angle	36
8	Experimental Press Brake Forming Limits of Recrystallized TD-NiCr Sheet for 120° Bend Angle	37
9	Effect of Die Span on Actual Brake Forming Limits of 0.5 mm (0.020 in.) Recrystallized TD-NiCr for 90° Bend Angle	48
10	Effect of Part Width on Experimental Press Brake Forming Limits of Recrystallized TD-NiCr for 90° Bend Angle	50
11	Test Results for Tensile Specimens Machined from Radius Portion of Brake Formed Parts of Recrystallized TD-NiCr Sheet	52
12	Summary of Effect of Brake Forming on Tensile Properties of Recrystallized TD-NiCr Sheet	52
13	Test Results for Tensile Specimens Machined from Brake Formed and Annealed 1.0 mm (0.040 in.) Recrystallized TD-NiCr Sheet - Heat 3715 (Code E1)	56
14	Summary of Effect of Annealing on Tensile Properties of Brake Formed 1.0 mm (0.040 in.) Recrystallized TD-NiCr Sheet - Heat 3715 (Code E1)	56
15	Experimental Corrugation Forming Limits of Recrystallized TD-NiCr for 45, 60 and 75 Degree Corrugation Angles	63
16	Joggling Tests on Recrystallized TD-NiCr Sheet	68
17	Dimpling Test Results for Recrystallized TD-NiCr Sheet	76
18	Dimpling Test Results for Recrystallized TD-NiCr Sheet with Dies Modified to a 0.5 mm (0.020 in.) Forming Radius	80
19	Beading Tests of Recrystallized TD-NiCr Sheet	91
20	Experimental Press Brake Forming Limits of Unrecrystallized TD-NiCr at 760C (1400F)	109
21	Effect of Hot Brake Forming on Tensile Properties of 0.5 mm (0.020 in.) Unrecrystallized Sheet - Heat 3709 (Code G)	112

LIST OF TABLES, Contd

Table		Page
22	Experimental Corrugation Forming Limits of Unrecrystallized TD-NiCr for 45, 60, and 75-Degree Corrugation Angles	115
23	Summary of Tensile-Shear Properties of Recrystallized TD-NiCr Sheet	128
24	Weld Parameter Optimization for L/L Orientation of Recrystallized Sheet (Surface Preparation D - Electropolished)	141
25	Tensile-Shear Test Data for Resistance Seam Welded (Solid-State) TD-NiCr Sheet	143
26	1204C (2200F) Stress Rupture Tests of Welded Lap Joint Specimens (Step A)	145
27	Tensile-Shear Tests of Resistance Seam Welded Lap Joint Specimens	156
28	982C (1800F) Stress-Rupture Tests of Resistance Seam Welded Lap Joint Specimens	157
29	1093C (2000F) Stress-Rupture Tests of Resistance Seam Welded Lap Joint Specimens	157
30	1204C (2200F) Stress-Rupture Tests of Resistance Seam Welded Lap Joint Specimens	158
31	Tensile-Shear Tests of Solid-State Spotwelded Joints of 0.25 mm (0.010 in.) Recrystallized TD-NiCr Sheet - Heat 3691 (Code L4)	168
32	Tensile-Shear Tests of Solid-State Spot Welded Joints of 0.25 mm (0.010 in.) Unrecrystallized TD-NiCr Sheet - Heat 3714 (Code J8)	172
33	Resistance Spotweld Schedules for 0.25 mm (0.010 in.) Recrystallized TD-NiCr Sheet	179
34	Results of Room Temperature Tensile Shear Tests and Metallographic Examination of Resistance Spotwelded 0.25 mm (0.010 in.) Recrystallized TD-NiCr Sheet - Heat 3691	181
35	Results of Tensile Shear and Stress Rupture Tests of Resistance Spotwelds (Fusion) of 0.25 mm (0.010 in.) Recrystallized TD-NiCr Sheet - Heat 3691	184
36	Raw Material Sources	186
37	Composition of TD-NiCr Braze Alloys	187
38	Test Results for Series 3 Braze Alloys	191
39	Test Results for Series 4 Braze Alloys	195
40	Braze Alloy Remelt Temperature Tests - Tensile Loaded T-Joints	203
41	Schedule of Testing - Brazement Evaluation	204
42	Braze Alloy Remelt Temperature Tests of Tensile Load T-Joints	205

LIST OF TABLES, Contd

Table		Page
43	Tensile Strength of Brazements	207
44	Parent-Material Tensile Properties of 0.25 mm (0.010 in.) TD-NiCr Sheet	208
45	Stress-Rupture Properties of Brazements at 1093C (2000F)	209
B-1	Tensile Properties of 0.25 cm (0.010 in.) Recrystallized TD-NiCr Sheet	219
B-2	Tensile Properties of 0.5 mm (0.020 in.) Recrystallized TD-NiCr Sheet	220
B-3	Tensile Properties of 1.0 mm (0.040 in.) Recrystallized TD-NiCr Sheet	221
B-4	Tensile Properties of 0.08 mm (0.003 in.) Recrystallized TD-NiCr Sheet	222
C-1	Tensile Properties of 0.25 mm (0.010 in.) Unrecrystallized TD-NiCr Sheet – Heat 3714 (Code K5)	223
C-2	Tensile Strain Measurements for 0.25 mm (0.010 in.) Unrecrystallized TD-NiCr Tensile Specimens – Heat 3714 (Code K5)	224
C-3	Tensile Properties of 0.5 mm (0.020 in.) Unrecrystallized TD-NiCr Sheet – Heat 3709 (Code G1)	225
C-4	Tensile Strain Measurements for 0.5 mm (0.020 in.) Unrecrystallized TD-NiCr Tensile Specimens – Heat 3709 (Code G1)	226
D-1	Tensile-Shear Test Results for Recrystallized TD-NiCr Sheet	227
D-2	Stress-Rupture Tests of Recrystallized TD-NiCr Sheet	228

SUMMARY

The dispersion-strengthened nickel-chromium alloys have promising properties for elevated temperature service in the 982 to 1204 C (1800 - 2200 F) range for applications such as the thermal protection systems of space shuttle vehicles. Utilization of these alloys requires development of suitable engineering data for design and fabrication of reliable hardware. This investigation was conducted to develop forming and joining techniques and properties data for thin-gage TD-NiCr sheet. Evaluation was conducted of material in the recrystallized and unrecrystallized conditions.

Theoretical and actual forming limits at ambient temperature were established for four gages of recrystallized sheet using five processes: brake forming, corrugation forming, joggling, dimpling, and beading. Theoretical and actual forming limits for two gages of unrecrystallized sheet were established at the optimum forming temperature for three processes: brake forming, corrugation forming, and dimpling. An optimum forming temperature of 760 C (1400 F) was determined for unrecrystallized material. Studies were conducted and data presented on grain orientation, microstructure, annealing, and tensile properties of formed parts for both material conditions. Satisfactory formability for the longitudinal orientation was demonstrated for both types of material and all processes except dimpling. Formability for the transverse orientation was poor, and forming in this direction should be avoided or the degree of strain minimized. The dimpling process involves severe strain in both the longitudinal and transverse directions, and further effort is required to develop satisfactory dimpling techniques. Several promising approaches are described.

Joining techniques and joint properties were evaluated for four processes: resistance seam welding (solid-state), resistance spot welding (solid-state), resistance spot welding (fusion), and brazing. Resistance seam welding (solid-state) was evaluated for both recrystallized and unrecrystallized sheet. Welding parameters and surface preparation were optimized to eliminate or minimize fine-grain recrystallization at the weldline. The optimum surface preparation was electropolishing, and this method was used for evaluation of joint efficiency. In tensile-shear and stress-rupture tests, seam-welded joints with 5t overlap failed in parent material for both material conditions.

Resistance spot welding (solid-state) was evaluated for recrystallized and unrecrystallized sheet using the Convair Aerospace-developed High Power Level (HPL) welding process. Welding parameter and surface preparation methods were evaluated by peel tests, metallography, and tensile-shear tests. Abrasive polishing gave the best joint properties of four surface preparations. However, further development of weld schedules for electropolished material is recommended to determine if results comparable to seam welding can be achieved.

Resistance spot welding (fusion) was evaluated for two gages of recrystallized sheet using conventional welding techniques. Weld schedules were developed and joint properties data were generated, which indicate best results for abrasive polishing surface preparation for 0.25 mm (0.010 in.) sheet and solvent cleaning for 0.08 mm (0.003 in.) cold rolled foil.

Brazing studies were conducted on twenty experimental brazing alloy compositions, a NASA-developed brazing alloy, and baseline TD-6 braze alloy. The braze alloys were evaluated on the basis of braze temperature, flow and filleting characteristics, and microstructure. Three braze alloys were selected for evaluation of brazement properties: experimental alloy NASA 18, the NASA developed B-2 alloy, and the reference TD-6 alloy. Testing included remelt temperature, tensile, and stress-rupture tests of brazed butt-joint specimens. The NASA18 alloy (Ni-16Cr-15Mo-8Al-4Si) revealed several areas of superiority in properties compared to TD-6, including lower brazing temperature, reduced reaction with TD-NiCr, and higher stress-rupture properties at 1093 C (2000 F). NASA18 brazing alloy is considered to have the potential for correcting several of the deficiencies of TD-6 alloy, and further evaluation is recommended.

1. INTRODUCTION

The dispersion strengthened nickel-base alloys are promising candidate materials for various high temperature applications requiring good creep strength and oxidation resistance. NASA is interested in this class of material for possible use in re-entry thermal protection systems for space shuttle vehicles and in high temperature components of jet engines (Ref. 1). The dispersion strengthened nickel-base alloy in the most advanced stage of development is TD-NiCr (Ni-20Cr-2ThO₂). This material appears promising for use in the 982 to 1204 C (1800 to 2200 F) range because it has better creep strength than conventional superalloys and good oxidation resistance. Thus, dispersion-strengthened nickel-base alloys could provide a more efficient and reliable material for a service temperature range between conventional superalloys and coated refractory alloys. To further the development of this type of alloy and explore its potential for use in space shuttle heat shields, NASA undertook an extensive technology program on dispersion-strengthened nickel-base alloys (Ref. 2). As part of this effort, NASA supported the development by Fansteel, Inc., of improved manufacturing processes for producing TD-NiCr sheet (Ref. 3). A standardized process was established for manufacture of thin-gage sheet, and a substantial quantity of material was produced for evaluation of design-allowable properties and development of fabrication processes for making heat shield panels. The physical and mechanical properties of the standardized process sheet material were determined under NASA contract by Metcut Research Associates (Ref. 4).

The lack of good engineering design data, as well as the potential for major improvement in formability and joinability of TD-NiCr, has been well recognized (Refs. 5, 6, 7). Fusion welding processes and conventional resistance spotwelding result in agglomeration of the dispersion strengthening thoria particles, which cause major loss of high-temperature strength. Solid-state welding and brazing offer the most promise as an alternative to fusion welding. However, one problem encountered with solid-state welding is the formation of small recrystallized grains at the interface, which results in lower strength at elevated temperatures. The small grains result from recrystallization of locally-strained material (caused by surface grinding and flattening of asperities) around the weld interface. This detrimental fine-grain recrystallization also occurs during forming of TD-NiCr sheet when the local straining is sufficiently severe to exceed the critical deformation limit, causing the small grains to form during annealing or high-temperature service.

A processing innovation that has received considerable interest is to conduct the forming and solid-state welding operations in the unrecrystallized condition (Refs. 8, 9). The formed and/or joined parts are then given a recrystallization anneal to develop the typical large-grain microstructure of recrystallized TD-NiCr that helps provide its good high temperature strength. Although this is a promising fabrication technique for TD-NiCr, there are certain disadvantages that should be explored in depth. Most notable is the poor ductility at room temperature of unrecrystallized TD-NiCr sheet, which makes it necessary to accomplish all forming at elevated temperature in the 649 to 971 C (1200 to 1600 F) range.

The purpose of this program was to develop forming and joining technology for TD-NiCr sheet. The study was conducted on material in two metallurgical conditions: recrystallized and unrecrystallized. The technology that was developed will provide baseline engineering data for the fabrication of reliable TD-NiCr hardware for applications such as the thermal protection systems of space shuttle vehicles. The specific goals were: (1) to establish the theoretical and actual formability limits for TD-NiCr sheet, (2) to evaluate solid-state and conventional resistance welding processes and establish joint efficiencies at ambient and elevated temperatures, and (3) to develop an improved brazing alloy for TD-NiCr.

The research study was conducted in three parts, each composed of several tasks as listed below:

Part I - Formability of Commercial (Recrystallized) TD-NiCr Sheet

- Brake Forming
- Corrugation Forming
- Joggling
- Dimpling
- Beading

Part II - Formability of Unrecrystallized TD-NiCr Sheet

- Brake Forming
- Corrugation Forming
- Dimpling
- Beading

Part III - Joining of TD-NiCr Sheet

Resistance Seam Welding (Solid-State)
Resistance Spot Welding (Solid-State)
Resistance Spot Welding (Fusion)
Brazing

The objective of Part I was to evaluate the formability at ambient temperature of recrystallized TD-NiCr sheet using five basic forming processes. This was accomplished by the following sequence of work:

- (1) Prediction of theoretical forming limits
- (2) Forming of experimental parts to determine actual forming limits
- (3) Evaluation of microstructure and mechanical properties of formed parts
- (4) Comparison of theoretical and actual forming limits

The objective of Part II was to evaluate the formability of unrecrystallized TD-NiCr sheet using four forming processes. To accomplish this objective, the optimum forming temperature for unrecrystallized sheet was established, and all forming studies were performed at this temperature. Part II was conducted using the same sequence of work as Part I, except that the formed parts were given a recrystallization anneal prior to evaluation of microstructure and mechanical properties.

The objective of Part III was to evaluate processes for joining recrystallized and unrecrystallized TD-NiCr sheet and to establish joint efficiencies at room and elevated temperatures for the optimized techniques. Investigation was conducted of two solid-state welding processes (resistance seam and spot welding), conventional resistance spot welding, and brazing. A major objective of the brazing effort was the correction of the deficiencies experienced with currently available braze alloys for thin-gage TD-NiCr sheet by development of a new braze alloy.

Page Intentionally Left Blank

2. MATERIALS

The TD-NiCr sheet material used in this program was produced by Fansteel Metallurgical Corporation, Baltimore, Maryland for NASA-Lewis Research Center under Contract NAS3-13490 (Ref. 3). The material was provided in two metallurgical conditions: recrystallized and unrecrystallized. Recrystallized sheet is the commercial-grade product and unrecrystallized sheet is termed "specially-processed." The principal difference between these two materials is that the final heat treatment is not performed on the unrecrystallized sheet. Parts fabricated from unrecrystallized sheet are given the standard recrystallization anneal of two hours at 1177 C (2150 F) in H₂ prior to evaluation or use.

Eleven heats of recrystallized sheet and three heats of unrecrystallized sheet were furnished by NASA for the forming and joining studies. The sheet gages were 0.08, 0.25, 0.5 mm, and 1.0 mm (0.003, 0.010, 0.020 and 0.040 in.) for the recrystallized material and 0.25 and 0.5 mm (0.010 and 0.020 in.) for the unrecrystallized material.

Each heat of material was examined for flatness and surface condition and measurements were made of sheet size and thickness. Material control was facilitated by assigning an identifying code letter to each heat and a code number to each sheet in the heat. A material record log was prepared for each heat and sheet of material. Test specimens were assigned identification numbers so that they could be traced back to their layout in the original sheet. Table 1 lists identification data for each heat of material.

Three different types of surface finish were present among the various heats of material, although all sheets within a given heat had the same finish. The heats of 0.5 and 1.0 mm (0.020 and 0.040 in.) recrystallized sheet and all heats of unrecrystallized sheet had a belt polished (surface ground) finish.

The two heats of 0.08 mm (0.003 in.) recrystallized foil had a typical cold rolled surface finish. All heats of 0.25 mm (0.010 in.) recrystallized sheet except Heat 3637 had a different type of cold rolled finish, which was obtained by a 5% cold roll pass after belt polishing. Heat 3637 had a belt polished finish.

**Table 1. List of Sheet Material Used for Forming
and Joining Development**

Fansteel Heat No.	Fansteel Sheet Serial No.	Convair Code No.*	Condition	Gage mm (in.)	Size cm (in.)	Total Quantity square meters (square feet)
3700	629 630 631 632 633 634	H1 H2 H3 H4 H5 H6	RX	0.25 (0.010)	51.3 x 144 (20.2 x 56.5) 55.1 x 162 (21.7 x 63.7) 55.1 x 145 (21.7 x 57) 55.9 x 107 (22 x 42) 55.9 x 86 (22.2 x 33.7) 55.9 x 155 (22 x 61.2)	4.37 (47)
3691	652 653 654 655 656 657 658 659 660	L1 L2 L3 L4 L5 L6 L7 L8 L9	RX	0.25 (0.010)	52.6 x 121 (20.7 x 47.5) 51.3 x 142 (20.2 x 50.2) 52.6 x 143 (20.7 x 56.2) 53.3 x 147 (21 x 57.7) 51.3 x 149 (20.2 x 58.5) 52.6 x 122 (20.7 x 48.2) 33.5 x 122 (13.2 x 47.7) 53.8 x 120 (21.2 x 47.2) 53.3 x 126 (21 x 49.5)	5.93 (63.8)
3637	457 458 557 558 559 560 561 562	F1 F2 F3 F4 F5 F6 F7 F8	RX	0.25 (0.010)	43.2 x 95 (17 x 37.5) 45 x 103 (17.7 x 40.5) 46.2 x 112 (18.2 x 44) 46.2 x 97 (18.2 x 38.2) 45.7 x 95 (18 x 37.5) 42.4 x 110 (16.7 x 43.2) 46.2 x 114 (18.2 x 44.7) 42.4 x 110 (16.7 x 43.1)	3.72 (40)
3635	448 450 453 454 455	C1 C2 C3 C4 C5	RX	0.25 (0.010)	47 x 176 (18.5 x 69.2) 49.5 x 120 (19.5 x 47.2) 48.8 x 110 (19.2 x 43.2) 46.2 x 177 (18.2 x 70.2) 47 x 180 (18.5 x 70.7)	3.63 (39)
3629	358 357 356 354	A1 A2 A3 A4	RX	0.5 (0.020)	45.7 x 105 (18 x 41.4) 42.4 x 130 (16.7 x 51.2) 43.2 x 106 (17 x 41.6) 34.3 x 118 (13.5 x 46.4)	1.86 (20)
3640	378 377 376 375 392 393 394 395 396	B1 B2 B3 B4 B5 B6 B7 B8 B9	RX	0.5 (0.020)	45.7 x 91 (18 x 36) 48.3 x 95 (19 x 37.4) 44.4 x 92 (17.5 x 36.2) 45 x 93 (17.7 x 36.6) 42.4 x 81 (16.7 x 31.8) 47.2 x 85 (18.6 x 33.4) 47.2 x 86 (18.6 x 33.7) 47.2 x 86 (18.6 x 34) 46.2 x 96 (18.2 x 38)	3.72 (40)
3507	196 197	R1 R2	RX	0.5 (0.020)	50 x 111 (19.7 x 43.6) 50.3 x 112 (19.8 x 44.2)	1.12 (12.1)
3708	547 544	D1 D2	RX	1.0 (0.040)	53.3 x 103 (21.8 x 40.5) 62.2 x 98 (24.5 x 38.5)	1.17 (12.6)
3715	571 572	E1 E2	RX	1.0 (0.040)	48.3 x 124 (19 x 49) 52 x 126 (20.5 x 49.8)	1.25 (13.4)
3702	Coil	M	RX	0.08 (0.003)	50.3 x 708 (19.8 x 279)	3.16 (34)
3523	Coil	P	RX	0.08 (0.003)	49.5 x 109 (19.5 x 42.8)	0.54 (5.8)

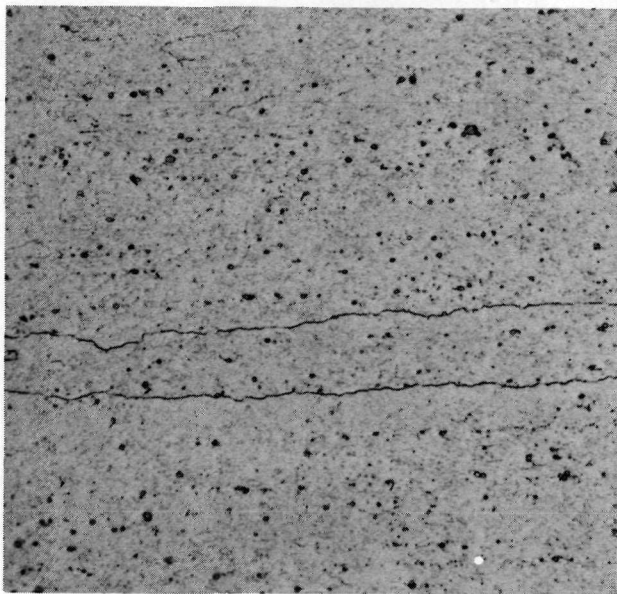
* Used for identification of all test specimens.

Table 1. List of Sheet Material Used for Forming and Joining Development (Continued)

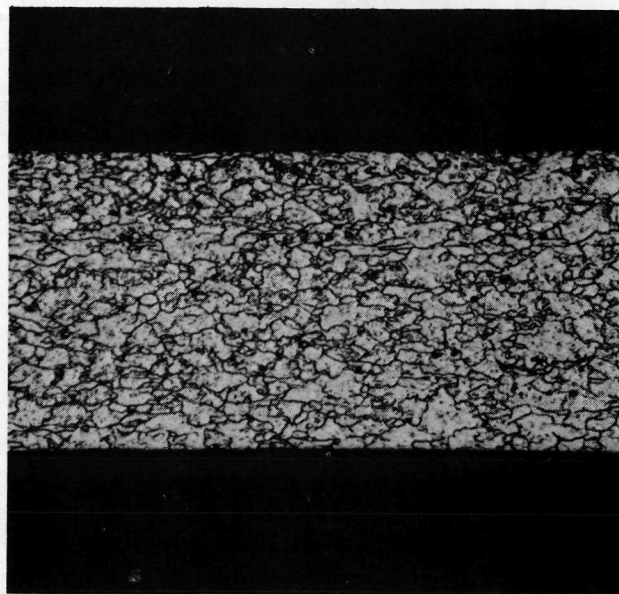
Fansteel Heat No.	Fansteel Sheet Serial No.	Convair Code No.	Condition	Gage mm (in.)	Size cm (in.)	Total Quantity square meters (square feet)
3709	540	G1	UNRX	0.5 (0.020)	44.4 x 187 (17.5 x 73.5)	3.41 (36.7)
	541	G2			45 x 195 (17.7 x 76.7)	
	542	G3			44.7 x 192 (17.6 x 75.7)	
	543	G4			44.7 x 193 (17.6 x 76)	
3689	635	J1	UNRX	0.25 (0.010)	57.2 x 97 (22.5 x 38.2)	4.88 (52.5)
	636	J2			57.2 x 99 (22.5 x 39)	
	637	J3			50.0 x 133 (19.7 x 52.2)	
	638	J4			57.2 x 99 (22.5 x 39)	
	639	J5			51.3 x 124 (21.2 x 49)	
	640	J6			51.3 x 128 (21.2 x 50.2)	
	641	J7			57.2 x 97 (22.5 x 38.2)	
	642	J8			52.6 x 70 (20.7 x 27.7)	
	643	J9			48.3 x 52.6 (19 x 20)	
3714	611	K1	UNRX	0.25 (0.010)	43.2 x 126 (17 x 49.5)	5.45 (58.6)
	612	K2			41.1 x 70 (16.2 x 28.2)	
	613	K3			41.1 x 105 (16.2 x 41.2)	
	614	K4			39.9 x 104 (15.7 x 40.7)	
	615	K5			39.9 x 107 (15.7 x 42)	
	616	K6			41.9 x 108 (16.5 x 42.2)	
	617	K7			43.2 x 108 (17 x 42.5)	
	618	K8			39.4 x 84 (15.5 x 33)	
	619	K9			41.1 x 126 (16.2 x 49.5)	
	620	K10			43.7 x 127 (17.2 x 49.7)	
	621	K11			40.6 x 125 (16 x 49.2)	
	622	K12			43.7 x 39 (17.2 x 15.2)	
	622A	K13			43.7 x 88 (17.2 x 34.7)	

The two heats of 0.08 mm (0.003 in.) sheet showed good flatness and an excellent cold rolled finish. The flatness and surface condition of the other heats varied considerably, but were judged to meet the requirements of Fansteel Product Specification S-TC-S-01-R-1 (Ref. 3) with the exception of Heat 3635 (Code C). The latter heat of 0.25 mm (0.010 in.) recrystallized sheet was judged marginal with respect to both flatness and surface quality, and was replaced by Heat 3637 (Code F). No properties or formability tests were conducted with Heat 3635, and it was subsequently used for forming tool tryout tests. Additional 0.5 mm (0.020 in.) recrystallized sheet was needed for beading tests and the two sheets of material from Heat 3507 (Code R) were provided for this purpose. This material was used only for preliminary bead forming studies and no properties or other evaluation tests were conducted.

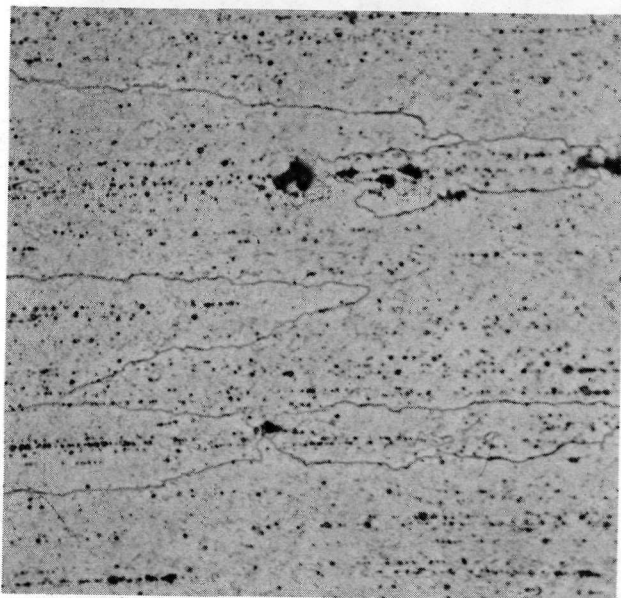
Typical microstructure of recrystallized and unrecrystallized sheet are shown in Figure 1. The fine grain structure of unrecrystallized sheet undergoes change during annealing at 1177 C (2150 F) into the same coarse grain structure of recrystallized material. The two thinner gages of recrystallized material have different microstructure than the thicker material. The 0.25 mm (0.010 in.) recrystallized sheet exhibits a



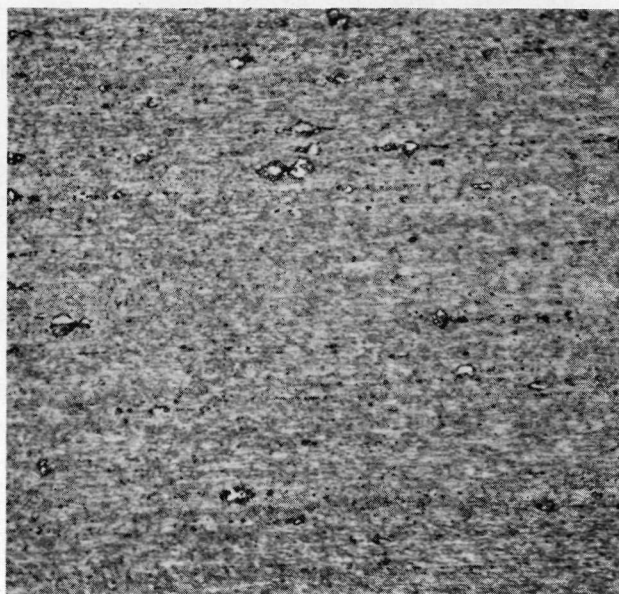
Neg. D3764 500X
Recrystallized 0.25 mm (0.010 in.)
sheet, Heat 3700 (Code H3)



Neg. D3763 500X
Recrystallized 0.08 mm (0.003 in.)
foil, Heat 3702 (Code M)



Neg. D3766 500X
Recrystallized 0.5 mm (0.020 in.)
sheet, Heat 3640 (Code B3)



Neg. D3765 500X
Unrecrystallized 0.5 mm (0.020 in.)
sheet, Heat 3714 (Code K9)
10% oxalic acid electrolytic etch

Figure 1. Typical Microstructure of Recrystallized and Unrecrystallized TD-NiCr Sheet

noticeably larger grain size than the heavier gages. The 0.08 mm (0.003 in.) foil, on the other hand, has a much finer grain size. The different thermo-mechanical processing applied to the thinner sheet gages are responsible for these variations in microstructure. The etchant employed to show the microstructure in Figure 1 was 10% oxalic acid electrolytic etch. This etchant was used to show the microstructure for all micrographs presented in this report unless otherwise noted.

Page Intentionally Left Blank

3. THEORETICAL FORMABILITY

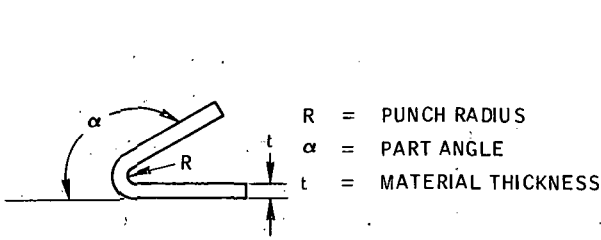
This section describes the approach used to predict the theoretical forming limits for both recrystallized and unrecrystallized TD-NiCr sheet. The outstanding formability work of W. W. Wood et al, performed for the USAF Materials Laboratory (Refs. 10, 11, 12) was selected for prediction of forming limits for the five basic forming processes studied in this program. Wood's studies were based on the premise that it is possible to predict the formability limits of individual forming processes based on characteristic failure types, theoretical analyses of the process, and mechanical properties of the materials to be formed. After defining these limits, he verified his predictions by actual forming tests using predicted values of forming variables.

The formability limits of each forming process are represented by specific predictability equations. Each equation is a function of the process, part shape and geometry, and material properties. Sketches of part shapes, definitions of geometric variables used in the equations, and illustrations of formability limit plots constructed using these equations are presented in Figure 2. It will be noted that two beading methods, rubber press and drop hammer, are included. Past experience in fabrication of beaded panels of thin-gage TD-NiCr indicates the possibility that either of the beading predictability equations developed by Wood might apply. It was planned, therefore, to develop limit curves for each beading process and to establish the best correlation with results of experimental forming.

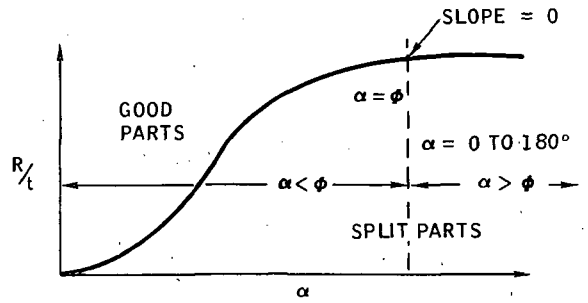
Definition of the symbols for mechanical properties data used in the theoretical formability equations is as follows:

$\epsilon_{2.0}$	= Elongation (strain) for 5.08 cm (2 in.) gage length
$(\epsilon_L)_{0.5}$	= Elongation (strain) for 1.27 cm (0.5 in.) gage length
$(\epsilon_W)_{0.5}$	= Strain 1.27 cm (0.5 in.) gage width
$(\epsilon_L)_{0.25}$	= Elongation (strain) for 0.63 cm (0.25 in.) gage length
$(\epsilon_W)_{0.25}$	= Strain 0.63 cm (0.25 in.) gage width
$\epsilon_{0.02}$	= Elongation (strain) for 0.05 cm (0.02 in.) gage length
S_{ty}	= Tensile strength at yield point
S_u	= Tensile strength at ultimate load
S_{cy}	= Compressive strength at yield point
E_c	= Compressive modulus of elasticity

BRAKE FORMING

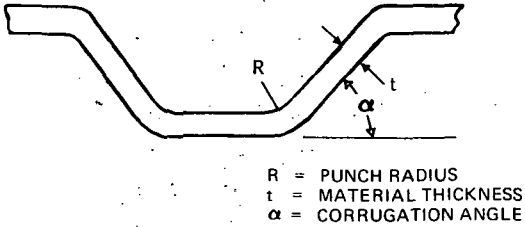


Variables for brake-formed part.

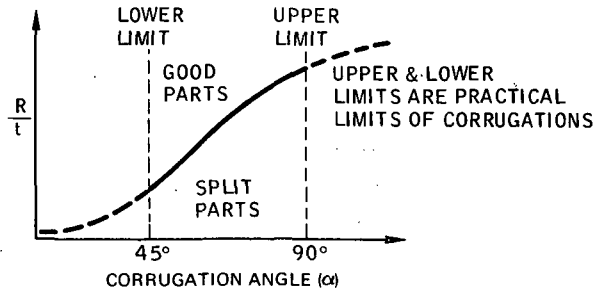


Formability envelope for brake forming.

CORRUGATION FORMING

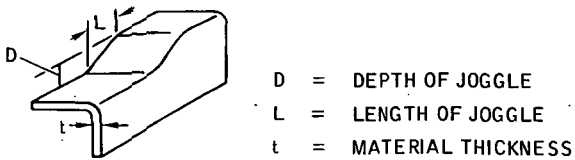


Variables for corrugation forming.

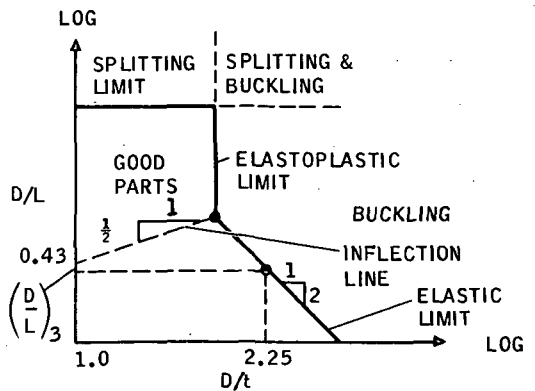


Formability envelope for corrugation forming (same as brake forming).

JOGGLING



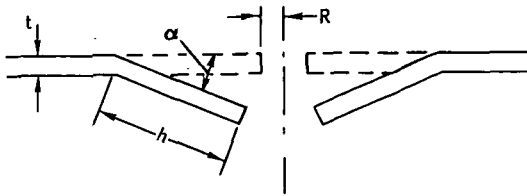
Variables for joggling.



Formability envelope for joggling.

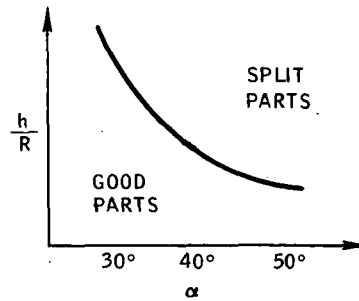
Figure 2. Geometric Variables and Formability Envelopes (Sheet 1 of 2)

DIMPLING



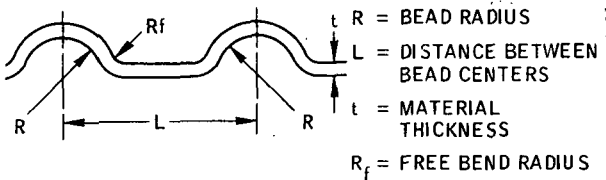
- R = INITIAL RADIUS OF PILOT HOLE
 α = ANGLE OF DIMPLE
 h = LENGTH OF DIMPLE FLANGE
 t = MATERIAL THICKNESS

Variables for dimpling.



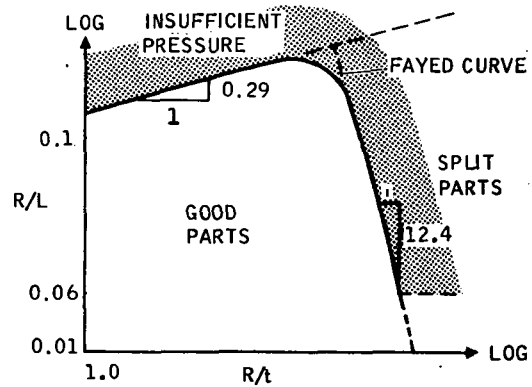
Formability envelope
for dimpling.

RUBBER PRESS BEADING



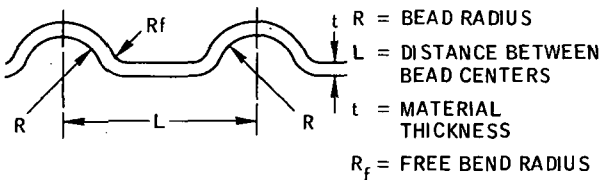
- R = BEAD RADIUS
 L = DISTANCE BETWEEN BEAD CENTERS
 t = MATERIAL THICKNESS
 R_f = FREE BEND RADIUS

Variables for rubber press beading.



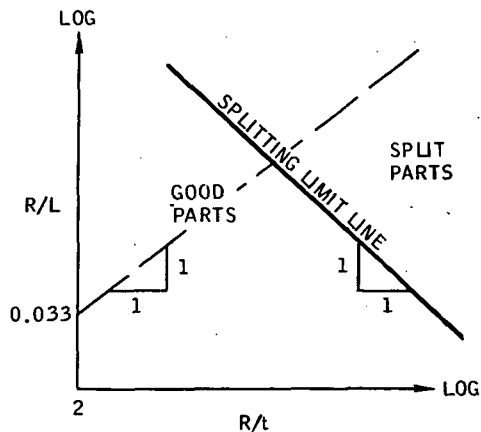
Formability envelope for
rubber press beading.

DROP HAMMER BEADING



- R = BEAD RADIUS
 L = DISTANCE BETWEEN BEAD CENTERS
 t = MATERIAL THICKNESS
 R_f = FREE BEND RADIUS

Variables for drop
hammer beading.



Formability envelope for
drop hammer beading.

Figure 2. Geometric Variables and Formability Envelopes (Sheet 2 of 2)

The theoretical formability equations that apply to each forming process used in this program are as follows:

(1) Brake Forming and Corrugation Forming

Given $(\epsilon_L)_{.25}$ and $(\epsilon_W)_{.25}$

Solve $(\bar{\epsilon}_L)_{.25} = \ln [1 + (\epsilon_L)_{.25}]$

$$(\bar{\epsilon}_W)_{.25} = \ln [1 + (\epsilon_W)_{.25}]$$

$$\bar{\epsilon}_{.25(\text{corr})} = (\bar{\epsilon}_L)_{.25} - \frac{(\bar{\epsilon}_W)_{.25}^2}{(\bar{\epsilon}_L)_{.25}}$$

Given $\alpha > \phi$ up to 180° , $\alpha \sim \beta$

Solve $\left(\frac{R}{t}\right)_{\max} = \frac{1}{e^{2[\bar{\epsilon}_{.25(\text{corr})}] - 1}}$

Given $\alpha < \phi$, $\alpha \sim \beta$

Solve $\frac{R}{t} = \frac{1}{2} \left[\left(\frac{R}{t}\right)_{\max} \right] \left[1 + \sin \left[\frac{15.21\alpha}{11.4 - \left(\frac{R}{t}\right)_{\max}} - 90^\circ \right] \right]$

Given $\alpha = \phi$, $\alpha \sim \beta$

Solve $\phi = \left[11.4 - \left(\frac{R}{t}\right)_{\max} \right] \div 0.0845$

(2) Jogging

Splitting Limit Line:

Given $\epsilon_{.02}$

Solve $\left(\frac{D}{L}\right)_1 = \left[\epsilon_{.02} (1.44 \epsilon_{.02} + 2.4) \right]^{1/2}$

Elasto-Plastic Limit Line:

Given E_c and S_{cy}

Solve $\frac{D}{t} = \left(0.0118 \frac{E_c}{S_{cy}} \right)^{2/5}$

Inflection Point (Elastic to Elasto-Plastic):

Solve $\left(\frac{D}{L} \right)_2 = 0.43 \left(\frac{D}{t} \right)^{1/2}$

Buckling Formability Index Point

Given $\frac{D}{t} = 2.25$

Solve $\left(\frac{D}{L} \right)_3 = \frac{E_c}{S_{cy}} \times 10^{-3}$

(3) Dimpling

Given $\epsilon_{2.0}$ and α

Solve $\frac{h}{R} = \frac{0.444 (\epsilon_{2.0})^{.253}}{1 - \cos \alpha}$

(4) Rubber Press Beading

Upper Pressure Limit Line

Given S_{ty} and $\frac{R}{t}$

Solve $\left(\frac{R}{L} \right)_1 = 0.065 \left(\frac{\frac{1}{S_{ty}} \times 10^4}{0.065} \right)^{.216} \left(\frac{R}{t} \right)^{.29}$

Splitting Line to Limit of Predictability

Given $\epsilon_{2.0}$ and S_u

Solve $\left(\frac{R}{L}\right)_2 = (6.0 \times 10^{-21}) (\epsilon_{2.0} S_u)^{9.3} \left(\frac{R}{t}\right)^{-12.4}$

Pressure Index Line

Solve $\left(\frac{R}{L}\right)_3 = 0.065 \left(\frac{R}{t}\right)^{.37}$

Splitting Index Line

Solve $\left(\frac{R}{L}\right)_4 = 6.84 \times 10^{-4} \left(\frac{R}{t}\right)^{1.5}$

(5) Drop Hammer Beading

Given $(\epsilon_L)_{.5}$ and $(\epsilon_W)_{.5}$

Solve $(\bar{\epsilon}_L)_{.5} = \ln \left[1 + (\epsilon_L)_{.5} \right]$

$(\bar{\epsilon}_W)_{.5} = \ln \left[1 + (\epsilon_W)_{.5} \right]$

$\epsilon_{.5(\text{corr})} = \ln^{-1} \left[(\bar{\epsilon}_L)_{.5} - \frac{(\bar{\epsilon}_W)_{.5}^2}{(\bar{\epsilon}_L)_{.5}} \right]^{-1}$

Splitting Limit Line

Solve $\left(\frac{R}{L}\right)_1 = (\epsilon_{.5(\text{corr})})^2 (60.6) \left(\frac{R}{t}\right)^{-1}$

Formability Index Line

Solve $\left(\frac{R}{t}\right)_1 = 60.6 \left(\frac{R}{L}\right)_1$

Upper and Lower Formability Limits

No limits will be established.

A computer program was written to solve the formability equations using geometric parameters and material properties as input. This program, given in Appendix A, was written in FORTRAN IV language for the CDC 6400 digital computer. Prior to use, the program was checked for completeness and accuracy using synthesized input data. The output data was verified three ways: (1) by plotting and checking resultant curves and lines for form and slope, (2) checking for rationality, and (3) checking against the results of manual calculations.

The mechanical properties data required to use the forming predictability equations are listed in Table 2.

Table 2. Tensile and Compressive Properties Data Required for Forming Predictability Equations (Room or Elevated Temperature)

Process	Material Properties									
	Elongation or Strain						Strength			Modulus
	$\epsilon_{2.0}$	$(\epsilon_L) 0.5$	$(\epsilon_W) 0.5$	$(\epsilon_L) 0.25$	$(\epsilon_W) 0.25$	$\epsilon_{0.02}$	S_{ty}	S_u	S_{cy}	E_c
Brake Forming				X	X					
Corrugation Forming				X	X					
Joggling						X			X	X
Dimpling	X									
Beading:										
Rubber Press	X						X	X		
Drop Hammer		X	X							

Page Intentionally Left Blank

4. FORMABILITY OF RECRYSTALLIZED TD-NiCr SHEET

The formability of recrystallized TD-NiCr sheet was evaluated at room temperature using five forming processes: brake forming, corrugation forming, joggling, dimpling, and beading. Under present material specifications, commercial (recrystallized) TD-NiCr sheet is given a high-temperature recrystallization anneal by the producer to enhance elevated temperature strength (Ref. 3). The material has reasonably good ductility (10 to 20%) at room temperature, but exhibits continuously decreasing ductility with increasing temperature to above 1204 C (2200 F). Since ductility is directly related to formability, no improvement can be obtained by forming at elevated temperatures.

The forming program for recrystallized sheet included the following studies: (1) material properties tests, (2) theoretical forming limit calculations, (3) fabrication of forming tools, (4) forming tests, (5) post-forming evaluation of microstructure and tensile properties, and (6) comparison of theoretical and actual forming limits.

Eight heats of material consisting of four gages (2 heats each) of recrystallized sheet were evaluated. Figure 3 shows the breakdown of material gages and heats and the post-forming evaluation studies for the various forming processes.

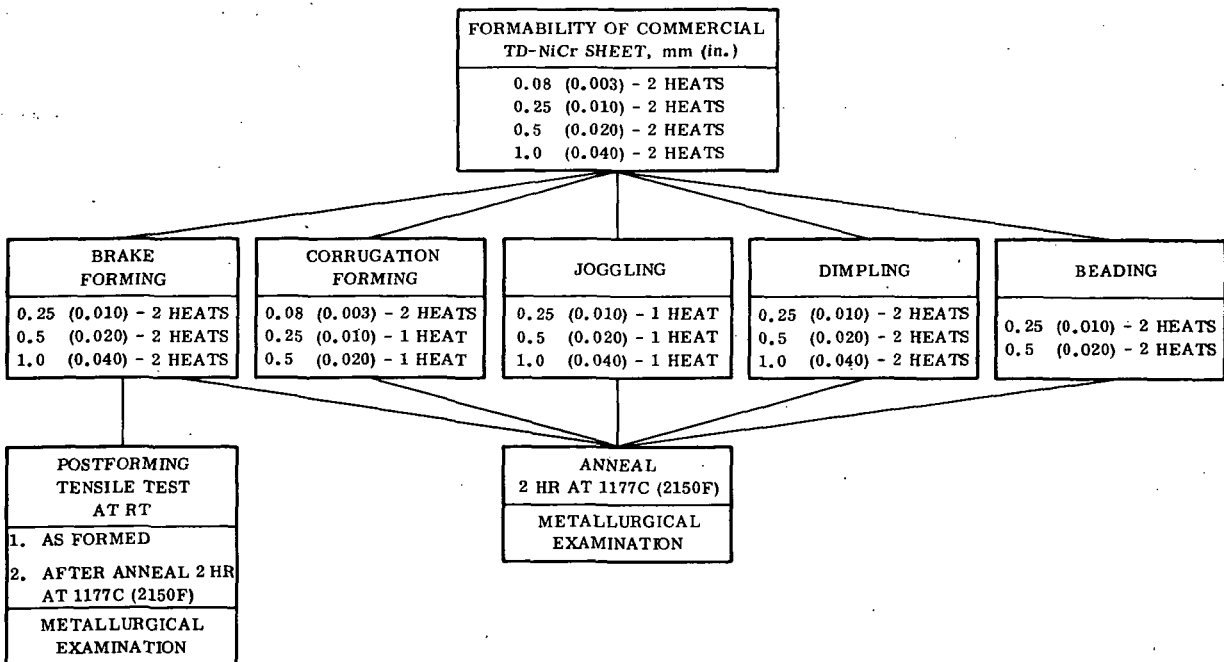


Figure 3. Material Breakdown and Test Plan for Recrystallized TD-NiCr Forming Evaluation

Material Properties

Tensile Properties - Tensile tests were conducted for eight heats of recrystallized sheet using the specimen configuration shown in Figure 4. Table 3 is a summary of tensile properties obtained for two heats each of 0.08, 0.25, 0.5 and 1.0 mm (0.003, 0.010, 0.020 and 0.040 in.) sheet in both the longitudinal and transverse grain directions. The complete test data are contained in Appendix B.

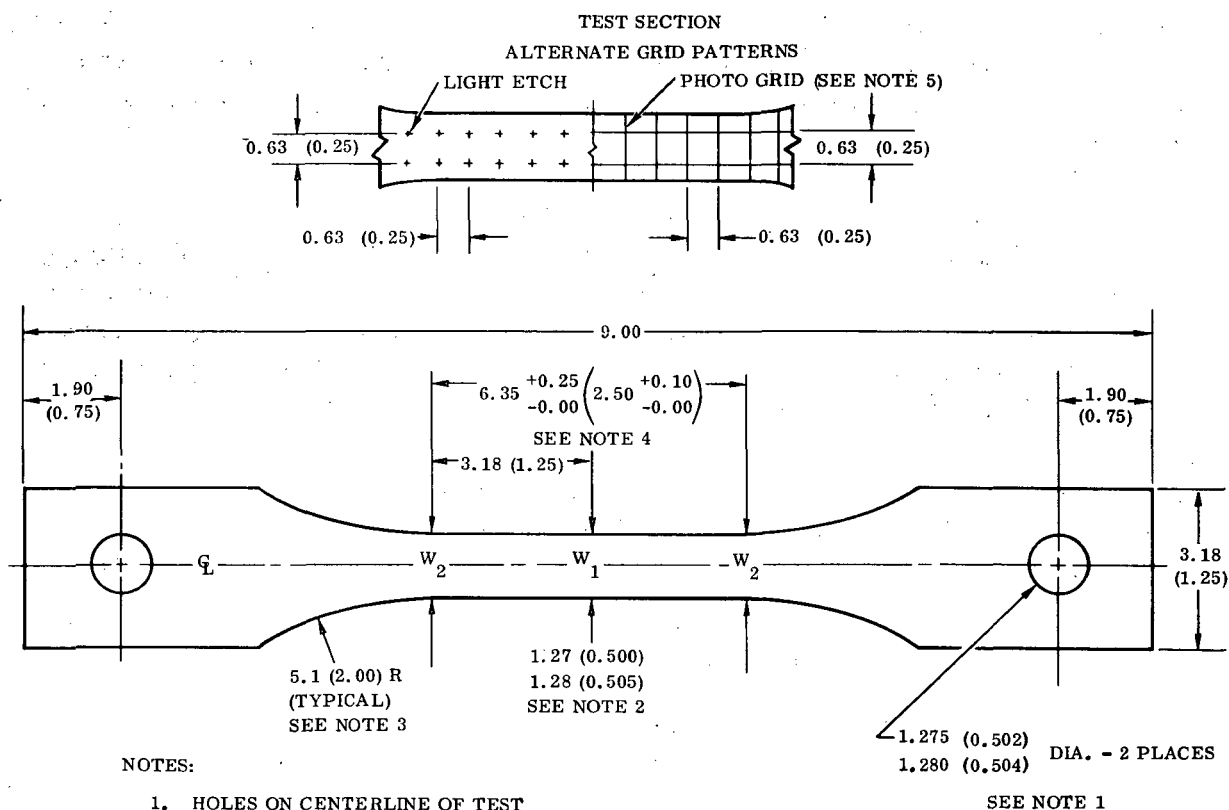


Figure 4. Tensile Specimen

Table 3. Summary of Tensile Properties of Recrystallized TD-NiCr Sheet

Sheet Thickness mm (in.)	Heat Number	Grain Direction	Specimen Code	Ultimate Tensile Strength MN/m ² (ksi)	Tensile Yield Strength MN/m ² (ksi)	Elongation or Strain, Percent								Indicated Modulus GN/m ² (10 ⁶ psi)
						ε 2.0	ε 1.0	(ε _L) 0.5	(ε _W) 0.5	(ε _L) 0.25	(ε _W) 0.25	ε 0.02		
0.25 (0.010)	3637	L	F1L	886 (128.5)	647 (93.8)	9.5	10.5	12.5	-4.5	15	-4	—	168 (24.4)	
		T	F1T	825 (119.7)	594 (86.1)	15.5	17.5	21	-13.5	27	-12	—	177 (25.6)	
	3700	L	H1L	847 (122.8)	640 (92.8)	9	10	11.5	-3	14	-2.5	19.5	141 (20.5)	
		T	H1T	729 (105.7)	555 (80.5)	19	21	25.5	-16	29	-16	33	170 (24.6)	
0.5 (0.020)	3629	L	A4L	891 (129.2)	618 (89.7)	16.5	18	21	-10	26	-5.5	—	144 (20.9)	
		T	A4T	843 (122.3)	595 (86.3)	18	21	26.5	-15.5	34	-15.5	—	170 (24.7)	
	3640	L	B2L	889 (129.0)	579 (84.0)	16	18	20.5	-7.5	24	-5.5	24	149 (21.6)	
		T	B2T	837 (121.4)	546 (79.2)	19	21	24.5	-14	28	-13.5	25	165 (23.9)	
1.0 (0.040)	3708	L	D2L	873 (126.6)	570 (82.7)	17	20	26	-9.5	32.5	-9.5	—	144 (20.9)	
		T	D2T	818 (118.6)	547 (79.3)	21	25.5	33	-20	40	-19	—	168 (24.4)	
	3715	L	E2L	868 (125.9)	714 (88.2)	17	19.5	26	-10.5	35.5	-9.5	49	141 (20.5)	
		T	E2T	801 (116.2)	537 (77.9)	21.5	26.5	33.5	-20.5	43	-19.5	48	164 (23.8)	
0.08 (0.003)	3702	L	ML	894 (129.7)	686 (99.5)	14.5	16.5	—	—	22	-7.5	—	228 (33.0)	
		T	MT	901 (130.7)	716 (103.8)	15.5	17.5	—	—	22.5	-9	—	272 (39.5)	
	3523	L	PL	883 (128.0)	748 (108.5)	6	6.5	—	—	9	-2.5	—	198 (28.7)	
		T	PT	863 (125.1)	751 (108.9)	4	5	—	—	8	-3.5	—	222 (32.2)	

Average of three specimens for each value.

Elongation and (ϵ_L) strain measurements made across fracture except $\epsilon_{0.02}$, which were made adjacent to fracture.

The tensile tests were performed at room temperature using a strain rate of 0.005 cm/cm/min (0.005 in./in./min) to 0.6 percent offset strain and then 0.05 cm/cm/min (0.05 in./in./min) to fracture in accordance with ASTM E8-69. Accurate measurement of elongation (strain) was obtained using precision grid patterns applied to the specimen by a photographic technique (Figure 4). An 0.63 cm (0.25 in.) photogrid pattern was applied to one side of each tensile specimen and in those cases where $\epsilon_{0.02}$ strain data were required, an 0.05 cm (0.02 in.) photogrid pattern was applied to the opposite side. The accuracy of the photogrid pattern is better than 0.5 percent of the grid spacing. Elongation (strain) was determined by measuring the grid spacings of fractured specimens at 30X magnification with a Unitron measuring microscope.

Also shown in Figure 4 is an 0.63 cm (0.25 in.) photoetched grid that was used for elevated temperature testing of unrecrystallized material, which is described in Section 5. This grid is in the form of small crosses lightly etched into the material at the 0.63 cm (0.25 in.) grid intersections. The etched-in grid pattern is necessary since the photographically-applied grids would be destroyed at elevated temperatures. Typical fractured tensile specimens with the three types of photogrid patterns are shown in Figure 5. Specimen No. B2T-2 illustrates the severe orange-peel surface condition characteristic of recrystallized TD-NiCr sheet plastically deformed transverse to the rolling direction. The tensile properties listed in Table 3 indicate a significant degree of anisotropy for recrystallized sheet. The ultimate and yield strengths are higher for the longitudinal than for the transverse direction, and the elongation and modulus are lower in the longitudinal direction. The tensile properties data show generally good agreement

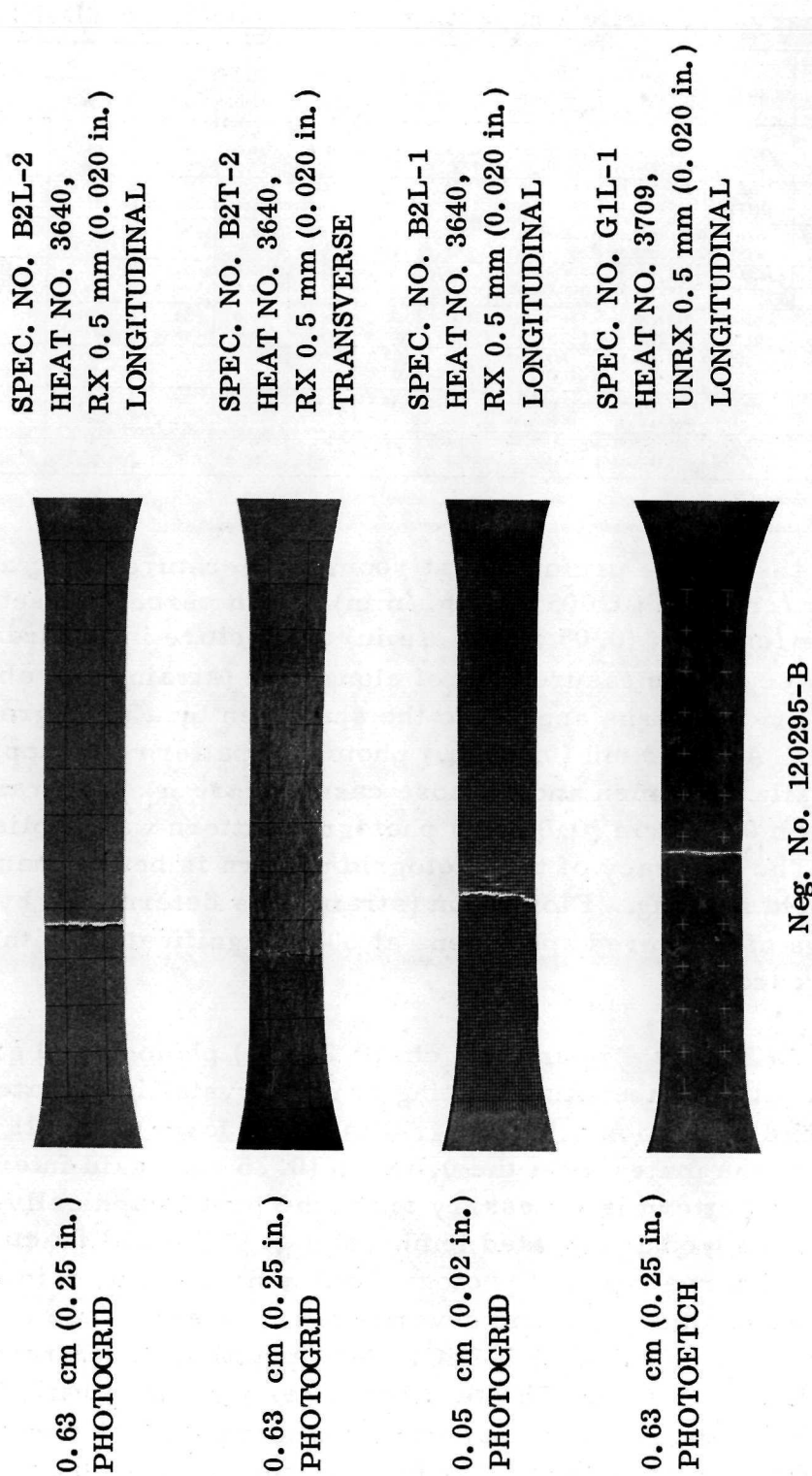


Figure 5. Fractured Tensile Specimens with 0.63 cm (0.25 in.) and 0.05 cm (0.02 in.) Grid Patterns

for the various gages and heats of material with the exception of the two 0.08 mm (0.003 in.) heats. The relatively low elongation (9 - 9.5%) in the longitudinal direction for 0.25 mm (0.010 in.) sheet from Heat 3700 appeared inconsistent, but three additional tensile tests confirmed that these data were valid.

The two heats of 0.08 mm (0.003 in.) sheet displayed only slight anisotropy, which is in contrast to the significant anisotropy for the thicker materials. Heat 3523 exhibited low elongation in both the longitudinal ($\epsilon_{2.0} = 7\%$) and transverse ($\epsilon_{2.0} = 4\%$) directions. This poor elongation is in marked contrast to Heat 3702 and the heats of thicker material.

It was reported that the processing procedures used for production of the foil were different for the two heats of material. Furthermore, Heat 3523 was not considered to be representative of material produced by the optimized rolling procedures for TD-NiCr foil. For this reason, studies of Heat 3523 were confined to a very limited investigation of forming characteristics. Since a large quantity of material was available for Heat 3702, this heat was used for both forming and joining studies.

The Fansteel material certifications for seven heats of 0.25, 0.5, and 1.0 mm (0.010, 0.020, and 0.040 in.) recrystallized TD-NiCr sheet give the transverse mechanical properties listed in Table 4. The Convair Aerospace test data show somewhat higher tensile strength and slightly lower elongation ($\epsilon_{1.0}$) than the material certifications, but the agreement is considered reasonably good. The material certifications indicate generally lower properties for 0.25 mm (0.010 in.) sheet than for the thicker material. The lower properties for 0.25 mm (0.010 in.) sheet are also reflected in the minimum requirements of the material specification. No tensile tests were conducted for one heat of 0.25 mm (0.010 in.) material listed in Table 4 (Heat No. 3691). Material from this heat was used for joining studies, and its properties were evaluated as a Part III task.

The transverse mechanical properties of the two heats of 0.08 mm (0.003 in.) material as reported by Fansteel (Ref. 3) are also listed in Table 4. The Fansteel data show even lower elongation (2.5%) for Heat 3523 and in addition show only 2.5% elongation for Heat 3702. Discussions with Fansteel personnel revealed that these low elongation values may have resulted from their use of specimen configuration and test procedures unsuitable for foil.

Table 4. Transverse Mechanical Properties of TD-NiCr Sheet from Fansteel Certifications

Fansteel Heat Number	Convair Heat Code No.	Sheet Thickness mm (in.)	Tensile Properties @ R. T.				Tensile Properties @ 1093°C(2000°F)				1093°C (2000°F) Stress Rupture		
			Ultimate Tensile Strength MN/m ² (ksi)	Tensile Yield Strength MN/m ² (ksi)	Elongation % in 2.54 cm (1.0 in.)	Ultimate Tensile Strength MN/m ² (ksi)	Tensile Yield Strength MN/m ² (ksi)	Elongation % in 1.54 cm (1.0 in.)	Stress MN/m ² (ksi)	Hours	Elong. % in 2.54 cm (1.0 in.)	105° Bend	
3637	F	0.25 (0.010)	801 (116.1)	564 (81.8)	17.0	102 (14.8)	102 (14.8)	2.0	31 (4.5)	exceeds 20	5.0	Passed	3T radius
3700	H	0.25 (0.010)	744 (107.9)	551 (79.9)	24.5	87 (12.6)	87 (12.6)	3.0	↑	↑	>1.5	↑	↑
3691	L	0.25 (0.010)	741 (107.5)	595 (86.3)	21.0	99 (14.3)	99 (14.3)	2.0	38 (5.5)	↑	2.0	↑	↑
3629	A	0.5 (0.020)	823 (119.3)	594 (86.2)	25.0	150 (21.7)	150 (21.7)	2.5	↑	↑	5.5	↑	↑
3640	B	0.5 (0.020)	776 (112.5)	531 (77.0)	22.5	142 (20.6)	142 (20.6)	3.5	↑	↑	6.5	↑	↑
3708	D	1.0 (0.040)	801 (116.1)	526 (76.3)	20.0	122 (17.7)	122 (17.7)	3.0	↑	↑	4.8	↑	↑
3715	E	1.0 (0.040)	822 (119.2)	548 (79.5)	23.0	123 (17.6)	121 (17.6)	2.9	↑	↑	6.5	↑	↑
3702	M	0.08 (0.003)	749 (108.7)	676 (98.1)	2.5	77 (11.2)	68 (9.9)	9.2	31 (4.5)	↑	not given	2T radius	2T radius
3523	P	0.08 (0.003)	980 (142.1)	909 (131.9)	2.5	77 (10.9)	75 (10.9)	2.0	31 (4.5)	↑	not given	2T radius	2T radius
Fansteel Product Specification S-TC-S-01-R-1 (Minimum Requirements)	to	0.5 (0.020)	758 (110.0)	517 (75.0)	10.0	103 (15.0)	*	1.0	38 (5.5)	20	*	Pass	3T radius
		0.5 (0.075)					*						
		0.25 (0.010) to <0.25 (<0.020)	690 (100.0)	448 (65.0)	8.0	69 (10.0)	*	1.0	28 (4.0)	20	*	Pass	3T radius

No certifications available for 0.08 mm (0.003 in.) heats; data taken from Reference 3.

Compressive Properties. - Compression tests were conducted for three heats of material: one heat each of 0.25, 0.5, and 1.0 mm (0.010, 0.020, and 0.040 in.) sheet thickness. Results of the compression tests are listed in Table 5. The tests were conducted with a Montgomery Templin Grip Compressometer, Model SC-1. The compression specimen is shown in Figure 6. Specimens for the 0.5 mm (0.020 in.) material were prepared by adhesive bonding together two thicknesses of sheet and then machining to final dimensions. The adhesive (3M Epoxy adhesive EC2216) was cured at room temperature for 16 hours, followed by 3 hours at 71 C (160 F). Compression test specimens for the 0.25 mm (0.010 in.) material were prepared by adhesive bonding four thicknesses of sheet using the same adhesive bonding technique as for the 0.5 mm (0.020 in.) specimens. Thickness measurements were made prior to adhesive bonding.

Table 5. Compressive Properties of Recrystallized TD-NiCr Sheet

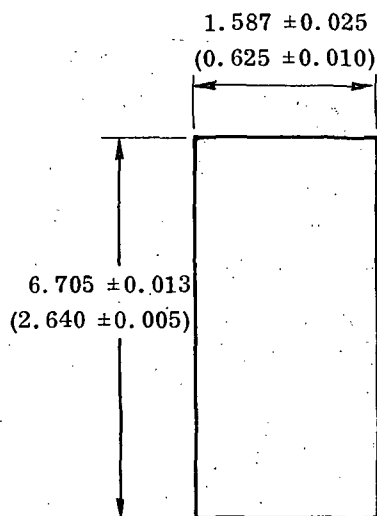
Sheet Thickness, mm (in.)	Heat Number (Fansteel)	Grain Direction	Specimen Number	Compressive Yield Strength MN/m ² (ksi)	Compressive Modulus GN/m ² (10 ⁶ psi)	Remarks
0.25 (0.010) ⁽¹⁾	3700	L	H1L-1		156 (22.6)	No yield, specimen buckled No yield, specimen buckled No yield, specimen buckled
			-5		148 (21.5)	
			-9		166 (24.1)	
			Average		156 (22.7)	
0.5 (0.020) ⁽²⁾	3640	L	H1T-1		207 (30.0)	No yield, specimen buckled No yield, specimen buckled No yield, specimen buckled
			-7		209 (30.3)	
			-9		206 (29.9)	
			Average		207 (30.1)	
		T	B2T-1		163 (23.6)	Yield not valid
			-3	596 (86.5)	163 (23.6)	
			-5	596 (86.5)	165 (24.0)	
			Average	596 (86.5)	164 (23.8)	
1.0 (0.040)	3715	L	B2T-1	596 (86.4)	189 (27.4)	
			-3	592 (85.8)	185 (26.9)	
			-5	592 (85.9)	180 (26.1)	
			Average	593 (86.0)	184 (26.8)	
		T	E2L-1	594 (86.2)	158 (22.9)	
			-2	568 (82.4)	154 (22.4)	
			-3	567 (82.3)	156 (22.6)	
			-4	568 (82.4)	162 (23.5)	
			-6	586 (85.0)	165 (24.0)	
			Average	577 (83.7)	159 (23.1)	
		T	E2T-1	592 (85.8)	179 (25.9)	
			-2	587 (85.1)	192 (27.8)	
			-3	588 (85.2)	179 (25.9)	
			Average	589 (85.4)	183 (26.5)	

(1) Four thicknesses of sheet, adhesive bonded.

(2) Two thicknesses of sheet, adhesive bonded.

No difficulties were encountered in compression testing of the 0.5 and 1.0 mm (0.020 and 0.040 in.) specimens, and the results agreed quite closely. The 0.25 mm (0.010 in.) specimens buckled near the top end prior to reaching yield. Compressive modulus test results for the transverse direction were significantly lower for the 0.25 mm (0.010 in.) specimens than for the thicker specimens. There is no present explanation for this discrepancy and the validity of the compressive modulus test data for the 0.25 mm (0.010 in.) material is questionable.

No corrective or alternate test procedure was available that had the capability of providing better compression test data for 0.25 mm (0.010 in.) gage material. For this reason, the compressive properties data of 0.5 mm (0.020 in.) sheet were used for determining theoretical forming limits for 0.25 mm (0.010 in.) sheet.



NOTES:

1. ENDS SHALL BE PARALLEL WITHIN 0.00063 (0.00025).
2. ENDS SHALL BE PERPENDICULAR TO SIDES WITHIN 0.25°.
3. ALL DIMENSIONS IN CM (IN.)

Figure 6. Compression Specimen

Theoretical Forming Limit Curves

Theoretical formability data were generated for eight heats of recrystallized sheet using the Formability Computer Program (Appendix A) with materials properties data from Table 3 and selected values of geometric parameters as input. The following formability curves were plotted from the output data:

Brake Forming	8 curves (4 heats/2 grain directions)
Corrugation Forming	Identical to brake forming
Joggling	4 curves (2 heats/2 grain directions)
Dimpling	8 curves (4 heats/2 grain directions)
Beading-Rubber Press	4 curves (2 heats/2 grain directions)
-Drop Hammer	4 curves (2 heats/2 grain directions)

Typical forming limit curves for each process are shown in Figures 7 through 11 for 0.5 mm (0.020 in.) sheet from Heat 3640. Plotted on these figures are data points for the selected parameter values. For example, in Figure 7, minimum bend radius (R/t) were calculated for selected part angles (α) of 30, 60, 90, 100 and 120 degrees.

Forming limit curves for the other heats of material are presented in later sections where actual forming limits are compared to the predicted forming limits.

The theoretical forming curves indicate only a small difference in forming limits between the longitudinal and transverse orientations.[†] The brake/corrugation (Figure 7) and drop hammer beading (Figure 11) curves show slightly better formability for the longitudinal direction, and the joggling (Figure 7), dimpling (Figure 8), and rubber press beading (Figure 9) curves show slightly better formability for the transverse direction.

A comparison was made of the theoretical formability in the transverse (T) and longitudinal (L) directions for eight heats of material and the five basic forming processes. Results of this comparison are as follows:

	Best Formability in Direction Indicated							
	0.25 mm (0.010 in.)		0.5 mm (0.020 in.)		1.0 mm (0.040 in.)		0.08 mm (0.003 in.)	
	Heat 3700(H)	Heat 3637(F)	Heat 3629(A)	Heat 3640(B)	Heat 3708(D)	Heat 3715(E)	Heat 3702(M)	Heat 3523(P)
Brake/ Corrugation Forming	T	T	L	L	L	L	L	L
Joggling	T	*	*	T	T	*	*	*
Dimpling	T	T	T	T	T	T	*	*
Beading-Rubber Press	T	T	T	T	*	*	*	*
-Drop Hammer	T	L	L	L	*	*	*	*
* Not included in study								

[†] The following definitions apply for both theoretical and experimental forming studies: a. Longitudinal Orientation - When the direction of maximum strain during forming is parallel to the rolling direction.
b. Transverse Orientation - When the direction of maximum strain is normal to the rolling direction.

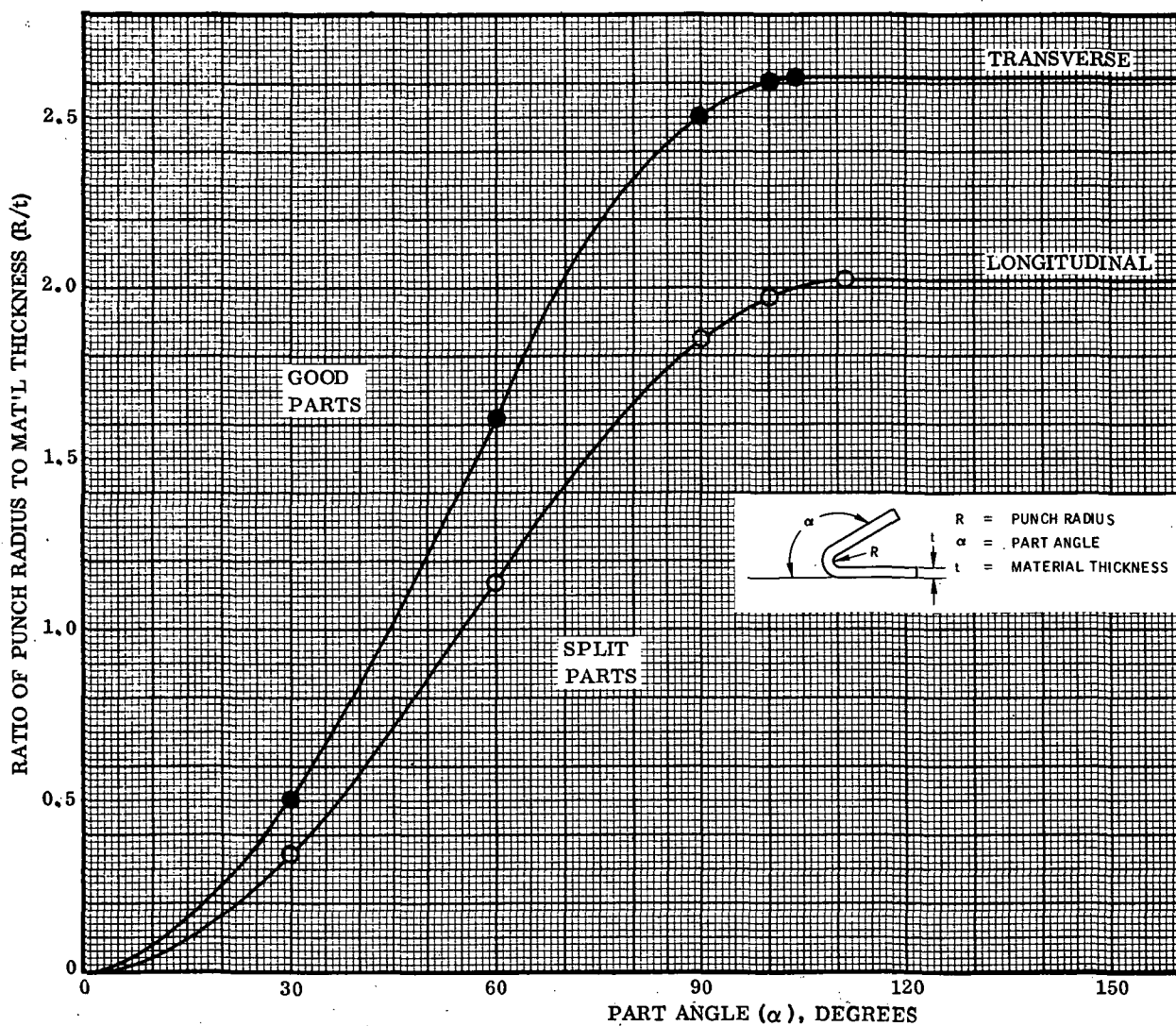


Figure 7. Theoretical Formability Curves for Brake and Corrugation Forming of 0.5 mm (0.020 in.) Recrystallized TD-NiCr Sheet - Heat 3640 (Code B2)

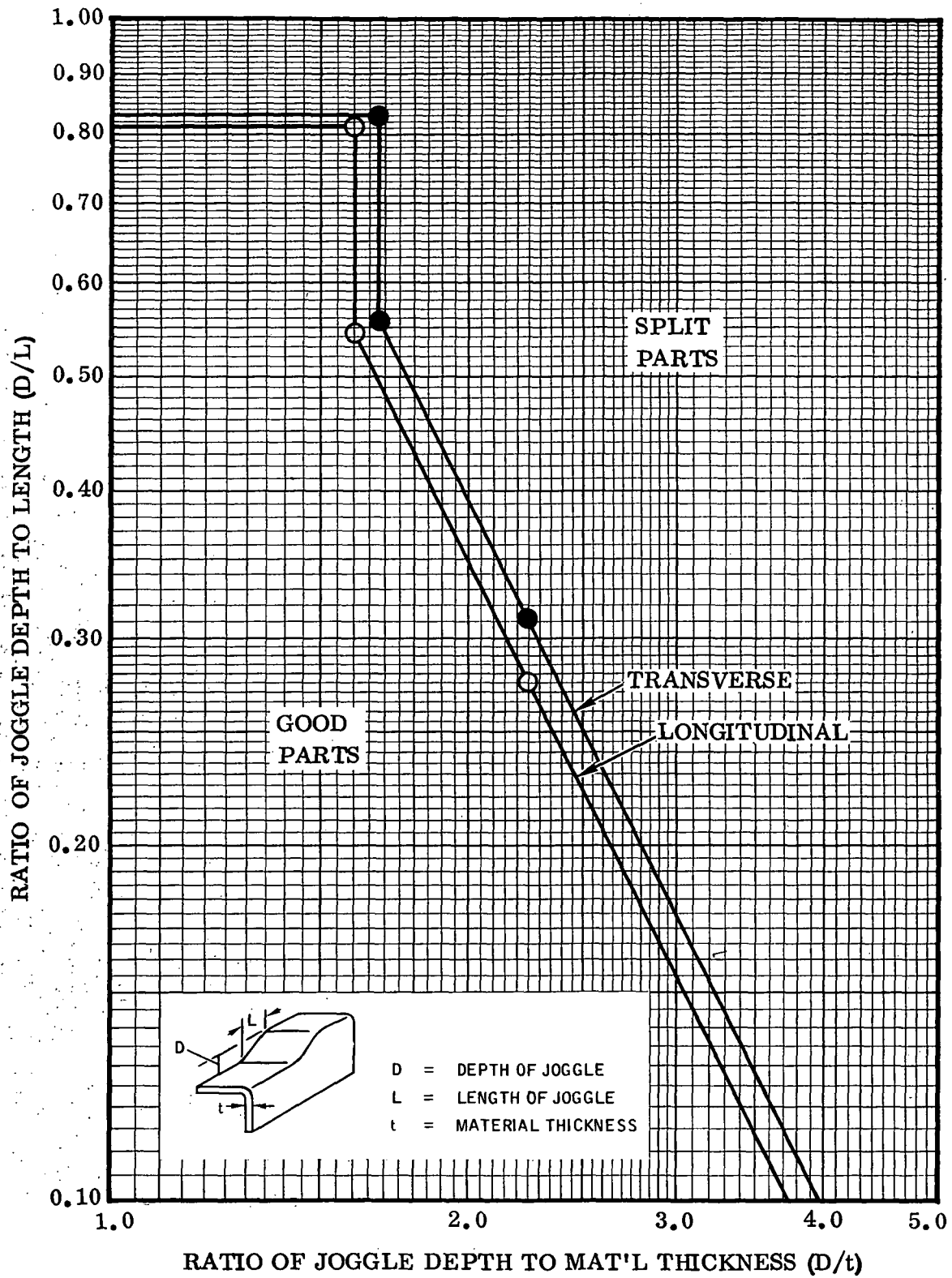


Figure 8. Theoretical Formability Curves for Jogging of 0.5 mm (0.020 in.) Recrystallized TD-NiCr Sheet-Heat 3640 (Code B2)

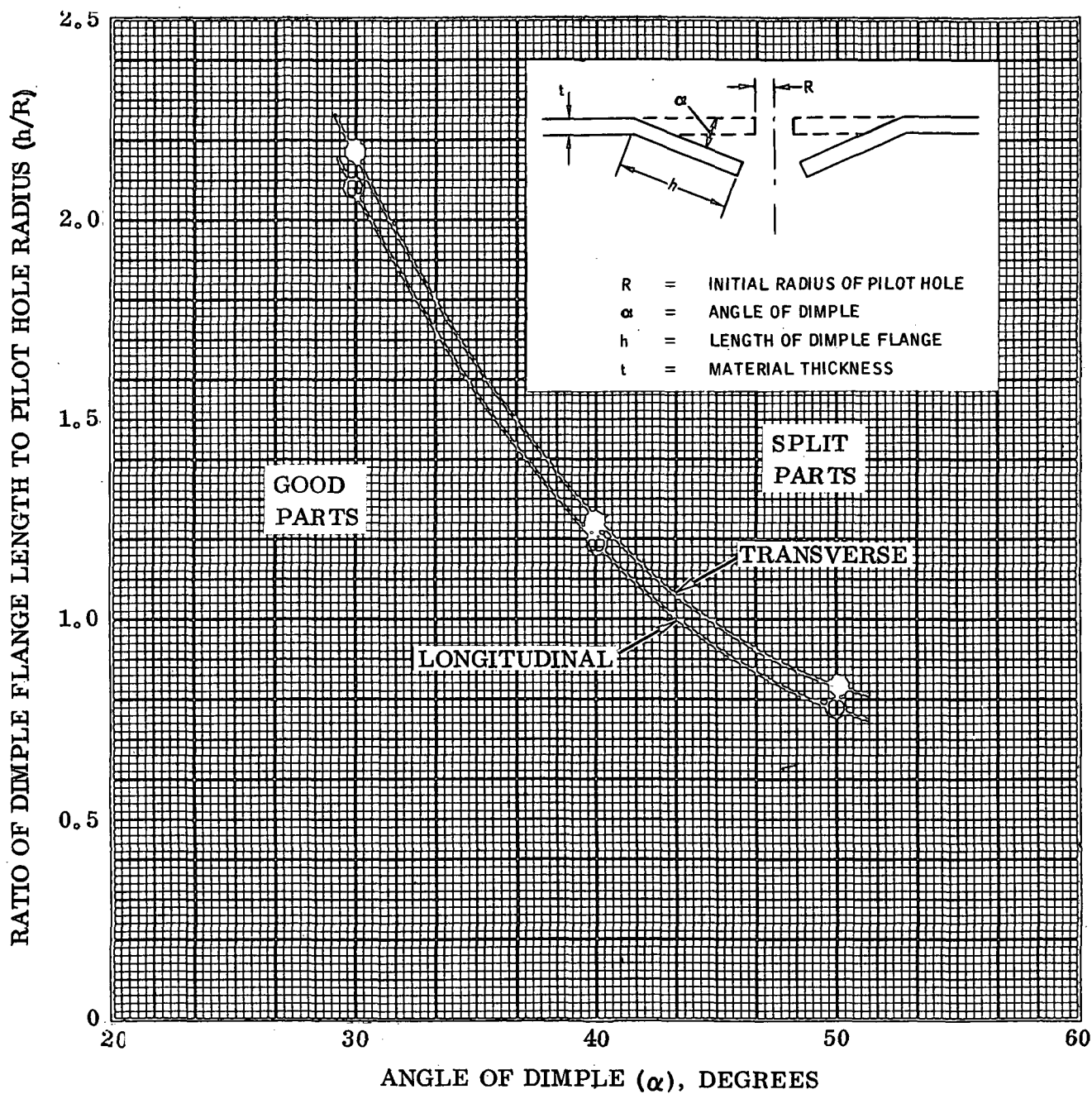


Figure 9. Theoretical Formability Curves for Dimpling of 0.5 mm (0.020 in.) Recrystallized TD-NiCr Sheet-Heat 3640 (Code B2)

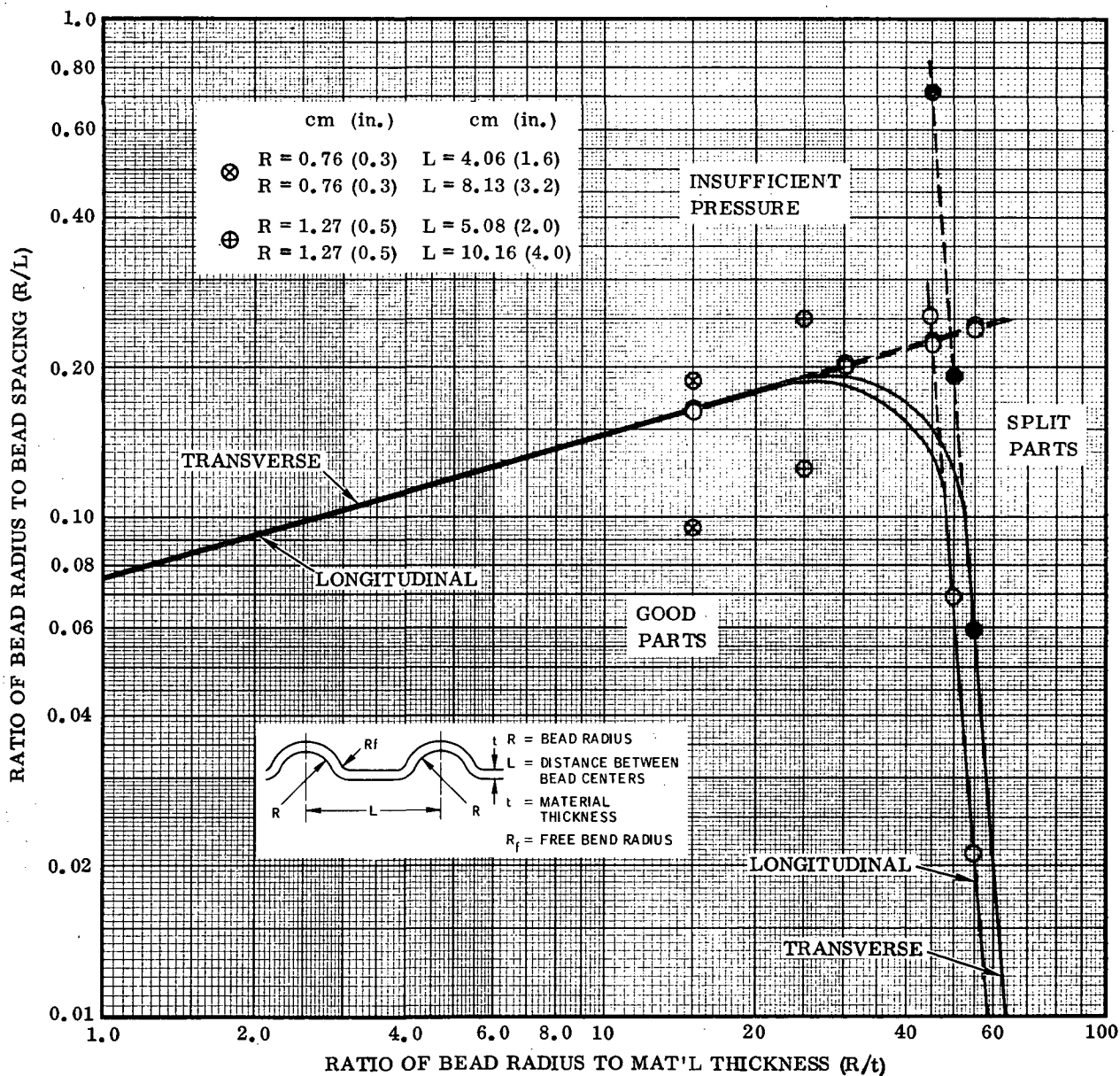


Figure 10. Theoretical Formability Curves for Rubber Press Beading of 0.5 mm (0.020 in.) Recrystallized TD-NiCr Sheet-Heat 3640 (Code B2)

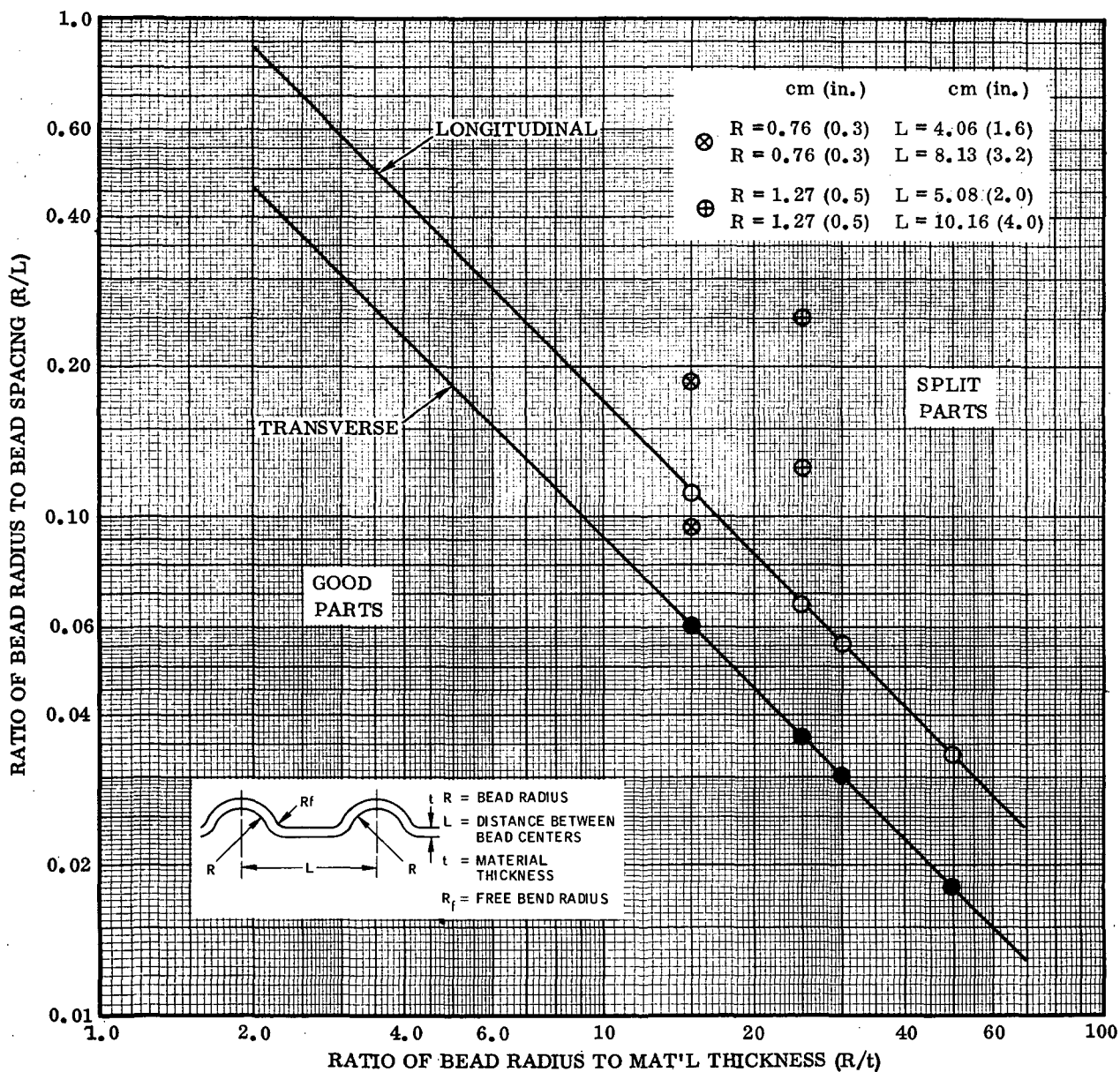


Figure 11. Theoretical Formability Curves for Drop Hammer Beading of 0.5 mm (0.020 in.) Recrystallized TD-NiCr Sheet-Heat 3640 (Code B2)

The theoretical formability data were used to help select test conditions for the forming test program to determine actual forming limits. For example, the bead configurations designated for experimental bead forming were as follows:

<u>Bead Radius, R,</u>		<u>Bead Spacing, L,</u>	
<u>cm</u>	<u>(in.)</u>	<u>cm</u>	<u>(in.)</u>
0.76	(0.3)	4.06	(1.6)
0.76	(0.3)	8.13	(3.2)
1.27	(0.5)	5.08	(2.0)
1.27	(0.5)	10.16	(4.0)

These bead sizes and spacings are considered reasonable for beaded components of thermal protection systems and hot structures for space shuttle vehicles. The calculated forming parameters for these bead configurations have been superimposed on the theoretical bead forming curves in Figures 10 and 11. The selected bead configurations appear suitable for evaluation of the formability of recrystallized TD-NiCr sheet.

Brake Forming

Brake Forming Limits. - Experimental brake forming tests were conducted with a Pneuco pneumatic 311 KN(35 ton)press brake using three types of press brake dies. The dies were:

- (a) Di Acro Rol-Form press brake die with 1.9 cm (0.75 in.) diameter rolls
- (b) Kaufman Urethane press brake die
- (c) Adjustable span air bending press brake die

Fifteen punches with radii ranging from 0.013 to 0.5 cm (0.005 to 0.2 in.) were available for use with the press brake dies. Forming tests showed that the adjustable span air bending die is the most suitable die for brake forming of TD-NiCr sheet. Sixty test blanks were brake formed to evaluate the Di Acro Rol-Form die. Results of these tests revealed that it was not possible to form small radii for 90 and 120 degree angle bends because sufficient pressure could not be applied to the work piece. The die span for the Di Acro die was not adjustable, and with the 1.9 cm (0.75 in.) diameter roller die, the span was so large that excessive radial and angular springback was obtained when punches with small radii were used.

Twenty-two brake forming tests were performed to evaluate a urethane press brake die manufactured by Kaufman Engineering Corp. The urethane die was found inadequate for the forming of the 0.5 and 1.0 mm (0.020 and 0.040 in.) TD-NiCr sheet. The small punch radii caused the urethane pad to split when sufficient pressure was applied to form the part. The advantage of an adjustable type of brake form die is that the die span can be adjusted for each test condition (bend radius and material thickness). An adjustable air bending brake die for use with the available punches was designed and fabricated. A sketch of the adjustable die is shown in Figure 12. The die span was adjusted for each test condition according to:

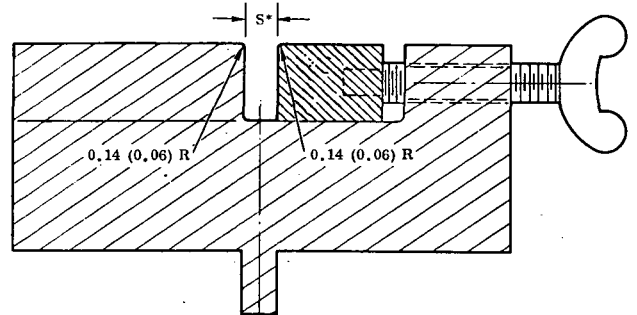
$$S = 2.55 R + 2t \quad (\text{Ref. 10})$$

where

S = Die Span

R = Punch radius

t = Material thickness



NOTE:
DIMENSIONS IN CM (IN.)

More than 200 brake forming tests with 5.1 x 10.2 cm (2 x 4 in.) blanks were conducted to establish forming limits for six heats of recrystallized TD-NiCr sheet. The forming parameters investigated included a minimum of three bend radii and three bend angles (45, 90, and 120 degrees) for two grain orientations (longitudinal and transverse), and two heats each of three sheet thicknesses, 0.25, 0.5, and 1.0 mm (0.010, 0.020, and 0.040 in.).

The actual brake forming limits are summarized in Table 6 for a 45-degree bend angle, in Table 7 for a 90-degree bend angle, and in Table 8 for a 120-degree bend angle. In addition to minimum punch radii, these tables also list the measured part radius and springback angle and provide the theoretical forming limit for comparison. The test results obtained with the Di Acro Rol-Form die and the Kaufman urethane die are not listed since these test conditions were repeated using the adjustable brake die.

Evaluation of the brake formed parts included examination for cracks at 10X to 30X magnification. The nature of the cracks and the surface condition of the material is such that in some cases relatively severe cracks cannot be seen at magnifications of less than 10X. It was necessary in some instances to examine the parts at 30X to positively identify rejectable cracks

**Table 6. Experimental Press Brake Forming Limits of Recrystallized
TD-NiCr Sheet for 45° Bend Angle**

Sheet Thickness mm (in.)	Heat Number	Grain ⁽¹⁾ Direction	Punch Radius (R/t)		Part Radius (R/t)		Springback Angle ⁽²⁾ (deg)	Theoretical Forming Limit (R/t)
			No Cracks	Cracks	No Cracks	Cracks		
0.25 (0.010)	3637 Code F2	L	3.7	3.0	3.7	3.2	9	1.5
		T	5.0	4.3	5.0	4.0	14	0.9
	3700 Code H2	L	1.0	0.5	3.0	2.0	10	1.6
		T	4.4	3.7	4.4	3.2	12	1.4
0.5 (0.020)	3629 Code A1	L	2.1	1.8	3.1	2.5	8	0.6
		T	5.5	5.0	5.5	4.7	9	0.8
	3640 Code B1	L	3.0	2.5	3.5	3.0	11	0.7
		T	5.5	5.0	5.2	4.7	12	1.0
1.0 (0.040)	3708 Code D2	L	2.5	2.2	2.9	2.7	8	0.5
		T	5.5	5.0	4.8	4.3	10	0.7
	3715 Code E2	L	0.9	0.8	1.4	1.2	10	0.4
		T	5.5	5.0	4.7	4.3	12	0.6

(1) L = Direction of bend (strain) parallel to rolling direction.

T = Direction of bend (strain) normal to rolling direction.

(2) Total overbend required to give a 45° bend angle.

**Table 7. Experimental Press Brake Forming Limits of Recrystallized
TD-NiCr Sheet for 90° Bend Angle**

Sheet Thickness mm (in.)	Heat Number	Grain ⁽¹⁾ Direction	Punch Radius (R/t)		Part Radius (R/t)		Springback Angle ⁽²⁾ (deg)	Theoretical Forming Limit (R/t)
			No Cracks	Cracks	No Cracks	Cracks		
0.25 (0.010)	3637	L	5.0	4.4	4.0	3.0	12	3.4
	Code F2	T	5.0	4.7	4.0	3.5	13	2.3
	3700	L	2.0	1.5	2.0	1.7	12	3.5
	Code H2	T	5.5	5.0	5.5	4.0	14	3.2
0.5 (0.020)	3629	L	2.6	2.1	2.2	2.1	8	1.7
	Code A1	T	5.5	5.0	5.5	4.0	13	1.9
	3640	L	4.0	3.5	4.0	3.4	10	1.8
	Code B1	T	5.5	5.0	4.7	4.0	11	2.5
1.0 (0.040)	3708	L	2.5	2.2	2.5	1.8	11	1.4
	Code D2	T	6.0	5.5	5.0	4.3	12	1.8
	3715	L	1.5	1.2	1.2	1.0	11	1.2
	Code E2	T	6.0	5.5	5.0	4.3	14	1.6

(1) L = Direction of bend (strain) parallel to rolling direction.

T = Direction of bend (strain) normal to rolling direction.

(2) Total overbend required to give a 90° bend angle.

Table 8. Experimental Press Brake Forming Limits of Recrystallized TD-NiCr Sheet for 120° Bend Angle

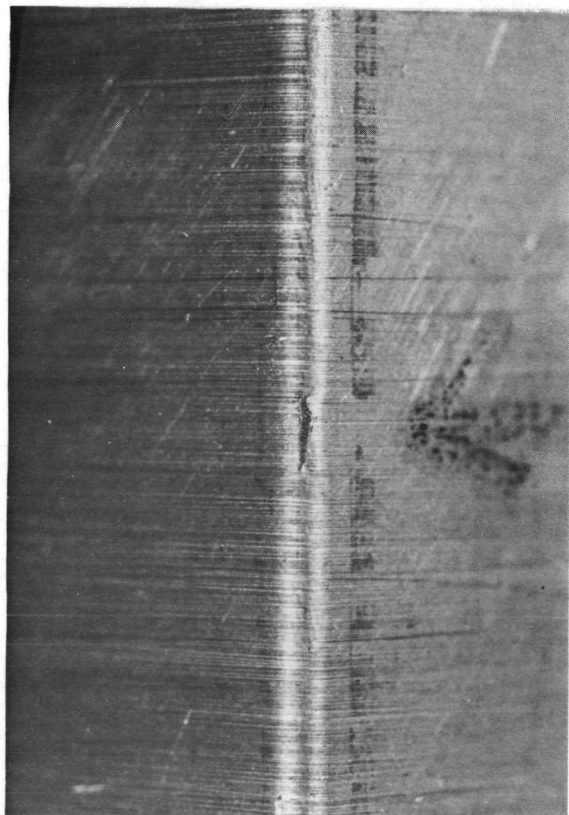
Sheet Thickness mm (in.)	Heat Number	Grain Direction	Punch Radius (R/t)		Part Radius (R/t)		Springback Angle ⁽¹⁾ (deg)	Theoretical Forming Limit (R/t)
			No Cracks	Cracks	No Cracks	Cracks		
0.25 (0.010)	3637 Code F2	L	5.0	4.3	4.5	3.2	14	3.5
		T	5.0	4.3	4.5	3.2	14	2.5
	3700 Code H2	L	2.5	2.0	3.0	1.8	13	3.5
		T	5.5	5.0	5.0	(2)	16	3.4
0.5 (0.020)	3629 Code A1	L	3.0	2.5	2.7	2.0	11	1.8
		T	6.5	6.0	6.5	5.5	14	2.1
	3640 Code B1	L	4.0	3.5	3.5	3.1	13	2.0
		T	5.5	5.0	5.2	4.5	14	2.6
1.0 (0.040)	3708 Code D2	L	3.0	2.5	2.7	2.2	11	1.6
		T	6.0	5.5	5.1	4.3	14	2.0
	3715 Code E2	L	2.2	1.7	2.0	1.5	10	1.4
		T	6.0	5.5	4.3	4.3	14	1.8

(1) Total overbend required to give a 120° bend angle.

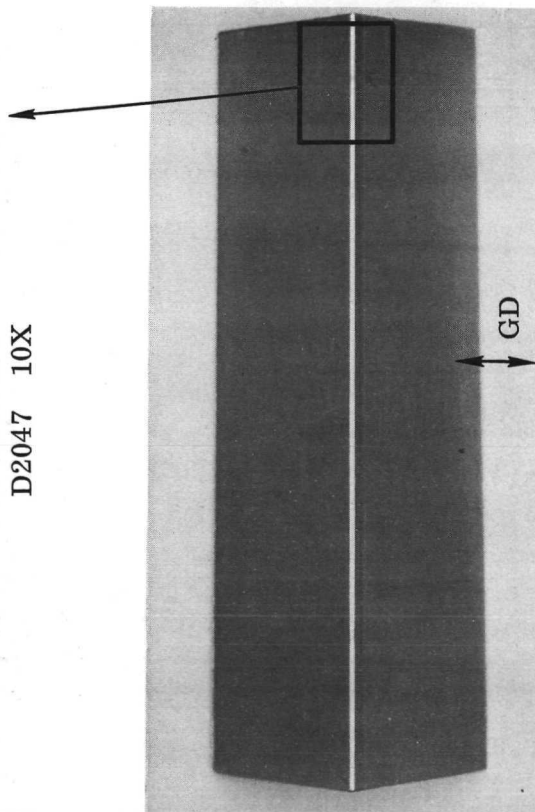
(2) Not measurable due to complete rupture.

after an initial examination at 10X magnification. Figure 13 shows typical small cracks in brake formed parts of 0.25 mm (0.010 in.) sheet and Figure 14 shows typical cracks in 1.0 mm (0.040 in.) sheet. Representative parts with and without cracks were examined metallographically. Typical surface cracks and associated deformation bands are shown in Figure 15 for 0.25 mm (0.010 in.) parts.

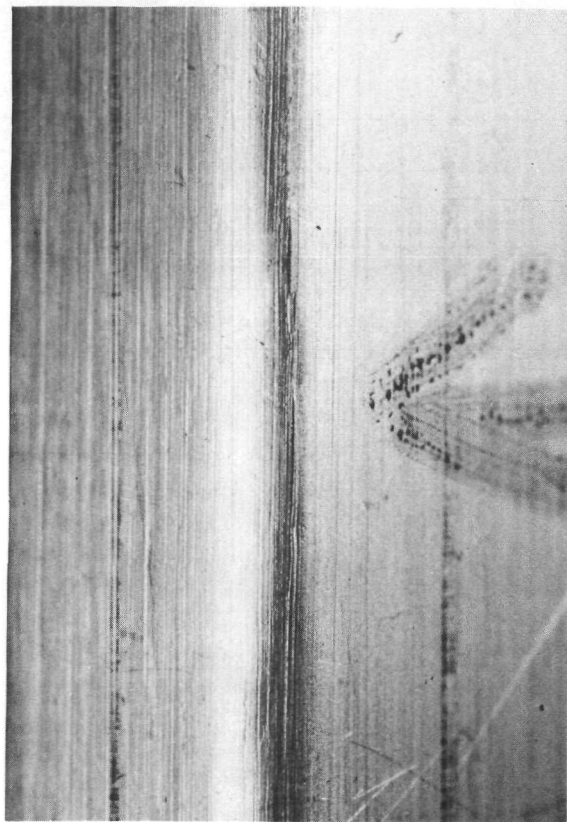
Dye penetrant inspection and metallographic examination were performed on selected parts to confirm results of visual examination. Specimens were re-examined for delayed cracking a minimum of five days after brake forming. No evidence of delayed cracking was observed.



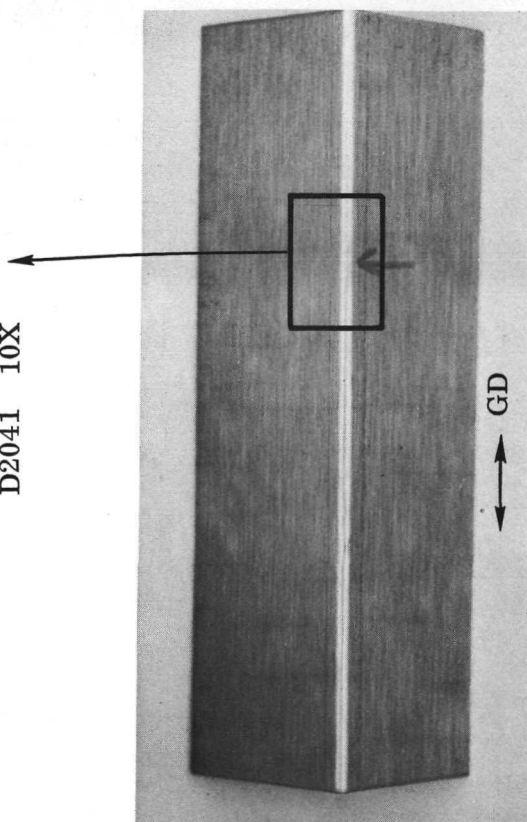
D2047 10X



D2046 Spec. H2L-33 1X

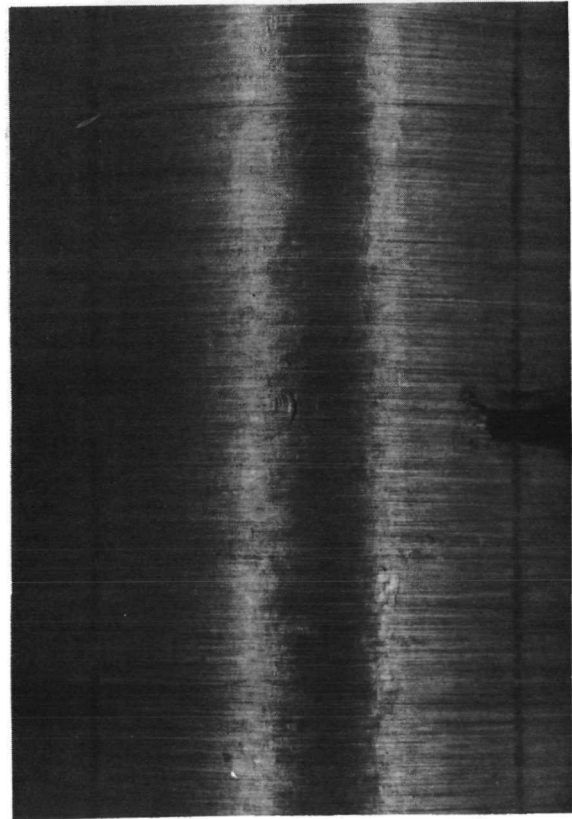


D2041 10X

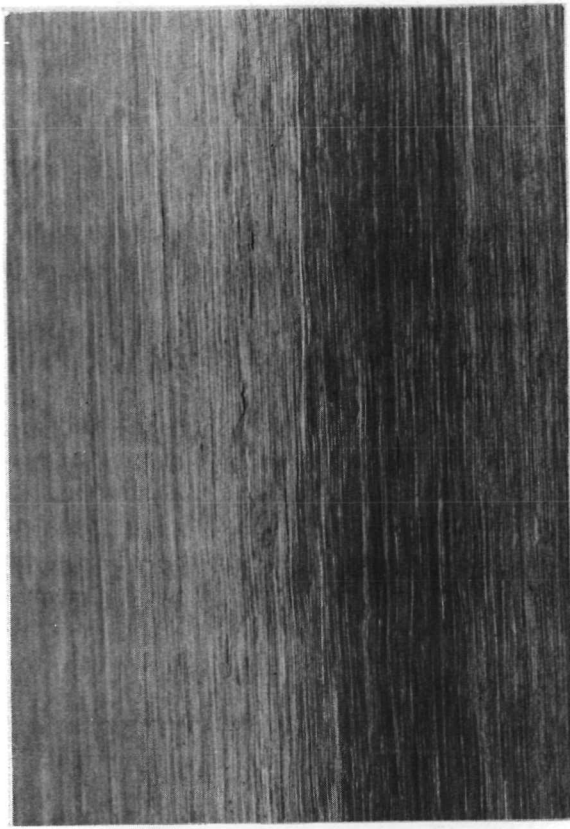


D2040 Spec. H2T-25 1X

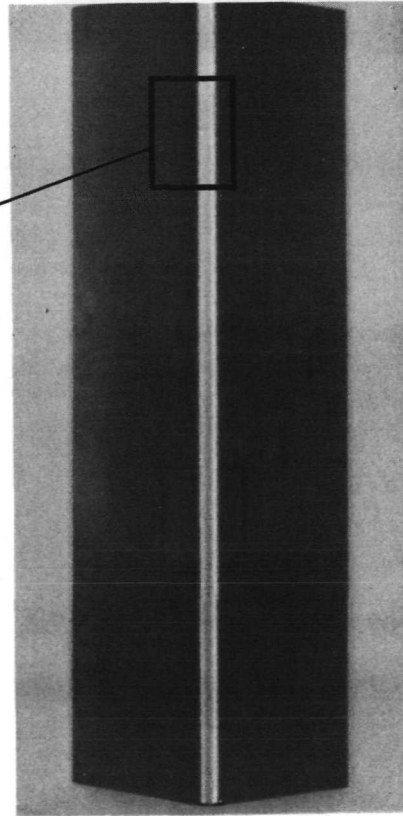
Figure 13. Brake Formed Parts of 0.25 mm (0.010 in.) Recrystallized TD-NiCr Sheet (Heat 3700) Showing Typical Small Cracks Parallel and Transverse to the Rolling Direction - Cold Rolled Surface Finish



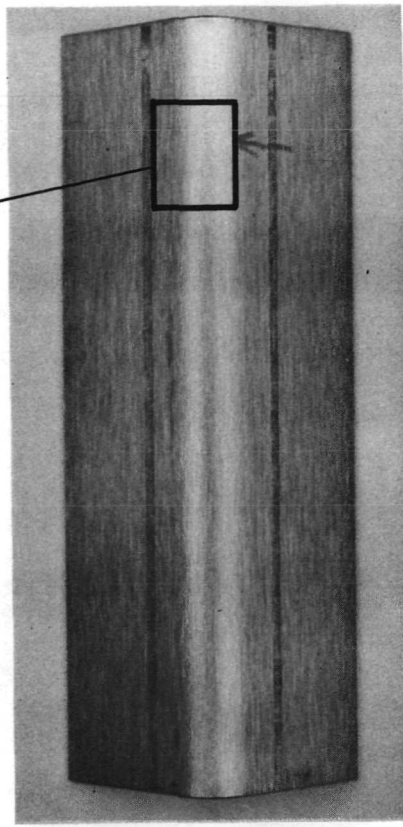
D2049 10X



D2043 10X

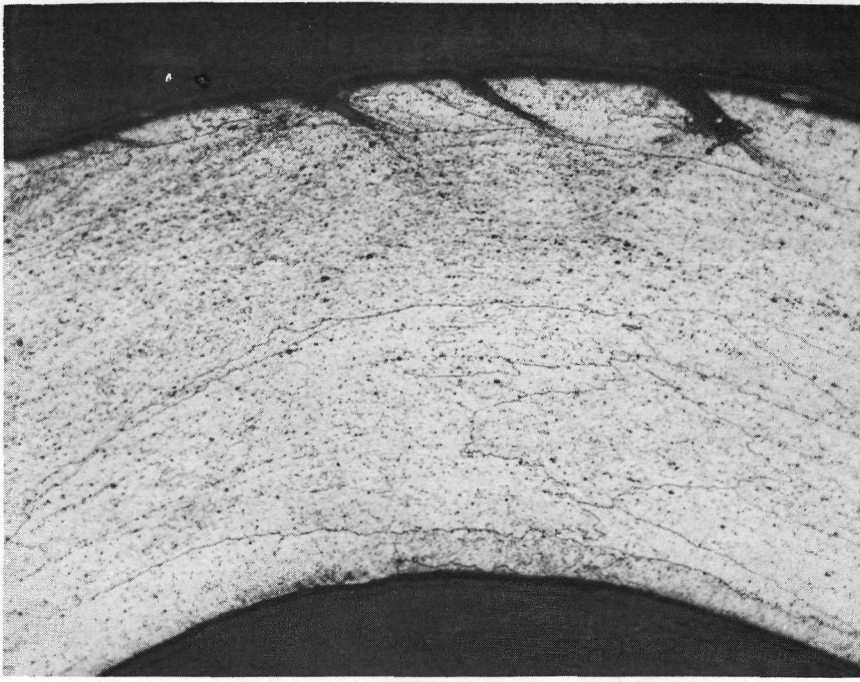


D2048 Spec. E2L-26 1X



D2042 Spec. E2T-16 1X

Figure 14. Brake Formed Parts of 1.0 mm (0.040 in.) Recrystallized TD-NiCr Sheet (Heat 3715) Showing Typical Small Cracks Parallel and Transverse to the Rolling Direction - Belt Polished Surface Finish



As-formed

Neg. D1858

250X



As-formed

Neg. D1856

40X

Figure 15. Typical Surface Cracks and Deformation Bands in Brake Formed 0.25 mm (0.010 in.) Recrystallized TD-NiCr Sheet- (Heat 3637, Specimen F2L-12, longitudinal orientation, 120° bend angle)

Comparison of predicted and actual forming limits for press brake forming is shown in Figures 16 through 21. Several observations can be made from these comparisons:

- (a) Actual forming limits show better formability in the longitudinal direction than in the transverse direction for all heats except Heat 3637, where the limits are approximately the same for both directions.
- (b) Actual forming limits show poorer formability than the predicted limits. The differences are greater for transverse than for longitudinal bends and greater for a bend angle of 45 degrees than for 90 and 120 degree bend angles.
- (c) The high strain values transverse to the rolling direction for TD-NiCr do not have the same relationship to formability as do the strain values in the longitudinal direction. This condition is attributed to the mode of crack initiation and propagation characteristic of dispersion-strengthened alloys and is also influenced by the belt polished surface condition.
- (d) The theoretical formability equations developed by Wood et al are not valid for predicting forming limits of TD-NiCr particularly for the transverse direction and bend angles less than 90 degrees.

Effect of Die Span. - Brake forming tests were conducted to establish the effect of die span on the minimum bend radius (MBR) for a 90-degree bend angle in 0.5 mm (0.020 in.) material for both the longitudinal and transverse orientations. Three different die spans were investigated using 5.1 by 10.2 cm (2 by 4 in.) wide blanks from Heat 3640. The three die spans were calculated from the following equations:

$$S = 2.55R + 2t \text{ (standard used for previous tests)}$$

$$S = 3.0R + 2t$$

$$S = 4.0R + 2t$$

where

S = die span

R = punch radius

t = material thickness

The span of the brake forming die was adjusted for each test condition in accordance with calculated values.

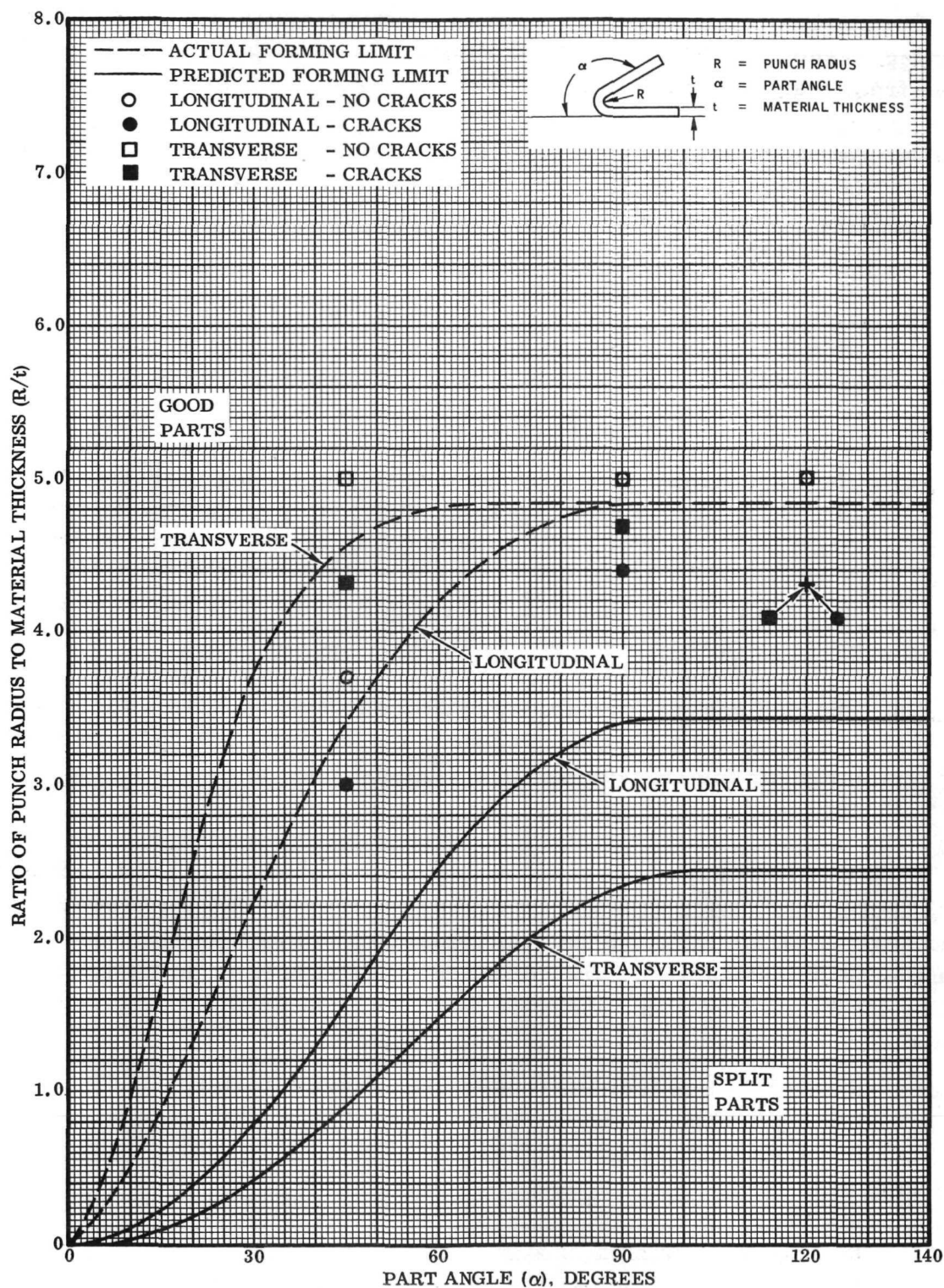


Figure 16. Theoretical and Actual Brake Forming Limit Curves for 0.25 mm (0.010 in.) Recrystallized TD-NiCr Sheet - Heat 3637 (Code F2)

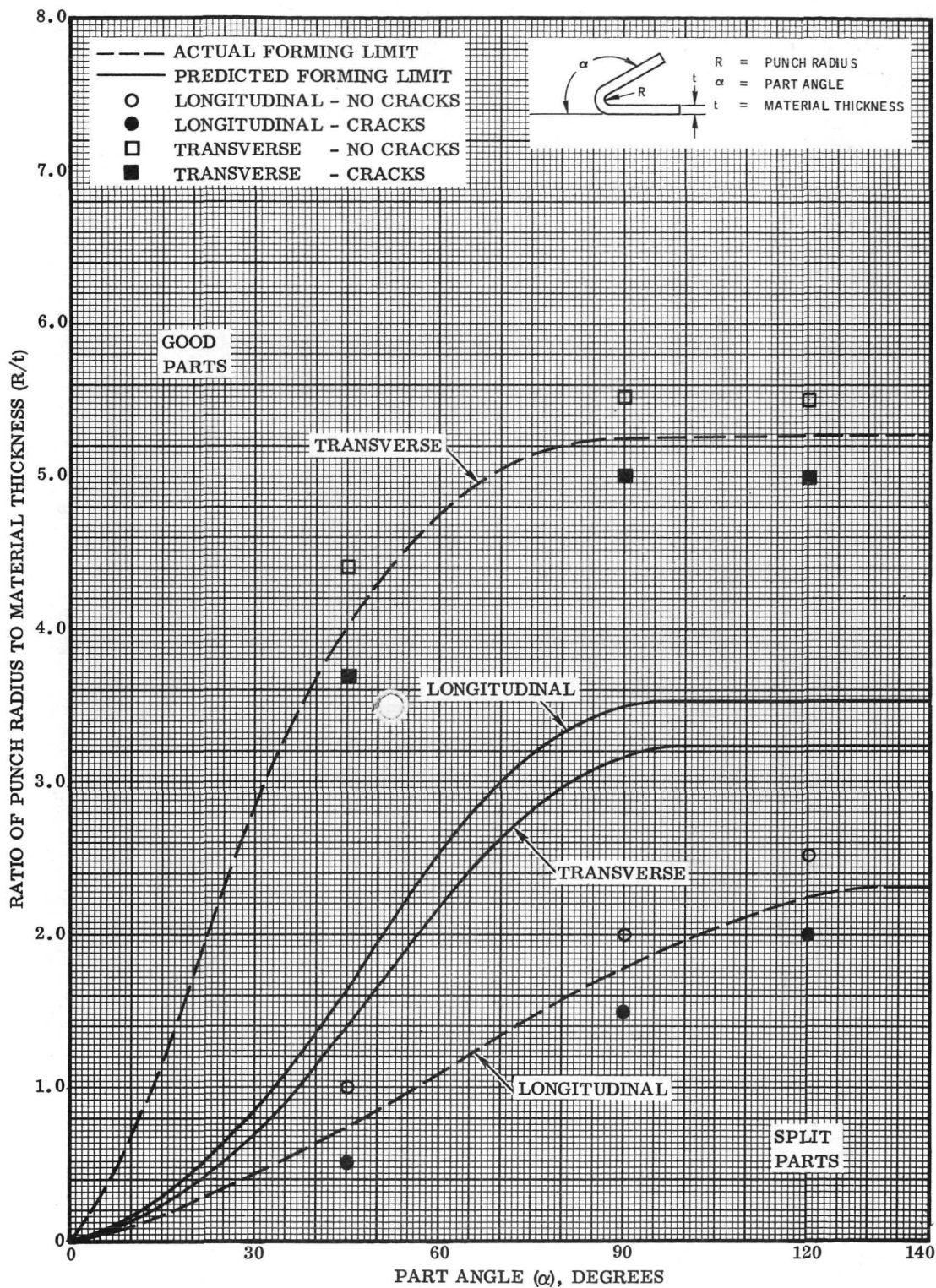


Figure 17. Theoretical and Actual Brake Forming Limit Curves for 0.25 mm (0.010 in.) Recrystallized TD-NiCr Sheet - Heat 3700 (Code H1)

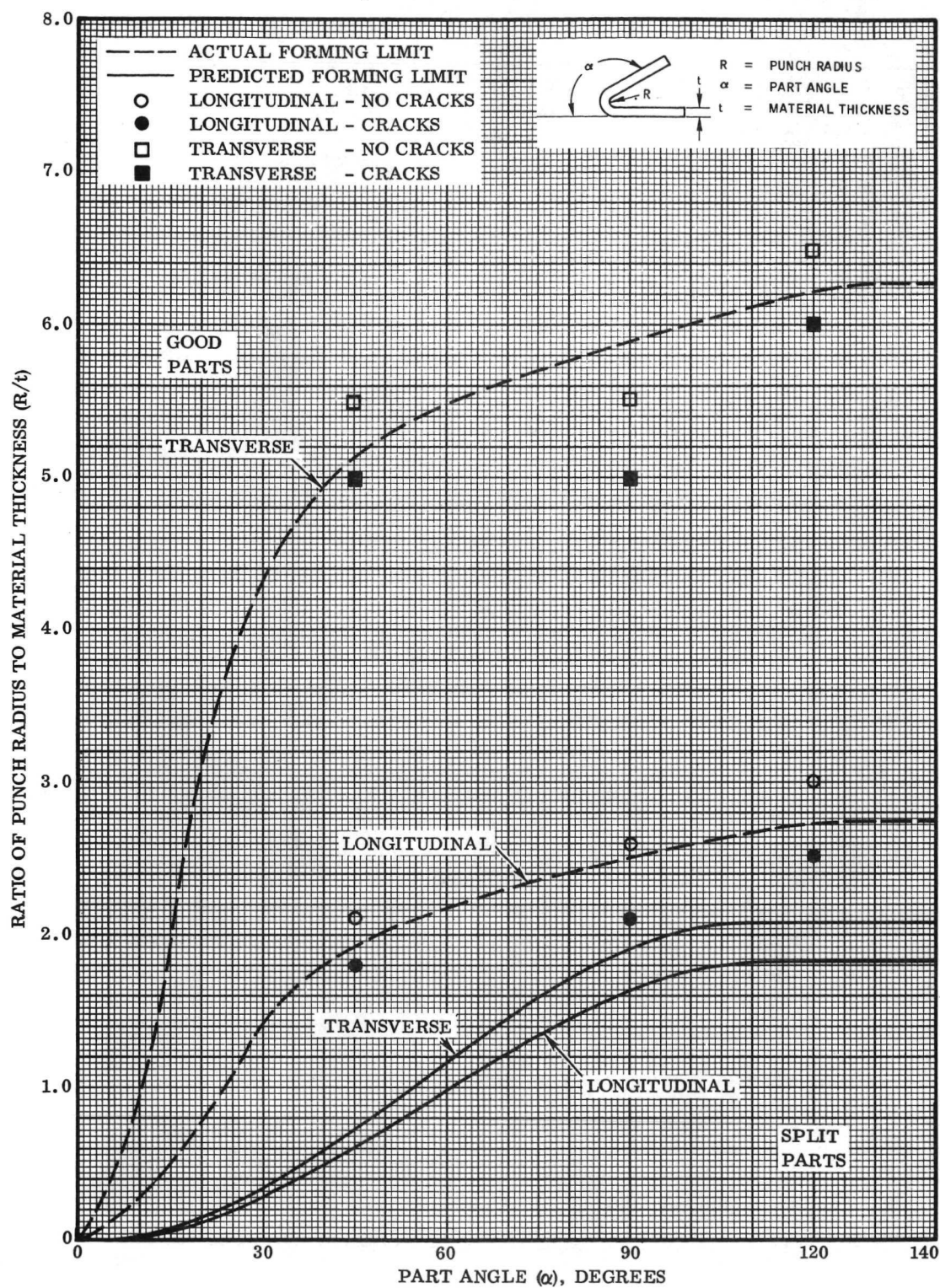


Figure 18. Theoretical and Actual Brake Forming Limit Curves for 0.5 mm (0.020 in.) Recrystallized TD-NiCr Sheet - Heat 3629 (Code A1)

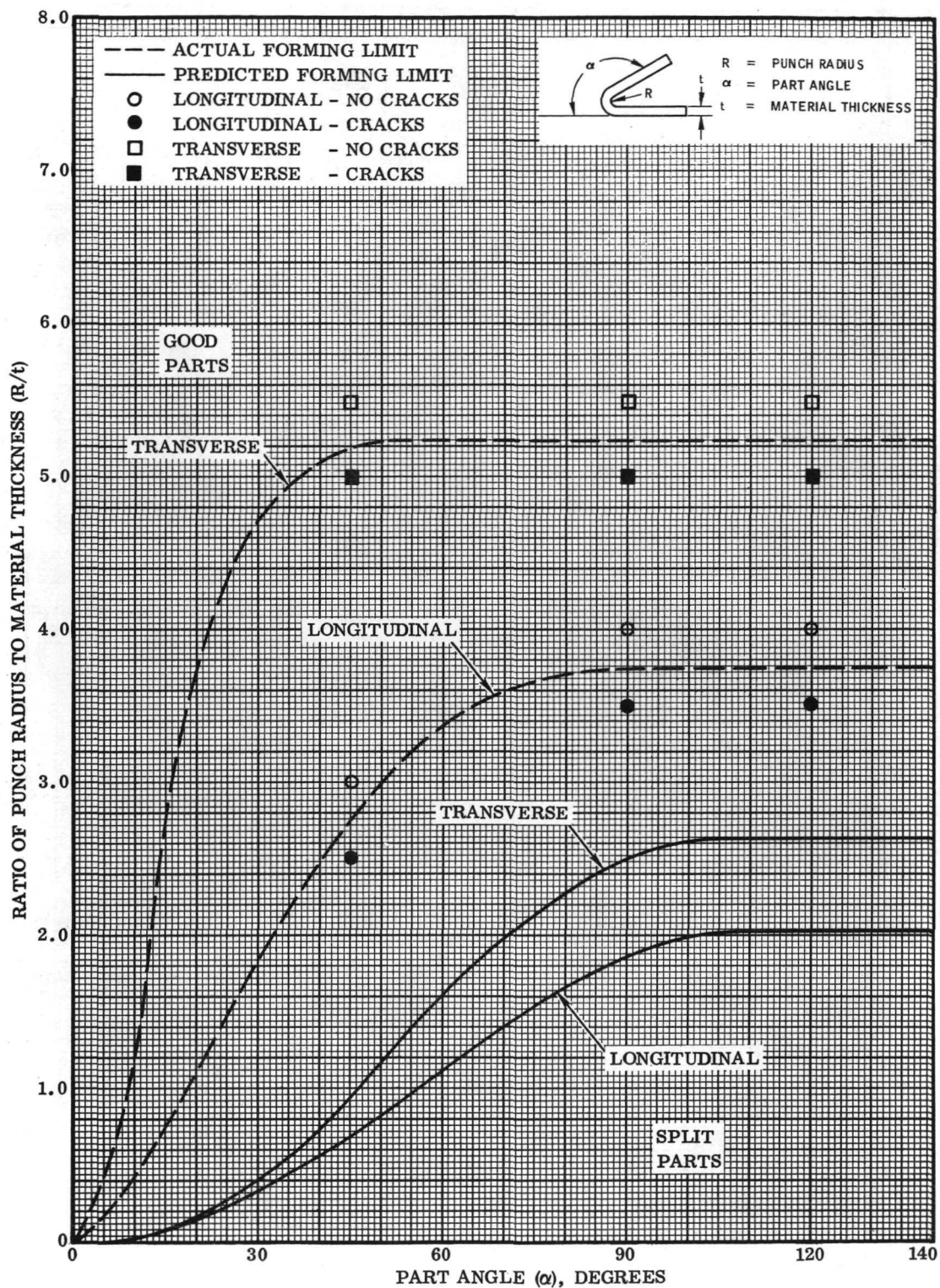


Figure 19. Theoretical and Actual Brake Forming Limit Curves for 0.5 mm (0.020 in.) Recrystallized TD-NiCr Sheet - Heat 3640 (Code B1)

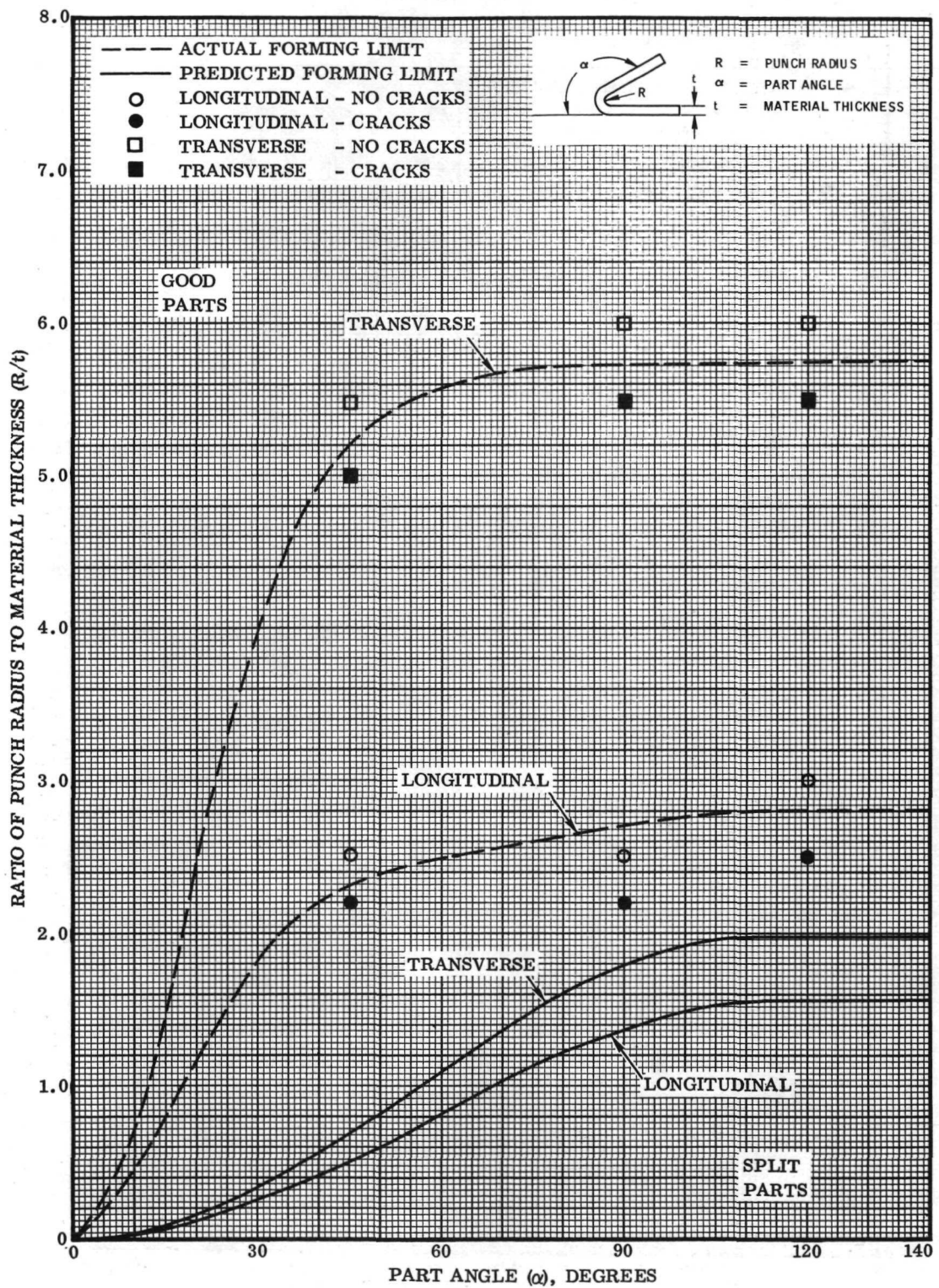


Figure 20. Theoretical and Actual Brake Forming Limit Curves for 1.0 mm (0.040 in.) Recrystallized TD-NiCr Sheet - Heat 3708 (Code D2)

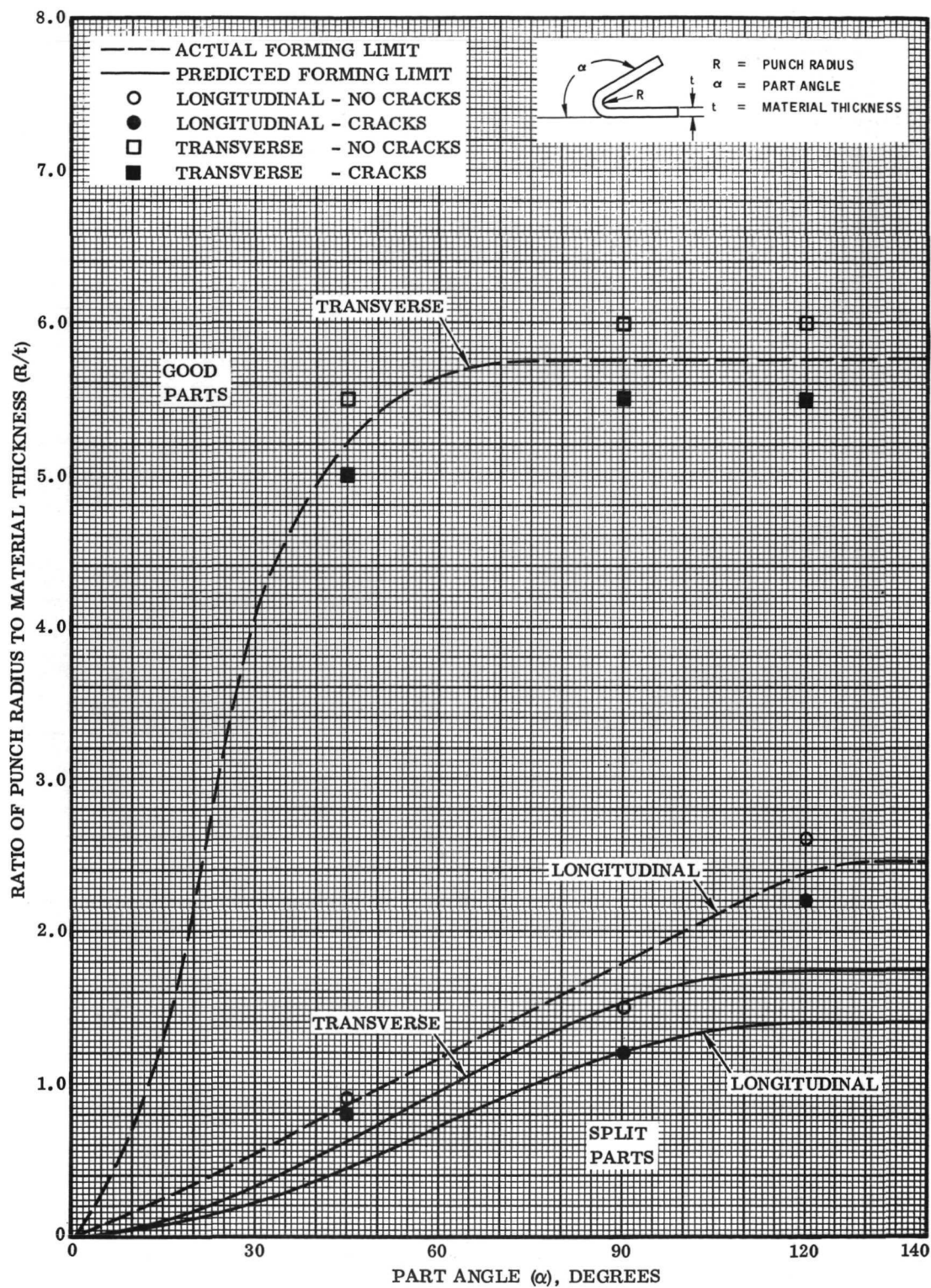


Figure 21. Theoretical and Actual Brake Forming Limit Curves for 1.0 mm (0.040 in.) Recrystallized TD-NiCr Sheet - Heat 3715 (Code E2)

The results of the die span studies are presented in Table 9. The brake forming tests were conducted on a different sheet of material (Code B6) from Heat 3640 than that used for the forming limit tests (Code B1). The latter tests from Table 7 are listed in Table 9 for comparison. These data show a considerable variation in MBR between the two sheets from the same heat.

Table 9. Effect of Die Span on Actual Brake Forming Limits of
0.5 mm (0.020 in.) Recrystallized TD-NiCr for 90°
Bend Angle

Heat Number	Grain Direction ⁽²⁾	Die Span	Ratio of Punch Radius to Material Thickness (R/t)		Ratio of Part Radius to Material Thickness (R/t)		Springback Angle ⁽³⁾ (degrees)
			No Cracks	Cracks	No Cracks	Cracks	
3640 Code B6	L	2.55R + 2t	2.5	2.2	1.9	2.0	10
		3.0R + 2t	2.5	2.2	1.8	1.6	11
		4.0R + 2t	2.2	1.8	1.6	1.6	10
	T	2.55R + 2t	5.0	4.5	4.8	3.9	10
		3.0R + 2t	4.5	4.0	4.2	3.9	10
		4.0R + 2T	4.0	3.5	4.2	3.4	10
3640 Code B1 (1)	L	2.55R + 2t	4.0	3.5	4.0	3.4	10
	T	2.55R + 2t	5.5	5.0	4.7	4.0	11

(1) From Table 7

(2) L = Direction of bend (strain) parallel to rolling direction.

T = Direction of bend (strain) normal to rolling direction.

(3) Total overbend required to give a 90-degree bend angle.

The forming limit (minimum bend radius) is plotted versus the die span in Figure 22. These data show that the MBR decreases (better formability) with increasing die span for the range of die span investigated. Further work is required to determine the optimum die span for TD-NiCr sheet; i. e., the die span for maximum formability (lowest MBR). However, this work is not within the scope of the present program. The use of a die span of $S = 2.55R + 2t$ was used for the studies even though it is recognized that a larger die span would provide a lower MBR.

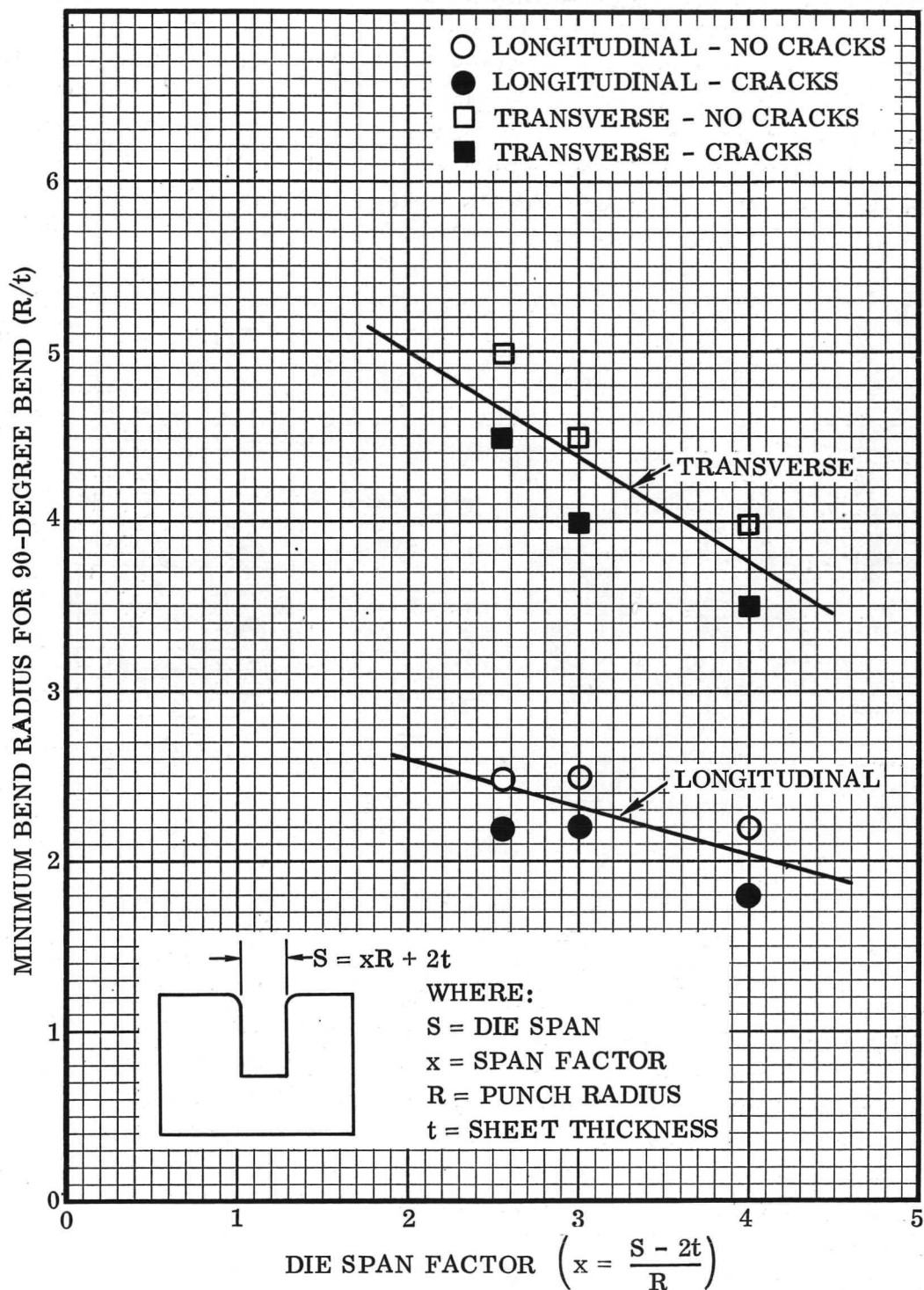


Figure 22. Effect of Die Span on Actual Brake Forming Limits of 0.5 mm (0.020 in.) Recrystallized TD-NiCr Sheet - Heat 3640 (Code B6)

Effect of Part Width. - Brake forming tests were conducted to establish the effect of sheet width on the minimum bend radius of one heat each of 0.25, 0.5, and 1.0 mm (0.010, 0.020, and 0.040 in.) TD-NiCr sheet in both the longitudinal and transverse directions. The tests were conducted with 5.1 by 45.7 cm (2 by 18 in.) wide test blanks, which were brake formed to a 90-degree angle using the same die span ($S = 2.55R + 2t$) that was used for the 10.2 cm (4 in.) part width test program. Results of these tests are summarized in Table 10 and compared with the previous forming limit data for 10.2 cm (4 in.) part width.

Table 10. Effect of Part Width on Experimental Press Brake Forming Limits of Recrystallized TD-NiCr for 90-Degree Bend Angle

Sheet Thickness mm (in.)	Heat Number	Grain Direction (1)	Actual Forming Limits for 45.7 cm (18 in.) Part Width					Comparison With 10.2 cm (4 in.) Part Width		
			Ratio of Punch Radius to Material Thickness (R/t)		Ratio of Part Radius to Material Thickness (R/t)		Springback Angle (2) (degrees)	Sheet Identification (3)	Actual Forming Limits (R/t)	Theoretical Forming Limit (R/t)
			No Cracks	Cracks	No Cracks	Cracks				
0.25 (0.010)	3700 Code H4	L	4.0	3.0	3.2	2.0	14	Code H2	2.0	3.5
		T	8.0	7.0	8.5	6.8	20	Code H2	5.5	3.2
0.5 (0.020)	3640 Code B6	L	2.5	2.0	1.9	1.5	11	Code B1	4.0	1.8
								Code B6(4)	2.5	
		T	5.0	4.5	4.7	3.9	11	Code B1	5.5	2.5
								Code B6(4)	5.0	
1.0 (0.040)	3715 Code E1	L	2.0	1.5	2.0	1.3	11	Code E2	1.5	1.2
		T	6.0	5.5	5.1	4.5	10	Code E2	6.0	1.6

(1) L = Direction of bend (strain) parallel to rolling direction.

(3) Data from Table 7 except as noted.

T = Direction of bend (strain) normal to rolling direction.

(4) Data from Table 9.

(2) Total overbend required to give a 90° bend angle.

Since there was insufficient material remaining from the same sheet used for the 10.2 cm (4 in.) wide bend tests, a different sheet from the same heat was used for the width effect studies. The large variation in minimum bend radius from sheet to sheet in the same heat has a tendency to overshadow the effects of sheet width on forming limits. However, bend test results for 10.2 cm (4 in.) wide blanks of the same sheet of 0.5 mm (0.020 in.) material are available from the die span studies. These data (also listed in Table 10) are more conclusive in showing that part width in the 10.2 cm (4 in.) to 45.7 cm (18 in.) range has no significant effect on forming limits.

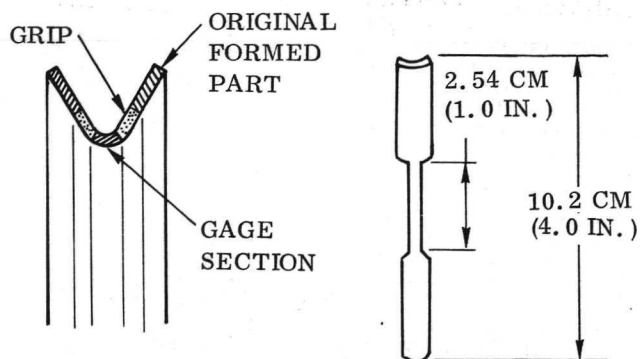


Figure 23. Specimen Configuration for Tensile Testing of Formed Parts

consisted of applying 0.05 cm (0.02 in.) photo grids on the tension side of the forming blank. The sheet thickness was measured prior to forming. The test section width was measured after machining by counting the number (and fractions) of grid lines with the aid of a microscope. However, this method proved insufficiently accurate and gave consistently low cross-section area values and unrealistically high strengths compared to parent metal properties. A second measurement method was found to give improved accuracy. This method consisted of measurements of thickness, radius, and chord length of machined specimens and calculation of cross-section area assuming it is a segment of two concentric circles. All data in this report on tensile specimens machined from formed parts were generated using the direct measurement method.

It was initially planned to prepare tensile specimens from the brake formed parts using conventional machining techniques. However, difficulties were encountered in achieving the required dimensional tolerances in the gage section due to pressure of the milling cutter. For this reason, the specimens were electrical discharge machined (EDM). The edges in the gage section were hand finished with a polishing stone to remove the heat-affected surface layer that resulted from the EDM operation. Table 11 shows tensile test results for specimens machined from the radius portion of brake formed parts in the as-formed condition. The formed parts represent two sheet thicknesses [0.5 and 1.0 mm (0.020 and 0.040 in.)], two grain directions (L and T), two bend angles (45° and 90°), and one bend radius (minimum bend radius). These data are summarized and compared with parent material properties in Table 12. The results indicate significant strain hardening has resulted from the brake forming operation. The more severe the forming (larger bend angle or smaller bend radius), the greater the amount of strain hardening (higher strength and lower ductility).

Tensile Properties of Formed Parts. - The specimen configuration used to determine the tensile strength and ductility of the radius portion of brake formed parts is shown in Figure 23. The specimen was machined to obtain the maximum amount of strained metal in the cross-section area. The principal problem with any irregular shaped tensile specimen is accurate measurement of area. The first method used in these tests

Table 11. Test Results for Tensile Specimens Machined from Radius Portion of Brake Formed Parts of Recrystallized TD-NiCr Sheet

Heat Number	Sheet Thickness mm (in.)	Grain (1) Direction	Bend Angle degrees	Part Radius cm (in.)	Specimen Number	Cross-section Area cm ² (in. ²)	Ultimate Tensile Strength MN/m ² (ksi)	Tensile Yield Strength MN/m ² (ksi)	Elongation % in 2.54 cm (1.0 in.)
3640 Code B2	0.5 (0.020)	T	45	0.35 (0.14) ⁽²⁾	B2L-7	0.0110 (0.00171)	886 (128.5)	728 (105.6)	7
					B2L-8	0.0128 (0.00198)	885 (128.4)	724 (105.0)	10
					B2L-9	0.096 (0.00149)	895 (129.8)	741 (107.5)	9
			Average		889 (128.9)	731 (106.0)	8.7		
			90	B2L-10	0.0113 (0.00175)	946 (137.2)	863 (125.2)	3	
				B2L-11	0.0110 (0.00171)	958 (139.0)	895 (129.8)	2	
		B2L-12		0.0109 (0.00169)	931 (135.0)	854 (123.8)	3		
		Average		945 (137.1)	871 (126.3)	2.7			
		L	45	0.28 (0.11)	B2T-8	0.0134 (0.00208)	934 (135.5)	670 (97.2)	10
					B2T-9	0.0084 (0.00130)	971 (140.8)	700 (101.5)	7
					Average		952 (138.1)	685 (99.3)	8.5
			90	0.33 (0.13)	B2T-11	0.0130 (0.00201)	925 (134.2)	717 (104.0)	7
B2T-12	0.0160 (0.00180)				900 (130.5)	683 (99.0)	7		
B2T-13	0.0108 (0.00167)				908 (131.7)	676 (98.0)	5		
Average		911 (132.1)	692 (100.3)	6.3					
3715 Code E1	1.0 (0.040)	T	45	0.23 (0.09)	E1L-1	0.0215 (0.00334)	913 (132.4)	790 (114.6)	7
					E1L-2	0.0219 (0.00340)	960 (139.2)	855 (124.0)	7
					E1L-3	0.0230 (0.00357)	886 (128.5)	769 (111.5)	7
					Average		920 (133.4)	805 (116.7)	7
			90	0.20 (0.08)	E1L-4	0.0175 (0.00271)	1044 (151.5)	932 (135.2)	3
					E1L-5	0.0177 (0.00274)	1008 (146.2)	945 (137.1)	2
					E1L-6	0.0166 (0.00258)	1014 (147.0)	952 (138.0)	4
					E1L-7	0.0171 (0.00265)	980 (142.2)	941 (136.5)	3
					Average		1011 (146.7)	949 (137.6)	3
		L	45	0.46 (0.18)	E1T-1	0.0199 (0.00308)	862 (125.0)	705 (102.2)	9
					E1T-2	0.0257 (0.00399)	876 (127.0)	681 (98.8)	9
					E1T-3	0.0221 (0.00343)	865 (125.5)	698 (101.2)	8
					Average		867 (125.8)	695 (100.8)	8.7
			90	0.58 (0.23)	E1T-4	0.0166 (0.00257)	873 (126.6)	684 (99.2)	6
		E1T-5			0.0177 (0.00275)	870 (126.2)	745 (108.0)	6	
		E1T-6			0.0165 (0.00255)	876 (127.0)	712 (103.2)	7.5	
		Average			875 (126.9)	714 (103.5)	6.5		

(1) L = Tension axis parallel to rolling direction, T = Tension axis normal to rolling direction.

(2) Inadvertently formed to 0.35 cm (0.14 in.) radius instead of 0.18 cm (0.07 in.) radius (MBR).

Table 12. Summary of Effect of Brake Forming on Tensile Properties of Recrystallized TD-NiCr Sheet

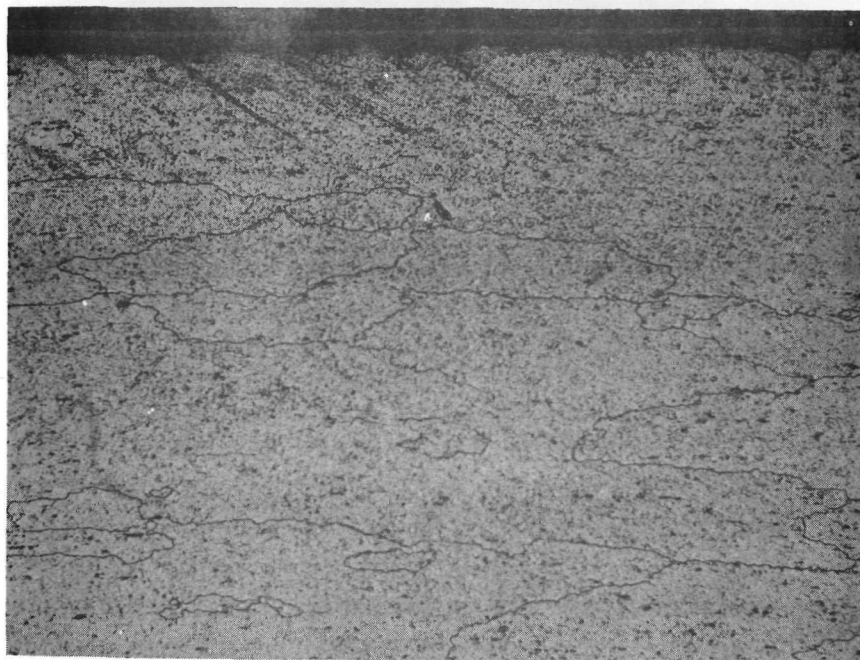
Heat No.	Sheet Thickness mm (in.)	Grain Direction(1)	Bend Angle (degrees)	Part Radius cm (in.)	Ultimate Tensile Strength MN/m ² (ksi)	Tensile Yield Strength MN/m ² (ksi)	Elongation % in 2.54 cm (1.0 in.)
3640 Code B2	0.5 (0.020)	T	45	0.35 (0.14)	889 (128.9)	731 (106.0)	8.7
			90	0.18 (0.07)	945 (137.1)	871 (126.3)	2.7
			parent metal	- -	837 (121.4)	546 (79.2)	21
		L	45	0.28 (0.11)	952 (138.1)	685 (99.3)	8.5
			90	0.33 (0.13)	911 (132.1)	692 (100.3)	6.3
			parent metal	- -	889 (129.0)	579 (84.0)	18
3715 Code E1	1.0 (0.040)	T	45	0.23 (0.09)	920 (133.4)	805 (116.7)	7
			90	0.20 (0.08)	1011 (146.7)	949 (137.6)	3
			parent metal	- -	801 (116.2)	537 (77.9)	26.5
		L	45	0.46 (0.18)	867 (125.8)	695 (100.8)	8.7
			90	0.58 (0.23)	875 (126.9)	714 (103.5)	6.5
			parent metal	- -	868 (125.9)	608 (88.2)	19.5

(1) L = Tension axis parallel to rolling direction, T = Tension axis normal to rolling direction.

Effect of Annealing. - Three annealing temperatures, 982, 1093, and 1177 C (1800, 2000, and 2150 F), were selected to investigate the effects of post-forming annealing on microstructure and tensile properties of brake formed parts.

Figures 24 and 25 show the microstructure of the radius portion of brake formed parts of 1.0 mm (0.040 in.) sheet for four conditions: as-formed, annealed at 982 C (1800 F), annealed at 1093 C (2000 F), and annealed at 1177 C (2150 F). The annealing treatments were for 2 hours in dry hydrogen. The as-formed microstructure shows the presence of deformation bands on the tension side of the bend. The annealed parts do not show deformation bands or fine grain recrystallization for any of the three annealing temperatures. The microstructure of parts annealed at 982 C (1800 F) and 1093 C (2000 F) appear identical. The 1177 C (2150 F) annealed microstructure contains an etch resistant layer at the tension side of the bend. This layer, which is 0.05 mm (0.002 in.) to 0.08 mm (0.003 in.) thick, is a chromium depleted zone caused by the high temperature annealing treatment. The chromium depletion is related to high residual stresses and does not occur at the compression side of the bend nor in the nondeformed metal adjacent to the bend. The presence of deformation bands in the as-formed microstructure and chromium depleted layer in the 1177 C (2150 F) annealed microstructure was also typical for brake formed parts of 0.25 mm (0.010 in.) and 0.5 mm (0.020 in.) sheet. Microstructural examination revealed no significant differences related to longitudinal and transverse grain orientation for as-formed or annealed parts.

Microhardness measurements showed 343 KHN for the as-formed condition and 300 to 305 KHN for the annealed conditions. The etch-resistant zone had equivalent hardness to the etched material. All three annealing treatments showed the same degree of hardness. The stress-accelerated chromium depleted surface layer could have a detrimental effect on the oxidation resistance of TD-NiCr.

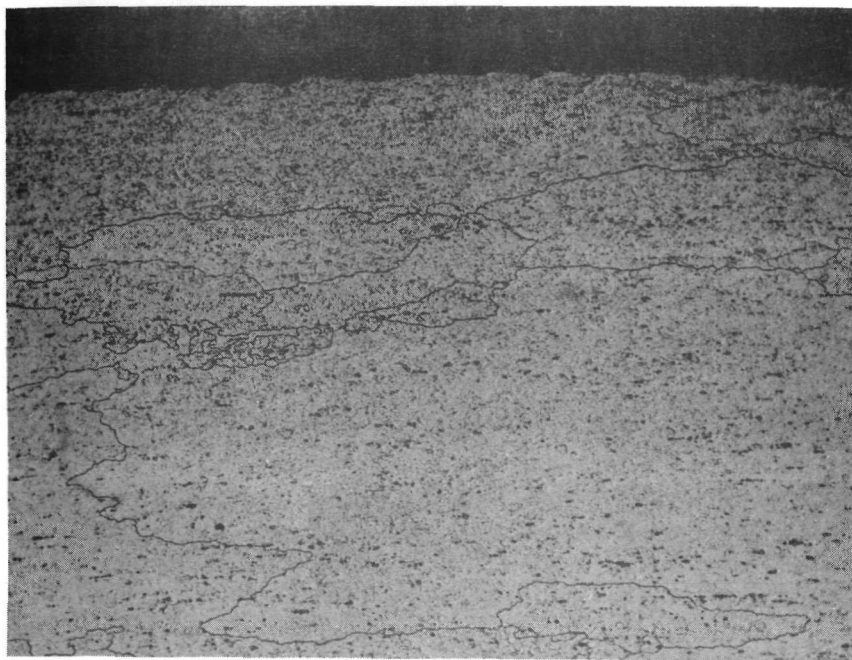


343 KHN

As-Formed

Neg. D2710

250X



300 KHN

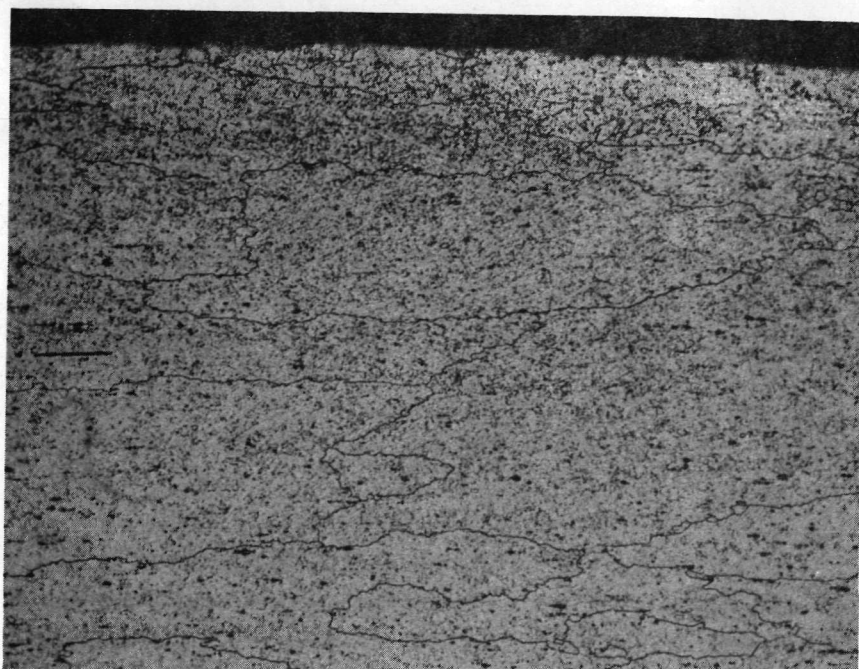
Annealed 982C (1800F)

Neg. D2716

250X

10% Oxalic Acid Electrolytic Etch

Figure 24. Microstructure of Brake Formed Part of 1.0 mm (0.040 in.) Recrystallized TD-NiCr Sheet As-Formed and After Annealing at 982C (1800F) - (Heat 3715, Specimen E2T-18, transverse orientation, 6t bend radius, 90-degree bend angle, annealed 2 hours in dry hydrogen.)

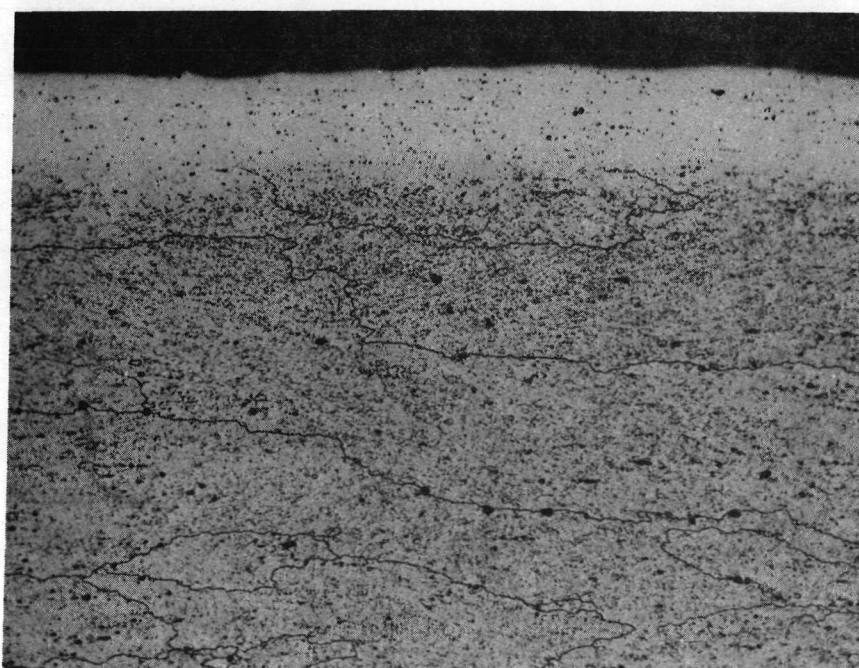


305 KHN

Annealed 1093C (2000F)

Neg. D2714

250X



302 KHN

304 KHN

Annealed 1177C (2150F)

Neg. D2712

250X

10% Oxalic Acid Electrolytic Etch

Figure 25. Microstructure of Brake Formed Part of 1.0 mm (0.040 in.) Recrystallized TD-NiCr Sheet After Annealing at 1093C (2000F) and 117C (2150F) - (Heat 3715, Specimen E2T-18, transverse orientation, 6t bend radius, 90-degree bend angle, annealed 2 hours in dry hydrogen.)

Test results for tensile specimens machined from brake formed parts annealed at the three different temperatures are listed in Table 13. The test parts represent one sheet thickness [1.0 mm (0.040 in.)], two grain directions (L and T), one bend angle (90°), and one bend radius (MBR). These data are summarized and compared to as-formed parts and parent material properties in Table 14. Annealing in the 982-1777 C (1800-2150 F) temperature range results in relief of strain hardening, but does not fully restore ductility. This lower ductility of annealed formed parts compared to parent metal properties appears to be a residual effect of the deformation, but specimen geometry may also be partly responsible.

Table 13. Test Results for Tensile Specimens Machined from Brake Formed and Annealed 1.0 mm (0.040 in.) Recrystallized TD-NiCr Sheet - Heat 3715 (Code E1)

Grain Direction (1)	Part Radius (2) cm (in.)	Annealing Temperature C (F)	Specimen No.	Cross-Section Area cm ² (in. ²)	Ultimate Tensile Strength MN/m ² (ksi)	Tensile Yield Strength MN/m ² (ksi)	Elongation % in 2.5 cm (1.0 in.)
T	0.020 (0.08)	982 (1800)	E1L-8	0.0182 (0.00282)	883 (128.0)	727 (105.5)	12
			E1L-9	0.0181 (0.00280)	888 (128.8)	738 (107.0)	10
			E1L-10	0.0173 (0.00268)	879 (127.5)	731 (106.0)	7
			Average		883 (128.1)	732 (106.2)	9.7
		1093 (2000)	E1L-11	0.0172 (0.00266)	910 (132.0)	731 (106.0)	9
			E1L-12	0.0165 (0.00255)	863 (125.2)	713 (103.4)	9
			E1L-13	0.0166 (0.00257)	888 (128.8)	731 (106.0)	10
			Average		887 (128.7)	725 (105.1)	9.3
		1177 (2150)	E1L-14	(3)	-	-	-
			E1L-15	0.0171 (0.00265)	876 (127.0)	712 (103.3)	10
			E1L-16	0.0172 (0.00266)	827 (120.0)	683 (99.0)	11
			Average		852 (123.5)	697 (101.1)	10.5
L	0.58 (0.23)	982 (1800)	E1T-7	0.0183 (0.00284)	801 (116.2)	683 (86.6)	10
			E1T-8	0.0199 (0.00308)	772 (112.0)	577 (83.7)	11.5
			E1T-9	0.0177 (0.00275)	824 (119.5)	618 (89.7)	10
			Average		799 (115.9)	598 (86.7)	10.5

(1) L = Tension axis parallel to rolling direction.

T = Tension axis normal to rolling direction.

(2) All specimens brake formed to a 90° bend angle.

(3) Test error.

Table 14. Summary of Effect of Annealing on Tensile Properties of Brake Formed 1.0 mm (0.040 in.) Recrystallized TD-NiCr Sheet - Heat 3715 (Code E1)

Grain Direction	Part Radius cm (in.) ⁽¹⁾	Annealing Temperature C (F)	Ultimate Tensile Strength MN/m ² (ksi)	Tensile Yield Strength MN/m ² (ksi)	Elongation % in 2.54 cm (1.0 in.)
T	0.20 (0.08) ↓ none	As-formed	1011 (146.7)	948 (137.6)	3.0
		982 (1800)	883 (128.1)	732 (106.2)	9.7
		1093 (2000)	887 (128.7)	725 (105.1)	9.3
		1177 (2150)	852 (123.5)	697 (101.1)	10.5
		Parent metal	801 (116.2)	537 (77.9)	26.5
L	0.58 (0.23) ↓ none	As-formed	875 (126.9)	714 (103.5)	6.5
		982 (1800)	799 (115.9)	598 (86.7)	10.5
		Parent metal	868 (125.9)	608 (88.2)	19.5

(1) All specimens brake formed to a 90° bend angle

As a result of the annealing studies, a stress relief annealing temperature of 1093C (2000F) for recrystallized TD-NiCr was selected for this program. For investigation of effects of forming and high temperature exposure on microstructure an annealing temperature of 1177C (2150F) was used. All annealing treatments were conducted for two hours at temperature in dry hydrogen.

Corrugation Forming

Corrugation Forming Limits - Corrugation forming evaluations were performed with the Pneuco pneumatic 311 kN (35 ton) press brake and closed die tooling. Closed die forming of a complete corrugation, four bends, was used for determining corrugation forming limits. This method, illustrated in Figure 26, was selected for the following reasons:

- It is a high-production process satisfactory for heat shield fabrication and for honeycomb core forming.
- It is a bending process that strains the material in a manner similar to the straining from brake forming.
- A range of sheet gages can be formed on the same tools without major modification.
- Forming of recrystallized and unrecrystallized materials can be accomplished using the same tools.

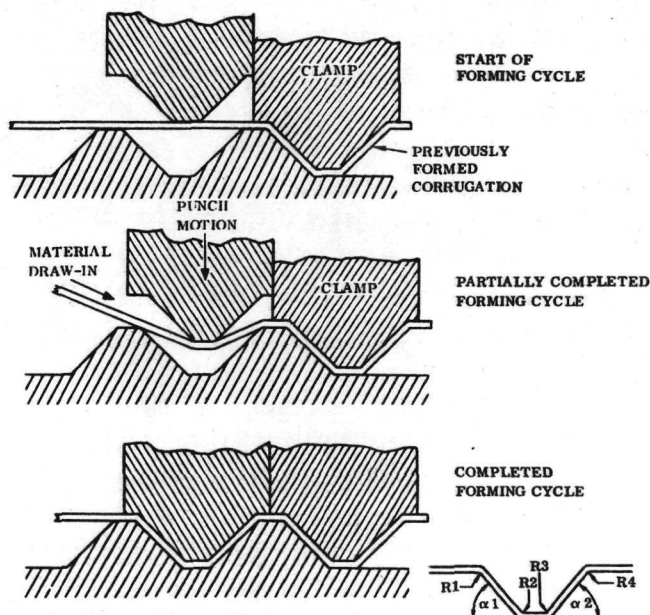


Figure 26. Corrugation Forming Cycle

Figure 27 is a sketch of the corrugation die designed and fabricated for the corrugation studies. Replaceable inserts are employed to accommodate the various corrugation angles, die radii, and material gages. Several sets of replaceable inserts with different radii were fabricated for each corrugation angle of 45, 60, and 75 degrees. Keys pressed into the dies are used to locate the inserts, and the inserts are also fastened to the dies with cap screws. Access holes are provided in the punch holder and the insulation containers so that the inserts can be replaced without disassembling the dies. Type 316 stainless steel was selected as the tool material for the inserts and die platens because of its good strength and oxidation resistance at elevated temperature, its availability, and relatively low cost.

The tool was designed so that a previously formed corrugation is held in place by a spring-loaded clamp while the next corrugation is being formed (see Figure 26). A complete corrugation with four bends is made at each stroke of the press. The requirement to form parts with three different corrugation angles required that the inserts be spaced at a constant pitch to simplify keying and fastening. This causes the width of flat to be different for each corrugation angle, varying from 0.96 cm (0.38 in.) for the 45-degree angle to 1.88 cm (0.74 in.) for the 75-degree angle. The difference in the length of flat is not considered significant to the forming evaluation of the three corrugation angles. Four stainless-steel stand-off spacers were used between the dies and the insulation container. For the hot-forming operation the space between the dies and the container is filled with insulation. The dies are gun drilled for installation of the cartridge heaters used for the hot-forming operation. Figure 28 shows the dies mounted in the press brake.

The forming studies were conducted on one heat each of 0.25 mm (0.010 in.) and 0.5 mm (0.020 in.) sheet for three corrugation angles (45, 60, and 75 degrees) and two heats of 0.08 mm (0.003 in.) sheet for one corrugation angle (45 degrees). Two grain orientations (longitudinal and transverse) were investigated for each set of conditions. Figure 29 shows typical corrugated test parts for the three corrugation angles studied.

The material was prepared for the corrugation tests by shearing to 10.2 by 30.5 cm (4 by 12 in.) blanks, deburring, and identifying with a vibro-pencil.

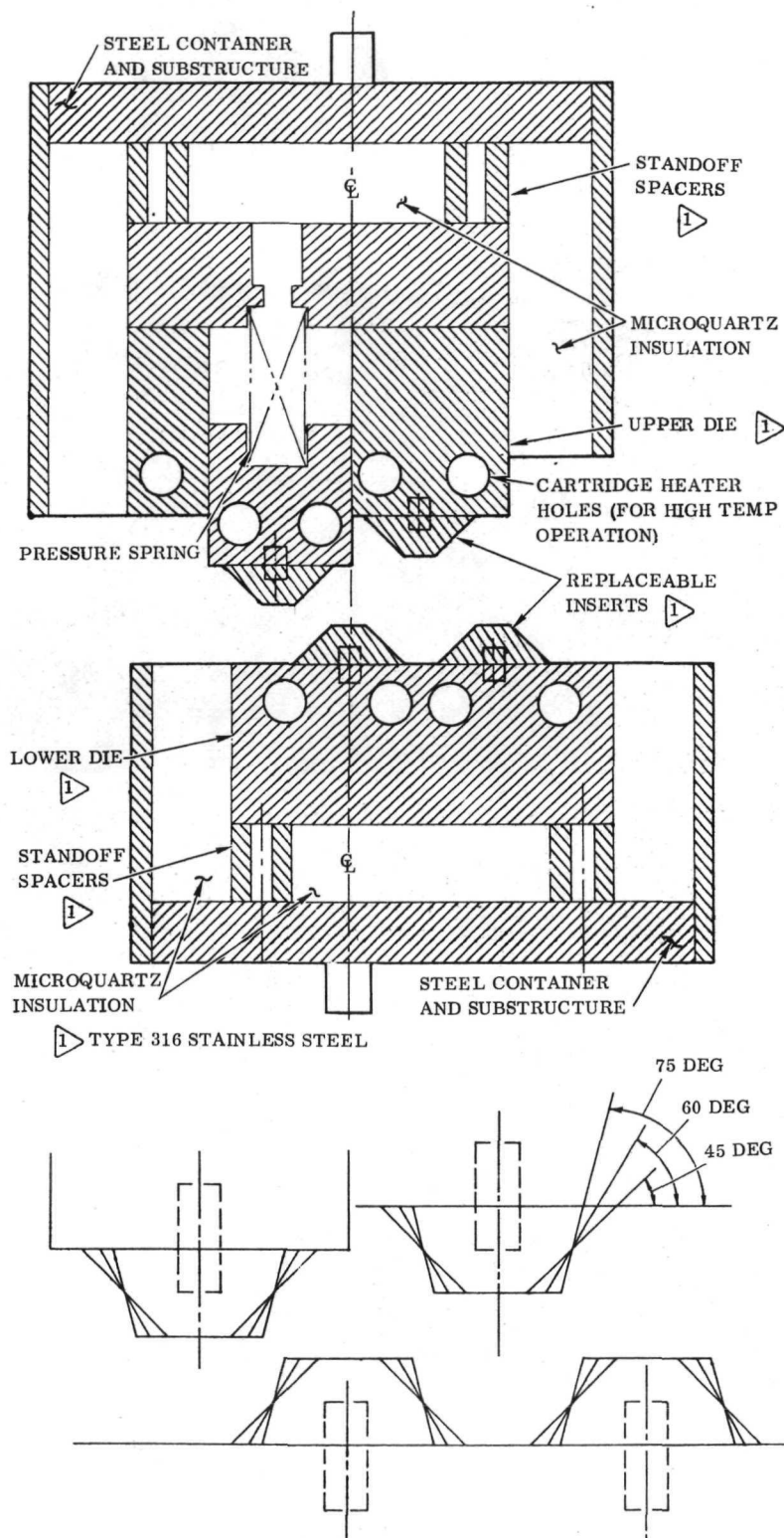


Figure 27. Corrugation Die Assembly with Replaceable Inserts

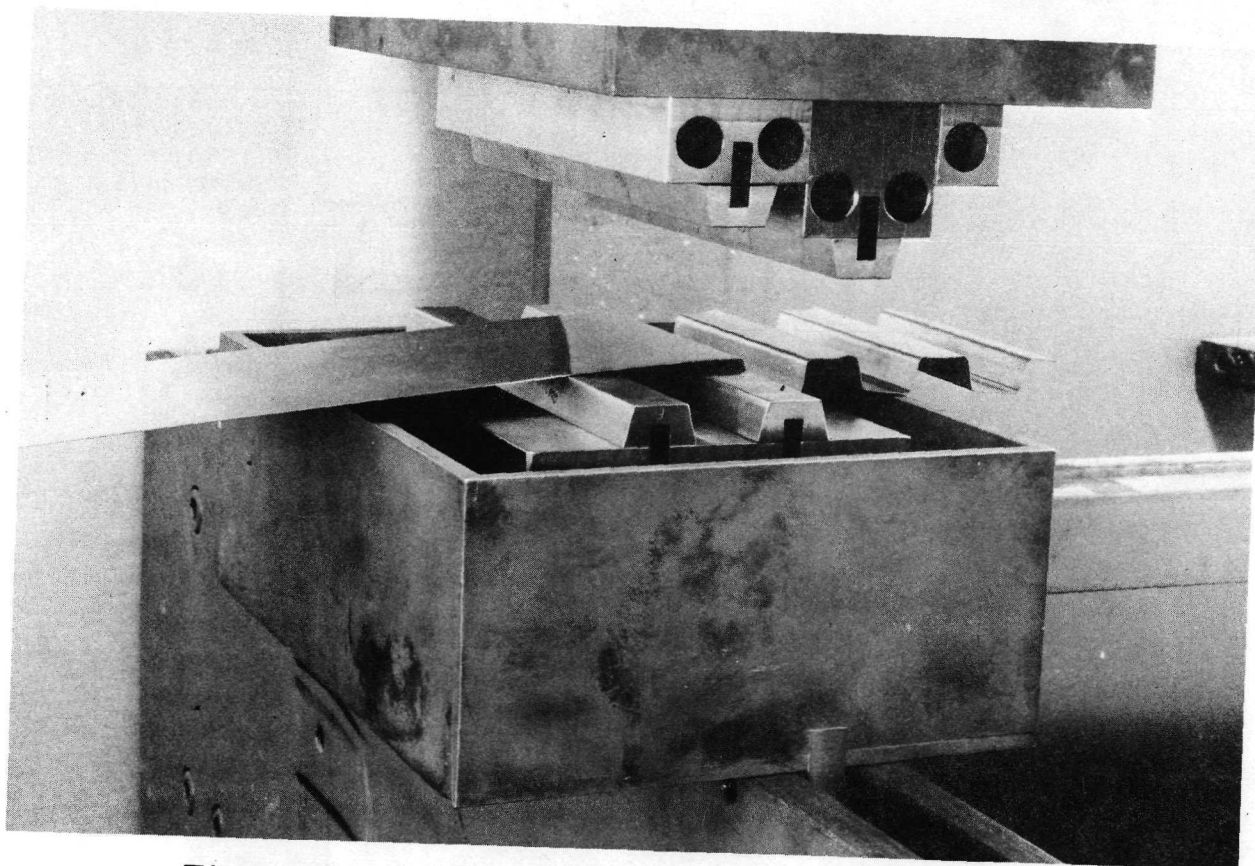


Figure 28. Corrugation Die Mounted in Press Brake Neg. 122573B

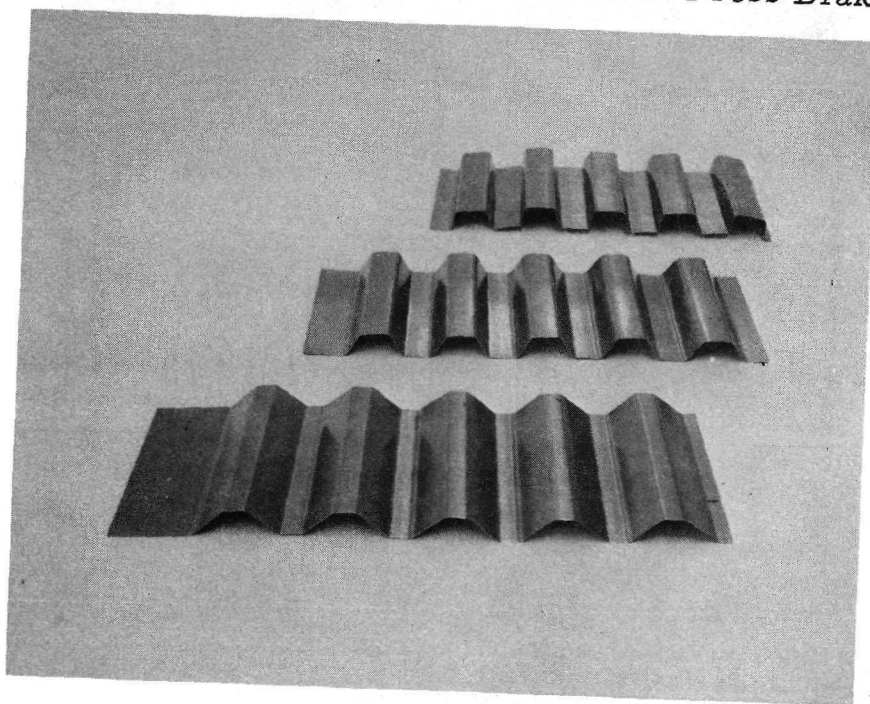


Figure 29. Corrugation Angles of 45, 60, and 75 Degrees Formed from 0.5 mm (0.020 in.) Recrystallized TD-NiCr Sheet Neg. 125794B

The corrugation dies were lubricated with Dow Corning No. 4 compound, a silicone lubricant, during all forming tests.

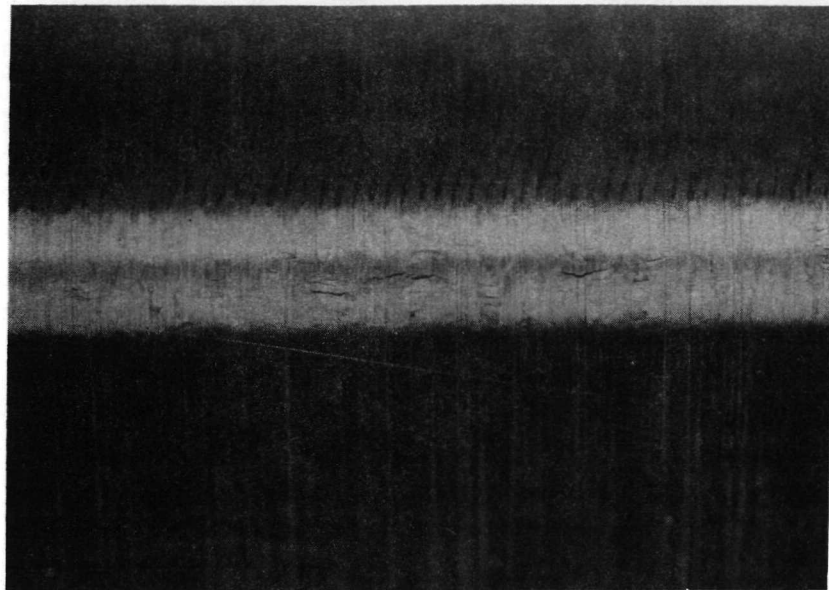
The test procedure for determining actual forming limits was to form corrugations with tool radii sufficiently tight to generate cracks, then progressively increase the tool radii until corrugations were formed without cracks. This was accomplished by removing the inserts and remachining the radii. In cases of fine cracks or severe orange peel, several additional corrugations would be formed to generate confidence in the results. Parts were examined at up to 30X magnification for cracks with both dye penetrant inspection and metallographic examinations employed to interpret borderline cases.

The type of cracking observed in the corrugation specimens is shown in Figures 30 and 31. Figure 30 shows typical cracks in a longitudinal specimen, and Figure 31 shows typical cracks in a transverse specimen. The radii on these specimens were just below the minimum bend radii. For radii that were significantly less than the minimum bend radii, cracks in the longitudinal specimens were of the same type and size shown in Figure 30 and did not propagate into large cracks. Cracks in the transverse specimen did propagate into long cracks for low R/t ratios.

Tool tryout tests verified that die clearance in the range of $0.1t$ to $1.0t$ was not critical and both 0.25 mm (0.010 in.) and 0.5 mm (0.020 in.) sheet could be formed with the same inserts. For the 0.08 mm (0.003 in.) material, a set of four 45-degree-angle inserts was ground to reduce the height from 1.27 cm (0.500 in.) to 1.21 cm (0.475 in.). This allowed closer meshing of the inserts, which then provided a die clearance of approximately $0.3t$. This minor modification allowed the use of the same tools for forming corrugations with the 0.08 mm (0.003 in.) foil.

Table 15 summarizes the results of the corrugation forming tests. These data show that the actual formability of 0.25 mm (0.010 in.) and 0.25 mm (0.020 in.) sheet is much better for the longitudinal direction than for the transverse direction. This confirms results of the brake forming evaluation.

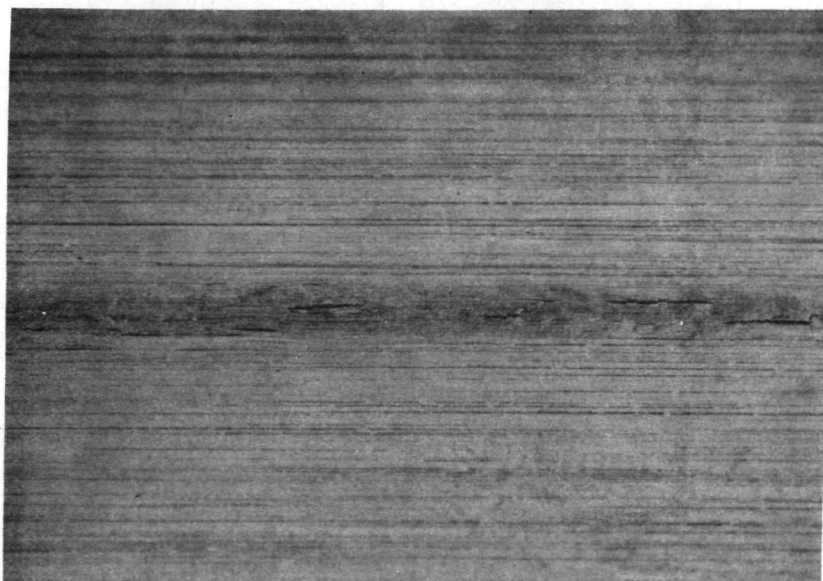
Large radial springback of the material for certain test conditions can be seen from Table 15 by comparing the tool radius (R/t) with the part radius (R/t). Because of the forming action imparted by making four bends at a time in the corrugation die, the part radius did not closely conform to the punch radius. Particularly large radial springback was experienced in the case of sharp punch radii and 45 degree corrugations.



Neg. D2689

10X

Figure 30. Typical Small Cracks in Radius of Corrugation Specimen of Recrystallized Sheet with Strain Longitudinal to the Rolling Direction



Neg. D2688

10X

Figure 31. Typical Small Cracks in Radius of Corrugation Specimen of Recrystallized Sheet with Strain Transverse to the Rolling Direction

Table 15. Experimental Corrugation Forming Limits of Recrystallized TD-NiCr for 45, 60 and 75 Degree Corrugation Angles

Corrugation Angle (degrees)	Sheet Thickness mm (in.)	Heat Number	Grain ⁽¹⁾ Direction	Ratio of Tool Radius to Material Thickness (R/t)		Ratio of Part Radius ⁽²⁾ to Material Thickness (R/t)		Springback ⁽³⁾ Angle (degrees)
				No Cracks	Cracks	No Cracks	Cracks	
45	0.08 (0.003)	3702 Code M	L	1.7	(4)	10.7	(4)	11
			T	1.7	(4)	10.7	(4)	13
		3523 Code P	L	1.7	(4)	10.7	(4)	10
			T	1.7	(4)	10.7	(4)	10
	0.25 (0.010)	3700 Code H3	L	0.5	(4)	6.2	(4)	4
			T	2.0	0.8	10.0	7.0	3
60	0.5 (0.020)	3640 Code B3	L	1.0	0.4	3.9	3.1	0
			T	(5)	2.4	(5)	6.2	6
	0.25 (0.010)	3700 Code H3	L	2.2	0.5	4.5	3.2	4
			T	6.2	4.7	7.8	6.2	7
	0.5 (0.020)	3640 Code B3 & B4	L	3.1	0.4	3.9	3.1	-3 (6)
			T	5.5	4.7	6.3	5.5	7
75	0.25 (0.010)	3700 Code H3	L	1.2	0.5	1.9	1.0	-6 (6)
			T	6.2	4.7	7.8	4.7	7
	0.5 (0.020)	3640 Code B3 & B4	L	3.1	2.4	3.9	2.4	1
			T	(5)	5.5	(5)	6.3	6

(1) L = direction of strain parallel to rolling direction.
T = direction of strain normal to rolling direction.

(2) Radius which provides most severe forming action. Radius R4 in sketch.

(3) Angle measured on specimen that did not crack. Angle α 2 in sketch.

(4) Sharpest radius that could be generated with 0.05 mm (0.002 in.) to 0.13 mm (0.005 in.) tool radii did not crack parts.

(5) Not determined.

(6) Negative springback.

The forming action also yielded a different degree of angular springback between the two sides of the corrugation angle. Looking at Figure 26, it can be seen that the radius identified as R4 is formed almost completely by stretch as the material locks on the edges of the inserts. Angular springback on the leg that forms this radius generally was in the order of 3 to 5 degrees. On the other hand, material is drawing in as radius R1 is formed. This leg is not strained to the same amount and springs back to a much larger extent. Angular springback for the R1 leg was generally 5 to 10 degrees greater than for the R4 leg. In addition, radial springback on radius R4 was the smallest of the four radii. Since the R4 radius provides the most severe forming action, this radius was used to check for formability. In many cases, this radius cracked, while the other radii did not.

Comparison of the actual and theoretical forming limits for 0.25 mm (0.010 in.) and 0.5 mm (0.020 in.) recrystallized TD-NiCr sheet are shown in Figures 32 and 33. For both material gages the actual forming limits for the transverse grain orientation are higher (poorer formability) than the theoretical limits. The actual forming limits for the longitudinal direction

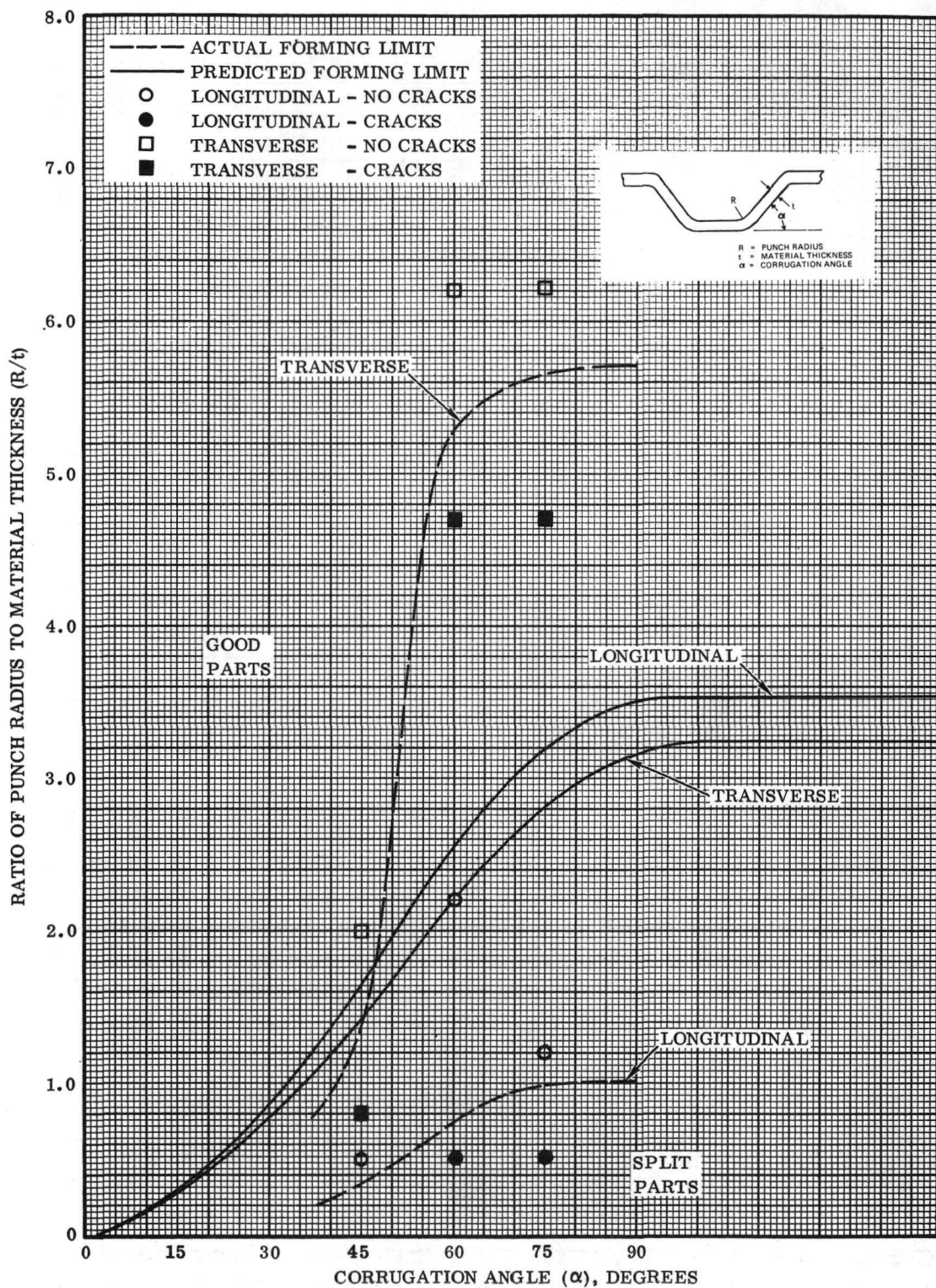


Figure 32. Theoretical and Actual Corrugation Forming Limit Curves for 0.25 mm (0.010 in.) Recrystallized TD-NiCr Sheet - Heat 3700 (Code H3)

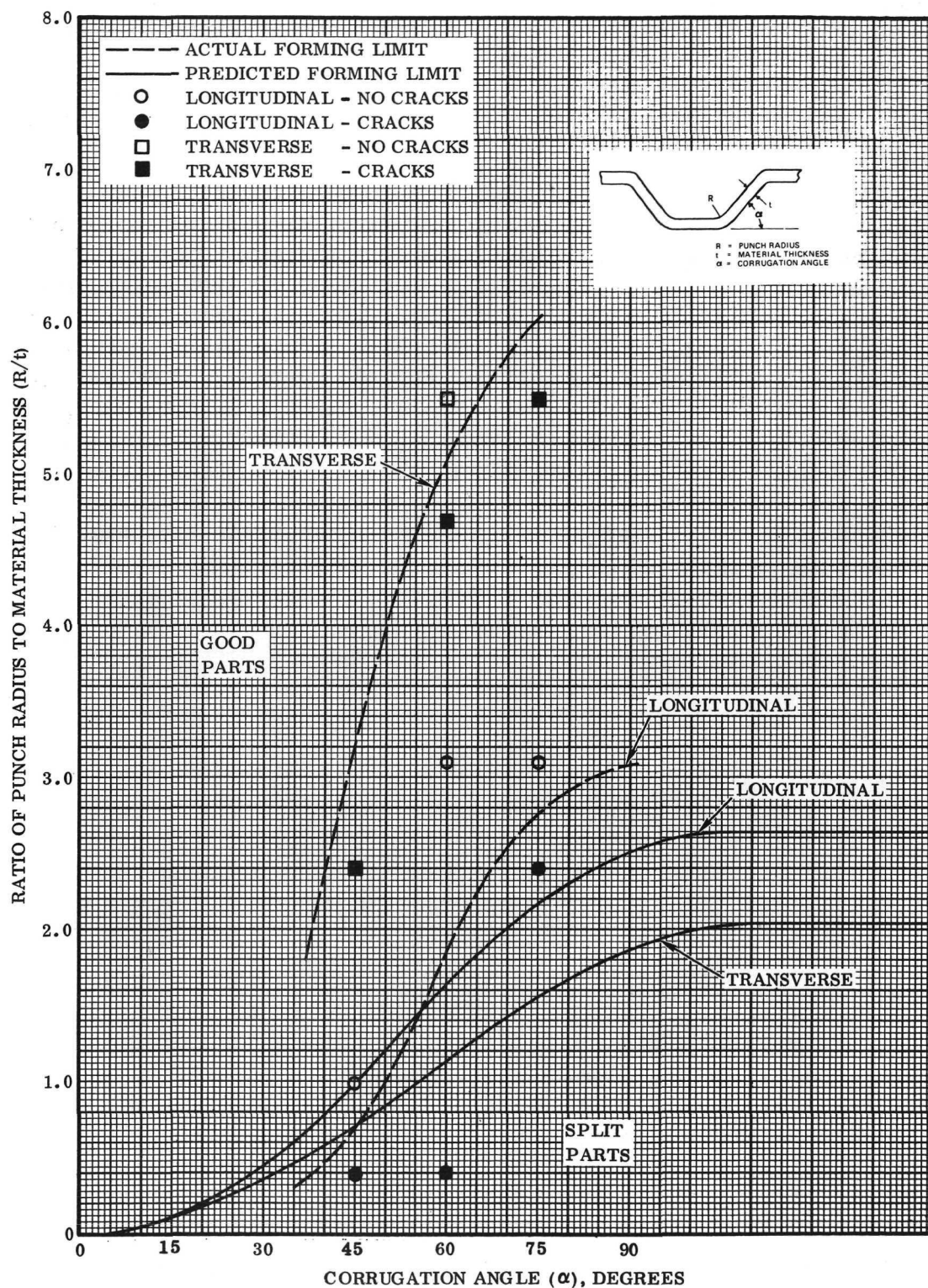


Figure 33. Theoretical and Actual Corrugation Forming Limit Curves for 0.5 mm (0.020 in.) Recrystallized TD-NiCr Sheet - Heat 3640 (Code B1)

show good agreement with the theoretical limits for 0.5 mm (0.020 in.) sheet but show better formability than predicted for 0.25 mm (0.010 in.) sheet. However, these curves are based on punch radius, and if consideration is given to the higher part radius values (see Table 15) the actual forming limits for the longitudinal direction are higher than the theoretical limits for both material gages.

Figure 34 shows the theoretical forming limits for 0.8 mm (0.003 in.) foil from Heat 3702 (Code M). and the forming test data points for the 45 degree corrugation. These data indicate good formability and no significant difference in formability due to grain orientation. This is not unexpected in view of the lack of anisotropy in tensile properties (Table 3), fine grain size, and excellent surface finish of the cold-rolled foil. Although this material exhibits good formability, the extremely large radial and angular spring-back (see Table 15) should be taken into consideration for both hardware and tool design. It is believed that formability data developed for closed die forming of a complete corrugation (4 bends per stroke) can also be used for the flip-flop corrugation method, in which only two bends are made for each stroke of the press.

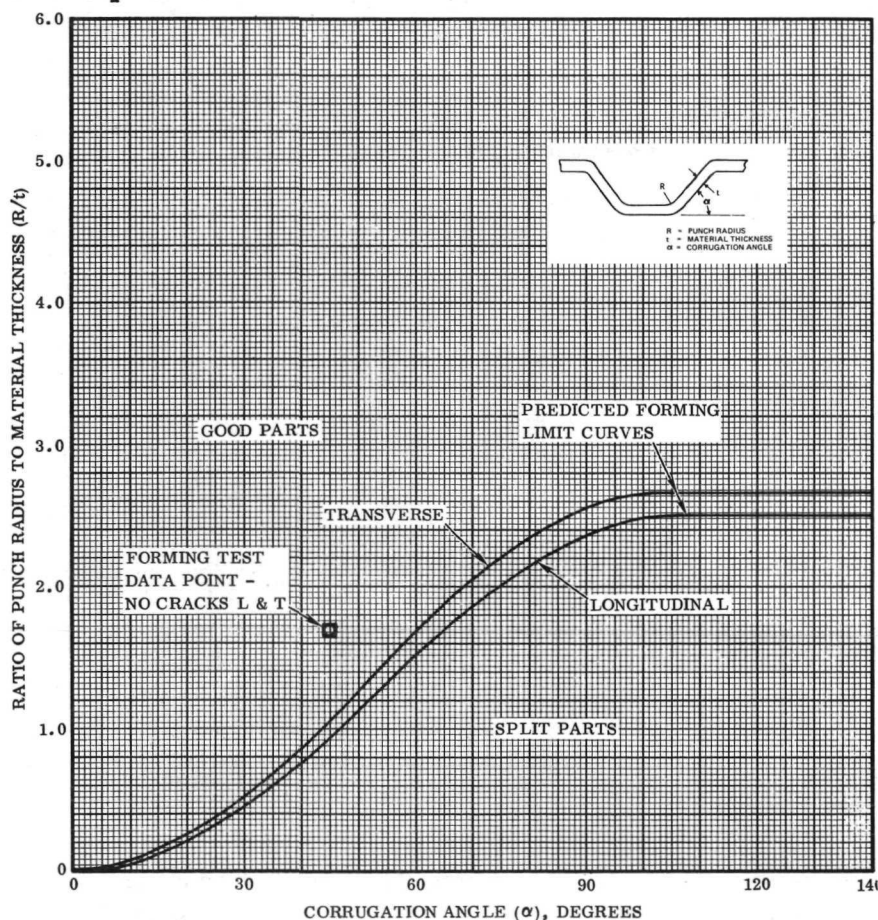


Figure 34. Theoretical Corrugation Forming Limit Curves and Actual Forming Data for 0.08 mm (0.003 in.) Recrystallization TD-NiCr Sheet - Heat 3702 (Code M)

Microstructure. - Metallographic examination was performed on typical corrugated parts encompassing the following parameters: three sheet thicknesses, two grain orientations (L and T), three corrugation angles (45, 60 and 75 degrees), two bend radii (MBR and <MBR), and two metallurgical conditions (as-formed and annealed). The annealing treatment was 2 hours at 1177C (2150F) in dry hydrogen. No microstructural effects were observed that would justify changes in the actual forming limits established by macroscopic examination. In most instances, some deformation bands were evident in the as-formed condition, which partially or completely disappeared upon annealing. The deformation was not sufficiently severe as to cause fine-grain recrystallization during annealing. Chromium depletion from annealing was evident at the tension side of the bend radius similar to that observed for brake forming.

Joggling

Joggle Limits - A Hufford Universal Joggling machine was used to evaluate joggling limits for three gages of recrystallized sheet. Three sets of joggle dies were designed and fabricated for use with the Hufford Joggler. The dies were designed to use joggle blanks with internal radii of 0.09, 0.22 and 0.51 cm (0.036, 0.085 and 0.200 in.). The joggle blanks were 90-degree angles with 2.54 cm (1.0 in.) legs prepared from brake-formed parts available from the brake forming study on sheet width effects. The dies were fabricated from cast kirksite, but the die surfaces and radii were machined after casting to obtain closer dimensional tolerances.

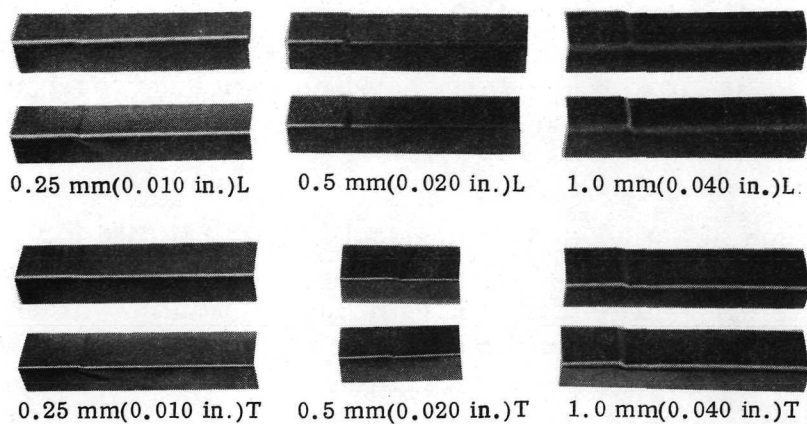
Results of joggling tests for three sheet thicknesses and two grain orientations (L and T) are presented in Table 16. The joggling parameters investigated were depth of joggle (D), length of joggle (L), and material thickness (t). A range of joggle depths was investigated for each material combination. The approach was to vary the joggle depth for each selected joggle length to establish the depth at which failure was observed.

The two major failures in joggling are splitting and shear buckling. Any evidence of splitting (cracks) was considered a failure. Many of the test parts showed various degrees of buckling, with the condition more severe for thinner sheet. Those parts with slight buckling that could be easily removed by flattening in accordance with common shop practice were judged good parts. Typical joggled parts of 0.25, 0.5 and 1.0 mm (0.010, 0.020 and 0.040 in.) sheet are shown in Figure 35. Buckling of the side leg is readily evident for the 0.25 mm (0.010 in.) material. A typical splitting failure of 1.0 mm (0.040 in.) sheet joggled transverse to the rolling direction is shown in Figure 36.

Table 16. Jogging Tests on Recrystallized TD-NiCr Sheet

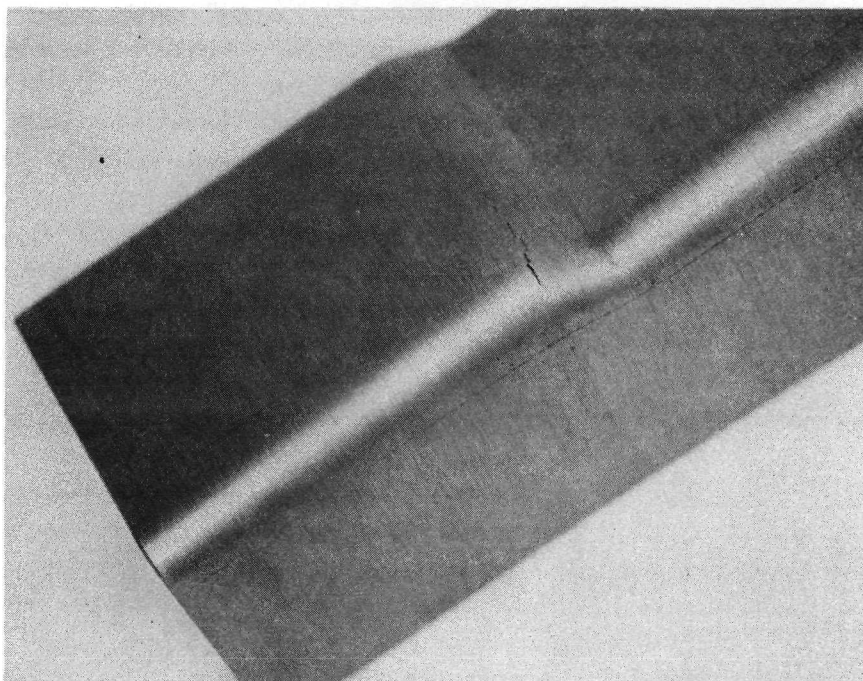
Material Thickness mm (in.)	Grain Direc- tion	L Joggle Length mm (in.)	D Joggle Depth mm (in.)	D/t Ratio	D/L Ratio	Results	Part Number	Metallo- graphic Examination
1.0 (0.040)	L	10.20 (0.40) ↓ 5.10 (0.20) ↓	1.02 (0.040)	1.0	0.10	good	E1T-3L-11	
			3.81 (0.150)	3.8	0.38	split	-21	
			1.52 (0.060)	1.5	0.15	good	-31	
			1.85 (0.073)	1.8	0.36	good	-12	
			1.55 (0.061)	1.5	0.30	good	E1T-1L-31	
			2.08 (0.082)	2.0	0.41	slight buckle	-2	X
			2.08 (0.082)	2.0	0.41	slight buckle	-32	
			1.42 (0.056)	1.4	0.28	good	-1	X
			1.42 (0.056)	1.4	0.28	good	E1T-2L-1	
	T	3.05 (0.12) 4.57 (0.18) 5.59 (0.22) ↓ 2.54 (0.10)	2.54 (0.100)	2.5	0.80	split	E1L-1L-32	
			3.18 (0.125)	3.1	0.70	split	-31	
			2.72 (0.107)	2.7	0.49	split & buckle	-22	
			1.98 (0.078)	2.0	0.35	slight buckle	E1L-4L-1	
			1.40 (0.055)	1.4	0.25	good	-2	X
			1.40 (0.055)	1.4	0.25	good	-3	
			2.64 (0.104)	2.6	0.47	split & buckle	E1L-3L-1	
			1.22 (0.048)	1.2	0.48	good	E1L-1L-11	
			1.17 (0.046)	1.1	0.46	good	E1L-3L-21	
			1.55 (0.061)	1.5	0.61	good	-31	X
			2.79 (0.11)	2.8	0.11	split	-32	
0.5 (0.020)	L	3.81 (0.15) ↓ 3.05 (0.12)	1.70 (0.067)	3.3	0.45	split & buckle	B6T-3L-11	
			1.27 (0.050)	2.5	0.33	buckle	B6T-2L-1	X
			0.89 (0.035)	1.7	0.23	good (1)	-2	X
			0.89 (0.035)	1.7	0.23	good (1)	-3	
			0.20 (0.008)	0.4	0.05	good	B6T-1L-11	
			0.58 (0.023)	1.1	0.15	good	-21	
			0.58 (0.023)	1.1	0.15	good	-3	
			0.89 (0.035)	1.7	0.29	split	-12	
	T	3.81 (0.15) ↓ 3.05 (0.12) 2.54 (0.10) ↓	3.05 (0.012)	0.6	0.08	good	B6L-3L-12	
			0.71 (0.028)	1.4	0.19	good (1)	-11	
			0.46 (0.018)	0.9	0.12	good	B6L-1L-1	
			0.58 (0.023)	1.1	0.15	good	-2	
			0.56 (0.022)	1.1	0.15	good	-3	
			1.04 (0.041)	2.0	0.27	good (1)	B6L-2L-11	X
			0.33 (0.013)	0.6	0.11	good	-1	
			0.91 (0.036)	1.8	0.36	good	B6L-3L-32	
			0.81 (0.032)	1.6	0.32	good	B6L-2L-21	X
			1.09 (0.043)	2.1	0.43	split & buckle	-31	
0.25 (0.010)	L	3.05 (0.12) ↓ 3.81 (0.15) ↓	0.51 (0.020)	2.0	0.17	buckle	H4T-2L-32	
			0.51 (0.020)	2.0	0.17	buckle	H4T-4L-1	
			0.33 (0.013)	1.3	0.11	good	-2	
			0.15 (0.006)	0.6	0.05	good	-3	
			0.51 (0.020)	2.0	0.13	good (1)	-12	X
			0.51 (0.020)	2.0	0.13	good (1)	H4T-5L-2	
			0.36 (0.014)	1.4	0.09	good (1)	-3	X
			0.36 (0.014)	1.4	0.09	good (1)	-1	
	T	3.05 (0.12) ↓ 3.30 (0.13) ↓ 3.05 (0.12)	0.36 (0.014)	1.4	0.09	good (1)	H4L-6L-1	X
			0.36 (0.014)	1.4	0.12	buckle	H4L-5L-11	
			0.23 (0.009)	0.9	0.08	good	-22	
			0.20 (0.008)	0.8	0.07	good (1)	H4L-3L-12	
			0.20 (0.008)	0.8	0.07	good (1)	-21	
			0.33 (0.013)	1.3	0.10	buckle	-32	
			0.51 (0.020)	2.0	0.15	buckle	H4L-6L-2	X
			0.51 (0.020)	2.0	0.15	buckle	-3	
			0.18 (0.007)	0.7	0.05	good	H4L-7L-31	
			0.18 (0.007)	0.7	0.05	good	-22	
			0.13 (0.005)	0.5	0.04	good	-11	

(1) Contained slight buckle that could be satisfactorily flattened by normal shop practice.



Neg. 127895B

Figure 35. Typical Joggled Parts of Recrystallized TD-NiCr Sheet



Neg. 127899B

Figure 36. Typical Splitting Failure of 1.0 mm (0.040 in.) Recrystallized Sheet Joggled Transverse to Rolling Direction

The radius used on the joggling dies is a critical factor in joggling of TD-NiCr sheet. The standard radius of 0.08 cm (0.032 in.) used in common shop practice will result in premature splitting if this radius is less than the minimum brake forming radius for the specific material thickness and orientation. A die radius of 1.27 mm (0.050 in.) was selected for the test program since TD-NiCr is somewhat less formable than conventional materials. However, it should be noted that a larger radius is needed for 1.0 mm (0.040 in.) material joggled in the transverse direction, since premature splitting was evident for some parts.

Comparison of actual and theoretical joggling limits for 0.25, 0.5, and 1.0 mm (0.010, 0.020, and 0.040 in.) sheet are shown in Figures 37, 38 and 39 respectively. The formability in the longitudinal direction is better than the transverse direction for all three material thicknesses. It is also evident that TD-NiCr is less formable than predicted from the theoretical joggling studies. For example the predicted splitting line in Figure 38 is near a D/L ratio of 0.8, whereas the experimental forming shows splitting for all tests conducted at D/L ratios greater than 0.4. The difference between actual and predicted joggling limits is in agreement with results from brake and corrugation forming investigations.

Microstructure. - Metallographic examinations were performed on representative joggled parts in the as-formed condition and after annealing for 2 hours at 1177C (2150F) in dry hydrogen. Observations were as follows:

- a. Joggling has no detrimental effect on microstructure of as-formed or annealed parts formed within the experimentally established forming limits.
- b. In some instances, slight-to-moderate deformation bands are visible in the as-formed condition, but there is little or no evidence of the plastically deformed zone after annealing.
- c. Microstructure of joggled parts is similar to that of brake formed parts.

Dimpling

An investigation was conducted on dimpling techniques, machines, and tooling used in the aerospace industry that might be applicable to TD-NiCr. A major objective was to determine if the same tooling could be used for both cold dimpling of recrystallized material and hot dimpling of unrecrystallized material. A visit was made to Zephyr Manufacturing Company, Inglewood, California for discussion and demonstration of Ram-Coin dimpling, Triple

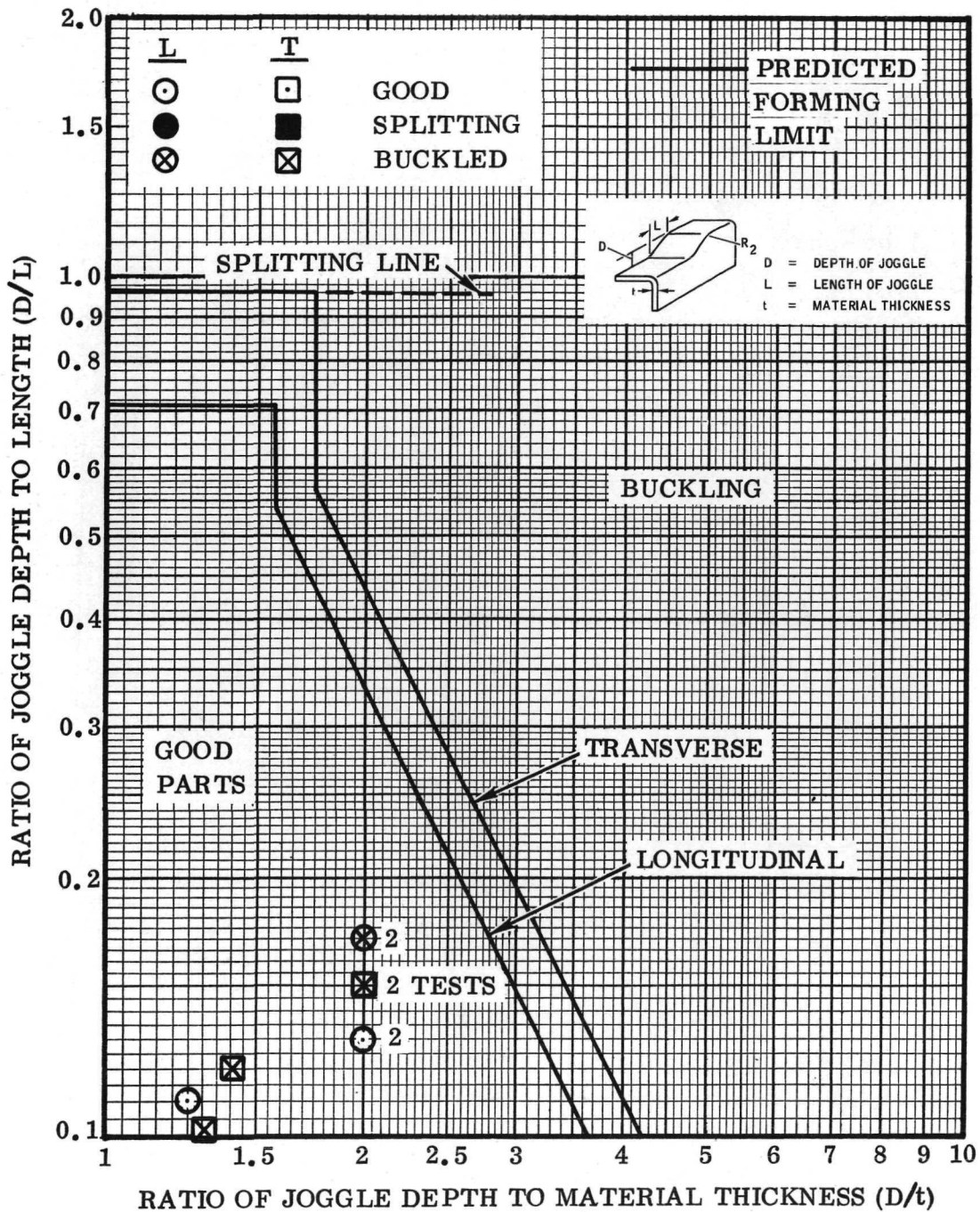


Figure 37. Actual Forming Data Superimposed on Theoretical Jogging Limit Curves for 0.25 mm (0.010 in.) Re-crystallized TD-NiCr Sheet - Heat 3700 (Code H1)

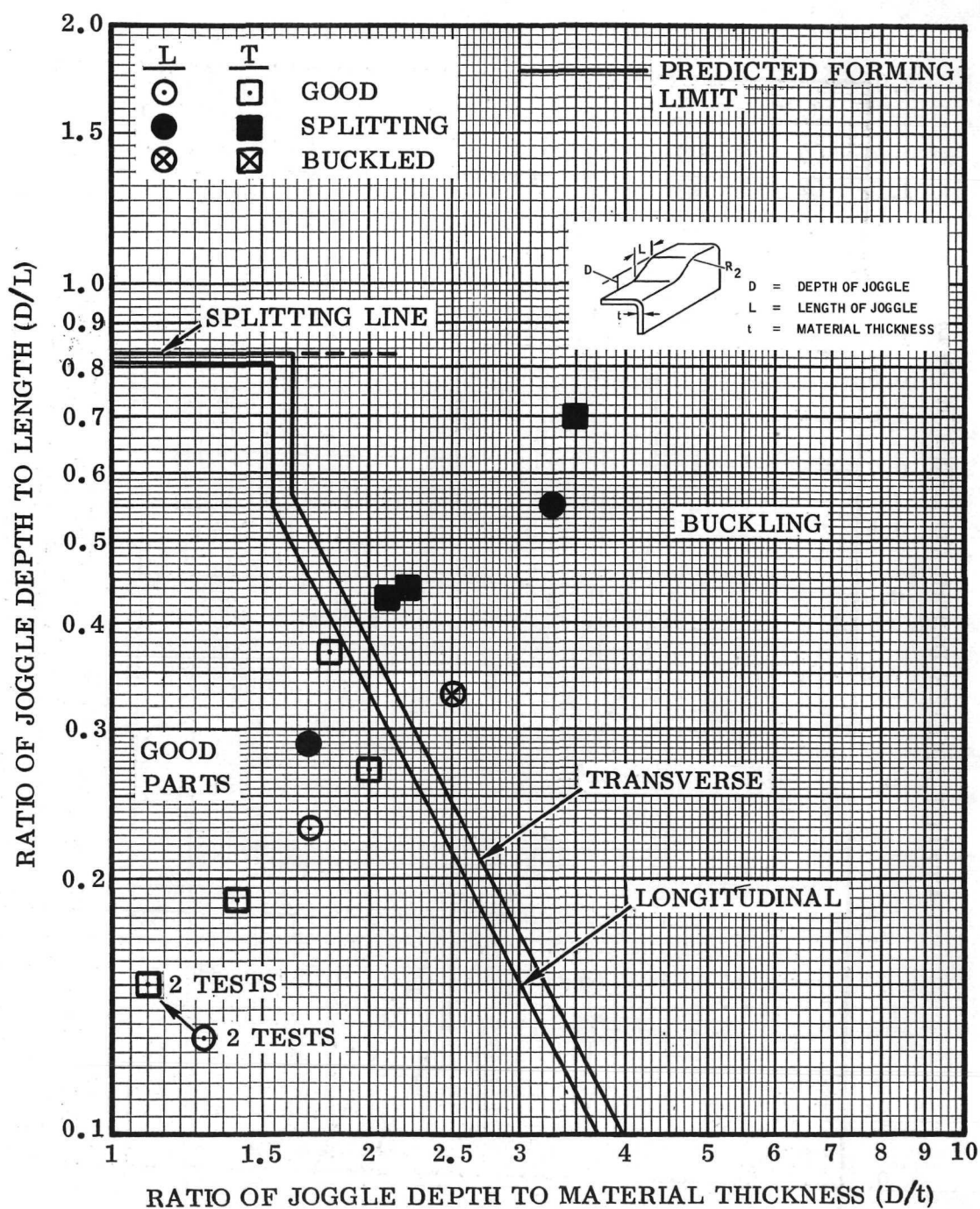


Figure 38. Actual Forming Data Superimposed on Theoretical Jogging Limit Curves for 0.5 mm (0.020 in.) Recrystallized TD-NiCr Sheet - Heat 3640 (Code B2)

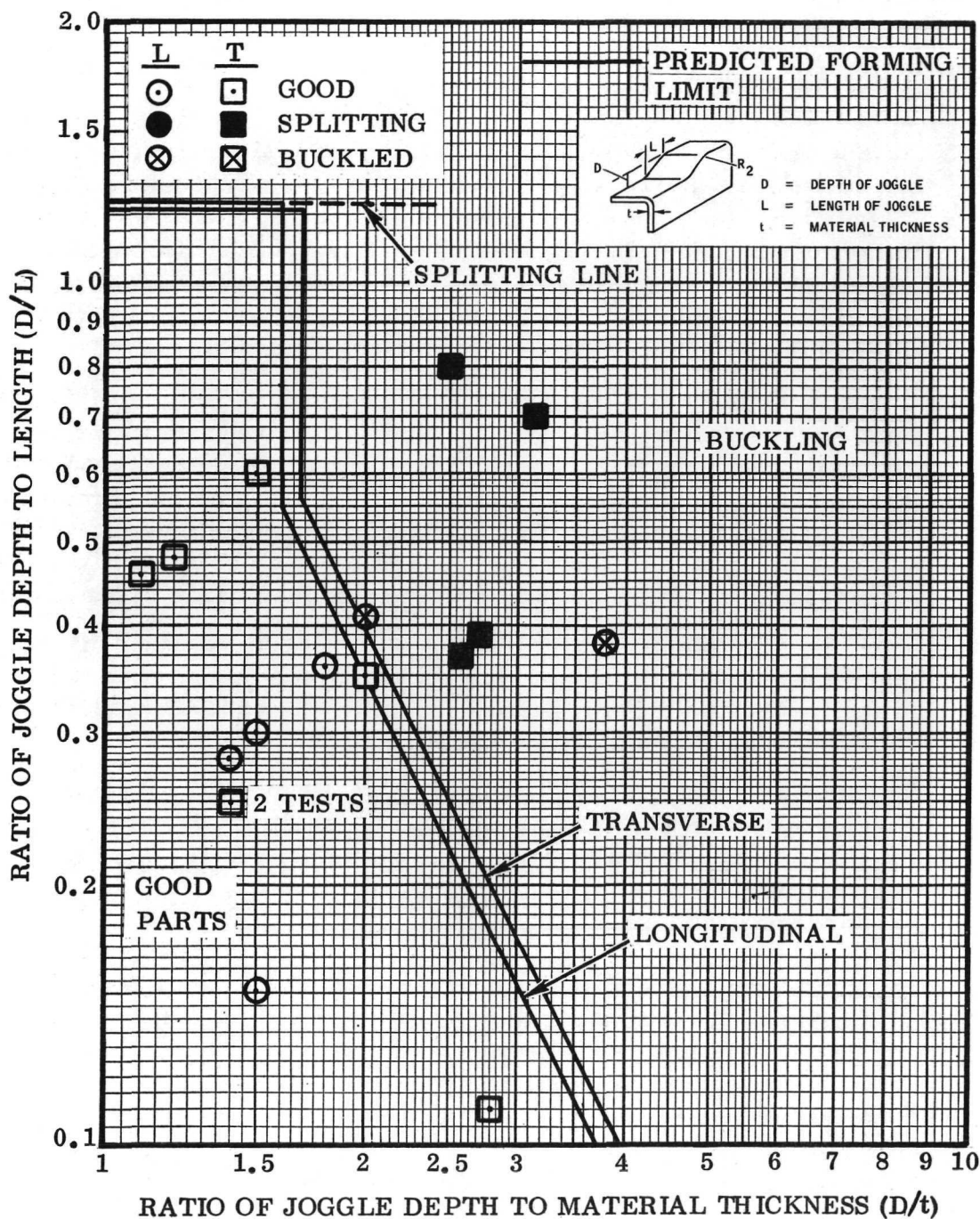


Figure 39. Actual Forming Data Superimposed on Theoretical Jogging Limit Curves for 1.0 mm (0.040 in.) Recrystallized TD-NiCr Sheet - Heat 3715 (Code E)

Action dimpling and Resistothermic dimpling. Ram-Coin and Triple-Action dimpling are the techniques most widely used for making aerospace hardware. Resistothermic dimpling is used when the temperature required for satisfactory dimpling of a particular material exceeds the capability of the other two methods.

Results of the investigation were as follows:

- a. Ram-Coin and Triple-Action dimpling are applicable to cold dimpling of recrystallized TD-NiCr. The tooling and machines for these techniques do not have the temperature capability for use in hot dimpling unrecrystallized TD-NiCr. Ram-coin dimpling has the advantage in tooling cost, delivery schedule, and availability of machines. Triple-action dimpling has the advantage of better dimensional control in materials difficult to dimple.
- b. Resistothermic dimpling was developed for dimpling materials at temperatures above 371C (700F). Resistothermic dimpling is generally used when satisfactory results cannot be achieved with Ram-Coin or Triple-Action dimpling. Resistothermic dimpling requires special procedures including: (1) close-tolerance drilling and deburring of pilot hole, (2) redrilling of holes after dimpling, and (3) a finish machining operation on the back side of the dimple.
- c. The use of common tooling for cold dimpling of recrystallized material and hot dimpling of unrecrystallized material is not practical for the test program because of the special procedures required for Resistothermic dimpling.
- d. The tooling required for the dimpling test program on TD-NiCr sheet favors the use of Ram-Coin dimpling on a cost basis. Of the three dimple configurations being considered (80, 100 and 120 degrees included angle), only the 100-degree rivet configuration is standard in the aerospace industry for thin-gage material.

Preliminary dimpling tests were performed at the Zephyr Manufacturing Company to compare the Ram-Coin and Triple-Action methods for cold dimpling recrystallized material. Dimples for the 3.97 mm (0.157 in.) diameter MS 20426 rivet were formed in 0.25 mm (0.010 in.) material (Heat 3700) supplied by Convair Aerospace. Radial cracks and circumferential cracks (with high ram pressures) were observed for both processes, with the cracking tendency less severe for Ram-Coin dimpling. The preparation of the pilot holes was very critical for dimpling TD-NiCr. Much of the radial cracking was attributed to cracks and severely deformed metal in the drilled holes. It was evident from these tests that precision drilled and deburred pilot holes must be used for dimpling TD-NiCr.

As a result of these investigations the Ram Coin process was selected for dimpling of recrystallized TD-NiCr.

Dimpling Limits. - Dimpling tests were conducted using a Chicago Pneumatic CP450A dimpling machine and Ram Coin dimpling dies purchased from Zephyr Manufacturing Company. The test program included nine dimple configurations and two heats each of three sheet thicknesses. The dimple configurations were the standard 100-degree included angle dimple (MS 20426 rivet) and two special configurations with 80- and 120-degree included angles. The hole diameters were 3.18, 3.97 and 4.76 mm (0.125, 0.157 and 0.188 in.) for each dimple angle.

Preparation of the test blanks involved drilling, reaming, and deburring 10 holes in each 3.8 cm by 20.3 cm (1.5 in. by 8 in.) blank. Test blanks for the dimpling tests were prepared representing two heats for each of three sheet thicknesses: 0.25, 0.5 and 1.0 mm (0.010, 0.020, and 0.040 in.)

Results of the dimpling tests are summarized in Table 17. A total of 54 test conditions were investigated (2 heats, 3 sheet thicknesses, 3 dimple angles, and 3 hole diameters). For 49 of the 54 test conditions, forming of dimples resulted in cracks. For five test conditions, 10 replicate dimples free from cracks could be formed. All of the dimples formed using the 120-degree included angle dies (30-degree formed angle) resulted in cracks. The dimpling dies for the five test conditions that produced crack-free dimples were for 100 and 80-degree included angles (40 and 50-degree formed angles).

The predominant failure mode was circumferential cracking; however, in 12 of the 49 test conditions that showed circumferential cracks, radial cracks were also observed.

Figure 40 shows photographs of typical circumferential and radial cracks. The circumferential occurred in the formed radius, primarily oriented transverse to the direction of strain. In a few severe cases, cracks were also observed longitudinal to the direction of strain. The radial cracks occurred at the edge of the hole at an angle of 45 degrees to the rolling direction. A typical metallographic cross section of a dimple containing circumferential cracks is shown in Figure 41. The 100X magnification micrograph reveals deformation bands associated with the circumferential cracks. These deformation bands are also present in the bend radius of uncracked dimples and testify as to the severity of the dimpling operation.

A number of dimpling tests were made with the test blanks at liquid nitrogen temperature to determine if the higher elongation at cryogenic temperatures would reduce or eliminate the radial and circumferential cracking. The tests were made with three thicknesses of material, and

Table 17. Dimpling Test Results for Recrystallized TD-NiCr Sheet

Specimen Number	Material Thickness mm (in.)	Heat Number	Dimple Angle (degrees)	Starting Hole Diameter mm (in.)	Final Hole Diameter mm (in.)	Ram Height† mm (in.)	Ram Pressure N/m ² (psi)	Results		
								Circumferential Cracks	Radial Cracks	No Cracks
H2L-43	0.25 (0.010)	3700	80	3.18	3.73 (0.147)	0.5 (0.020)	69 (10)	X	X	
F3-1	0.25 (0.010)	3637	↓	(0.126)	3.73 (0.147)	0.8 (0.030)	↓	X	X	
A2-1	0.5 (0.020)	3629	↓	↓	3.66 (0.144)	↓	↓	X		
B7-1	0.5 (0.020)	3640	↓	↓	3.66 (0.144)	↓	↓	X		
E2L-44	1.0 (0.040)	3715	↓	↓	3.30 (0.130)	0.5 (0.020)	↓			X
D2L-44	1.0 (0.040)	3708	↓	↓	3.30 (0.130)	0.5 (0.020)	↓			X
H2L-44	0.25 (0.010)	3700	100	3.18	3.66 (0.144)	0.6 (0.025)	69 (10)	X		
F3-2	0.25 (0.010)	3637	↓	(0.126)	3.66 (0.144)	0.6 (0.025)	↓	X		
A2-2	0.5 (0.020)	3629	↓	↓	3.50 (0.138)	0.5 (0.020)	↓	X		
B7-2	0.5 (0.020)	3640	↓	↓	3.50 (0.138)	↓	↓	X		
E2L-45	1.0 (0.040)	3715	↓	↓	3.25 (0.128)	↓	↓	X		
D2L-45	1.0 (0.040)	3708	↓	↓	3.25 (0.128)	0.4 (0.015)	138 (20)	X		
H2L-45	0.25 (0.010)	3700	120	3.18	3.45 (0.136)	0.8 (0.030)	69 (10)	X		
F3-3	0.25 (0.010)	3637	↓	(0.126)	↓	↓	↓	X		
A2-3	0.5 (0.020)	3629	↓	↓	↓	↓	↓	X		
B7-3	0.5 (0.020)	3640	↓	↓	↓	↓	↓	X		
E2L-46	1.0 (0.040)	3715	↓	↓	3.30 (0.130)	↓	↓	X		
D2L-46	1.0 (0.040)	3708	↓	↓	3.30 (0.130)	↓	↓	X		
H2L-52	0.25 (0.010)	3700	80	3.97	4.70 (0.185)	0.5 (0.020)	69 (10)	X	X	
F3-4	0.25 (0.010)	3637	↓	(0.157)	4.70 (0.185)	0.8 (0.030)	↓	X	X	
A2-4	0.5 (0.020)	3629	↓	↓	4.62 (0.182)	↓	↓	X		
B7-4	0.5 (0.020)	3640	↓	↓	4.62 (0.182)	↓	↓	X		
E2L-47	1.0 (0.040)	3715	↓	↓	4.27 (0.168)	↓	↓	X		
D2L-47	1.0 (0.040)	3708	↓	↓	4.27 (0.168)	0.5 (0.020)	↓	X		
H2L-53	0.25 (0.010)	3700	100	3.97	4.50 (0.177)	0.8 (0.030)	69 (10)			X
F3-5	0.25 (0.010)	3637	↓	(0.157)	4.50 (0.177)	0.8 (0.030)	69 (10)			X
A2-5	0.5 (0.020)	3629	↓	↓	4.37 (0.172)	0.5 (0.020)	138 (20)	X		
B7-5	0.5 (0.020)	3640	↓	↓	4.37 (0.172)	↓	↓	X		
E2L-48	1.0 (0.040)	3715	↓	↓	4.11 (0.162)	↓	↓	X		
D2L-48	1.0 (0.040)	3708	↓	↓	4.11 (0.162)	↓	↓			X
H2L-54	0.25 (0.010)	3700	120	3.97	4.29 (0.169)	0.5 (0.020)	69 (10)	X		
F3-6	0.25 (0.010)	3637	↓	(0.157)	↓	↓	↓	X		
A2-6	0.5 (0.020)	3629	↓	↓	↓	↓	↓	X		
B7-6	0.5 (0.020)	3640	↓	↓	↓	↓	↓	X		
E2L-49	1.0 (0.040)	3715	↓	↓	4.09 (0.161)	↓	138 (20)	X		
D2L-49	1.0 (0.040)	3708	↓	↓	4.09 (0.161)	↓	138 (20)	X		
H2L-49	0.25 (0.010)	3700	80	4.76	5.82 (0.229)	0.5 (0.020)	69 (10)	X	X	
F3-7	0.25 (0.010)	3637	↓	(0.188)	5.82 (0.229)	↓	↓	X	X	
A2-7	0.5 (0.020)	3629	↓	↓	5.61 (0.221)	↓	↓	X	X	
B7-7	0.5 (0.020)	3640	↓	↓	5.61 (0.221)	↓	↓	X	X	
E2L-50	1.0 (0.040)	3715	↓	↓	5.21 (0.205)	↓	↓	X		
D2L-50	1.0 (0.040)	3708	↓	↓	5.18 (0.204)	↓	138 (20)	X		
H2L-50	0.25 (0.010)	3700	100	4.76	5.41 (0.213)	0.5 (0.020)	69 (10)	X	X	
F3-8	0.25 (0.010)	3637	↓	(0.188)	↓	0.5 (0.020)	↓	X	X	
A2-8	0.5 (0.020)	3629	↓	↓	↓	0.8 (0.030)	↓	X		
B7-8	0.5 (0.020)	3640	↓	↓	↓	0.8 (0.030)	↓	X		
E2L-51	1.0 (0.040)	3715	↓	↓	5.18 (0.204)	0.5 (0.020)	↓	X		
D2L-51	1.0 (0.040)	3708	↓	↓	5.18 (0.204)	0.5 (0.020)	138 (20)	X		
H2L-51	0.25 (0.010)	3700	120	4.76	5.18 (0.204)	1.0 (0.040)	69 (10)	X	X	
F3-9	0.25 (0.010)	3637	↓	(0.188)	↓	1.0 (0.040)	↓	X	X	
A2-9	0.5 (0.020)	3629	↓	↓	↓	0.8 (0.030)	↓	X		
B7-9	0.5 (0.020)	3640	↓	↓	↓	0.8 (0.030)	↓	X		
E2L-52	1.0 (0.040)	3715	↓	↓	5.05 (0.199)	0.5 (0.020)	138 (20)	X		
D2L-52	1.0 (0.040)	3708	↓	↓	5.05 (0.199)	0.5 (0.020)	138 (20)	X		

† Ram height = distance ram surface is below die face. Tests conducted at room temperature.

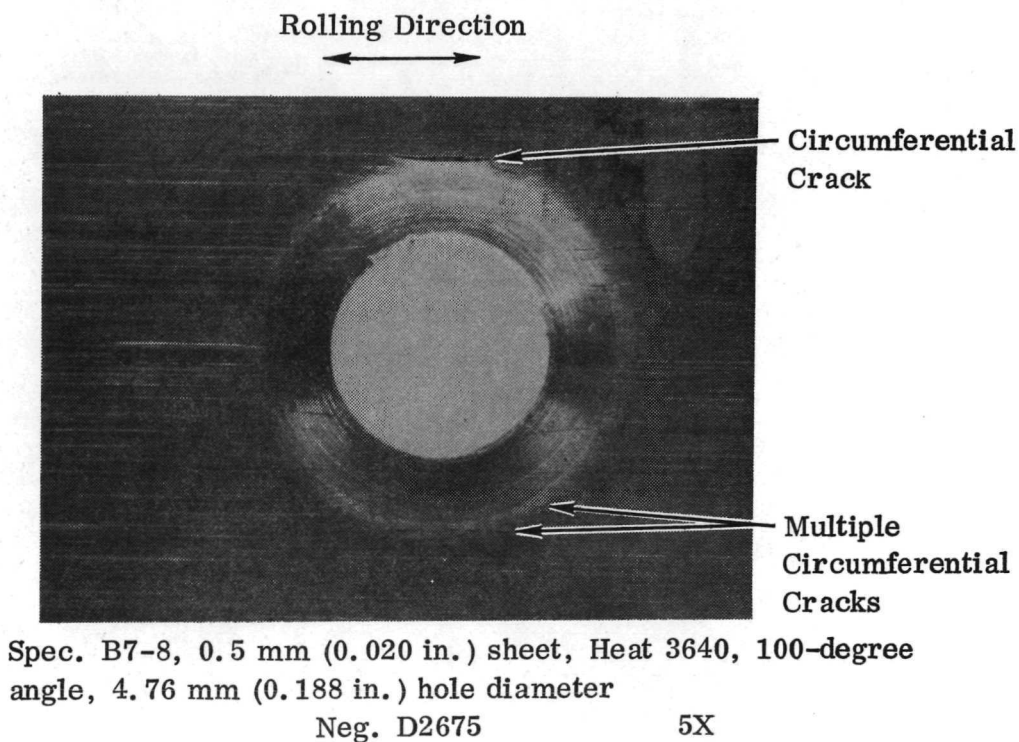
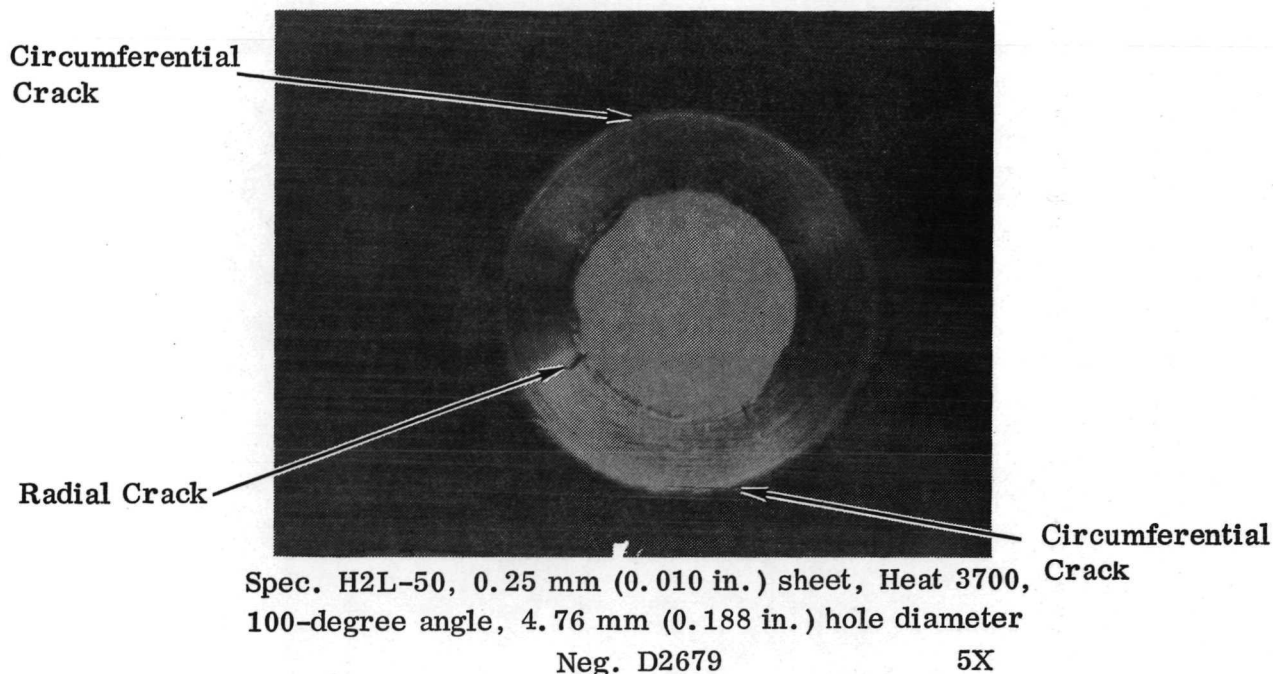
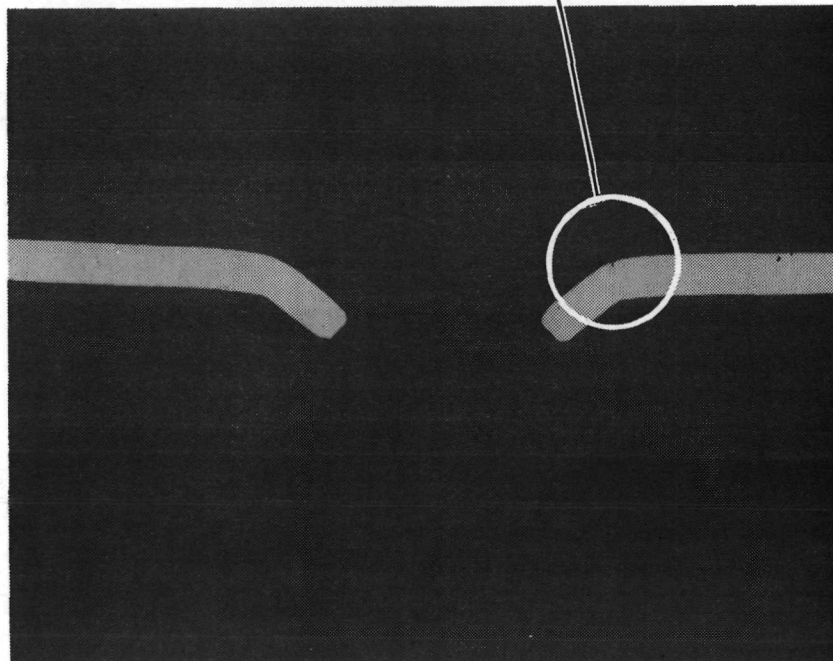


Figure 40. Typical Circumferential and Radial Cracks in Dimples in Recrystallized TD-NiCr Sheet Formed with Ram Coin Dimpling Dies



Neg. D2814

100X



Neg. D2789

5X

Figure 41. Microstructure of a Dimple Containing Circumferential Cracks in 1.0 mm (0.040 in.) recrystallized sheet - Heat 3708 (Code D2), Spec. D26-51, 100-degree dimple angle, 4.76 mm (0.188 in.)

the easiest-to-form 120-degree angle dimpling tools. The material to be dimpled was first submerged in a Dewar flask of liquid nitrogen, held submerged until all bubbling action stopped, and then quickly dimpled before much temperature rise could occur. These tests resulted in no apparent reduction in the amount or type of cracking as compared to the room temperature tests. The use of cryogenic cooled dimpling dies would be necessary to fully explore the effects of cryogenic dimpling.

Additional tests were conducted to evaluate dimpling of recrystallized material at room temperature using the 100-degree angle tooling fabricated for hot dimpling. The spot welder was used to apply the forming pressure to the tool set. Test results revealed circumferential or radial cracks in dimples for eight out of the nine test conditions investigated.

A more successful investigation involved modification of the Zephyr Ram Coin dimpling dies to increase the forming radius. The circumferential cracking is believed to be the result of the dimpling dies having a forming radius smaller than the minimum bend radius (MBR) for forming TD-NiCr (see Figure 41). The die radius for several sets of dimpling tools was measured with an optical comparator using a plastic cast of the die. The radius was found to be 0.05 mm (0.002 in.) for each die set.

To verify that the forming radius on the standard Ram Coin dimpling dies is too sharp for TD-NiCr, three sets of 100-degree dimpling dies were reground to a radius of 0.5 mm (0.020 in.). Blanks of all three sheet thicknesses were dimpled with the modified dies.

Results are presented in Table 18 for dimpling tests performed with the dimpling dies machined to an 0.5 mm (0.020 in.) forming radius. Six of the 18 test conditions had circumferential cracks. Results for the same 18 test conditions with the standard dies 0.05 mm (0.002 in.) forming radius had previously shown 15 test conditions with circumferential cracks. It is believed that a further increase in forming radius on the dies would eliminate the circumferential cracking problem. Occurrence of radial cracks was not improved by the modified dies. Since the radial cracks occurred primarily in the thinnest material, the use of a stainless steel caul sheet may alleviate this problem.

The results to date have demonstrated that modification of the Ram-Coin dimpling dies will permit satisfactory dimpling for most of the dimple configurations and material gages investigated.

Comparison was made of dimpling test results obtained with standard and modified Ram Coin dimpling dies with theoretical forming limits in Figures 42, 43 and 44. The theoretical forming limits are based on tensile

Table 18. Dimpling Test Results for Recrystallized TD-NiCr
Sheet with Dies Modified to a 0.5 mm
(0.020 in.) Forming Radius

Specimen No.	Material Thickness mm (in.)	Heat Number	Dimple Angle (degrees)	Starting Hole Diameter mm (in.)	Final Hole Diameter mm (in.)	Ram Height mm (in.)	Ram Pressure N/m ² (psi)	Results		
								Circumferential Cracks	Radial Cracks	No Cracks
H21-50	0.25 (0.010)	3700	100	4.76 (0.188)	5.41 (0.213)	0.51 (0.020)	6.9 (10)	X	X	
F3-8	0.25 (0.010)	3637	↓	↓	↓	↓	↓	X	X	
A2-8	0.5 (0.020)	3629								X
B7-8	0.5 (0.020)	3640								X
E2L-51	1.0 (0.040)	3715			5.18 (0.204)					X
D2L-51	1.0 (0.040)	3708	↓	↓	5.18 (0.204)	↓	13.8 (20)			X
H2L-53	0.25 (0.010)	3700	100	3.97 (0.157)	4.57 (0.180)	0.76 (0.030)	6.9 (10)	X	X	
F3-5	0.25 (0.010)	3637	↓	↓	4.57 (0.180)	0.76 (0.030)	6.9 (10)	X		
A2-5	0.5 (0.020)	3629			4.50 (0.177)	0.51 (0.020)	13.8 (20)	X		
B7-5	0.5 (0.020)	3640			4.50 (0.177)	↓	↓	X		X
E2L-48	1.0 (0.040)	3715	↓	↓	4.11 (0.162)	↓	↓			X
D2L-48	1.0 (0.040)	3708	↓	↓	4.11 (0.162)	↓	↓			
H2L-44	0.25 (0.010)	3700	100	3.18 (0.126)	3.66 (0.144)	0.64 (0.025)	6.9 (10)			X
F3-2	0.25 (0.010)	3637	↓	↓	3.66 (0.144)	0.64 (0.025)	↓			X
A2-2	0.5 (0.020)	3629			3.56 (0.140)	0.51 (0.020)				X
B7-2	0.5 (0.020)	3640			3.56 (0.140)	0.76 (0.030)				X
E2L-45	1.0 (0.040)	3715	↓	↓	3.25 (0.128)	0.51 (0.020)	↓			X
E2L-45	1.0 (0.040)	3708	↓	↓	3.25 (0.128)	0.51 (0.020)	↓			X

Ram height = distance ram surface is below die face. Tests conducted at room temperature.

properties using strain for 5.08 cm (2 in.) gage length for each heat of material, and represent the limits only for radial cracking. However, the experimental data are plotted to indicate failure due to both radial and circumferential cracking. Circumferential cracking is a result of bending, which is strongly affected by the coining action and material thickness. The material will conform to the small radius (R) of the die, and fail by circumferential cracking if R/t is less than that for brake forming the same material.

The theoretical and actual dimpling limits for the second heat of material for each gage was very similar to that of the heats shown.

Microstructure. - Metallographic examinations were performed on representative specimens in the as-formed condition and after annealing for 2 hours at 1177C (2150F) in dry hydrogen. These included three sheet thicknesses, three hole diameters, and three dimple configurations. Dimples with and without visible cracks were included in the studies. Approximately half of the dimples examined were made with the modified dies.

The examinations disclosed deformation bands in the bend area and adjacent to the pilot hole (see Figure 45). The annealing treatment resulted in recrystallization of small size grains in the severely deformed areas (see Figure 46). The presence of fine grain recrystallization indicates that the critical deformation limit has been exceeded (Ref. 13, 14). The severity of the deformation bands and fine grain recrystallization was greatest for the

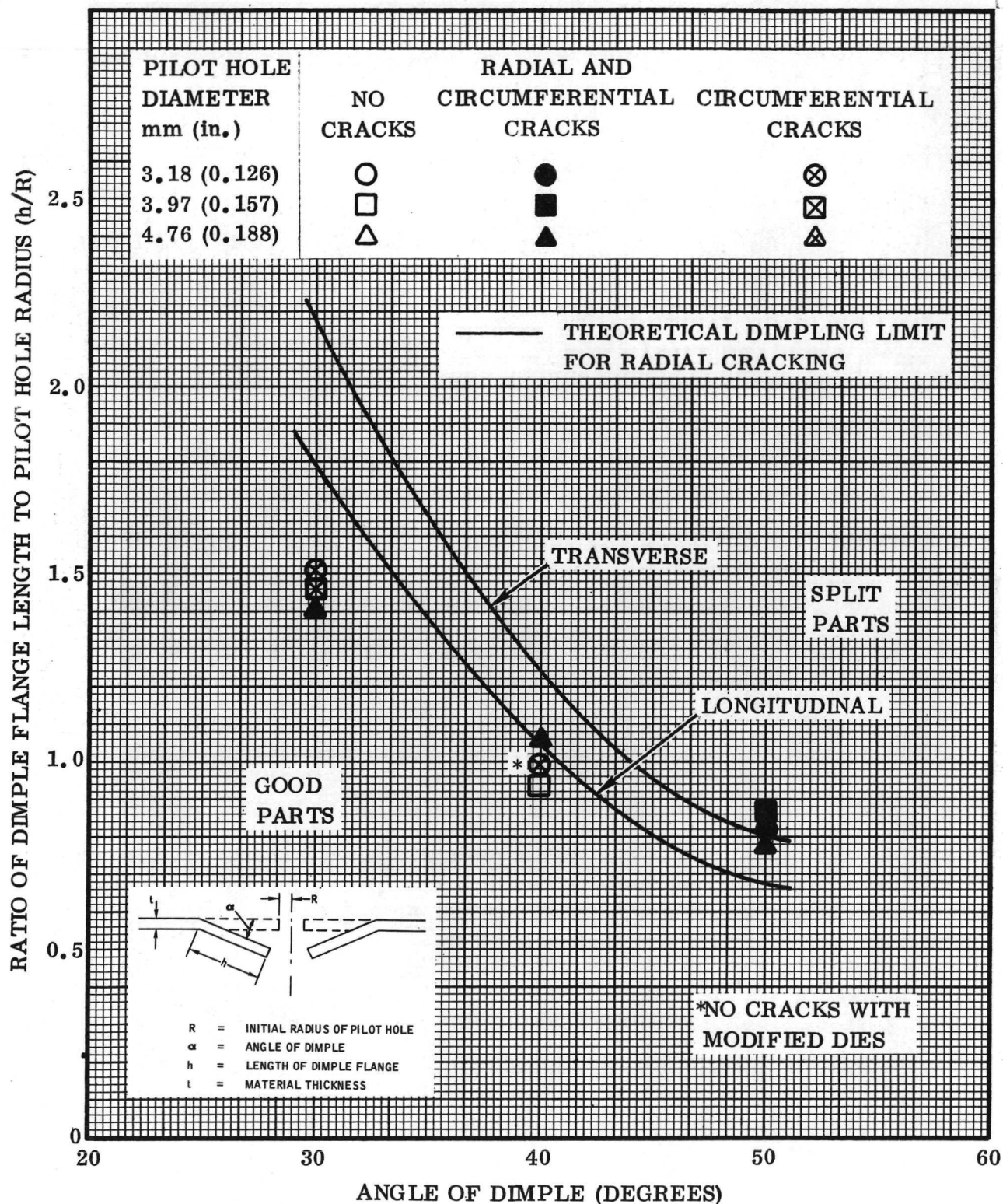


Figure 42. Comparison of Dimpling Test Results with Theoretical Dimpling Limits for 0.25 mm (0.010 in.) Recrystallized TD-NiCr Sheet - Heat 3700 (Code H)

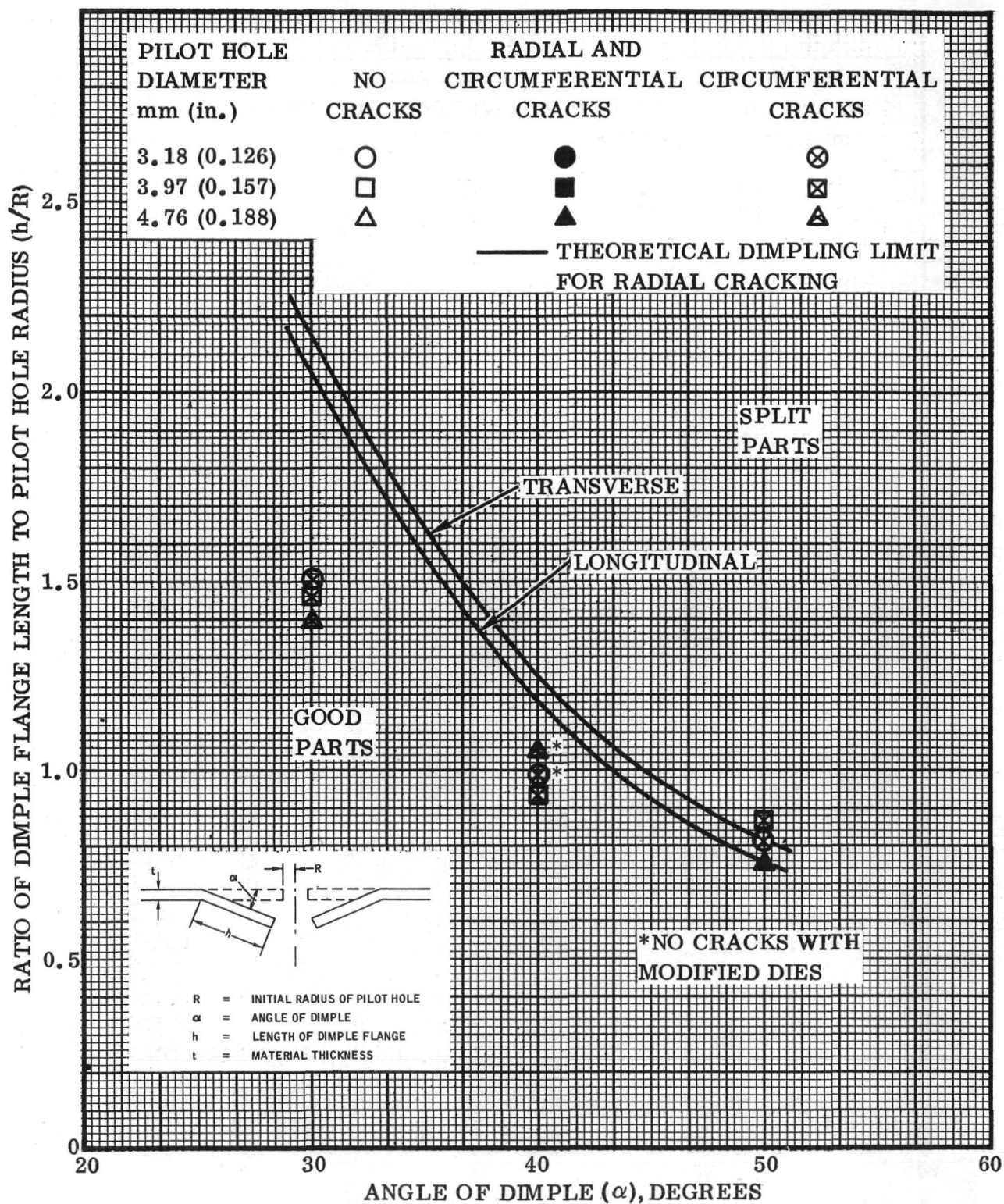


Figure 43. Comparison of Dimpling Test Results with Theoretical Dimpling Limits for 0.5 mm (0.020 in.) Recrystallized TD-NiCr Sheet - Heat 3640 (Code A)

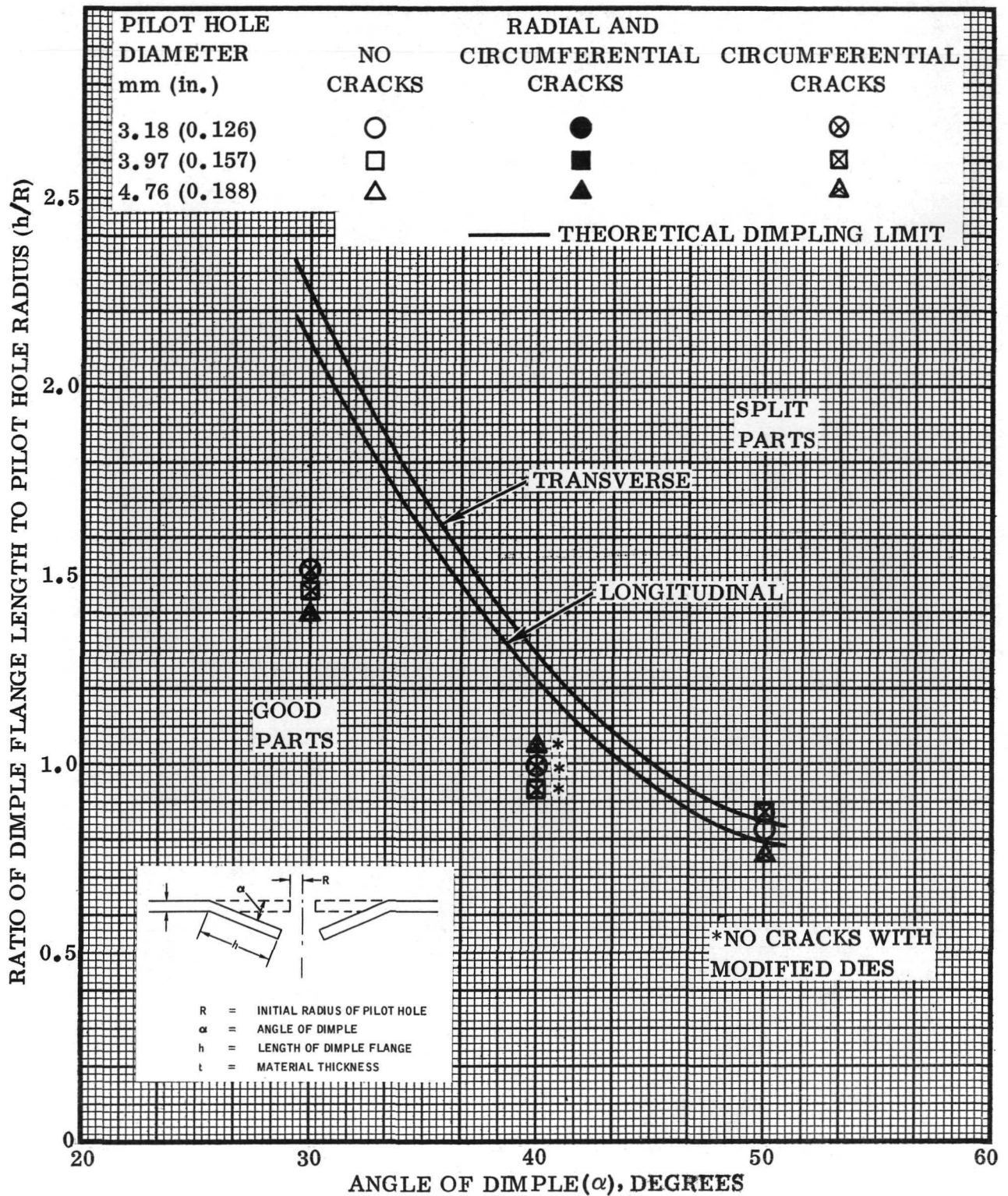
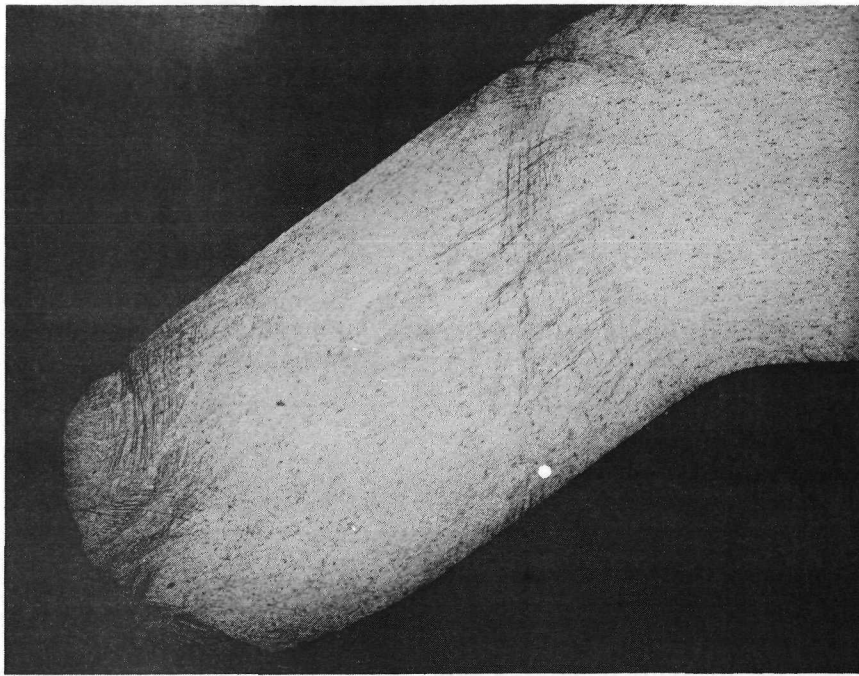


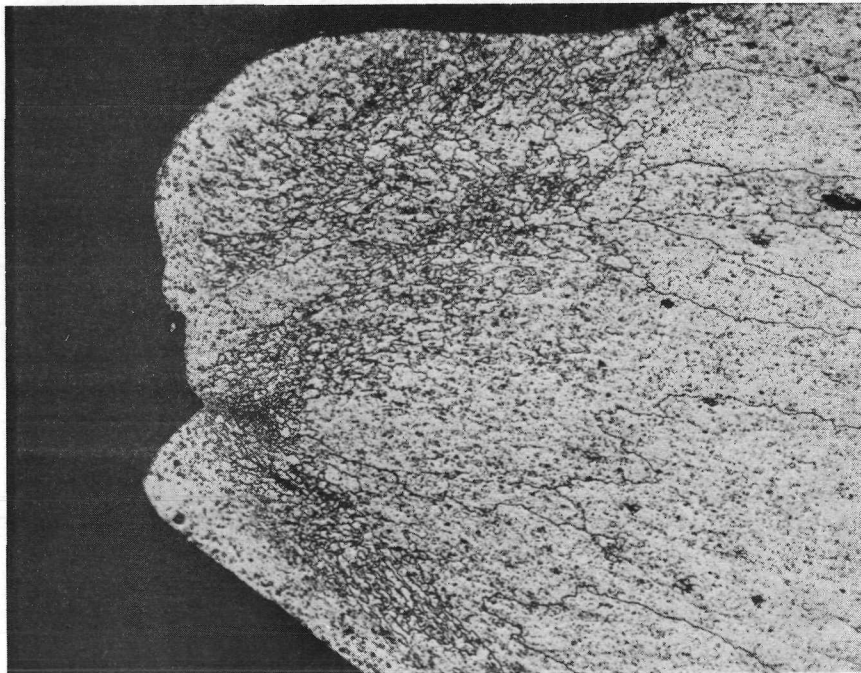
Figure 44. Comparison of Dimpling Test Results with Theoretical Dimpling Limits for 1.0 mm (0.040 in.) Recrystallized TD-NiCr Sheet - Heat 3714 (Code E)



Neg. D3757

50X

Figure 45. Microstructure of As-Formed Dimple in 1.0 mm (0.040 in.) Recrystallized TD-NiCr Sheet - Heat 3715 (Code E), Modified 100° Die, 3.97 mm (0.157 in.) Hole Diameter



Neg. D3758

250X

Figure 46. Microstructure Adjacent to Hole of Annealed Dimple in 0.5 mm (0.020 in.) Recrystallized Sheet - Heat 3640 (Code B), Modified 100° Die, 3.97 mm (0.157 in.) Hole Diameter

80-degree dimple configuration and least for the 120-degree dimple configuration. In a few instances, small surface cracks were present that were not observed during visual examination of the dimples. These were shallow cracks transverse to the rolling direction, and generally initiated at the bottom of deep scratches from the belt polishing operation. Since further development of dimpling dies is required to optimize dimpling of recrystallized TD-NiCr, no attempt was made to assess the overall effects of the deformation bands, small grain recrystallization, and small surface cracks on potential service performance or to adjust forming limits indicated in Figures 42 to 44.

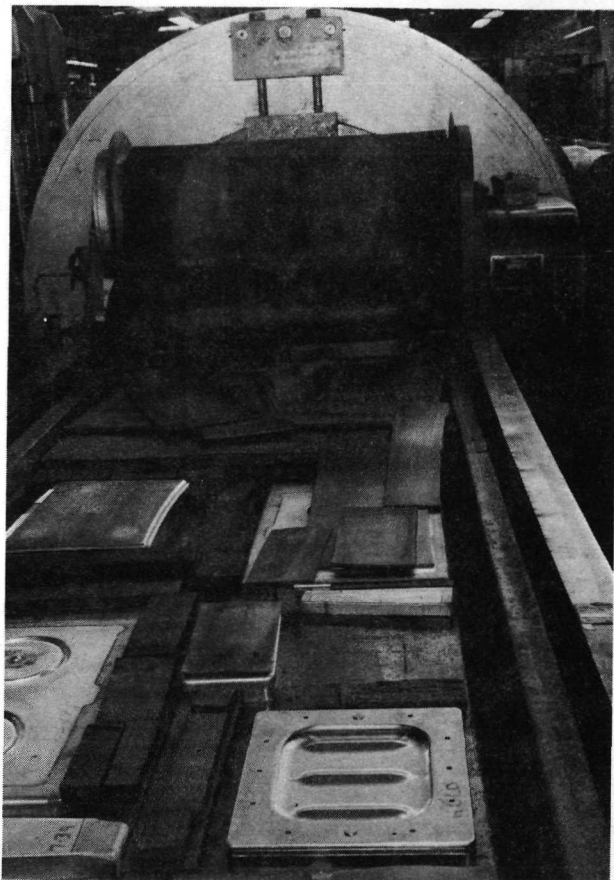
Beading

The rubber press and drop hammer beading processes are used to form beads in sheet metal for stiffening. Rubber press beading is the most commonly used process, but is usually restricted to the lower strength materials because of the high rubber pressure required to produce parts of good definition. Drop hammer beading also employs the "trapped rubber" principle but uses repeated blows of a drop hammer ram. This process imparts greater pressures and achieves better bead definition due to the greater strain the metal part undergoes during forming.

Previous work at Convair Aerospace (Ref. 15, 16, 17) resulted in development of rubber press techniques for fabrication of bead-stiffened TD-NiCr heat shield panels. These studies showed that at low pressures [$<20.7 \text{ MN/m}^2$ (3000 psi)] it was not possible to obtain the required definition of the flat land area between beads needed to join the stiffener to a skin, and severe buckling occurred along the ends of the beads. It became necessary to increase the pressure and to introduce methods for clamping the material to prevent buckling during forming. Panel splitting also was a major problem, solved only by forming with maximum strain in the longitudinal direction, use of a caul sheet for gages less than 0.5 mm (0.020 in.), and using an in-process anneal before final forming stages.

Based on past successful experience at Convair Aerospace, the rubber press process was selected for evaluation of beading of recrystallized TD-NiCr sheet. Although the Woods' theoretical forming limits for rubber press beading were established for 20.7 MN/m^2 (3000 psi) maximum pressure, the studies reported here used higher pressures to obtain improved bead definition.

Beading Limits. - Evaluation of rubber press beading of recrystallized TD-NiCr sheet was performed with a 69 MN/m^2 (10,000 psi) Verson-Wheelon press shown in Figure 47. Tools were designed and fabricated with the



Neg. 125840B

Figure 47. Verson Wheelon Rubber Press with a TD-NiCr Beaded Panel Shown on the Press Table

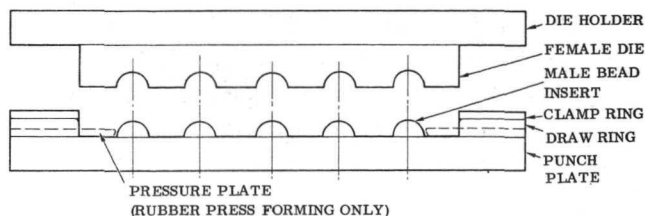
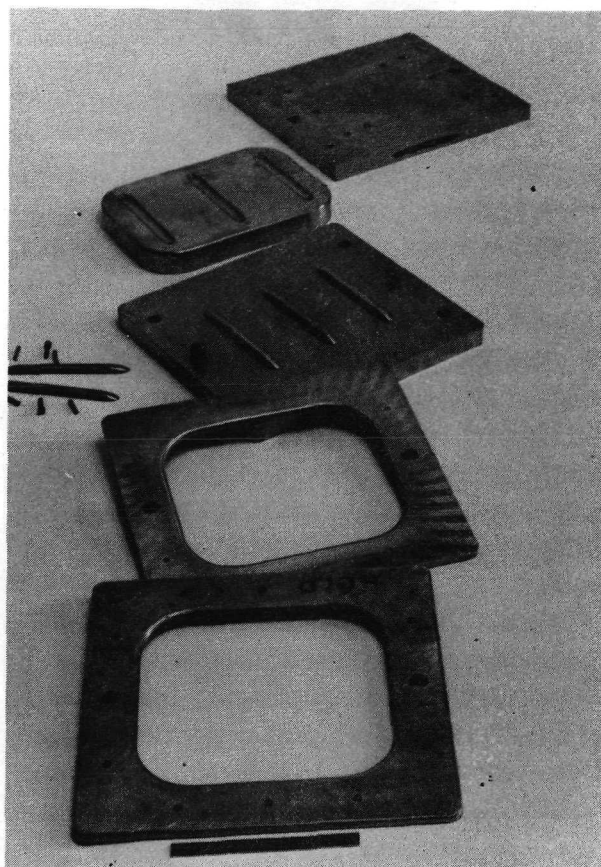


Figure 48. Sketch of Beading Die Configuration

capability for both room temperature rubber press beading of recrystallized sheet and elevated temperature closed die beading of unrecrystallized sheet. Figure 48 is a sketch of the beading die configuration. The tools consist of two complete sets of matched male and female bead dies. One set of dies was designed for forming an 0.76 cm (0.3 in.) radius bead, while the other set of dies will form a 1.27 cm (0.5 in.) radius bead. The beading die was made from Type 316 stainless steel. The tools are designed to form R/L ratios (bead radius to bead spacing) of 0.25, 0.188, 0.125, 0.094 and 0.075. The male die for each die set contains five male bead inserts that are doweled and bolted to a punch plate. The inserts are spaced 5.1 cm (2 in.) apart for the 1.27 cm (0.5 in.) radius bead and 4.06 cm (1.6 in.) apart for the 0.76 cm (0.3 in.) radius bead. The second and fourth beads can be removed from the plate to obtain a three-bead array with a spacing of 10.16 cm (4.0 in.) and 8.13 cm (3.2 in.) respectively for the two bead sizes. Figure 49 shows a set of beading tools for forming panels with 0.76 cm (0.3 in.) radius beads.

The male die for each set is matched to female bead die plates containing five cavities and three cavities. Generally, for room temperature forming of the recrystallized material, only the male die is used. The matched die sets were designed to be mounted on heated platens for hot forming the unrecrystallized material.



Neg. 125835B

Figure 49. Set of Beading Tools for Forming 0.76 cm (0.3 in.) Radius Beads (The female bead die and die holder at the top of the photograph are designed for use with the male tooling for hot forming unrecrystallized TD-NiCr)

For the rubber press preforming operation with the male die, the blank is first placed on the draw ring and clamped. It is then formed with a pressure of 13.8 MN/m^2 (2000 psi) to draw the material down over the beads. The clamp ring and draw ring are then removed and a pressure plate placed over the partially formed panel. The pressure plate is in the form of a picture frame that has a small clearance with the beaded portion of the panel. The purpose of the pressure plate is to minimize buckling and wrinkling of the panel (Ref. 17). The final beading operation is performed at 34.5 MN/m^2 (5000 psi) pressure. The lubricant used for all beading tests was Oakite Special Drawing Compound, a soap and fatty oil paste.

The beading evaluation of recrystallized sheet was performed on the following combinations of bead radii, bead spacing and bead arrays:

<u>Bead Radius, R</u> mm (in.)	<u>Bead Spacing, L</u> mm (in.)	<u>Bead Array</u>
0.76 (0.3)	4.06 (1.6)	Five bead
0.76 (0.3)	8.13 (3.2)	Three bead
0.76 (0.3)	10.16 (4.0)	Three bead
1.27 (0.5)	5.08 (2.0)	Five bead
1.27 (0.5)	10.16 (4.0)	Three bead

In addition to determining the beading limits of TD-NiCr sheet and comparing these with the theoretical forming limits, investigations were conducted to evaluate the effects of the following factors on the forming limits.

- a. Use of caul sheet.
- b. Preforming on male die.
- c. Preforming on female die.
- d. Intermediate annealing.

The beading tests have shown that use of a caul sheet is essential when forming 0.25 mm (0.010 in.) sheet. At 34.5 MN/m^2 (5000 psi) good parts could be made using a caul sheet, whereas all test blanks formed without the caul sheet fractured. Beading tests were conducted to evaluate the use of 0.25, 0.4 and 0.5 mm (0.010, 0.016 and 0.020 in.) stainless steel caul sheets between the die and the TD-NiCr blank. Two formed parts with two different gages of stainless steel sheets are shown in Figure 50. The part on the right was formed with an 0.25 mm (0.010 in.) caul sheet, and fractures can be seen on the outside of both outer beads. The part on the left in Figure 50 did not fracture; the same pressure was used for this part, but with an 0.5 mm (0.020 in.) caul sheet. Stainless steel caul sheets of 0.4 mm (0.016 in.) thickness were also found satisfactory, and were used extensively in beading studies of 0.25 mm (0.010 in.) TD-NiCr sheet.

Initial investigations on preforming were conducted with the male die, which resulted in frequent premature splitting between the draw ring and the outer beads. Additional tests were conducted with pressures as low as 3.45 MN/m^2 (500 psi) with similar results. The cause of the premature splitting was attributed to insufficient clearance between the draw ring and the outer bead, which imparted severe local strains. This problem could be solved by increasing the clearance, but this would require modification of the draw ring and clamp as well as a significant increase in the size of the TD-NiCr



Neg. 125836B

Figure 50. Partially Formed 0.25 mm (0.010 in.) TD-NiCr Beaded Panels and Stainless Steel Caul Sheets After Preform Operation (The annealed stainless steel caul sheets are shown above the TD-NiCr blanks. The blank on the right was formed with an 0.25 mm (0.010 in.) caul sheet and fractured. The blank on the left was formed with an 0.5 mm (0.020 in.) caul sheet and did not fracture.

blank. For this reason, the female die, which had been fabricated for forming of unrecrystallized sheet, was employed for the preforming operation. The female die eliminated the problem of premature cracking at the edge of the outer beads. However, the test results showed that with most bead configurations the preform operation did not improve the formability of the panel with respect to cracking. The major advantage of the preform operation was to minimize buckling in the blank. This was especially true with the 0.25 mm (0.010 in.) material.

Intermediate annealing was investigated for partially formed parts that were preformed using both male and female dies. The annealing treatment was 2 hours at 1093C (2000F) in dry hydrogen. The annealed parts were given a final strike on the male dies at 34.5 MN/m^2 (5000 psi) pressure. The intermediate anneal did not provide any significant improvement with respect to cracking for the bead configurations investigated. The major

advantage of intermediate annealing was better bead definition and reduction in buckling.

Results of the final series of beading tests are listed in Table 19 and include preforming steps, intermediate anneals, and tests conducted without either preforming or intermediate anneals. The primary evaluation criteria were splitting (cracks) and insufficient pressure to form a minimum flat of 1.27 cm (0.5 in.) between beads. Additional formability data including bead radius, free bead radius, bead depth, and severe buckling were measured and/or noted. Typical good parts are shown in Figure 51 and a typical cracked part is shown in Figure 52.

The maximum forming pressure was set at 34.5 MN/m^2 (5000 psi) due to a leakage problem on the press at the time the tests were conducted. Although this pressure is considerably lower than the 69 MN/m^2 (10,000 psi) maximum potential pressure on the press, it was believed that the 34.5 MN/m^2 (5,000 psi) was sufficiently high to provide formability data for TD-NiCr in the 0.25 mm (0.010 in.) and 0.5 mm (0.020 in.) sheet thicknesses. This pressure is also reasonable compared to the 20.7 MN/m^2 (3000 psi) forming pressure used for the theoretical formability data.

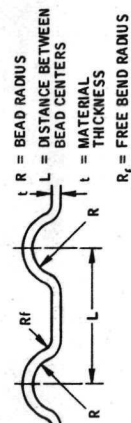
Heat 3637 (Code F) and 3700 (Code H) were used for beading evaluation of 0.25 mm (0.010 in.) sheet, and Heats 3629 (Code A) and 3640 (Code B) for the 0.5 mm (0.020 in.) tests. Heat 3507 (Code R) was used to fill in certain data points where insufficient material from Heat 3629 (Code A) was available.

Comparison of actual forming data with the theoretical forming limits for rubber press beading is shown in Figures 53 and 54. Although the predicted limits indicated reasonably good formability for the transverse direction, the actual formability was poor for this orientation.

Actual formability in the longitudinal direction agrees fairly well with the predicted forming limits for Heat 3637 (Figure 53), but somewhat lower formability than predicted is evident for Heat 3629. The theoretical forming limits were almost identical for the two heats of each gage; however, the actual formability in the longitudinal direction for the 0.25 mm (0.010 in.) sheet from Heat 3700 was poorer than Heat 3637 (see Table 19). The actual formability was the same for the two heats of 0.5 mm (0.020 in.) material. Better formability for the longitudinal than for the transverse orientation observed for beading is in agreement with results for the other four forming processes.

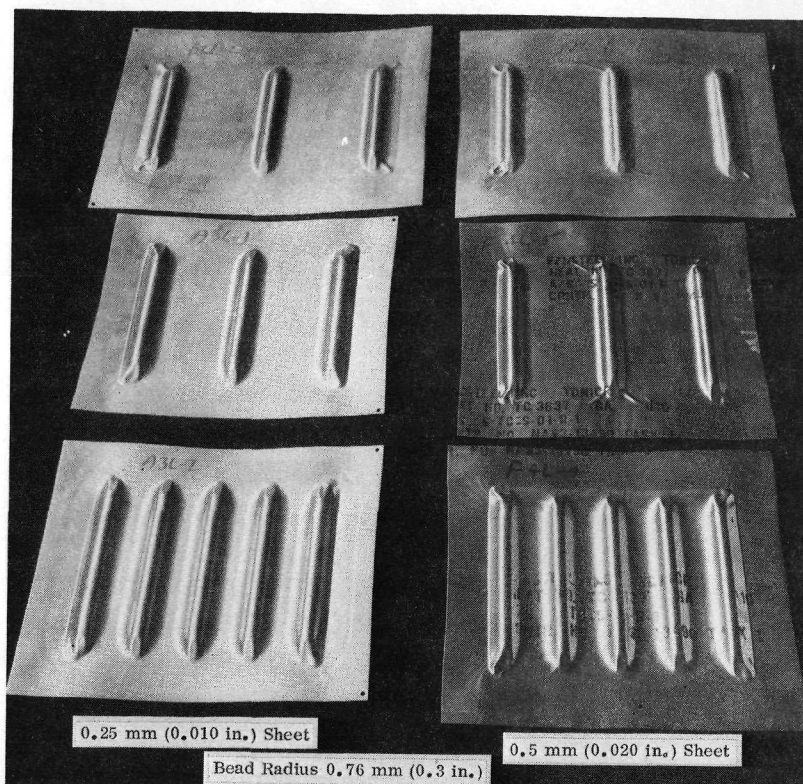
Table 19. Beading Tests of Recrystallized TD-NiCr Sheet

Heat No.	Spec. No.	Matl. Gage mm (in.)	(1) Grain Direc.	Bead Configuration Radius cm (in.) Spacing cm (in.)	Caul Sheet (2)	Pre-form (3)	(4) Anneal	Bead Depth cm (in.)	Bead Radius R cm (in.)	Free-Bend R_f cm (in.)	Width of flat cm (in.)	(5) Rating	Remarks
3637 Code F	F4L-4	0.25	L	0.76 (0.3)	yes	no	no	-	-	-	-	C	
	F4L-2	(0.010)		4.06 (1.6)	yes	yes-F	yes-F	-	-	-	-	C	
	F4L-6			4.06 (1.6)	yes	yes	yes	-	-	-	-	C	
	F4L-1			8.13 (3.2)	no	no	no	-	-	-	-	C	
	F4L-5				yes	yes	yes-M	0.74 (0.29)	0.79 (0.31)	1.43 (0.56)	1.27 (0.5)	Good	severe buckling, met. exam.
	F6T-4		T		yes	no	no	0.69 (0.27)	0.87 (0.34)	1.27 (0.5)	-	C	
	F6T-3		T		yes	yes	yes-F	-	-	-	-	C	
	F8L-1		L		yes	yes	yes-M	0.74 (0.29)	0.79 (0.31)	1.59 (0.63)	1.27 (0.5)	Good	met. exam.
3700 Code H	F8L-1		T		yes	yes	yes-M	-	-	-	-	C	cracked in preform operation
	F5L-3		L		yes	-	-	-	-	-	-	C	
	F5L-1		L		yes	yes	yes-F	-	-	-	-	C	
	H6L-6	0.25	L	0.76 (0.3)	no	no	no	-	-	-	-	C	
	H6L-7	(0.010)		8.13 (3.2)	yes	yes	yes-M	0.71 (0.28)	0.87 (0.34)	1.75 (0.68)	1.27 (0.5)	Good	met. exam. possible surface flaws
	H5L-3				yes	yes	yes-M	-	-	-	-	C	
	H6T-1		T		yes	yes	yes-M	-	-	-	-	C	
	H5L-2		L		yes	yes	yes-F	-	-	-	-	C	
3629 Code A	H5L-1		L		yes	yes	yes-F	-	-	-	-	C	
	A3L-3	0.5	L	0.76 (0.3)	no	no	no	0.76 (0.30)	0.79 (0.31)	1.9 (0.75)	0.47 (0.19)	IP	met. exam.
	A3L-2	(0.020)		4.06 (1.6)	yes	yes	yes-F	0.71 (0.28)	0.79 (0.31)	1.75 (0.68)	0.79 (0.31)	IP	met. exam.
	A3L-1			8.13 (3.2)	yes	yes	yes-M	0.74 (0.29)	0.79 (0.31)	1.43 (0.56)	1.27 (0.5)	Good	cracked in preform operation
	A3T-2		T		-	-	-	-	-	-	-	C	cracked in preform operation
	A3T-1		T		-	-	-	-	-	-	-	C	
	A3L-4		L		yes	yes	yes-F	-	-	-	-	C	
	A3L-3		L		yes	yes	yes-F	-	-	-	-	C	
3507 Code R	R1L-3	0.5	L	0.76 (0.3)	no	yes	yes-M	0.69 (0.27)	0.79 (0.31)	1.59 (0.63)	1.27 (0.5)	Good	cracked in preform operation
	R1L-2	(0.020)		4.06 (1.6)	no	-	-	-	-	-	-	C	
	R2L-3			5.08 (2.0)	yes	no	no	1.17 (0.46)	1.27 (0.5)	2.54 (1.0)	1.27 (0.5)	Good	severe buckling
	R2L-2		L		yes	yes	yes-M	0.74 (0.29)	0.79 (0.31)	1.9 (0.75)	0.63 (0.25)	IP	
	B9L-2	0.5	L	0.76 (0.3)	no	no	no	-	-	-	-	C	
	B9L-1	(0.020)	T	4.06 (1.6)	yes	yes	yes-M	0.74 (0.29)	0.79 (0.31)	1.43 (0.56)	1.27 (0.5)	Good	met. exam.
	B9L-3		L		yes	yes	yes-M	0.71 (0.28)	0.79 (0.31)	1.59 (0.63)	1.27 (0.5)	Good	met. exam.
	B9T-1		T		no	no	no	0.76 (0.30)	0.87 (0.34)	2.38 (0.94)	1.27 (0.5)	Good	met. exam.
3640 Code B	B9T-3		T		yes	yes	yes-M	0.76 (0.30)	0.87 (0.34)	2.06 (0.81)	1.27 (0.5)	Good	met. exam.
	B2L-2		L		yes	yes	yes-M	0.74 (0.29)	0.79 (0.31)	1.27 (0.5)	1.27 (0.5)	Good	
	B2L-1		L		yes	yes	yes-F	-	-	-	-	C	
	B2L-3		L		yes	yes	yes-F	-	-	-	-	C	
	B2L-2		L		yes	yes	yes-F	-	-	-	-	C	
	B2L-1		L		yes	yes	yes-F	-	-	-	-	C	
	B2L-3		L		yes	yes	yes-F	-	-	-	-	C	
	B2L-1		L		yes	yes	yes-F	-	-	-	-	C	



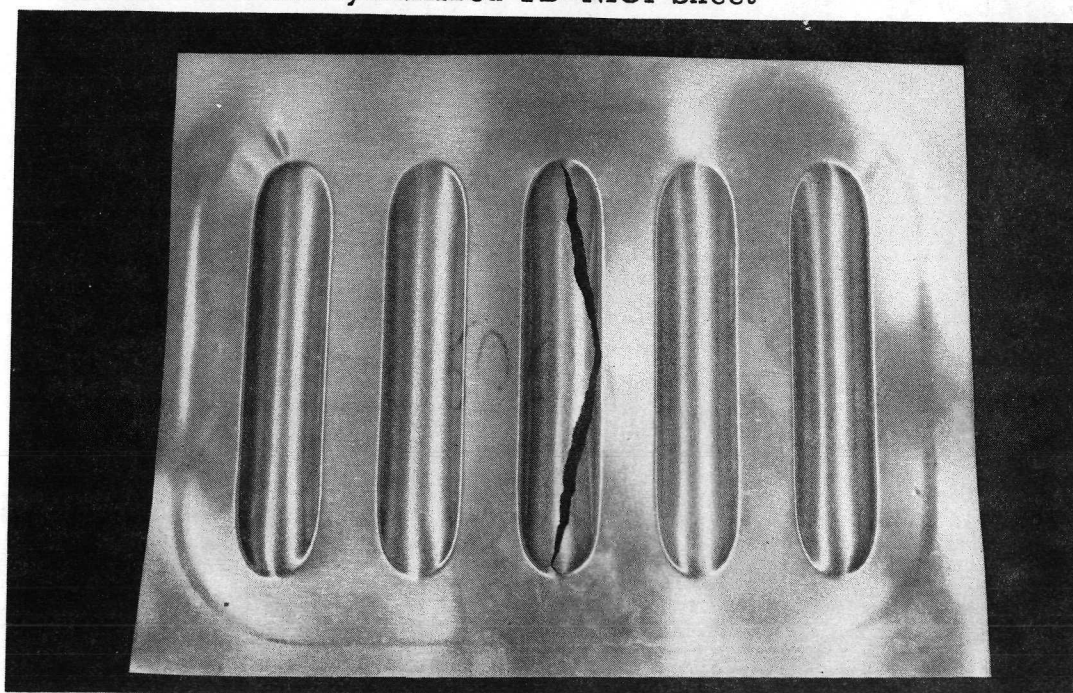
- (1) L = longitudinal; T = transverse
 (2) 0.41 mm (0.016 in.) annealed stainless steel
 (3) Preformed @ 13.8 MN/m² (2000 psi) in female die
 (4) Annealed @ 1093C (2000F) for 2 hrs. in dry hydrogen
 F - After preform on female die at 13.8 MN/m² (2000 psi)
 M - After preform on female die at 13.8 MN/m² (2000 psi) plus one strike on male die at 13.8 MN/m² (2000 psi)
 (5) Good - good parts with 1.27 mm (0.5 in.) minimum flat between beads
 IP = insufficient pressure
 C = cracks

All tests conducted on Verson Wheelon rubber press @ 34.5 MN/m² (5000 psi) except as noted for operations prior to anneal.



Neg. 131303B

Figure 51. Typical Rubber Press Beaded Test Panels of Recrystallized TD-NiCr Sheet



Neg.
131044B

Figure 52. Typical Splitting Failure During Beading Test of TD-NiCr Sheet, Preformed on Female Die, Heat 3637, 1.27 cm (0.5 in.) Bead Radius, 5.08 cm (2.0 in.) Bead Spacing

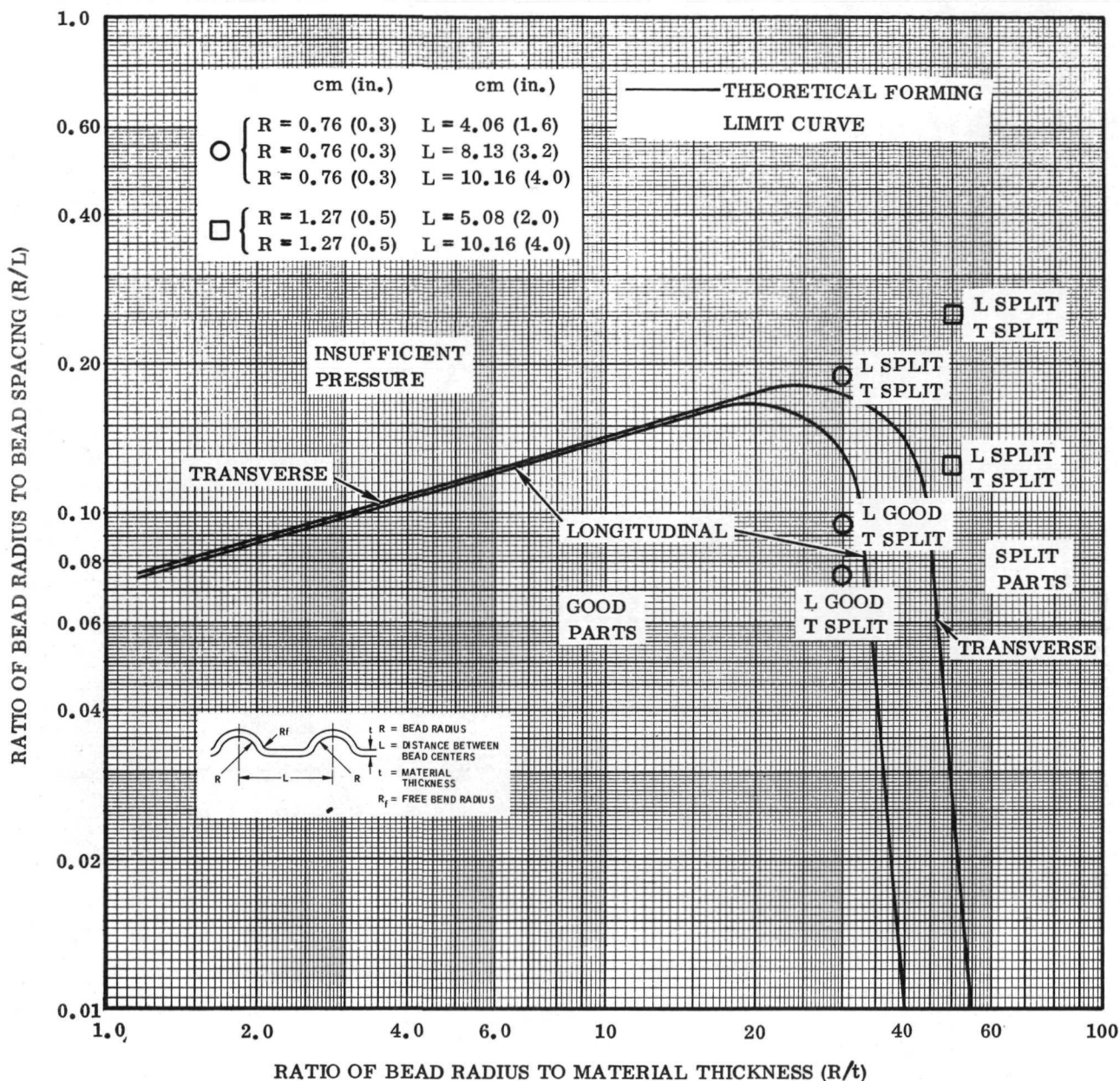


Figure 53. Theoretical and Actual Forming Limits for Rubber Press Beading of 0.25 mm (0.010 in.) Recrystallized TD-NiCr Sheet - Heat 3637 (Code F1)

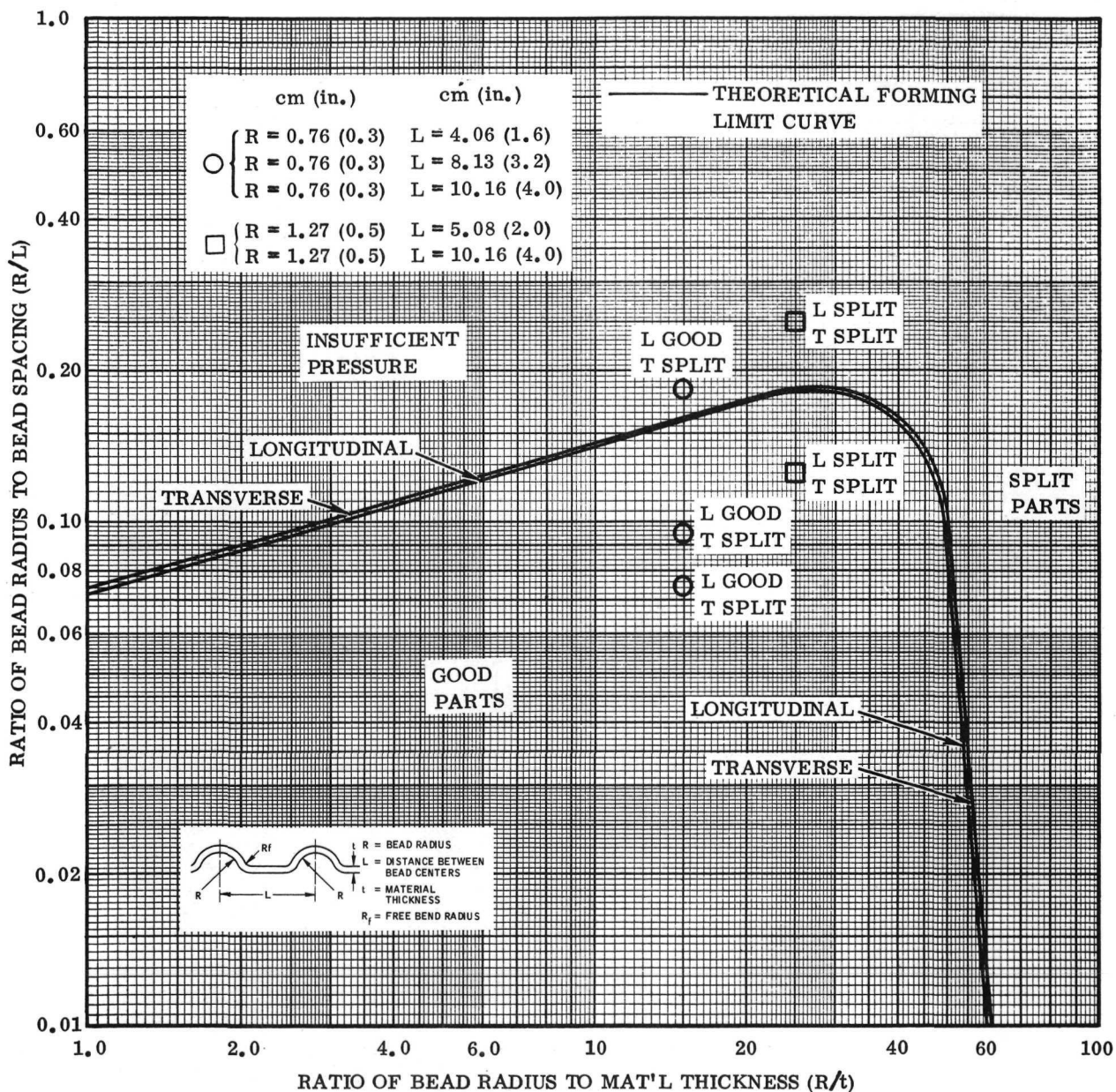


Figure 54. Theoretical and Actual Forming Limits for Rubber Press Beading of 0.5 mm (0.020 in.) Recrystallized TD-NiCr Sheet - Heat 3629 (Code A4)

Microstructure. - Metallographic examinations were conducted on specimens from selected panels in the as-formed condition and after annealing for 2 hours at 1177C (2150F). The test parts examined represent two sheet thicknesses, two grain directions (L and T), and three variations of forming severity. Included were beaded panels that had been formed with and without an intermediate anneal. No detrimental effects of beading were observed for either as-formed or annealed microstructure. Deformation bands in the as-formed condition such as observed in microstructure of recrystallized sheet formed by the other four processes were not evident in the case of beaded parts.

Page Intentionally Left Blank

5. FORMABILITY OF UNRECRYSTALLIZED TD-NiCr SHEET

The formability of unrecrystallized material was evaluated for four forming processes:

- (1) Brake forming
- (2) Corrugation forming
- (3) Dimpling
- (4) Beading*

Unrecrystallized TD-NiCr has different properties than commercial (recrystallized) TD-NiCr. The unrecrystallized material has poor ductility at ambient temperature but good ductility at elevated temperatures in the range 649 to 871C (1200 to 1600F). This means that forming operations on unrecrystallized material must be performed at elevated temperature.

A major advantage of forming TD-NiCr in the unrecrystallized condition is that the material is not subject to detrimental recrystallization effects from postforming annealing as is the case for recrystallized material when its critical deformation limit is exceeded. When unrecrystallized material has been hot formed into the desired configuration, the part is given a final recrystallization anneal. This results in uniform coarse grain structure with elevated temperature strength equivalent to recrystallized sheet material that has not been formed.

All forming evaluations were conducted in the 649-871C (1200-1600F) range. The selection of the optimum forming temperature was based on tensile properties and microstructure evaluation. The same forming temperature was used for all forming processes. Following hot forming, the parts were given the standard recrystallization anneal of two hours at 1177C (2150F) in dry hydrogen.

One heat of material for each of two gages, 0.25 and 0.5 mm (0.010 and 0.020 in.) were investigated for all four forming processes as shown in Figure 55.

The establishment of theoretical and actual formability data for unrecrystallized TD-NiCr followed the same methods for the particular processes as for recrystallized TD-NiCr.

*Theoretical forming limits were determined and tooling was fabricated for hot beading of unrecrystallized sheet. However, cost limitations prevented conducting a test program to establish the actual beading limits for unrecrystallized material.

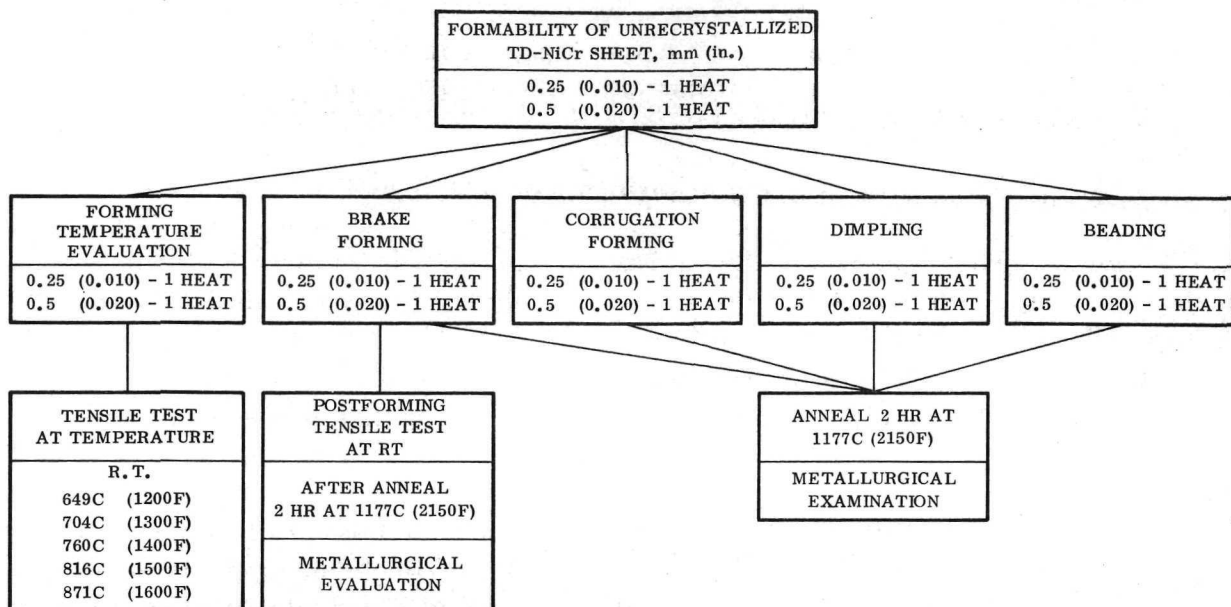


Figure 55. Material Breakdown and Test Plan for Unrecrystallized TD-NiCr Forming Evaluation

Material Properties

Theoretical forming studies for 0.25 and 0.5 mm (0.010 and 0.020 in.) unrecrystallized TD-NiCr sheet require tensile strength and strain data at the forming temperature for 5.08, 1.27 and 0.63 cm (2.0, 0.5, and 0.25 in.) gage lengths. Since the photogrid patterns used for tensile tests of recrystallized TD-NiCr would be destroyed during elevated temperature testing, a photoetched grid pattern was used for the unrecrystallized specimens.

Techniques were developed for application of 0.63 cm (0.25 in.) grids to tensile specimens by the photoetching process. A photoetched grid pattern consisting of 0.19 by 0.19 cm (0.075 by 0.075 in.) crosses at each corner of the 0.63 cm (0.25 in.) square grid was selected to minimize notch effects (see Figure 4). The crosses forming the grid pattern were very lightly etched into the material with a ferric chloride etchant. Checkout samples of the cross grid patterns were measured for accuracy and legibility with a Unitron measuring microscope at 30X magnification. Accuracy was found equal to that of the photogrid patterns. Figure 5 shows a typical cross-grid pattern for an unrecrystallized TD-NiCr tensile specimen tested at room temperature. Tensile tests conducted at temperatures up to 871C (1600F) in air showed good retention of the photoetched grid pattern, and photoetching had no apparent effect on elongation or initiation of fracture.

Tensile properties of 0.25 and 0.5 mm (0.010 and 0.020 in.) unrecrystallized sheet were determined at room temperature, 649, 704, 760, 816 and 871C (1200, 1300, 1400, 1500 and 1600F) in both the longitudinal and transverse directions. Testing was conducted in accordance with ARTC standard testing procedures (Ref. 18). Results of these tests are presented in Appendix C.

Figure 56 shows the tensile strength and elongation of 0.5 mm (0.020 in.) unrecrystallized TD-NiCr sheet plotted as a function of temperature. The elongation at 760 and 816C (1400 and 1500F) is about the same, and the ductility maxima appear to fall between these two temperatures.

One problem was encountered in elevated temperature tensile tests of the 0.25 mm (0.010 in.) material. When the specimen fractured, lateral movement of the extensometer bent the lower half of the thin-sheet specimen. This prevented good fit-back of the two specimen halves and reduced accuracy of the strain measurements. This is not a problem with thicker material, since the stiffer specimen can satisfactorily resist the lateral movement of the extensometer when the specimen fractures. The test procedures were modified to restrict the vertical and lateral movement of the extensometer sliding arms after the specimen fractured. The accuracy of the elongation measurements was significantly improved by this change.

The tensile properties of the 0.25 mm (0.010 in.) material are plotted as a function of temperature in Figure 57. These data indicate the ductility maximum for the transverse direction is at or near 816C (1500F), and the maximum for the longitudinal direction is between 760 and 816C (1400 and 1500F). This is in agreement with the results observed for the 0.5 mm (0.020 in.) unrecrystallized sheet.

Strain measurements for 1.27 and 0.63 cm (0.5 and 0.25 in.) gage length and width were performed on 0.25 mm (0.010 in.) tensile specimens tested at 760 and 816C (1400 and 1500F) and at 704, 760 and 816C (1300, 1400 and 1500F) for 0.5 mm (0.020 in.) specimens. These results are presented in Appendix C (Tables C-3 and C-4). Comparison of the strain data at 760 and 816C (1400 and 1500F) for the two sheet thickness reveal higher elongation values transverse to the rolling direction for both heats of material. The strain values are slightly higher for the 0.50 mm (0.020 in.) material than for the 0.25 mm (0.010 in.) material.

Theoretical Forming Limit Curves

Theoretical formability data for hot forming of unrecrystallized TD-NiCr at 704, 760 and 816C (1300, 1400 and 1500F) were generated using the Formability Computer Program (Appendix B) with the material properties data from Appendix C and selected values of geometric variables as input.

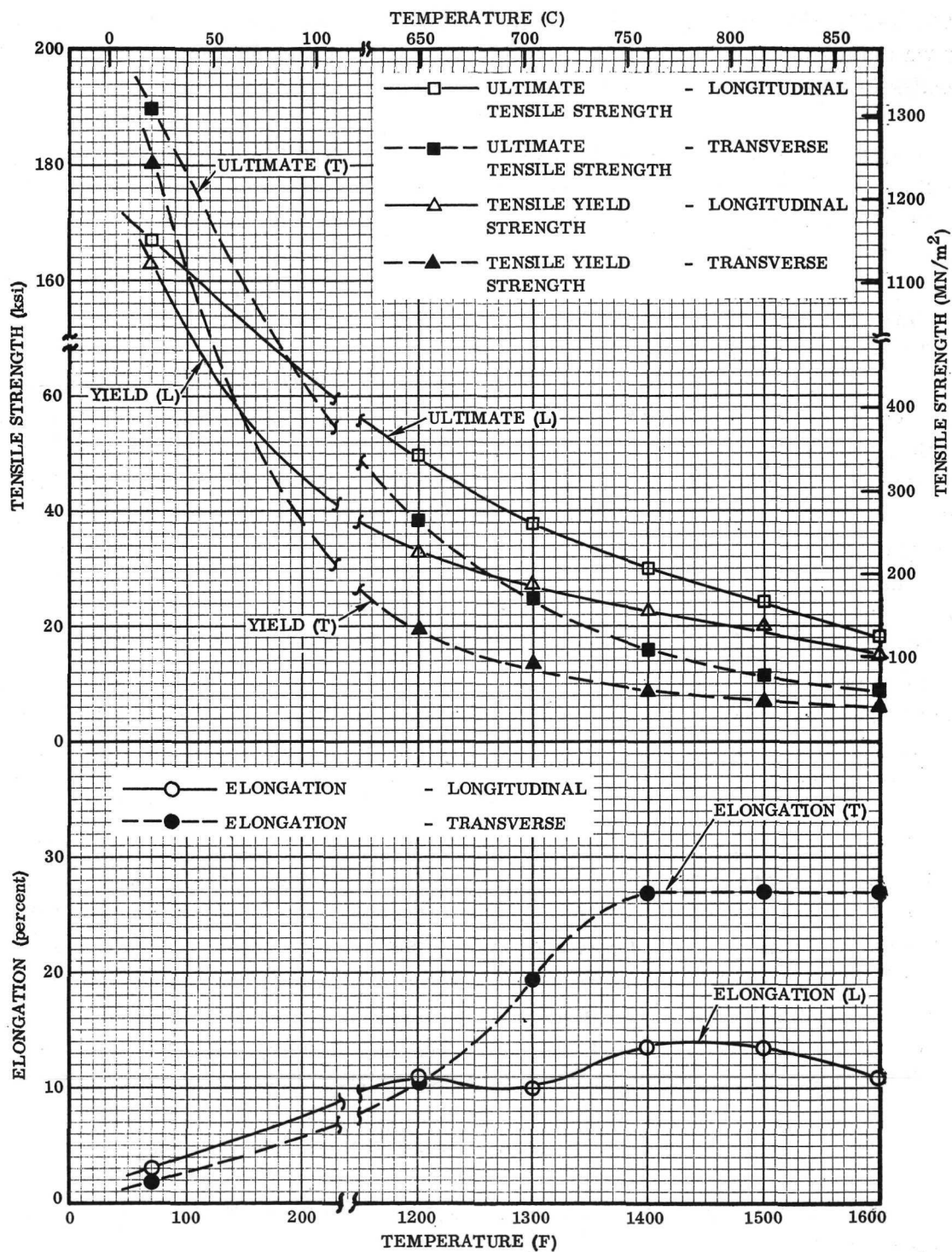


Figure 56. Tensile Properties of 0.5 mm (0.020 in.) Unrecrystallized TD-NiCr Sheet - Heat 3709 (Code G1)

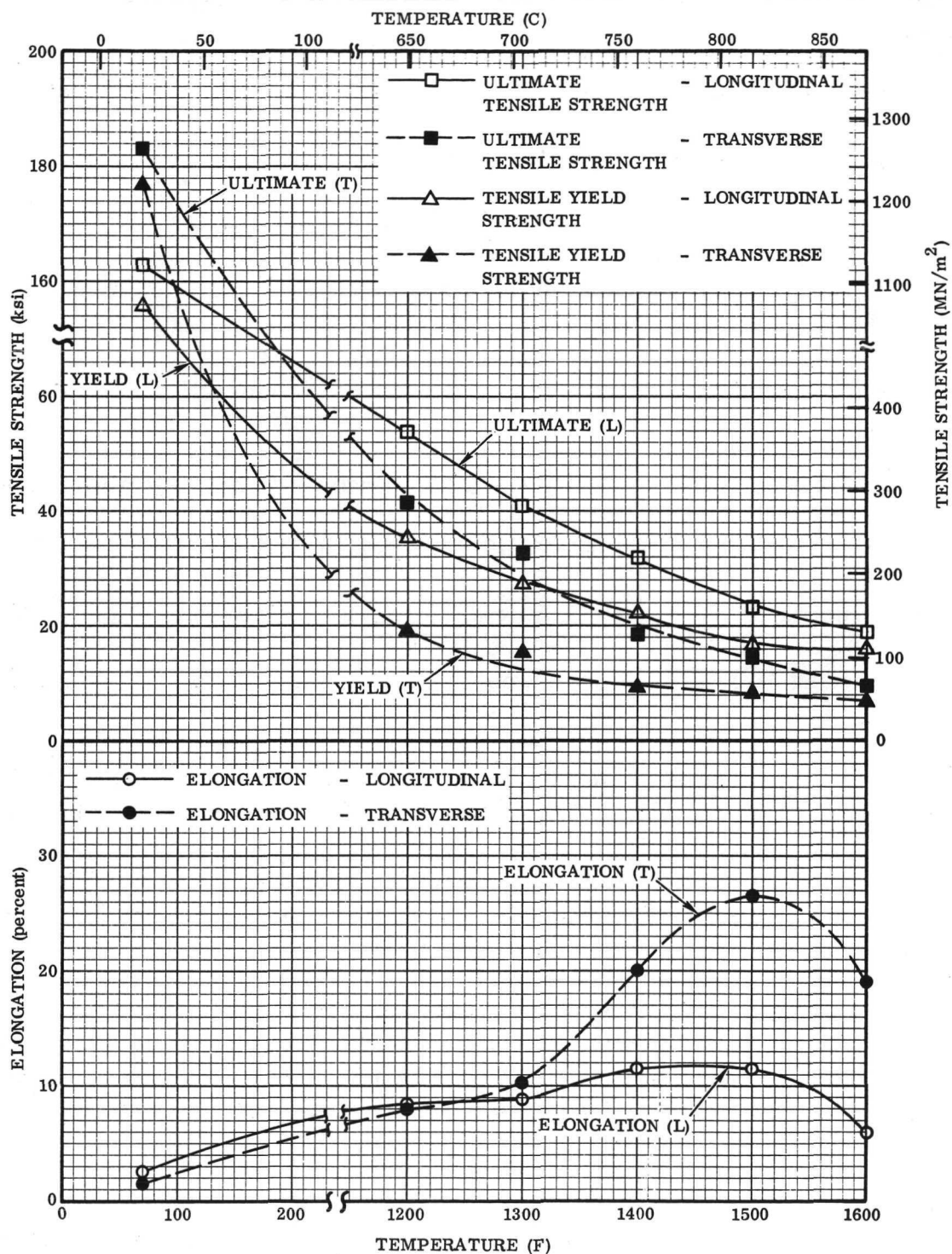


Figure 57. Tensile Properties of 0.25 mm (0.010 in.) Unrecrystallized TD-NiCr Sheet - Heat 3714 (Code K5)

The following formability curves for 0.5 mm (0.020 in.) sheet were prepared from the computer output:

Brake Forming	6 curves (3 temperatures/1 heat/2 grain directions)
Corrugation Forming	Identical to brake forming
Dimpling	6 curves (3 temperatures/1 heat/2 grain directions)
Beading-Drop Hammer	6 curves (3 temperatures/1 heat/2 grain directions)

Theoretical forming limits were established for 0.25 mm (0.010 in.) unrecrystallized sheet as follows:

Brake Forming	4 curves (2 temperatures/1 heat/2 grain directions)
Corrugation Forming	Identical to brake forming
Dimpling	6 curves (3 temperatures/1 heat/2 grain directions)
Beading-Drop Hammer	4 curves (2 temperatures/1 heat/2 grain directions)

Representative theoretical curves for 0.5 mm (0.020 in.) sheet are shown in Figures 58 through 60 and for 0.25 mm (0.010 in.) sheet are shown in Figures 61 and 62.

The theoretical forming limits are similar for the two gages of unrecrystallized sheet. These data indicate formability is better when strain is parallel to the rolling direction (longitudinal) than normal to the rolling direction (transverse).

The theoretical forming curves indicate the best hot formability for unrecrystallized material is in the range 760 to 816 C (1400 to 1500 F). Major concern on forming at higher temperature is the onset of normal recrystallization, which can occur as temperatures approach 871-927C (1600-1700 F) (Ref. 3) and limitations on tooling operating at these high temperatures.

The bead radii and spacing parameters of the bead forming tools are superimposed on the theoretical beading limit curves in Figure 60. This comparison indicates that the experimental beading parameters straddle the limits for drop hammer beading. This selection of parameters for experimental beading studies is excellent if actual closed die press beading follows the relationships of drop hammer beading.

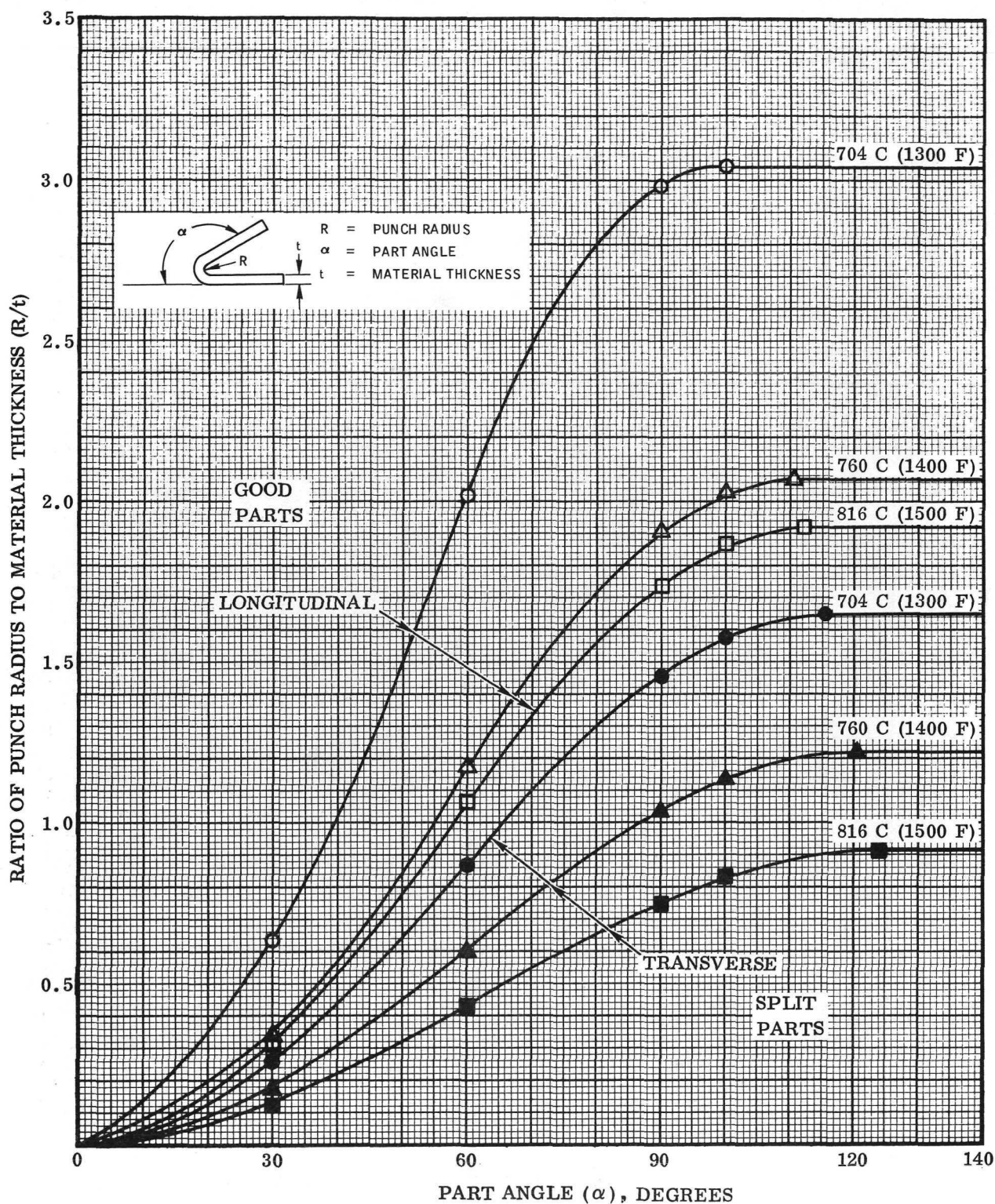


Figure 58. Theoretical Formability Curves for Hot Brake and Corrugation Forming of 0.5 mm (0.020 in.) Unrecrystallized TD-NiCr Sheet - Heat 3709 (Code G1)

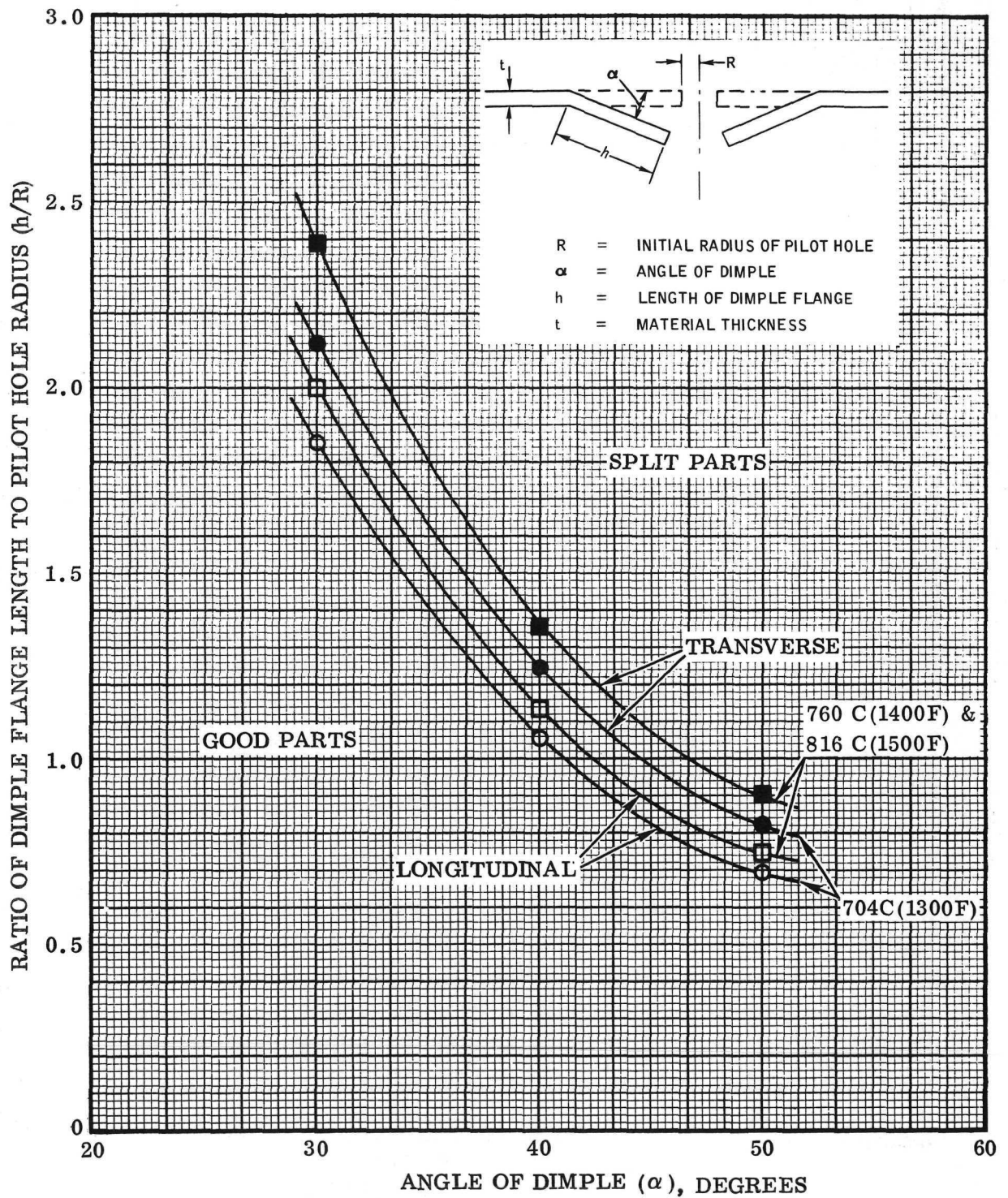


Figure 59. Theoretical Formability Curves for Hot Dimpling of 0.5 mm (0.020 in.) Unrecrystallized TD-NiCr Sheet — Heat 3709 (Code G1)

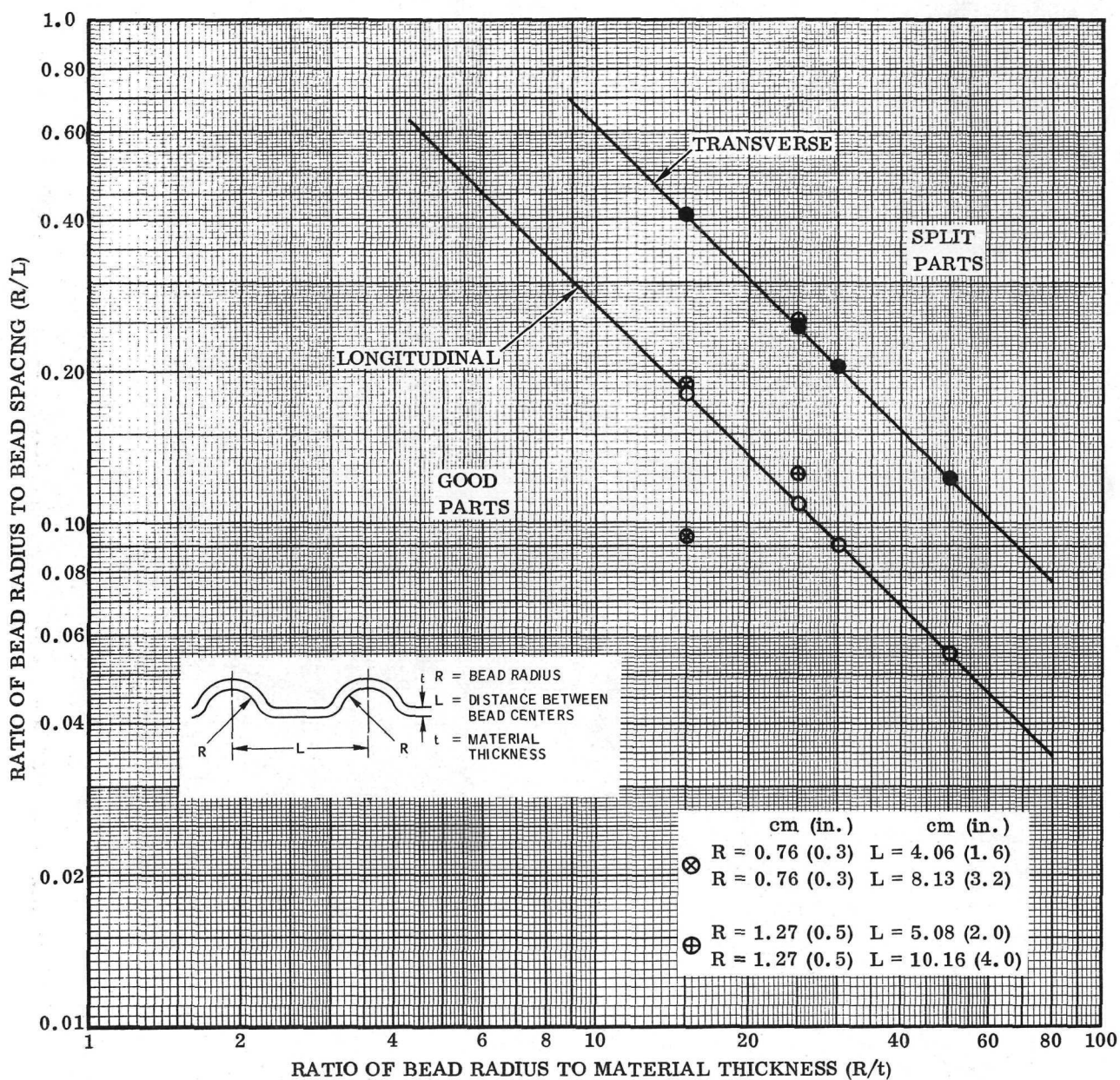


Figure 60. Theoretical Formability Curves for Drop Hammer Beading of 0.5 mm (0.020 in.) Unrecrystallized TD-NiCr Sheet at 760C(1400F)— Heat 3709 (Code G1)

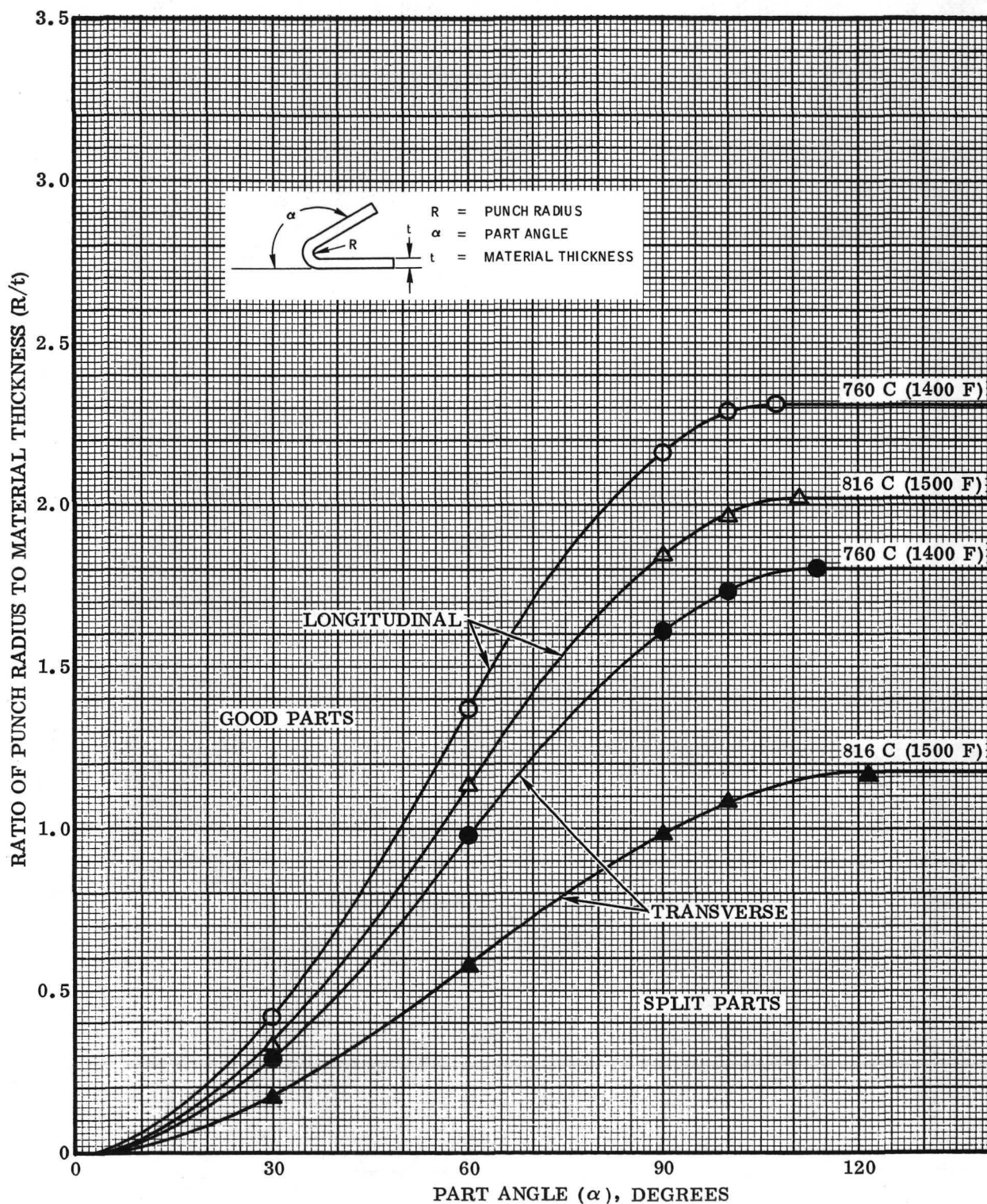


Figure 61. Theoretical Formability Curves for Hot Brake and Corrugation Forming of 0.25 mm (0.010 in.) Unrecrystallized TD-NiCr Sheet - Heat 3714 (Code K5)

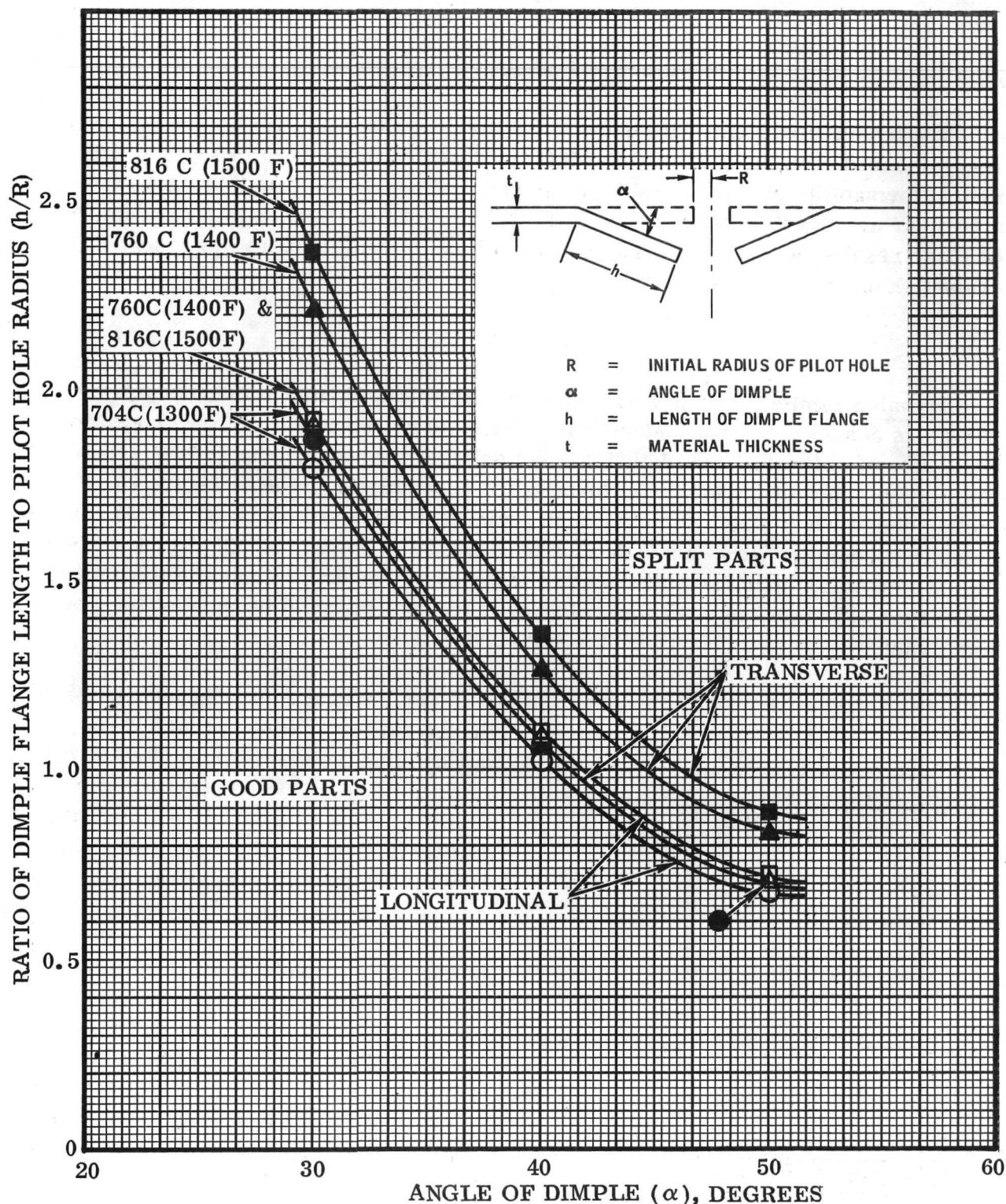


Figure 62. Theoretical Formability Curves for Hot Dimpling of 0.25 mm (0.010 in.) Unrecrystallized TD-NiCr Sheet — Heat 3714 (Code K5)

Selection of Forming Temperature

The tensile properties data indicate the maximum ductility for both gages of unrecrystallized sheet is in the 760 to 816C (1400 to 1500F) temperature range. Theoretical formability studies based on these properties data indicate that the best formability for unrecrystallized material is in the 760 to 816C (1400 to 1500F) range. Based on these results, an optimum forming temperature of 760C (1400F) was selected for evaluation of actual forming limits.

Brake Forming

Forming Limits.— Matched die tooling for hot brake forming of unrecrystallized sheet was designed and fabricated. The adjustable span brake forming die used for evaluation of recrystallized material is not suitable for hot forming at 760C (1400F). The configuration of the hot brake forming die assembly is shown in Figure 63. The tooling concept is a matched die set with replaceable dies and punches. Three replaceable die assemblies were fabricated for bend angles of 45, 90 and 120 degrees. Heating was accomplished with cartridge heaters inserted in gun-drilled holes in the die assembly. Type 316 stainless steel was selected as the tool material because of its elevated temperature properties, availability, and relatively low cost.

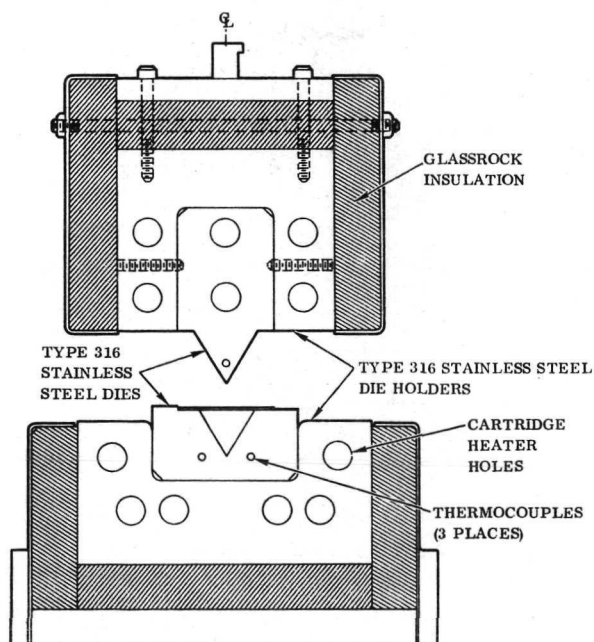


Figure 63. Hot Brake Forming Die Assembly

The hot brake forming tests were conducted with the Pneuco press brake. All forming tests were conducted at 760C (1400F). The blank temperature was measured by means of a chromel-alumel thermocouple inserted at the point of contact between the punch and part and removed just prior to forming. The blanks and dies were sprayed with graphite-base dry-film lubricant (Formkote T-50, Everlube Corporation, North Hollywood, California).

Actual forming limits of 0.25 and 0.5 mm (0.010 and 0.020 in.) unrecrystallized sheet were determined for two grain directions (L and T) and three bend angles (45, 90 and 120 degrees). Test results are summarized in Table 20.

In some instances, there was a large difference between the punch radius and the actual measured part radius. For

**Table 20. Experimental Press Brake Forming Limits of
Unrecrystallized TD-NiCr at 760C (1400F)**

Sheet Thickness mm (in.)	Heat Number	Bend Angle (Deg)	Grain Direction	Punch Radius (R/t)		Part Radius (R/t)		Springback Angle (Deg)	Theoretical Forming Limit (R/t)
				No Cracks	Cracks	No Cracks	Cracks		
0.25(0.010)	3714 Code K 7 Code K 8	45	L	0.5	ND ⁽¹⁾	3.5	ND	5	0.9
			T	2.0	1.0	6.2	5.0	3	0.6
	3714 Code K 7 Code K 8	90	L	3.7	2.8	5.5	4.2	-6 ⁽²⁾	2.2
			T	7.2	6.6	7.0	5.4	-7	1.6
	3714 Code K 7 Code K 7	120	L	2.7	2.2	2.6	1.7	6	2.3
			T	12.5	10.2	11.7	9.4	-2	1.8
0.5(0.020)	3709 Code G1	45	L	0.3	ND	2.5	ND	5	0.7
			T	7.2	6.2	6.2	5.0	2	0.4
		90	L	4.6	4.1	3.9	3.1	-5	1.9
			T	8.1	7.5	7.5	6.7	-1	1.1
		120	L	6.2	5.1	5.5	4.9	2	2.1
			T	7.2	6.2	6.6	Fractured	1	1.2

(1) ND = No data established. (2) Negative springback.

example, the 45-degree bends showed a much larger part radius than the punch radius. On the other hand, the 90- and 120-degree bends generally revealed a slightly smaller part radius than the punch radius.

Comparison of actual and theoretical forming limits are shown in Figures 64 and 65. It should be noted that the part radius is used in these figures rather than punch radius, since the former appears to be more meaningful. These results indicate that hot brake forming of unrecrystallized sheet follows the same general trend shown for room temperature brake forming of recrystallized TD-NiCr. The actual forming limits are higher (less formable) than the predicted limits, and the formability in the longitudinal direction (strain parallel to the rolling direction) is better than transverse to the rolling direction.

Figures 64 and 65 show several anomalies in the test data, which should be resolved by additional hot brake forming studies. Notably, in two instances, the minimum bend radius (MBR) is shown to be less for a bend angle of 120 degrees than for a bend angle of 90 degrees.

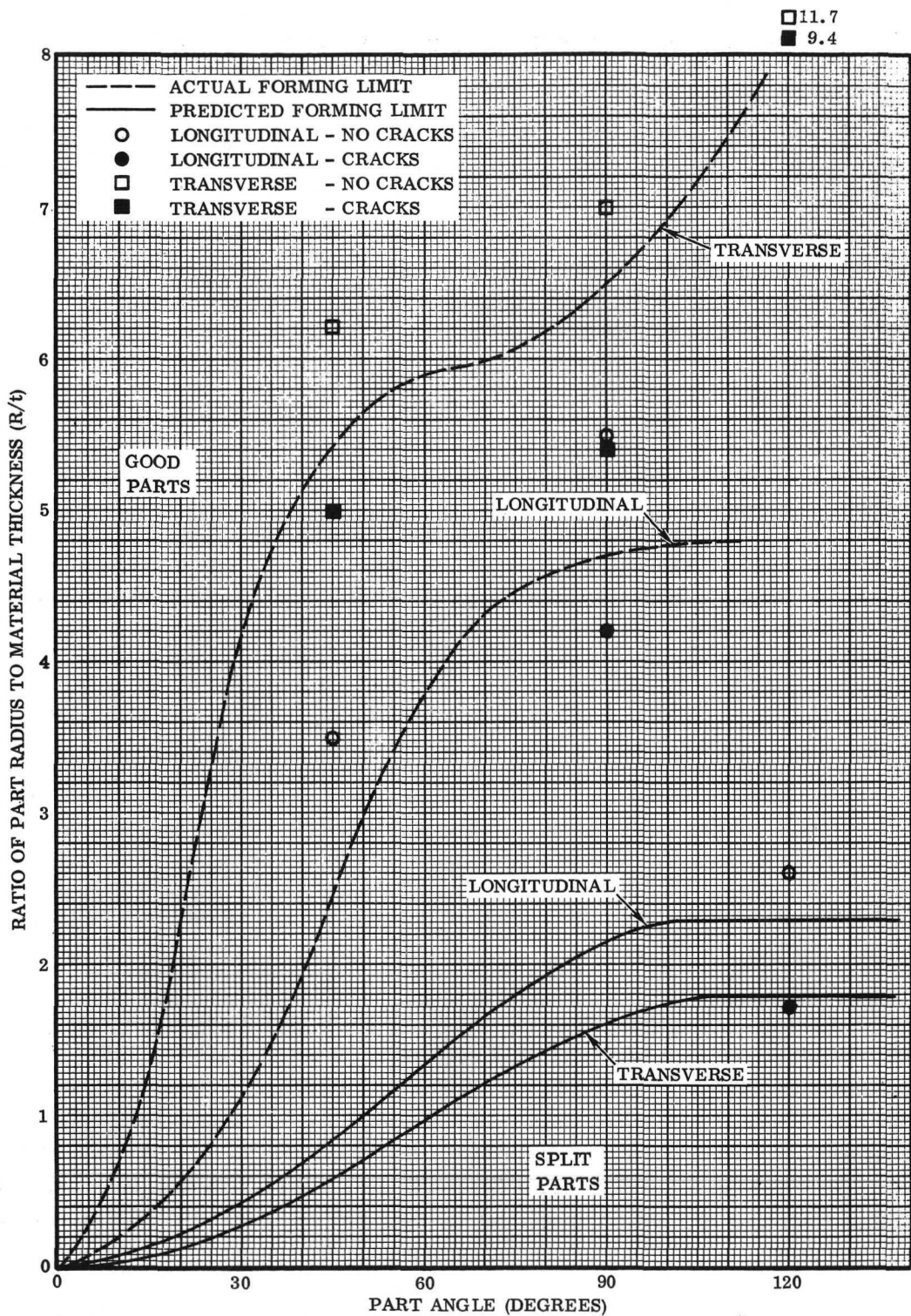


Figure 64. Actual and Predicted Brake Forming Limits at 760C (1400F) for 0.25 mm (0.010 in.) Unrecrystallized TD-NiCr Sheet - Heat 3714 (Code K7 and K8)

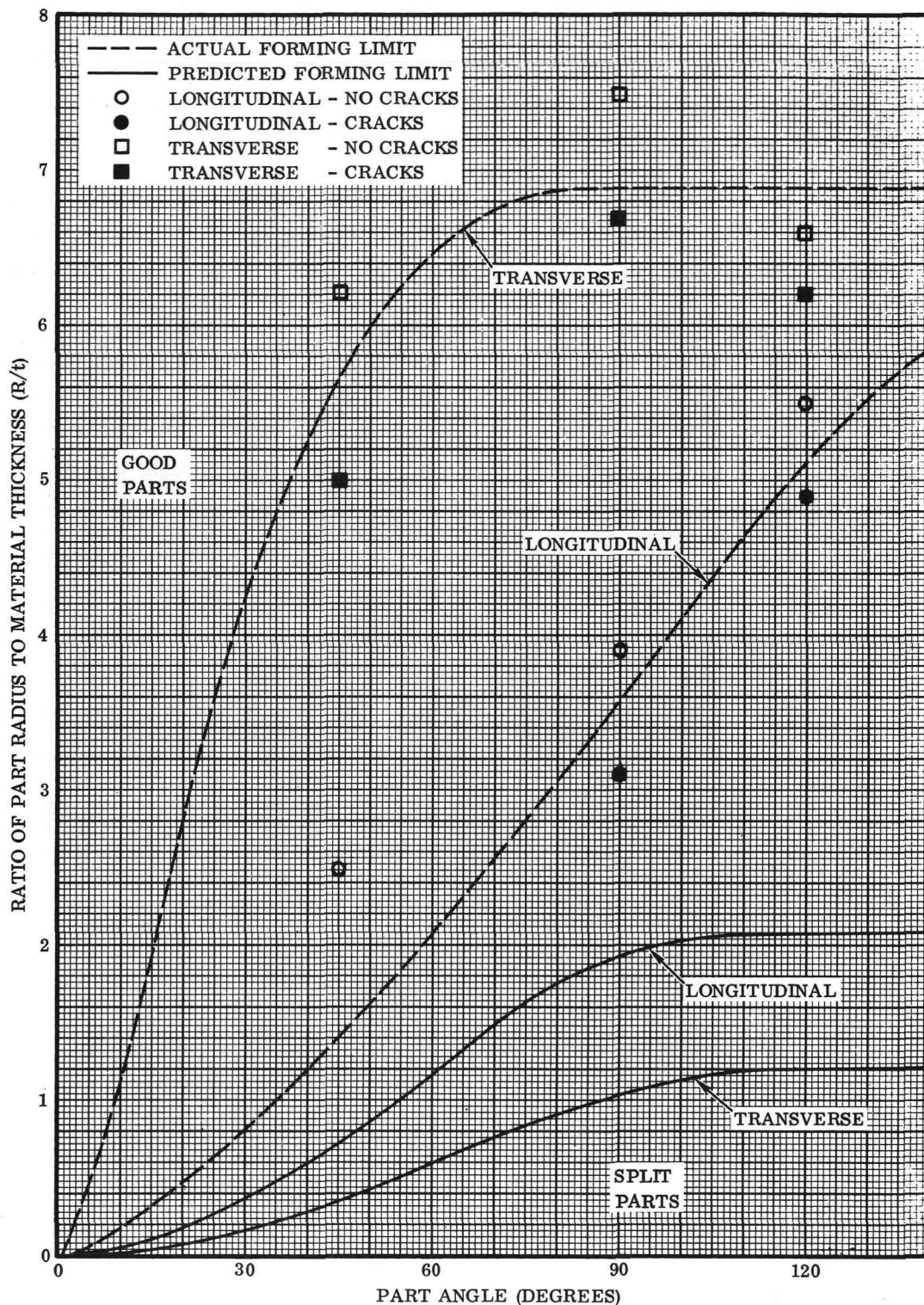


Figure 65. Actual and Predicted Brake Forming Limits at 760C (1400F) for 0.5 mm (0.020 in.) Unrecrystallized TD-NiCr Sheet - Heat 3709 (Code G1)

It is concluded from these studies that unrecrystallized TD-NiCr sheet can be hot brake formed satisfactorily at 760C (1400F) with the use of a suitable bend radius and grain orientation. The effects of hot brake forming on tensile properties and microstructure are discussed in the following sections.

Tensile Properties of Formed Parts.— Tensile tests were conducted on specimens machined from the radius portion of hot brake formed parts of 0.5 mm (0.020 in.) material to evaluate effect of hot brake forming on strength and ductility. The specimens represent the MBR for a 90-degree bend angle for two grain orientations (L and T), and were annealed 2 hours at 1177C (2150F) after machining. Specimen configuration and test procedures were the same as described for tensile tests of brake formed parts of recrystallized sheet.

Test results are given in Table 21. These data show good strength and ductility for hot brake formed parts, indicating no properties degradation as a result of hot forming. Comparison with results for brake formed parts of recrystallized sheet in Tables 12 and 14 show greatly superior ductility for hot brake formed parts.

Table 21. Effect of Hot Brake Forming on Tensile Properties of 0.5 mm (0.020 in.) Unrecrystallized Sheet – Heat 3709 (Code G)

Grain Orientation ^(a)	Specimen Number	Cross-Section Area cm ² (in. ²)	Ultimate Tensile Strength MN/m ² (ksi)	Tensile Yield Strength MN/m ² (ksi)	Elongation % in 2.54cm (1.0 in.)
L	GIT-31 ^(b)	0.0143 (0.00222)	845 (122.5)	530 (76.8)	15
	GIT-32	0.0142 (0.00221)	858 (124.4)	538 (78.0)	17
	GIT-67	0.0152 (0.00235)	836 (121.3)	519 (75.3)	12
			Avg. 846 (122.7)	529 (76.7)	14.7
T	GIL-19 ^(c)	0.0138 (0.00214)	789 (114.5)	528 (76.6)	18
	GIL-20	0.0151 (0.00234)	796 (115.4)	530 (76.9)	21
	GIL-21	0.0145 (0.00235)	952 (113.8)	527 (76.4)	20
			Avg. 789 (114.4)	528 (76.6)	19.7

(a) Rolling direction perpendicular (T) or parallel (L) to tensile specimen axis.

(b) Formed 90° bend with 7t radius.

(c) Formed 90° bend with 4t radius.

Microstructure.— Metallographic examinations were conducted on hot brake formed parts representing two sheet thicknesses, two grain directions (L and T), and two bend angles (45 and 90 degrees). Parts were examined that were formed to the MBR as well as more severely formed parts containing cracks. All specimens were given a recrystallization anneal for 2 hours at 1177C (2150F) prior to examination.

Comparison of the microstructure of the formed metal in the bend area with that of the parent metal disclosed change in grain size and shape resulting from the forming process. The parent material exhibited typical recrystallized microstructure consisting of very large elongated grains. The microstructure of the deformed metal was different in two respects: (1) the grains, although still very large, were smaller than the parent metal, and (2) the grains were more nearly equiaxed. This effect was more pronounced in the 90-degree bend specimens than for the less severely formed 45-degree bend specimens. Typical microstructure of deformed and nondeformed regions of a hot brake formed part after annealing is shown in Figure 66. The relatively small reduction in grain size resulting from hot brake forming is not considered to have a serious effect on high temperature strength of TD-NiCr sheet.

Corrugation Forming

Forming Limits.—Evaluation of the actual corrugation forming limits of unrecrystallized sheet was accomplished with the Pneuco press brake and the matched dies (Figures 27 and 28) used for forming of recrystallized sheet. The tooling was modified for hot forming by assembly of heaters and installation of insulation material. The design of the spring used for clamping the preformed corrugation was modified for elevated temperature forming. René 41 was used for the spring material, and the spring was increased to a 10.2 cm (4.0 in.) free length rather than 5.1 cm (2.0 in.) as in the original design. All corrugation forming tests were conducted at 760C (1400F), which required the tools to be heated in the range 788 to 816C (1450 to 1500F). The same graphite base dry-film lubricant was applied to test blanks and dies as used for hot brake forming.

Figure 67 is a photograph showing hot corrugation forming of unrecrystallized sheet. Actual forming limits of 0.25 and 0.5 mm (0.010 and 0.020 in.) unrecrystallized material were evaluated for two grain directions (L and T) and three corrugation angles (45, 60, and 75 degrees). Several bend radii were tested for each condition. Results of these tests are summarized in Table 22.

Comparison of these data with Table 15 for recrystallized material shows considerably less springback during elevated temperature forming of unrecrystallized material. However, part radius is considerably greater than punch radius for corrugations of unrecrystallized sheet.

Figure 68 shows a comparison of theoretical and actual forming limit curves for 0.25 mm (0.010 in.) material for the longitudinal and transverse directions. The forming limit curves for the 0.5 mm (0.020 in.) material are shown in Figure 69. In all cases, higher actual forming limits (poorer formability) were obtained for the transverse grain orientation than for longitudinal. This is the opposite of the predicted



Neg. D3759

250X

(a) Deformed metal in bend

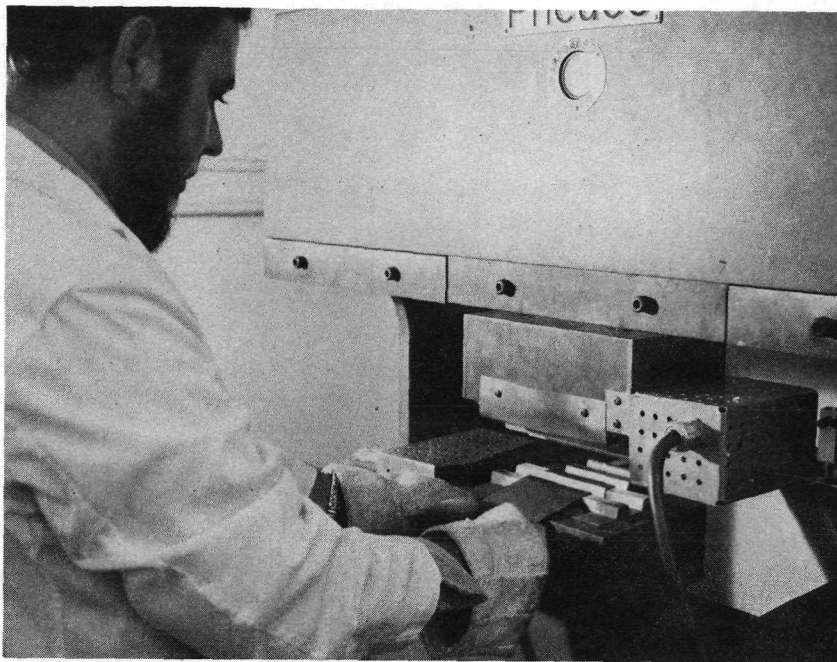


Neg. D3760

250X

(b) Non-deformed region

Figure 66. Typical Microstructure of Hot Brake Formed 0.5 mm (0.020 in.) Unrecrystallized Sheet After Recrystallization Anneal



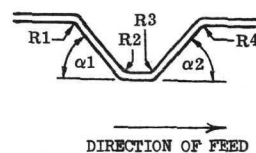
Neg. 127945B

Figure 67. Hot Corrugation Forming of Unrecrystallized TD-NiCr Sheet

Table 22. Experimental Corrugation Forming Limits of Unrecrystallized TD-NiCr for 45, 60, and 75-Degree Corrugation Angles

Corrugation Angle (degrees)	Sheet Thickness mm (in.)	Heat Number	Grain ⁽¹⁾ Direction	Ratio of Punch Radius to Material Thickness (R/t)		Ratio of Part Radius ⁽²⁾ to Material Thickness (R/t)		Springback ⁽³⁾ Angle (degrees)
				No Cracks	Cracks	No Cracks	Cracks	
45	0.25 (0.010)	3714 Code K6	L T	0.4 2.0	(4) 0.8	6.2 9.3	(4) 4.7	1 0
	0.5 (0.020)	3709 Code G-3	L T	0.4 1.0	(4) 0.4	2.4 5.5	(4) 6.3	-2 (5) -3
60	0.25 (0.010)	3714 Code K6 & K9	L T	0.5 7.8	(4) 6.2	3.2 11.0	(4) 7.8	0 0
	0.5 (0.020)	3709 Code G-3	L T	1.6 3.1	0.9 2.4	3.9 3.9	3.9 3.9	0 -2
75	0.25 (0.010)	3714 Code K6 & K9	L T	4.7 7.8	0.4 6.2	6.2 10.9	3.2 6.2	1 1
	0.5 (0.020)	3709 Code G-3	L T	3.1 6.3	2.4 5.5	7.1 7.1	3.1 5.5	3 2

- (1) L = direction of strain parallel to rolling direction
T = direction of strain normal to rolling direction
(2) Radius R₄ (See sketch)
(3) Angle measured on specimen that did not crack
Angle α_2 (see sketch)
(4) Sharpest radius that could be generated with 0.01 to 0.02 mm (0.004 to 0.008 in.) tool radii did not crack parts
(5) Negative springback



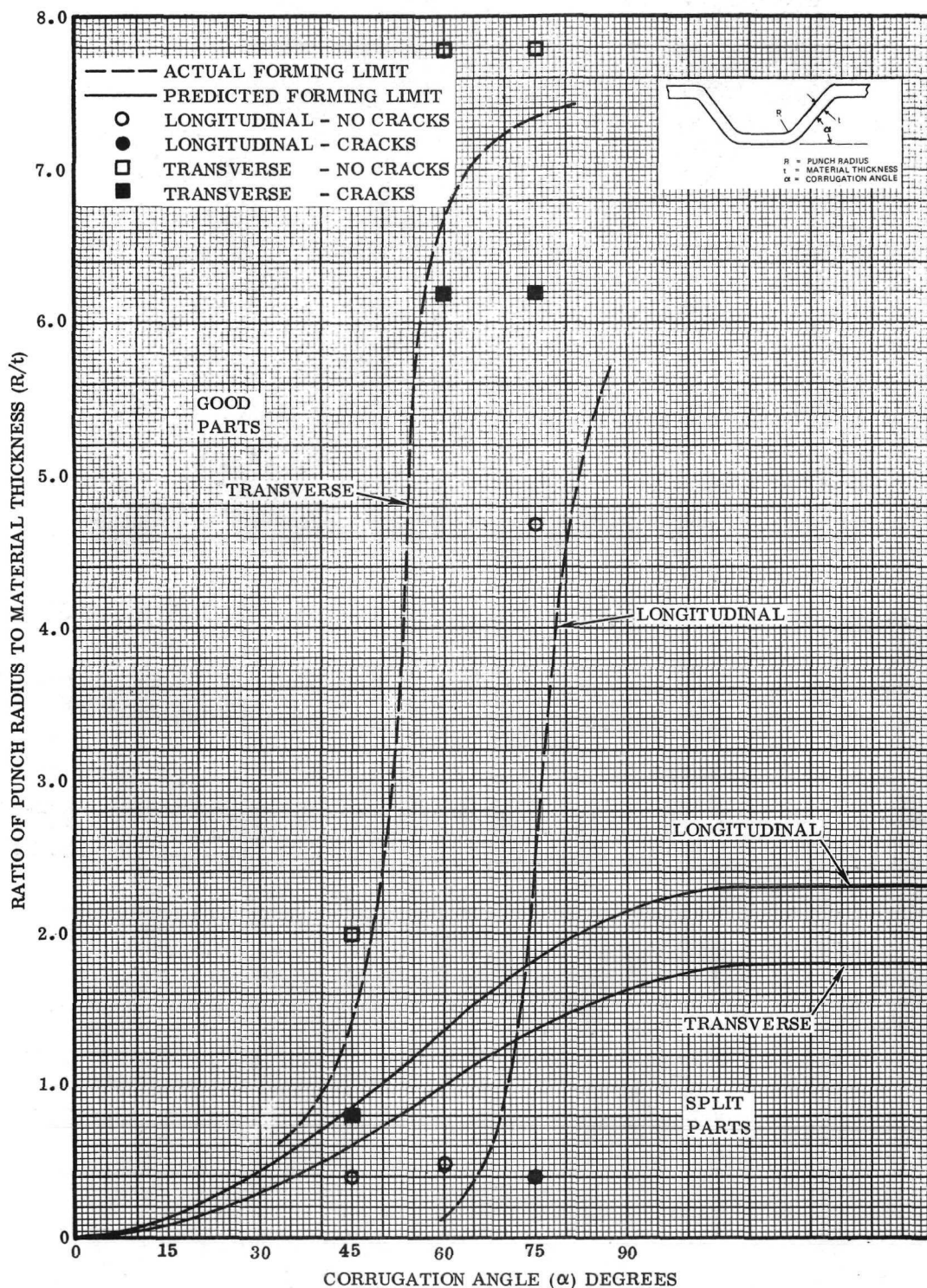


Figure 68. Theoretical and Actual Corrugation Forming Limit Curves at 760C (1400F) for 0.25 (0.010 in.) Unrecrystallized TD-NiCr Sheet — Heat 3714 (Code K6 and K7)

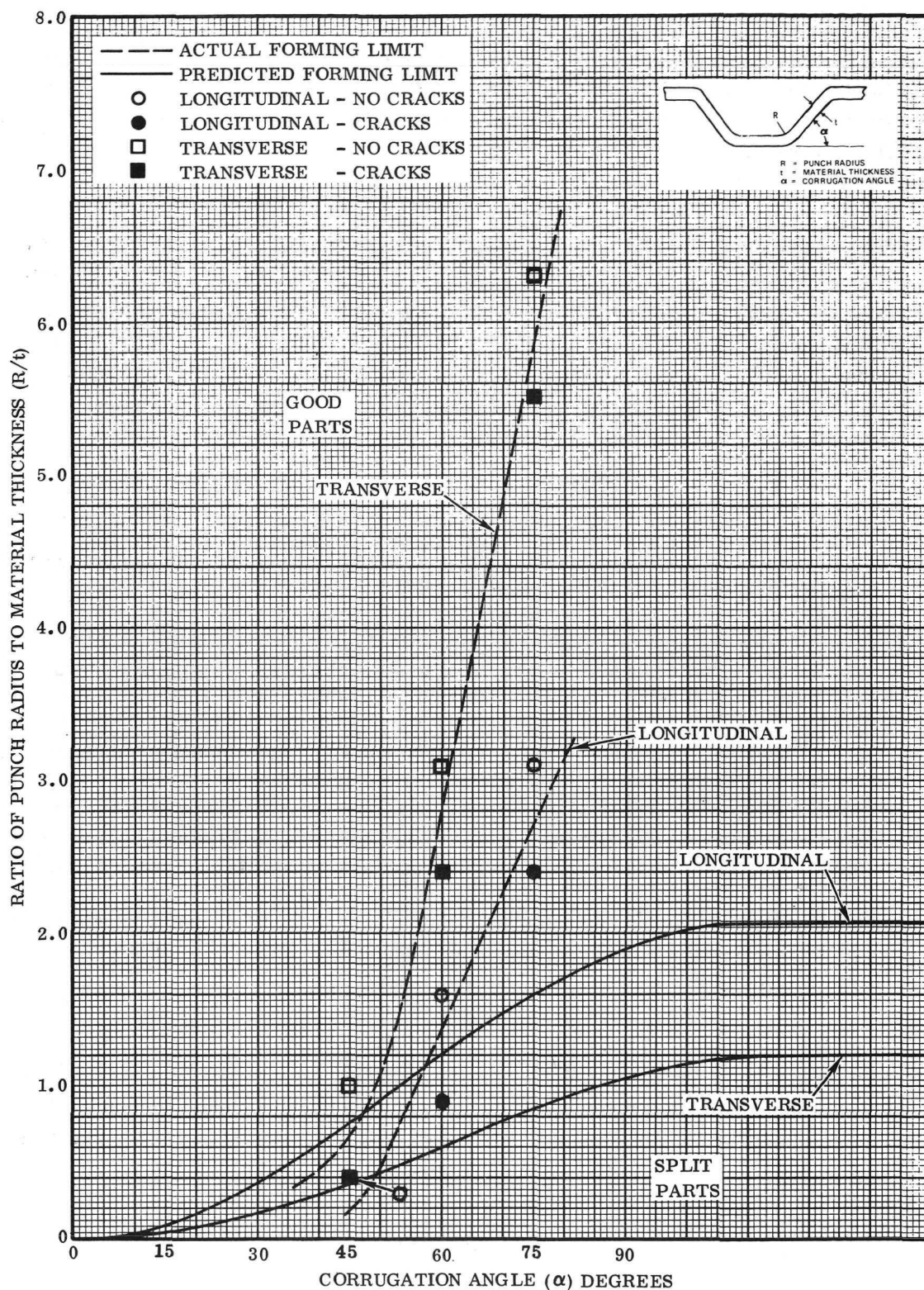


Figure 69. Theoretical and Actual Corrugation Forming Limit Curves at 760C (1400F) for 0.5 mm (0.020 in.) Unrecrystallized TD-NiCr Sheet - Heat 3709 (Code G3)

forming limit curves. Figures 68 and 69 show that the actual forming limits are generally higher (poorer formability) than the theoretical forming limits. In those instances where lower actual forming limits are indicated, it is evident from Table 22 that actual limits would have been much higher if part radius was considered rather than punch radius.

Microstructure. - Metallographic examinations were conducted on hot corrugation formed parts after annealing for 2 hours at 1177C (2150F) in hydrogen. The test parts examined represented two sheet thicknesses, two grain orientations (L and T), and three corrugation angles (45, 60 and 75 degrees). Two corrugation bend radii; minimum bend radius (MBR), and a radius greater than the (MBR) were examined for each forming parameter. The microstructure of the corrugations were compared to that of parent metal with the same annealing treatment.

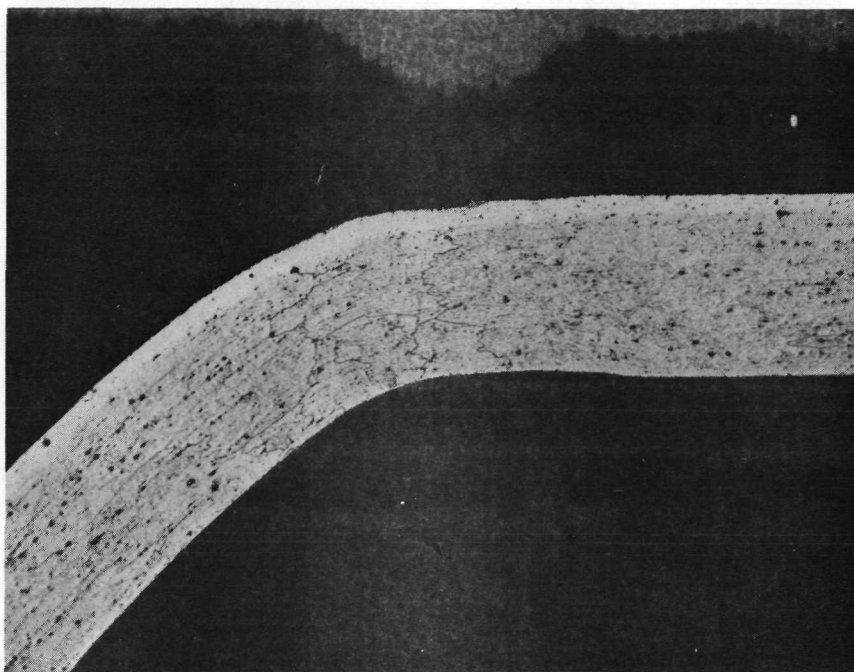
Observations were as follows:

- (1) Microstructure of hot formed corrugations is almost identical to that of hot brake formed parts
- (2) Grain size of plastically deformed metal (bend area) is somewhat smaller than nondeformed metal, and the more severe the deformation, the smaller the grain size
- (3) The nondeformed areas of the corrugated parts have identical microstructure to the annealed parent metal
- (4) Cracks were observed in transverse 60 degree corrugations of 0.25 mm (0.010 in.) sheet, which necessitated adjustment of the forming limit curve
- (5) Although the smaller grain observed in the bend area would tend to reduce the elevated temperature strength of corrugated parts, the degree of properties loss is not believed to be significant

Characteristic microstructure of hot corrugated parts after recrystallization annealing are shown in Figure 70. The upper micrograph (Figure 70 (a)) shows the reduced grain size in the bend area for a 60-degree corrugation formed in the longitudinal direction. The lower micrograph shows a typical crack in a 60-degree corrugation formed transverse to the rolling direction.

Dimpling

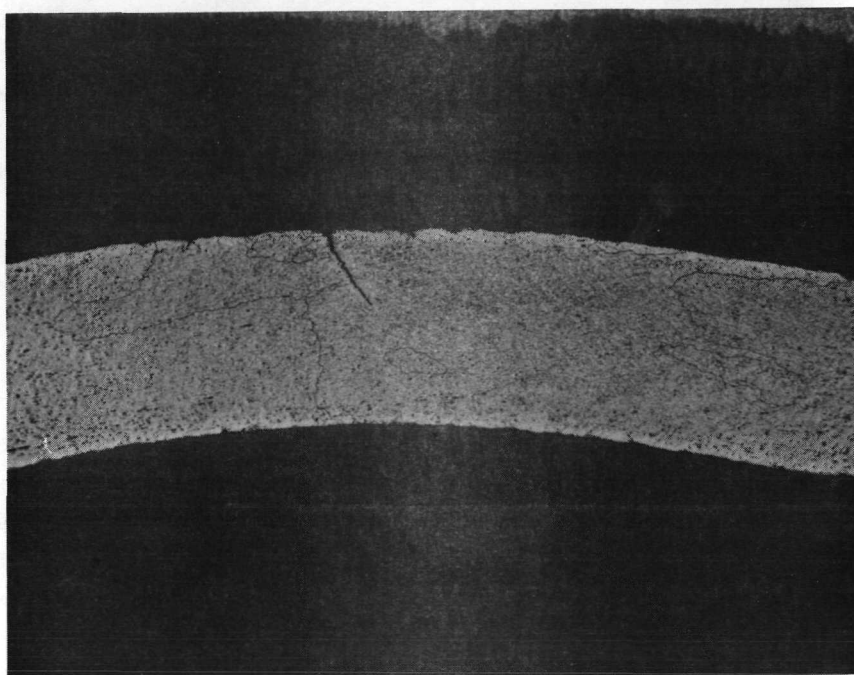
Various dimpling processes were investigated that might be applicable to hot dimpling of unrecrystallized TD-NiCr. The Ram-Coin and Triple-Action methods used for recrystallized material have a maximum heating limit of 370C (700F). Three



Neg. D3761

100X

(a) Longitudinal 60° bend, 0.5t radius



Neg. D3762

100X

(b) Transverse 60° bend, 6.2t radius

Figure 70. Microstructure of Hot Corrugated Parts of 0.25 mm (0.010 in.) Unrecrystallized TD-NiCr Sheet

methods have the required 760C (1400F) temperature capability: Resistothermic dimpling (Zephyr Mfg. Co.), induction heating dimpling (Aerospace Tooling, Inc.), and a resistance-heated dimpling process developed by Convair Aerospace. A description of these processes and their application to development of hot dimpling techniques for titanium alloys is given in Reference 19. The conclusion from the titanium program is that Resistothermic dimpling is the best method for dimpling titanium when satisfactory dimpling cannot be achieved at temperatures less than 371C (700F).

Preliminary evaluation of Resistothermic dimpling of unrecrystallized sheet was conducted at Zephyr Manufacturing Co., Inglewood, California. The experimental dimpling tests of 0.25 and 0.5 mm (0.010 and 0.020 in.) sheet revealed that the maximum heating diameter that could be achieved with Resistothermic dimpling was not sufficient to prevent circumferential cracks. Discussion of the problem with Zephyr personnel disclosed that the cost and time schedule to develop modified Resistothermic tooling for successful hot dimpling of TD-NiCr would exceed the scope of the present program. As a result, plans to procure Resistothermic dimpling tools were cancelled.

Aerospace Techniques, Inc. (ATI) of Escondido, California, was contacted concerning the induction-heated dimpling process they developed a number of years ago. This process achieved a much larger heated zone area than the Resistothermic process (Ref. 19). ATI (formerly Aircraft Tools, Inc.) advised that they had discontinued the development of induction heated dimpling techniques several years previously and had no tooling or dimpling machines available.

The resistance-heated dimpling process previously investigated by Convair Aerospace for titanium uses a resistance spotwelding machine and Class 3 electrodes with Class 10 electrode tips for forming the dimples (Ref. 19). The configuration of the dies and operational sequence for hot dimpling by this process are illustrated in Figure 71.

The principal disadvantage of any resistance-heated dimpling process is control of the heat pattern and measurement of the part temperature during the forming operation. However, the Convair Aerospace hot dimpling process offers the greatest versatility in development of techniques and tooling for hot dimpling. For this reason the Convair Aerospace resistance-heated dimpling process was selected for evaluation of unrecrystallized TD-NiCr Sheet.

Dimpling Limits. - Resistance heated dimpling dies were designed and fabricated to the general concept shown in Figure 71. The dimpling electrodes were made by brazing machined tips of Inconel 718 nickel-base superalloy to 1.59 cm (0.63 in.) diameter RWMA Class 3 copper electrodes. Inconel 718 was selected as the tip material because of its strength at elevated temperatures. Dies were fabricated for three dimple angles and three rivet diameters. Hot dimpling techniques were developed using a conventional three-phase 125 kVA resistance welding machine. Typical machine settings for dimpling 0.5 mm (0.020 in.) unrecrystallized sheet are as follows:

Pre-dimpling Force	445 N (100 lb)
Dimpling Force	1556 N (350 lb)
Preheat	10%
Dimpling Heat	15%
Heating Time	5 cycles
Cooling Time	5 cycles
Dimpling Impulses	15

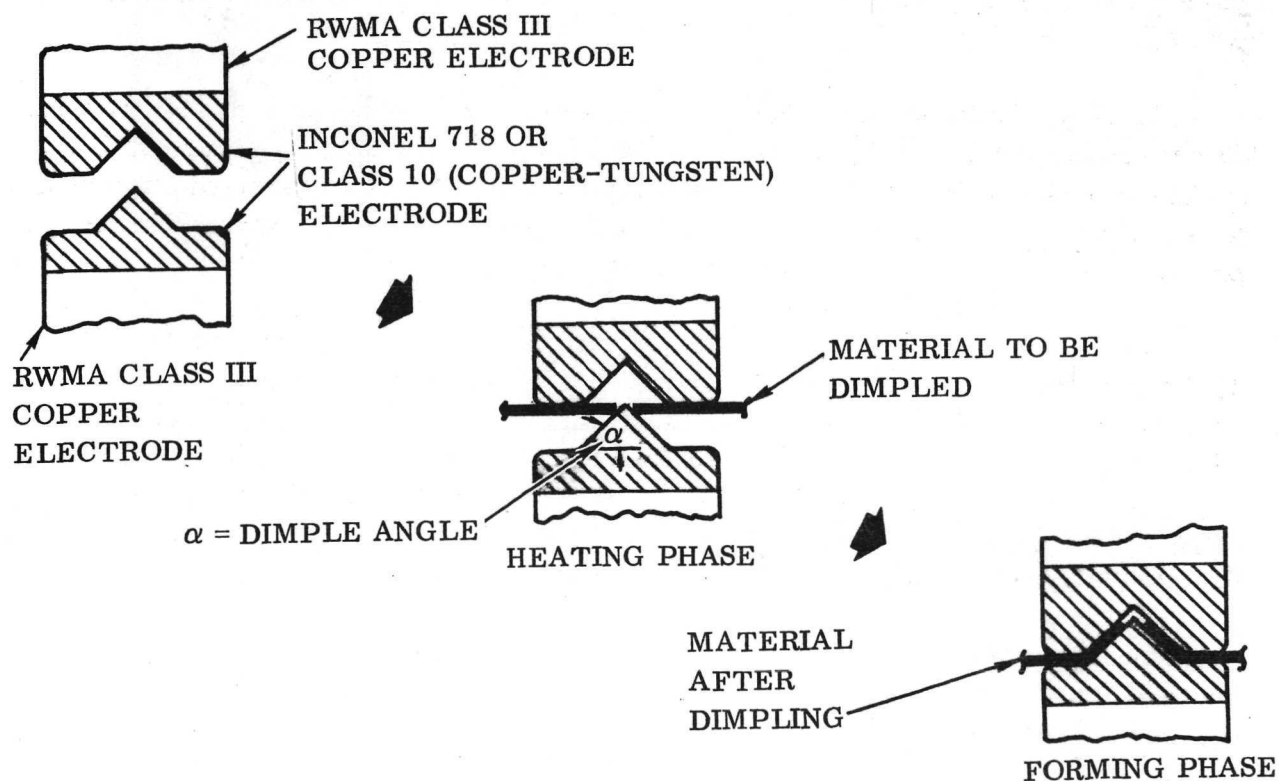


Figure 71. Details of Dies and Operational Sequence for Hot Dimpling by Resistance Heating on a Spotwelder

Since single action dimpling dies were used (no coining action to size the hole and flatten the bottom of the dimple), the holes were prepared undersized. Hole diameters of 2.56, 3.25 and 4.39 mm (0.101, 0.128 and 0.173 in.) were used for rivet diameters of 3.18, 3.97 and 4.76 mm (0.125, 0.157 and 0.188 in.) respectively. Hot formed dimples require a drilling and spot facing operation to complete dimple preparation. Test blanks were prepared by drilling, reaming, and deburring the holes in the same manner as for recrystallized material.

Difficulties were experienced in controlling temperature uniformity over the entire dimple area. Problems were encountered with circumferential cracks, radial cracks, and overheating. The circumferential cracks occurred at the bend, parallel to the rolling direction (strain transverse to rolling direction) when the temperature was too low. Radial cracks, originating from the hole, occurred at both low and high temperatures. In the latter case, fine-grain recrystallization also occurred near the hole due to overheating.

Dimpling tests were conducted for 0.25 and 0.5 mm (0.010 and 0.020 in.) sheet and dimples evaluated for a range of heat levels from too low (radial cracks) to satisfactory (no cracks) to too high (radial cracks). Temperatures during dimpling cannot be accurately measured, and the various heat levels were defined by heat input. Development of satisfactory dimpling schedules proved to be more difficult for the thinner material.

Machine schedules for the 100- and 120-degree (included angle) dimple configuration produced visually acceptable dimples, but the 80-degree dimple configuration could not be fully formed without cracks. The ductility of unrecrystallized TD-NiCr at the optimum forming temperature is not sufficient to permit the severe forming required for the 80-degree dimple configuration.

As discussed in the following section, metallographic examination of the 100- and 120-degree dimples disclosed that in most cases fine-grain recrystallization had occurred apparently due to the combination of high heat input and severe deformation. This type of recrystallization has a detrimental effect on elevated temperature strength of TD-NiCr and although containing no cracks, these dimples are not considered satisfactory. Further development of machine schedules and die configurations is required for successful hot dimpling of unrecrystallized sheet.

Comparison of hot dimpling test results with the theoretical dimpling limits at 760C (1400F) is shown in Figures 72 and 73. It should be noted that the 30, 40 and 50-degree dimple angles are equivalent to 120-, 100- and 80-degree included angles respectively. In the final analysis, no dimpling schedules were developed for the resistance-heated dimpling method that could consistently produce fully formed

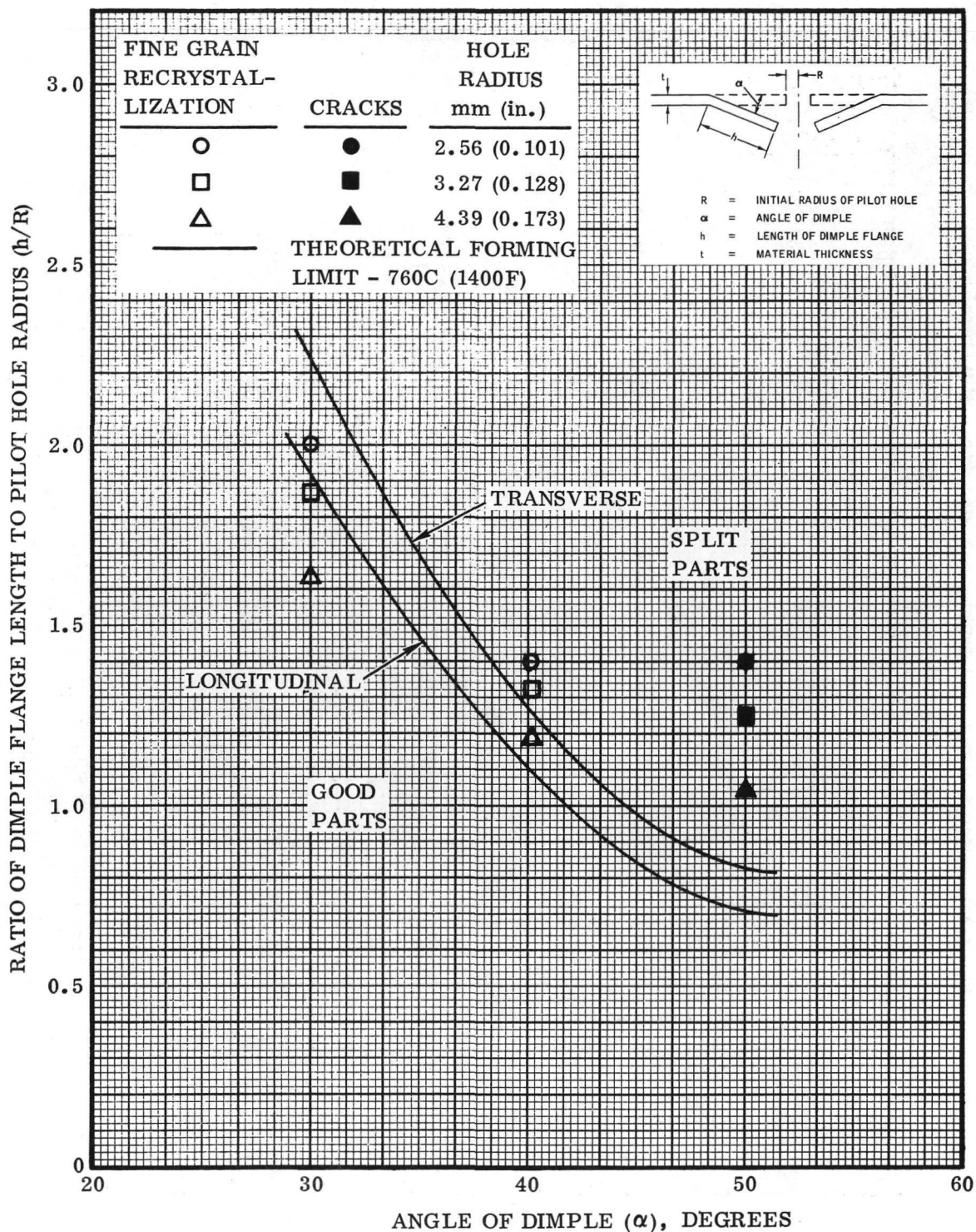


Figure 72. Actual Forming Data Superimposed on Theoretical Formability Curves for Hot Dimpling of 0.25 mm (0.010 in.) Unrecrystallized TD-NiCr Sheet - Heat 3714 (Code K)

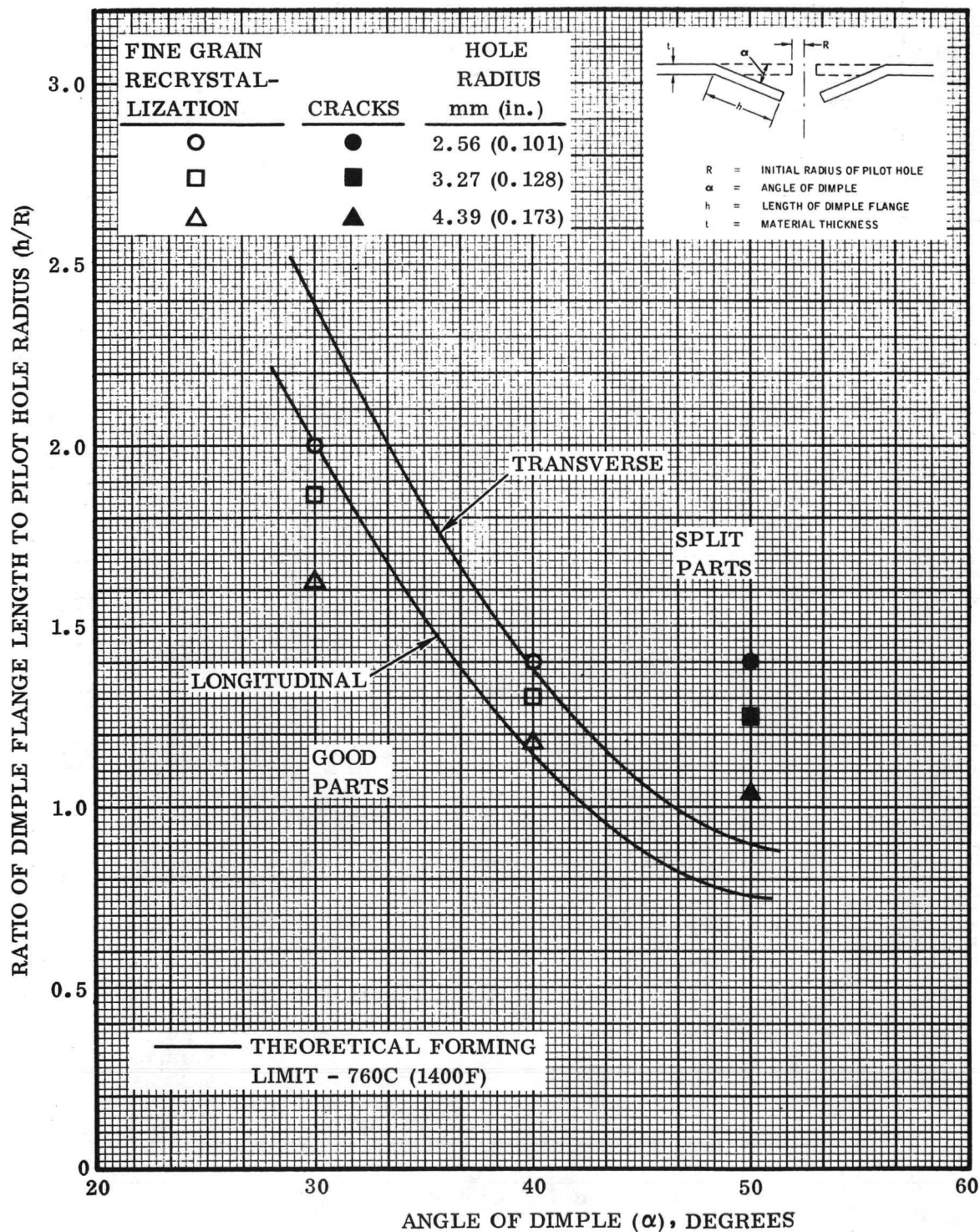


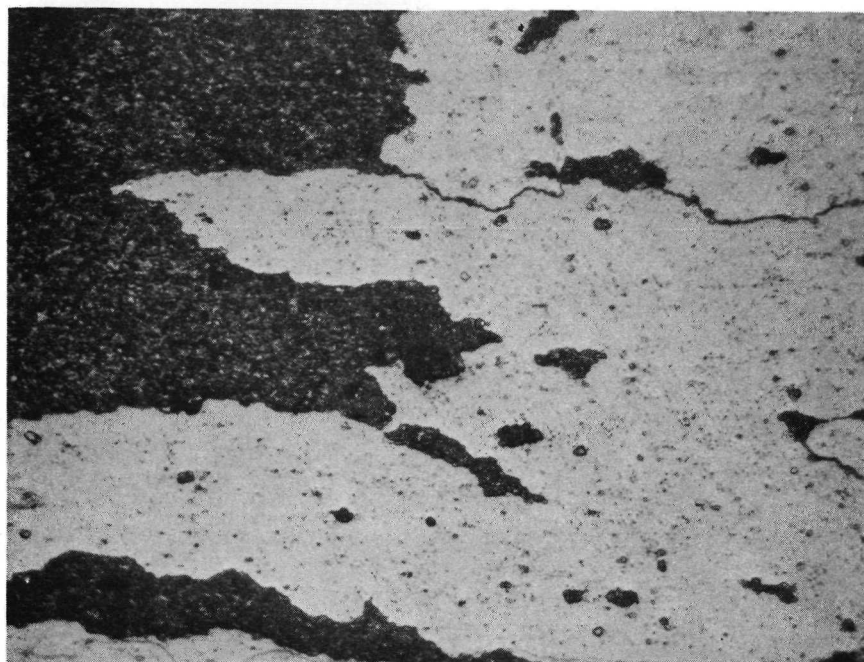
Figure 73. Actual Forming Data Superimposed on Theoretical Formability Curves for Hot Dimpling of 0.5 mm (0.020 in.) Unrecrystallized TD-NiCr Sheet - Heat 3709 (Code G)

dimples with no cracks or detrimental overheating. The predicted limits indicate better formability for the transverse orientation, but the experimental dimpling tests revealed better resistance to cracking for the longitudinal orientation. This agrees with results for brake and corrugation forming of unrecrystallized material as well as forming of recrystallized material.

It is evident that better control of heat input is necessary to prevent localized overheating during hot dimpling by the resistance-heating method. One approach for accomplishing this is changing to the use of refractory metal electrode tips for the dimpling dies. The present die material, Inconel 718 nickel-base superalloy, was selected so that the dies could operate at relatively high temperatures. However, poor temperature uniformity and short die life with Inconel 718 was evident during the hot dimpling tests. The use of copper-tungsten alloy for resistance dimpling dies was successful for hot dimpling of titanium alloys in previous Convair Aerospace studies.

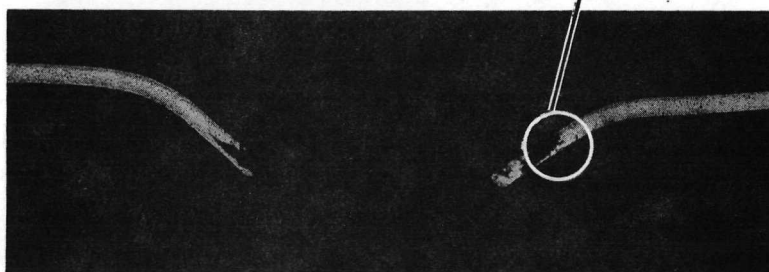
Microstructure. - Metallographic examinations were conducted on hot dimpled specimens of 0.25 and 0.5 mm (0.010 and 0.020 in.) unrecrystallized sheet. The samples were 100 and 120 degrees (included angle) dimple configurations for three rivet sizes representing the best schedules for the resistance-heated dimpling method. All specimens were given a recrystallization anneal for 2 hours at 1177C (2150F) in hydrogen prior to examination.

Results of the metallographic analyses disclosed detrimental effects on the microstructure due to localized overheating for more than one-half of the dimple specimens examined. Excessive heating adjacent to the pilot hole resulted in areas of fine-grained recrystallization that did not respond to the subsequent recrystallization anneal. Since fine-grain microstructure has lower strength at elevated temperatures than the normal large-grain recrystallized structure, this condition is undesirable. Figure 74 shows typical microstructure of hot formed dimples with fine-grain recrystallization (black patches) adjacent to the hole.



(a) Same as (b) showing fine-grain recrystallization following grain boundaries.

500X
Neg. D3786



(b) 100° dimple, 3.25 mm (0.128 in.) hole diameter, 0.25 mm (0.010 in.) sheet.

10X
Neg. D3784



(c) 120° dimple, 2.56 mm (0.101 in.) hole diameter, 0.5 mm (0.020 in.) sheet.

10X
Neg. D3785

Figure 74. Microstructure of Hot Formed Dimples in Unrecrystallized TD-NiCr Sheet

6. JOINING OF TD-NiCr SHEET

Joining techniques for TD-NiCr sheet were evaluated using four joining techniques: (1) resistance seam welding (solid state), (2) resistance spot welding (solid-state), (3) resistance spot welding (fusion), and (4) brazing. The two solid-state welding processes were used to evaluate joining of both recrystallized and unrecrystallized material. Previous studies have attributed the low strength of TD-NiCr welds at elevated temperatures to the interruption of microstructure at the joint (Ref. 8,9). Since the elevated temperature strength is dependent upon grain size and grain boundaries, solid-state welding of unrecrystallized material offers the best chance to eliminate the presence of equiaxed grains and a residual grain boundary at the weld line.

The approach used for the present program was to optimize the welding parameters for both types of material and evaluate the optimized weldments by metallography, by tensile shear testing at ambient and elevated temperatures, and by stress rupture testing at elevated temperatures. Joint efficiencies were determined by comparison of properties of optimized weldments with parent material properties. The approach used for the brazing study was to evaluate several brazing alloy compositions and develop an improved braze alloy for TD-NiCr with properties superior to TD-6 braze alloy. An earlier study led to identification of TD-6 as the best of the commercially available braze alloys for thin gage TD-NiCr sheet for reentry use. However, the TD-6 alloy was developed for brazing heavy sections of TD-NiCr for use in gas turbine components. In heavy sections, erosion of the substrate is not a critical problem but becomes more significant as sheet thickness decreases. A further disadvantage of TD-6 is that the braze temperature is high. Other problems include excessive reaction with TD-NiCr, low strength in stress rupture, and somewhat marginal oxidation resistance.

Several new brazing alloy compositions were developed and properties of brazements of these alloys were evaluated and compared with TD-6. Joint efficiencies were determined by comparison of tensile-shear and stress-rupture properties with parent material properties.

For use in evaluation of joint efficiencies, parent material tensile-shear and stress-rupture tests were conducted for one heat each of 0.08 mm (0.003 in.) and 0.25 mm (0.010 in.) recrystallized sheet and one heat of 0.25 mm (0.010 in.) unrecrystallized sheet.

Figure 75 shows a breakdown of materials used for each of the joining tasks.

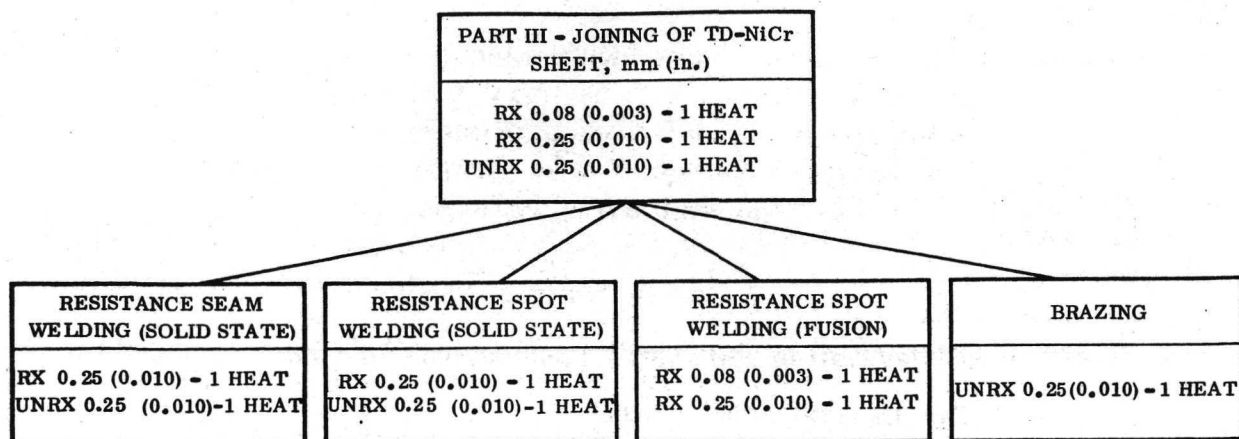


Figure 75. Material Matrix for Joining Development

Parent Material Properties Tests

Tensile-Shear Tests. - Tensile-shear properties of the three heats of material used for joining studies were determined at room temperature, 1093C (2000F), and 1316C (2400F). The unrecrystallized sheet (Heat 3689) was given a recrystallization anneal of 2 hours at 1177C (2150F) prior to testing. Test results are listed in Appendix D. The tensile-shear properties of the three heats of material are summarized in Table 23.

Table 23. Summary of Tensile Shear Properties of Recrystallized TD-NiCr Sheet

Test Temp. C (F)	Shear Direction ^(a)	Tensile Shear Strength MN/m ² (ksi)		
		0.25 mm (0.010 in.) Heat 3691	0.25 mm (0.010 in.) Heat 3689 ^(b)	0.08 mm (0.003 in.) Heat 3702
RT	L	535 (77.6)	461 (66.8)	398 (57.7)
	T	537 (77.6)	480 (69.6)	416 (60.4)
1093 (2000)	L	86 (12.5)	94 (13.7)	52 (7.5)
	T	100 (14.5)	94 (13.6)	54 (7.9)
1316 (2400)	L	70 (10.2)	61 (8.9)	43 (6.2)
	T	73 (10.6)	57 (8.3)	37 (5.3)

(a) L = Shear direction parallel to rolling direction.

T = Shear direction normal to rolling direction.

(b) Unrecrystallized sheet annealed 2 hours at 1177C (2150F) prior to test.

The specimen configuration used for the tensile-shear tests is shown in Figure 76. Two specimen configurations were considered, single and double shear, prior to selection of the double-shear specimen. The advantages of the double-shear configuration are: (1) more uniaxial loading (less bending moment), (2) the specimen is more rigid and, therefore, less subject to damage in handling and installing in the test machine, and (3) it gives an average shear value for two locations in the specimen. A previous configuration was modified to provide a short shear path and narrow center slot to overcome the tendency of thin-gage material to buckle and tear laterally. This condition had not been encountered in previous tests made with heavier gage material. An untested specimen and typical fractured specimens are shown in Figure 77.

Stress-Rupture Tests. - Stress-rupture properties of parent material were determined at 982, 1093, and 1204C (1800, 2000, and 2200F) for the same three heats as the tensile-shear tests. Test results are presented in Appendix D. The stress-rupture properties are plotted in Figures 78 through 86.

The specimen configuration for the parent-material stress-rupture tests is the same 22.8 cm (9.0 in.) long tensile specimen used for the forming studies (Figure 4). The unrecrystallized specimens were given a recrystallization anneal of 2 hours at 1177C (2150F) in dry hydrogen after machining. Stress-rupture tests were conducted using Satec creep-rupture machines with platinum element resistance-heated furnaces. Test temperature was controlled with Pt/Pt-13% Rh thermocouples attached to the gage section of each specimen. The initial tests revealed several problems related to test procedures for the thin-gage material. Six failures occurred during or immediately after loading, and two specimens failed at the pin hole.

Two revisions were made to the test procedures: tighter attachment of the mechanical doublers and adaption of dead-weight loading. The principal cause of the premature failures was a high load temporarily applied during automatic leveling of the loading arm. The 53.4 and 89 kN (12,000 and 20,000 lb) capacity Satec creep machines are not sufficiently sensitive for use with loads less than 222 N (50 lb) that are required for the 0.25 mm (0.010 in.) thick test specimens. Subsequent tests were conducted with the revised test procedures using dead-weight loading. Although some additional specimens failed during or immediately after loading, these tests were conducted at high stress levels, and there is no evidence the results are not valid. The only additional changes necessary for stress-rupture testing of 0.08 mm (0.003 in.) material was the use of Inconel X750 nickel-base superalloy doublers spot welded to both sides of the grip ends of each specimen. A total of 97 tests were performed to establish the stress-rupture properties of the three heats of material.

NOTES:

1. 1.02 (0.400) SLOT TO BE CENTERED ON ϕ OF HOLES WITHIN ± 0.013 (± 0.005) AND \perp TO ϕ OF HOLES WITHIN 1° .
2. THE TWO SHEAR PATHS TO BE EQUAL WITHIN 0.005 (0.002).
3. ALL DIMENSIONS IN CENTIMETERS (INCHES).

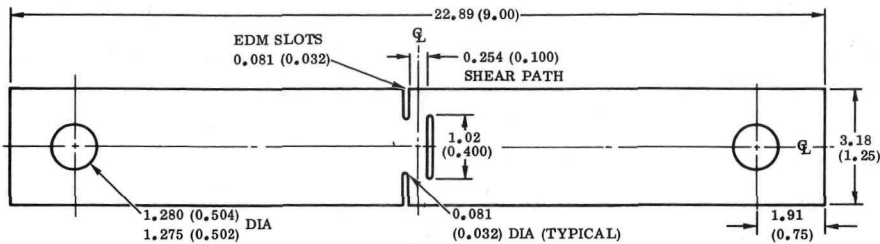
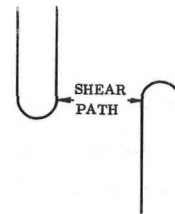
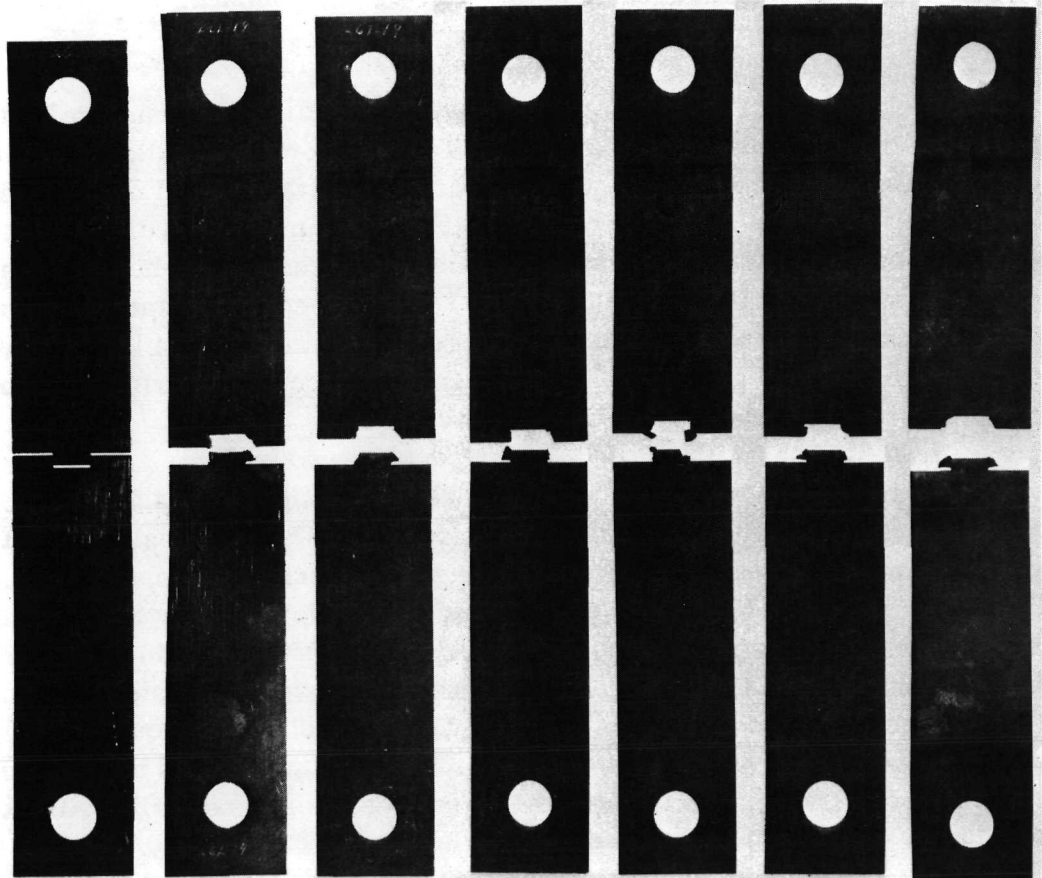


Figure 76. Double Shear Specimen Configuration for Parent Material Tensile Shear Tests



Neg. 112579B

SPEC. NO.	L6T-30	L6L-19	L6T-19	L6L 20	L6T-28	L6L-25	L6T-24
GRAIN DIRECTION	T	L	T	L	T	L	T
TEST TEMP C (F)	UNTESTED	RT	RT	982 (2000)	982 (2000)	1316 (2400)	1316 (2400)

Figure 77. Typical Fractures in Tensile-Shear Specimens of 0.25 mm (0.010 in.) Recrystallized TD-NiCr - Heat 3691 (Code L6)

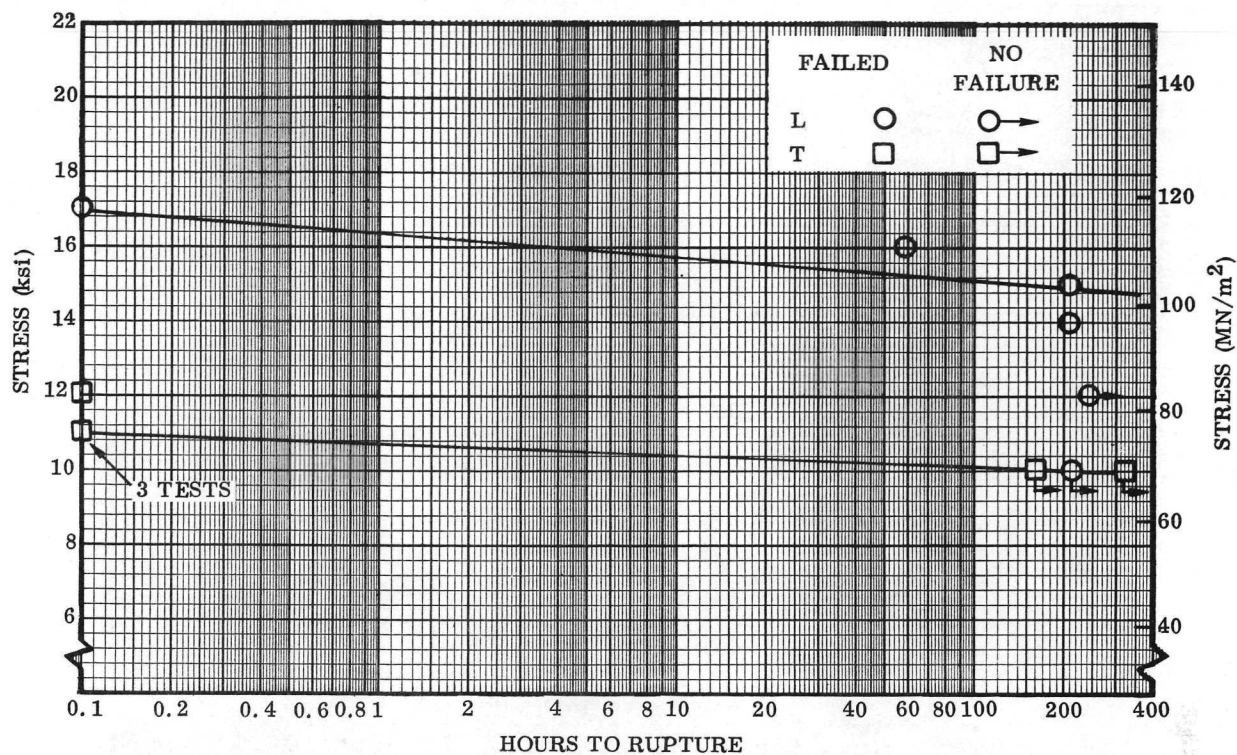


Figure 78. Stress-Rupture Properties of 0.25 mm (0.010 in.) TD-NiCr Sheet at 982C (1800F) — Heat 3691 (Code L6)

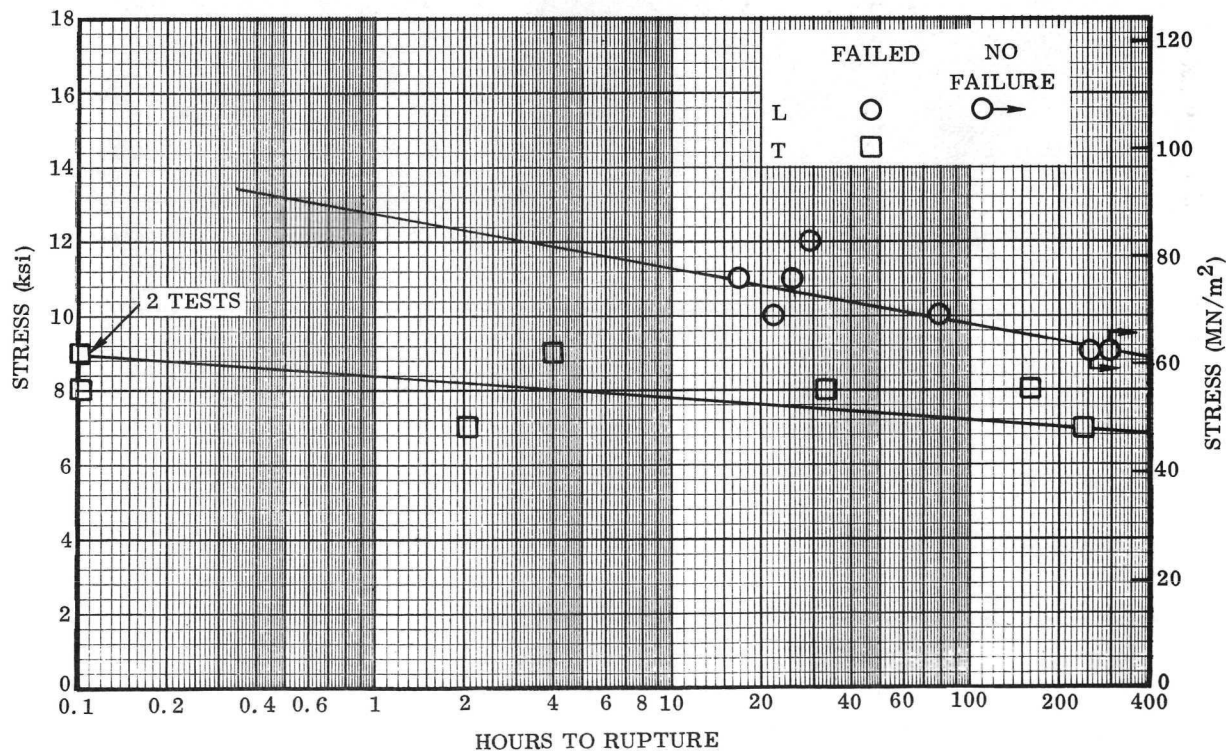


Figure 79. Stress-Rupture Properties of 0.25 mm (0.010 in.) TD-NiCr Sheet at 1093C (2000F) — Heat 3691 (Code L6)

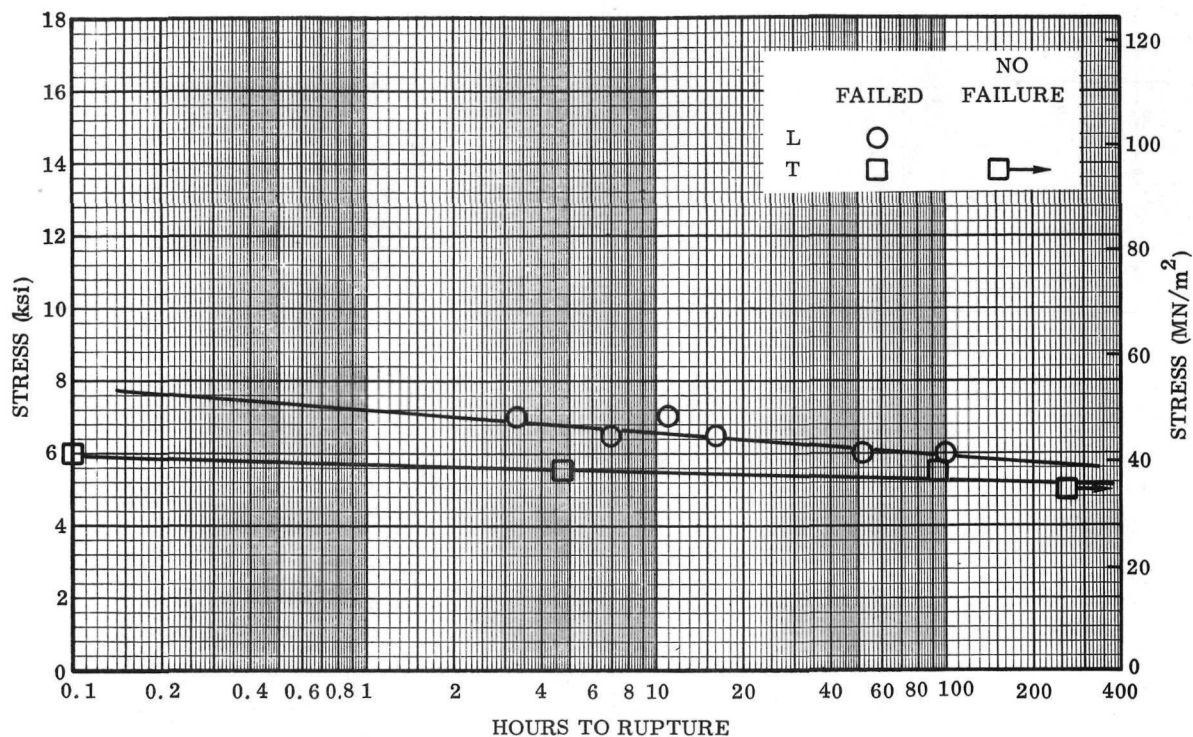


Figure 80. Stress-Rupture Properties of 0.25 mm (0.010 in.) TD-NiCr Sheet at 1204C (2200F) - Heat 3691 (Code L6)

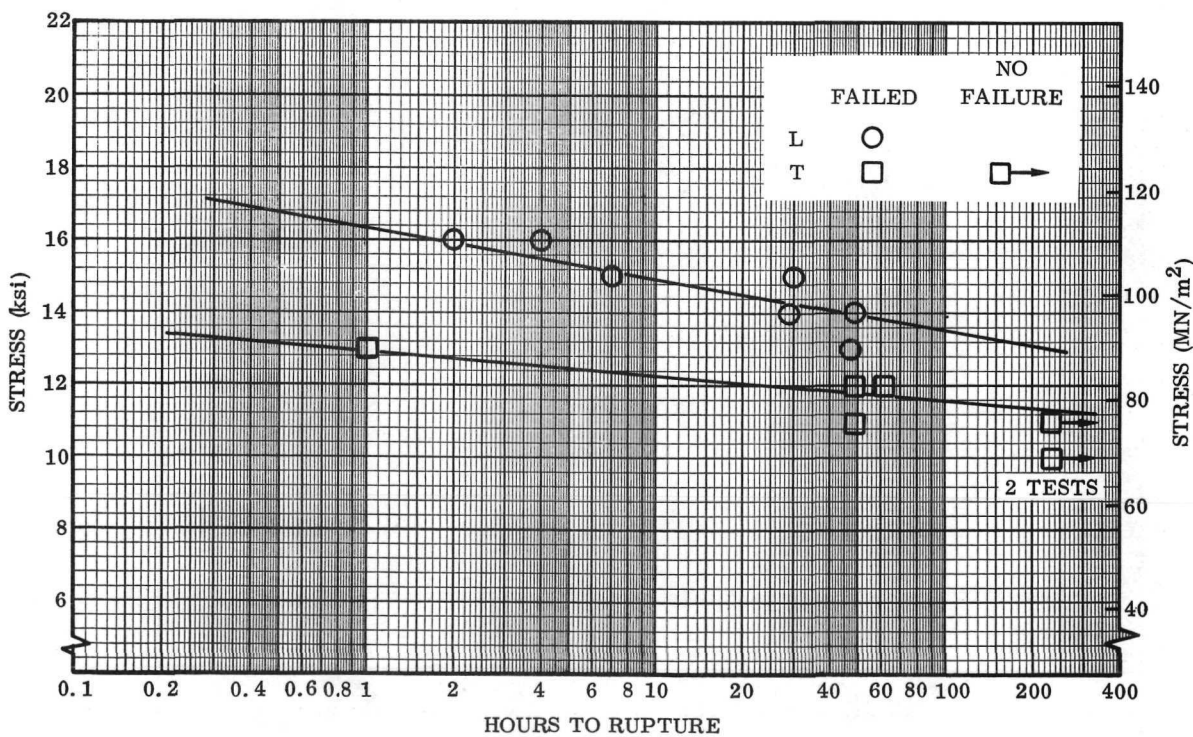


Figure 81. Stress-Rupture Properties of 0.25 mm (0.010 in.) TD-NiCr Sheet at 982C (1800F) - Heat 3689 (Code J1)

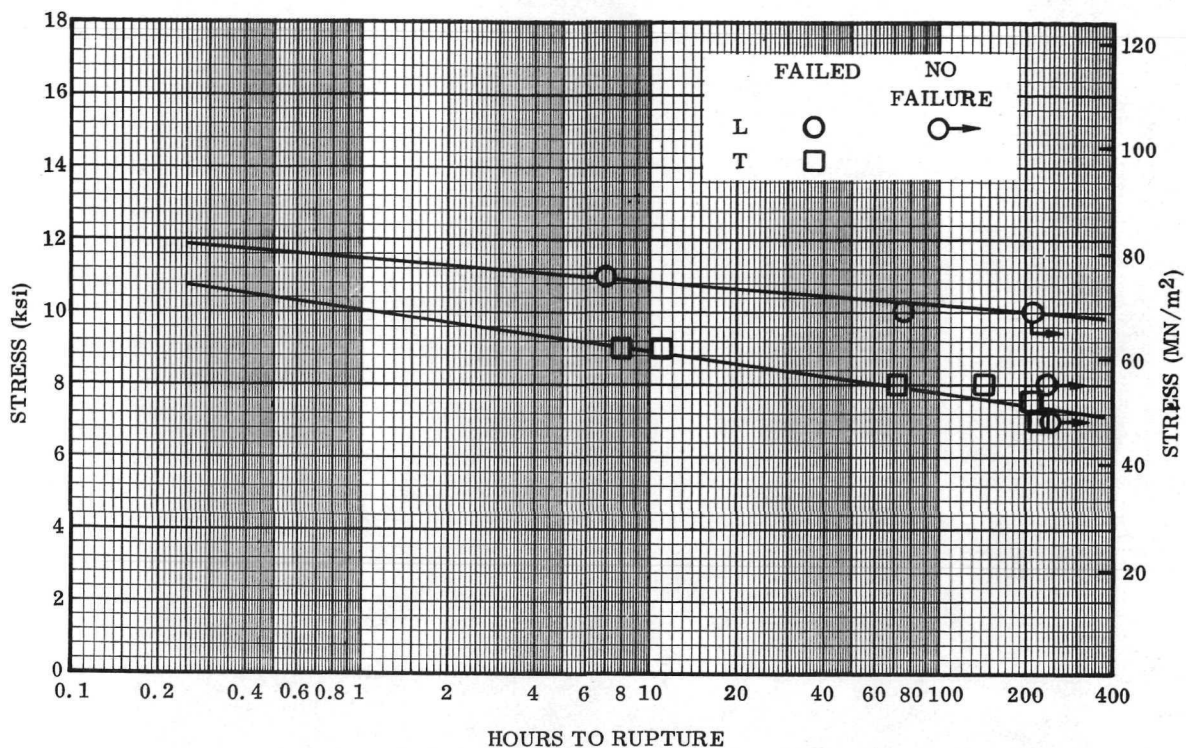


Figure 82. Stress-Rupture Properties of 0.25 mm (0.010 in.) TD-NiCr Sheet at 1093C (2000F) — Heat 3689 (Code J1)

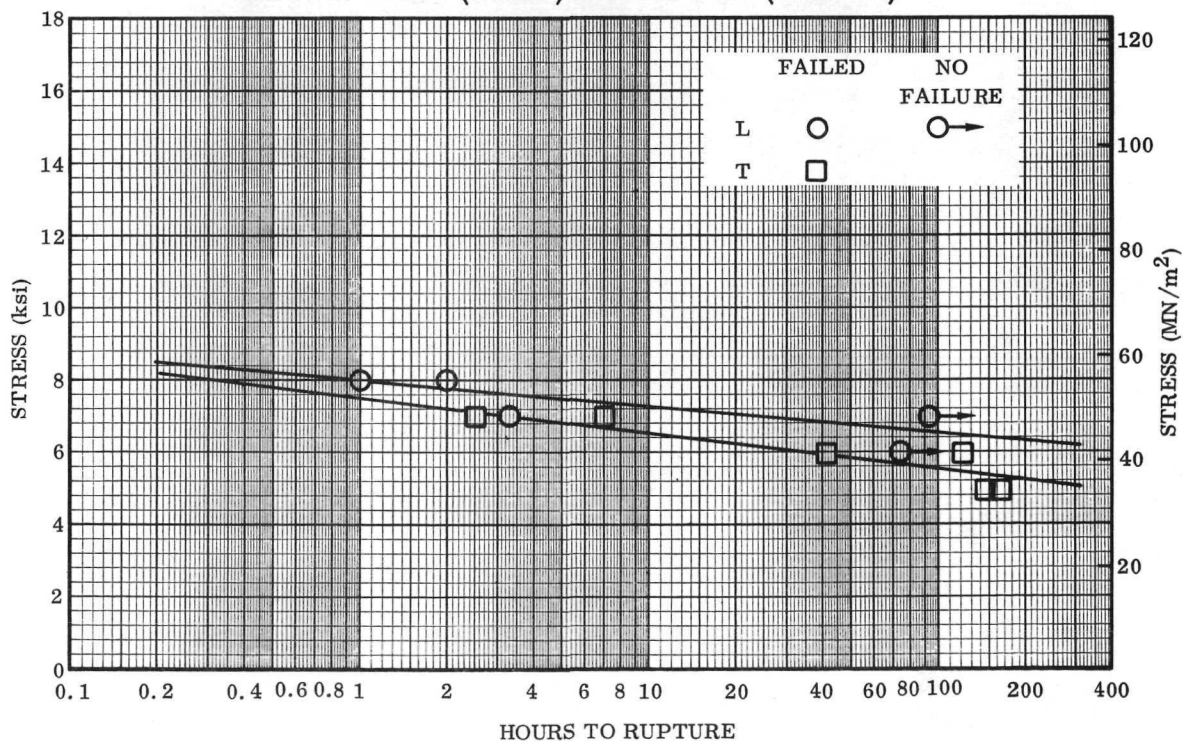


Figure 83. Stress-Rupture Properties of 0.25 mm (0.010 in.) TD-NiCr Sheet at 1204C (2200F) — Heat 3689 (Code J1)

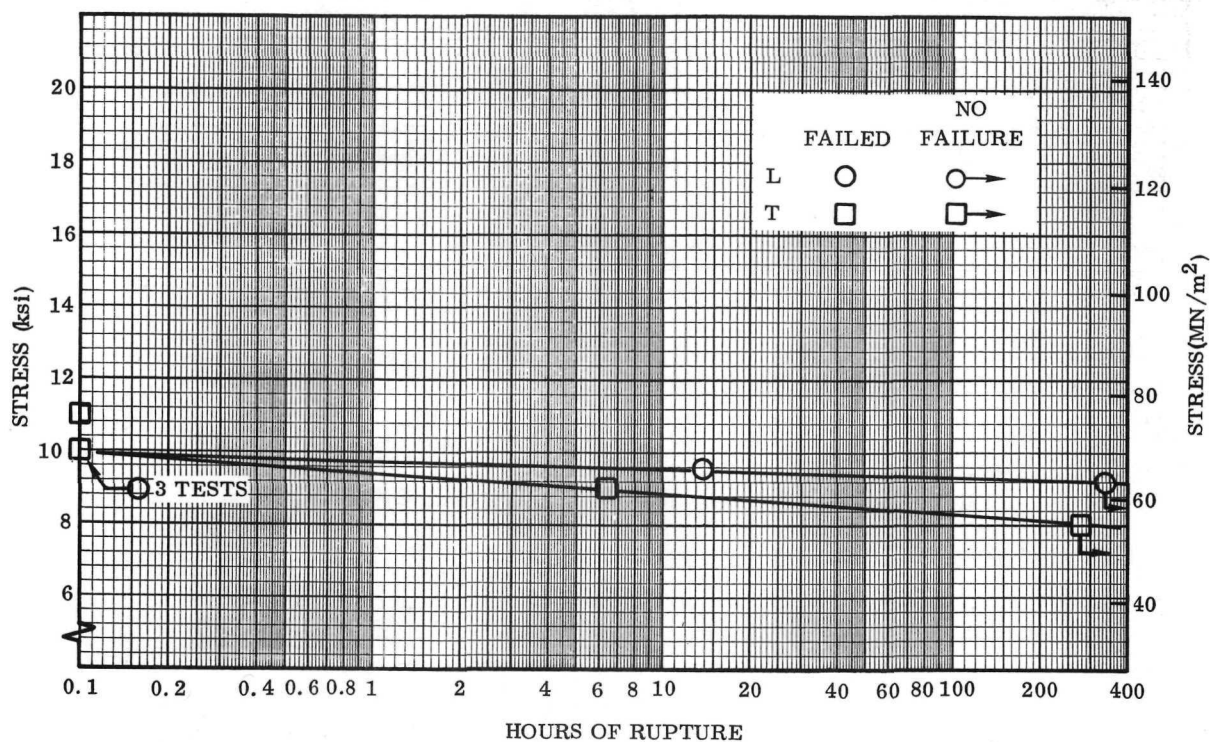


Figure 84. Stress-Rupture Properties of 0.08 mm (0.003 in.) TD-NiCr Sheet at 982C (1800F) — Heat 3702

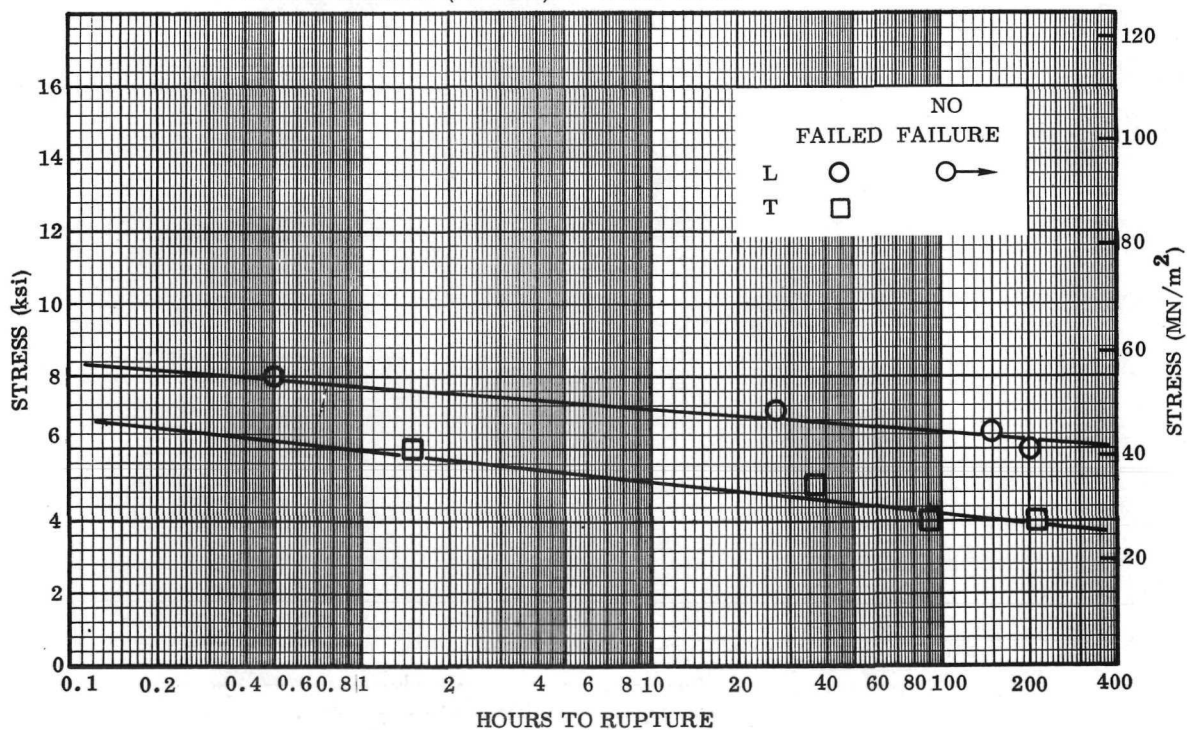


Figure 85. Stress-Rupture Properties of 0.08 mm (0.003 in.) TD-NiCr Sheet at 1093C (2000F) — Heat 3702 (Code M)

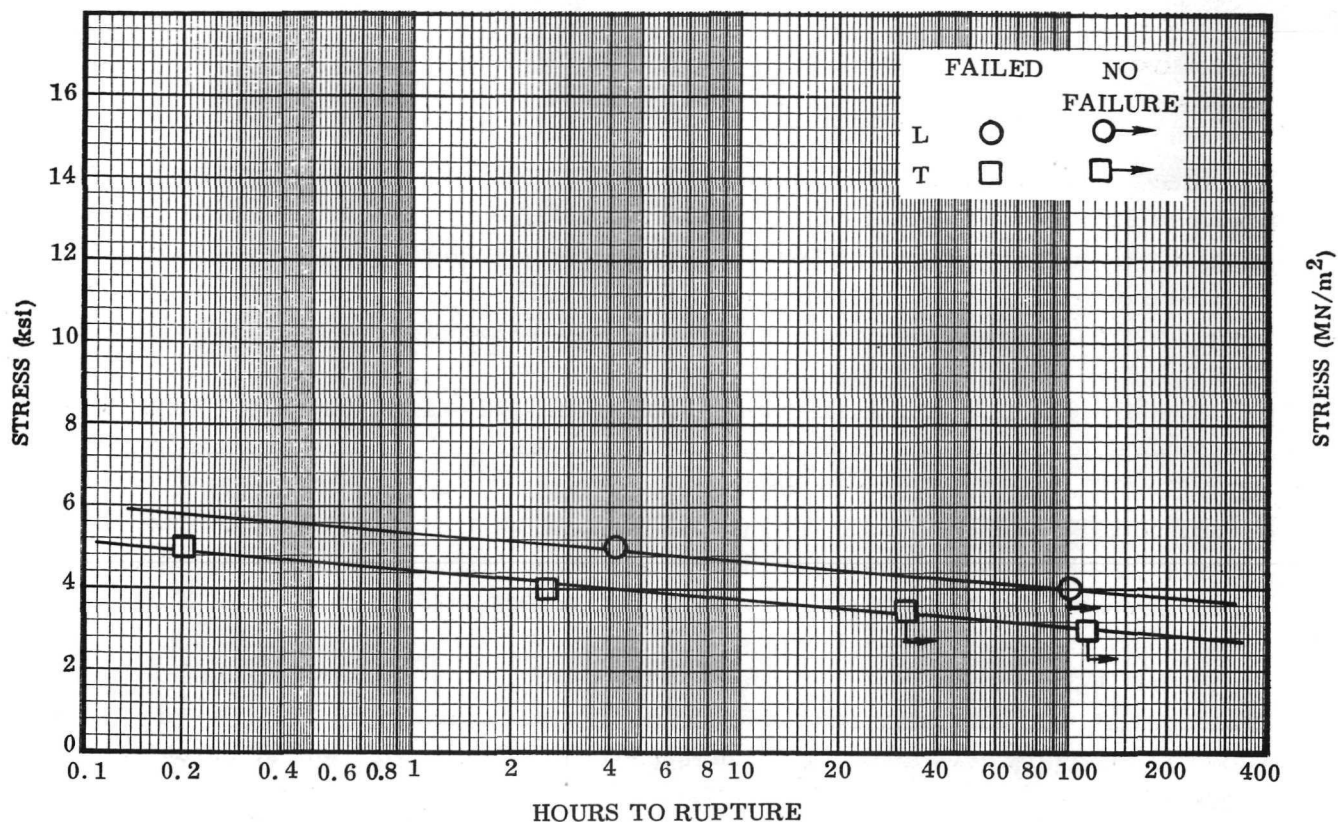


Figure 86. Stress-Rupture Properties of 0.08 mm (0.003 in.) TD-NiCr Sheet at 1204C (2200F) - Heat 3702 (Code M)

Resistance Seam Welding (Solid-State)

Resistance hot-press welding methods often cause excessive distortion in thin sheet material panels. The continuous resistance seam welding process developed by Solar* reduces the distortion very markedly because the heating times are reduced by an order of magnitude compared to heating times of several seconds used in (static) resistance hot press welding. The local heat input is the major factor in reducing distortion of flat panels to a minimum. The process uses refractory metal wheel electrodes to develop localized heating at the joint and to apply welding pressure. Temperature is programmed from a special power supply, pressure is controlled by wheel force, and time is controlled by speed. The process is performed in a protective inert gas atmosphere.

* Solar proprietary "Continuous Seam Diffusion Bonding Process," U.S. Patent 3,644,698, Issued February 22, 1972.

The experimental approach for evaluation of resistance seam welding (solid-state) procedures for TD-NiCr sheet material was divided into two steps, summarized as follows:*

Step A. - Three parameters of the welding process and four parameters of surface preparation were evaluated on two types of material, commercial (recrystallized) and specially-processed (unrecrystallized) sheet. Evaluation proceeded in a three tier sequence of testing through room temperature tensile shear, 1093C (2000F) tensile shear, and 1204C (2200F) stress rupture, all with associated metallographic analysis.

Step B. - The optimum surface preparation and welding parameters established in Step A were used to fabricate test specimens in both recrystallized and unrecrystallized TD-NiCr sheet. These specimens were tested in tensile shear at ambient temperature, 1093C (2000F) and 1316C (2400F); and in stress rupture at 982C (1800F), 1093C (2000F) and 1204C (2200F). These data were referenced to baseline data generated in tests of sheet from the same heats of parent metal.

The TD-NiCr sheet material used for the resistance seam welding (solid-state) development was recrystallized 0.25 mm (0.010 in.) sheet, Heat 3691, Sheet No. 653 (Code L2) and unrecrystallized 0.25 mm (0.010 in.) sheet, Heat 3689, Sheet No. 637 (Code J3).

Establishing Weld Parameters - Step A. - The criteria for screening the welding schedule were established as:

- (1) Minimum recrystallization at the joint interface
- (2) A thickness reduction in welding of less than 5 percent
- (3) Parent material failure in tensile tests

Welding parameters that were varied to achieve optimum properties included:

- (1) Surface preparation
- (2) Weld speed
- (3) Weld temperature
- (4) Squeeze force

* The resistance seam welding development work was performed by the Solar Division of the International Harvester Company. The description of this subcontracted work was extracted from Solar Report RDR 1721-4 (Ref. 20).

A set of lap joint specimens was prepared to study the effect of surface preparation on the resistance seam welding (solid state) of recrystallized TD-NiCr. Surface conditions evaluated were obtained through the following treatments:

Condition A - Hot alkaline degrease; deionized water/air blast rinse; warm air dry

Condition B - Hot alkaline degrease; tap water rinse; abrade through 600 grit emery paper (weld side only); rinse deionized water/air blast; warm air dry

Condition C - Preparation B plus: electropolish in Summa* solution (27 to 38C (80 to 100F), 8 volts, 1.5 minutes); rinse deionized water/air blast; dry with warm air

Condition D - Preparation A plus: electropolish in Summa solution as above.

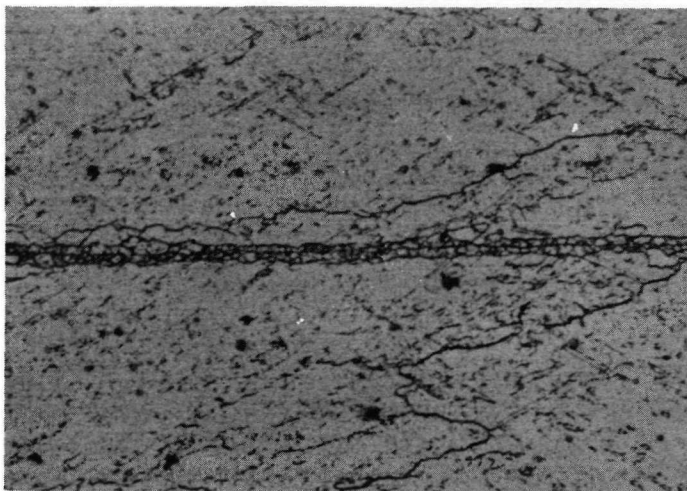
Three lap joint specimens, each surface treated according to one of the conditions above, were fabricated using the following welding parameters:

- (1) 0.125 cm (0.050 in.) overlap (5t) with L/L orientation**
- (2) 1379 N (310 lb) squeeze force
- (3) 20.3 cm (8 in.) per minute weld speed
- (4) 1316C (2400F) (estimated) weld temperature

Metallography of the joints after recrystallization annealing for 2 hours at 1177 C (2150 F) is shown in Figure 87. Surface treatments A and B (Figure 87a and 87b) are characterized by recrystallization along the joint interface. This recrystallization is from two to three grains wide. It was felt that a worked surface resulting from the supplier's final treatment of the sheet (cold rolling after belt polish) gave rise to the recrystallization. The 600 grit abrading (Condition B) is also undesirable as it adds additional surface work to the as-received condition. Surface condition C strikingly reveals the superiority of the electropolish relative to the other surface preparations. Electropolishing apparently is effective in removing the heavily worked surface, even though less than 5×10^{-4} cm (2×10^{-4} in.) of metal is removed per surface.

* Summa electropolishing is a proprietary process of Moleetrics, Inc., Inglewood, Calif.

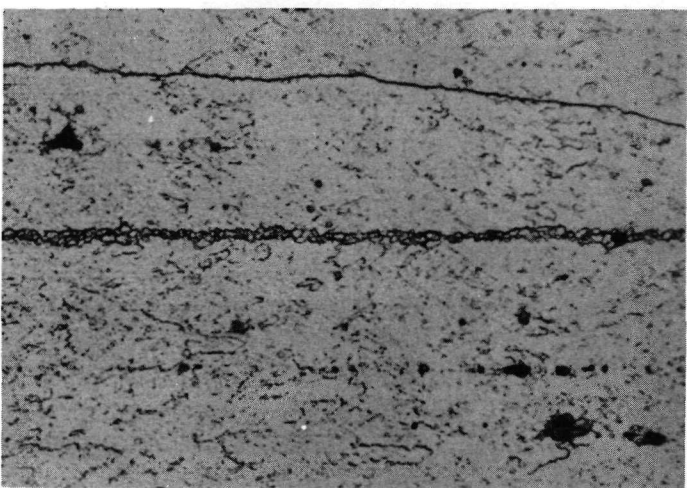
** Sheet Orientations at Joint: Rolling direction of sheet in both members of lap joint at right angle to seam constitutes a longitudinal/longitudinal (L/L) orientation. Rolling direction of sheet in one member of lap joint at right angle to seam with other member parallel to seam constitutes a longitudinal/transverse (L/T) orientation.



(a) Preparation A

Alkaline degrease plus rinse

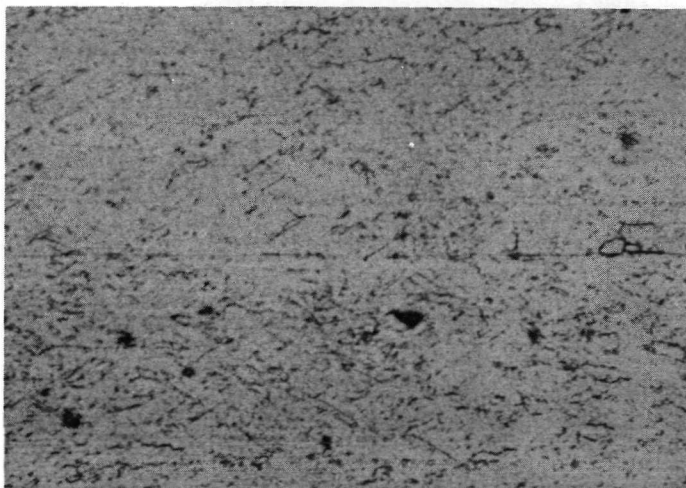
Log 4172



(b) Preparation B

Alkaline degrease plus 600
grit abrade plus rinse

Log 4173



(c) Preparation C

Alkaline degrease plus 600
grit abrade plus electro-
polish plus rinse

Log 4174A

Magnification 1000X

Figure 87. Lap Joints of 0.25 mm (0.010 in.) Recrystallized TD-NiCr
Showing Effects of Various Pre-weld Surface Treatments
(Post-weld Annealed for 2 hours at 1177C (2150 F) in dry hydrogen)

After annealing at 1177C (2150F) for 2 hours in dry hydrogen, lap joints produced with the above schedule with surface preparation D showed no recrystallization at the weld interface that could be discerned at 1000X magnification (Figure 88).

Four creep rupture tests were performed at 1171C (2140F) in air on specimens prepared by surface treatment D with the above schedule. Originally, it was planned to perform the stress-rupture tests at 1204C (2200F); however, during the first test the Satec creep machine furnace in the Solar Laboratories was found incapable of its maximum rated temperature of 1204C (2200F). The 1171C (2140F) test temperature was also used on the three subsequent tests to enable data comparison with the first test. Subsequent tests were performed at 1204C (2200F) in a platinum resistance furnace as described in Appendix E. The four test results are shown plotted in Figure 89 as a function of uniaxial tensile stress versus log time. The use of uniaxial tensile stress in the sheet neglects bending stress due to rotation of the lap joint and stress concentration at the change of section of the joint.

The first test, performed at 34.5 MN/m^2 (5 ksi) was terminated unfailed after 93 hours. The other three tests at higher stresses all ruptured in the parent material adjacent to the lap joint. Examination of the specimens indicated the following: (1) failure in each case originated at the change of section of the lap joint, and (2) the fracture did not extend into the joint interface.

The sequence of steps used to arrive at the optimum weld parameters (weld speed, squeeze, and current) for the L/L orientation joints in recrystallized material with surface preparation D (electropolish) are presented in Table 24. The evaluation criteria used in Table 24 were: presence of melt, occurrence of excessive deformation, buckling of the sheets, visibility of bondline, and presence of fine recrystallized grains on the bondline.

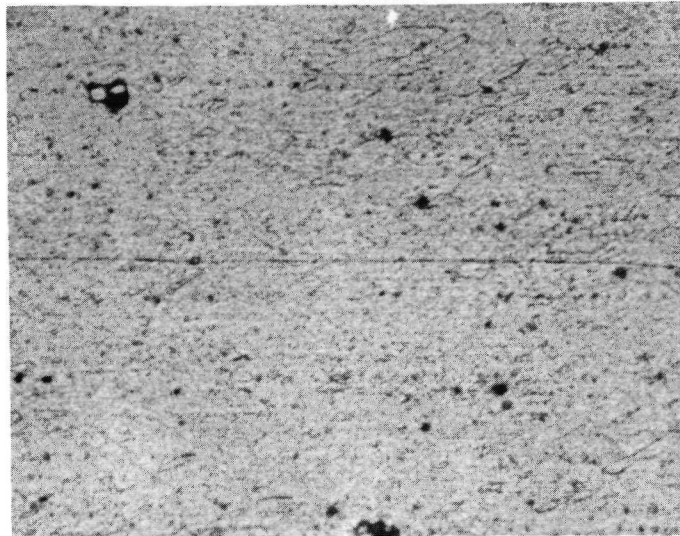
Using the optimized weld parameters, further evaluation of resistance seam welding was conducted for both recrystallized (R) and unrecrystallized (U) material, two grain orientations (L/L and L/T), and four surface conditions.

Lap seam welds were produced in 25.4 cm (10 in.) lengths for each material type, sheet orientation, and surface preparation by joining two 11.4 cm (4.5 in.) by 25.4 cm (10 in.) sheets.

All specimens were welded using the following parameters:

0.125 cm (0.050 in.) nominal overlap (5t)

1379 N (310 lb) squeeze force



Preparation D

Alkaline degrease
plus electropolish
plus rinse

Post-weld annealed
2 hours at 1177C
(2150F)

Log 4174B

Magnification: 1000X

Figure 88. Microstructure of Joint Interface of Lap Joint
Made in 0.25 mm (0.010 in.) Recrystallized
TD-NiCr Sheet by Resistance Seam Welding

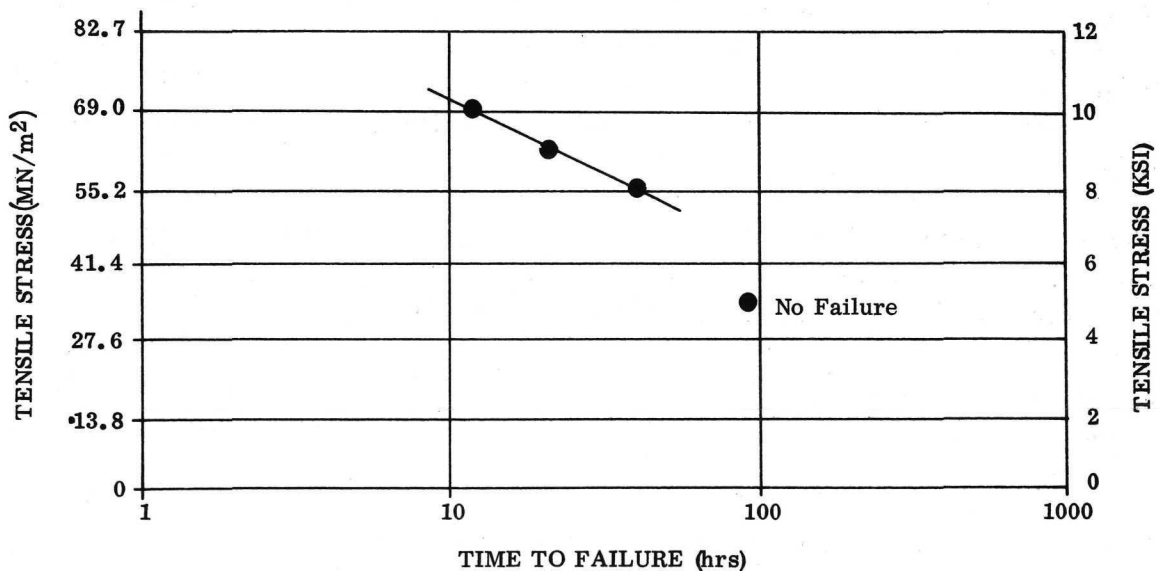


Figure 89. Tensile Stress as a Function of Time to Rupture for
Resistance Seam Welded Lap Joints in 0.25 mm
(0.010 in.) Recrystallized TD-NiCr Sheet

Table 24. Weld Parameter Optimization for L/L Orientation of Recrystallized Sheet (Surface Preparation D - Electropolish)

Weld Parameters			Joint Evaluation				
Speed cm/min. (in/min)	Squeeze Force N (lbs)	Current (amps)	Visual Examination			Metallographic	
			Melt	Thinning (%)	Buckling	Jointline	Jointline Recryst
8.9 (3.5)	2046 (460)	80	None	9.5-12	Severe		
		100	None	12-19	Severe		
		110	Minor	19	Severe		
		120	Minor	19	Severe		
		130	Severe	19	Severe		
8.9 (3.5)	2046 (460)	85	None	13	Severe		
		90	None	13-16	Severe		
		95	None	20	Severe		
		100	None	20	Severe		
8.9 (3.5)	1379 (310)	60	None	9	Moderate	Visible	None
		70	None	9	Moderate	Visible	None
		80	None	12	Moderate	Visible	None
		90	None	19	Moderate	Visible	None
15.2 (6.0)	1379 (310)	60	None	0*	Light	Visible	None
		70	None	0	Light	Visible	
		80	None	0	Light	Visible	
		90	None	6	Light	Visible	
30.5 (12.0)	1379 (310)	50	None	0	Light	Visible	None
		60	None	0	Light	Visible	None
		70	None	3-6	Light	Visible	None
15.2 (6.0)	1379 (310)	40	None	0	Light	Visible	None
		50	None	0	Light	Visible	None
		60	None	6	Light	Visible	None
15.2 (6.0)	1379 (310)	40	None	0	None	Visible	None
20.3 (8.0)	1379 (310)	60	None	0-4	Minimal	Not Visible	None

* Zero thinning means less than 0.64×10^{-3} cm (0.00025 inch) decrease in joint thickness.

Weld speed: 20.3 cm (8 in.)/minute

Weld heat: 60 amperes (1316C (2400F) estimated)

The joints were evaluated by a three-tier sequence of mechanical screening tests, supplemented by metallographic analysis. The mechanical tests that are progressively more critical of joint quality are:

Room-temperature tensile shear

1093C (2000F) tensile shear

1204C (2200F) stress rupture

Tensile-Shear Tests. - The room temperature tensile-shear tests were conducted in duplicate on 14 combinations of material type, sheet orientation, and surface preparation. The test procedure and equipment are described in Appendix E. All specimens showed good strength and toughness with fracture occurring in the parent material either at the change in section at the edge of the joint, or removed from the joint within the reduced section. The ultimate uniaxial tensile stress in the parent material and the level of shear stress attained in the lap joints are tabulated for each test in the upper portion of Table 25.

Very weak welds were produced in recrystallized sheet with longitudinal/transverse orientation when electropolishing was the final step in the preparation of the surface for welding. Good welding was not achieved with this combination, even though the welding current was varied in 5-ampere steps from a low of 50 amperes to the 75-ampere level. It was interesting to find that good welds were achieved with this same material and surface preparation when the sheet orientation was either L/L or T/T, but not for the mixed combination, L/T. The reason for the sensitivity of weld quality to sheet orientation is not well understood but may be related to anisotropy of the thin sheet with regard to thermal expansion, elasticity/plasticity, and other properties. The relatively rough surface finish of Conditions A and B appear to outweigh the directional effect by recrystallization at the weld line.

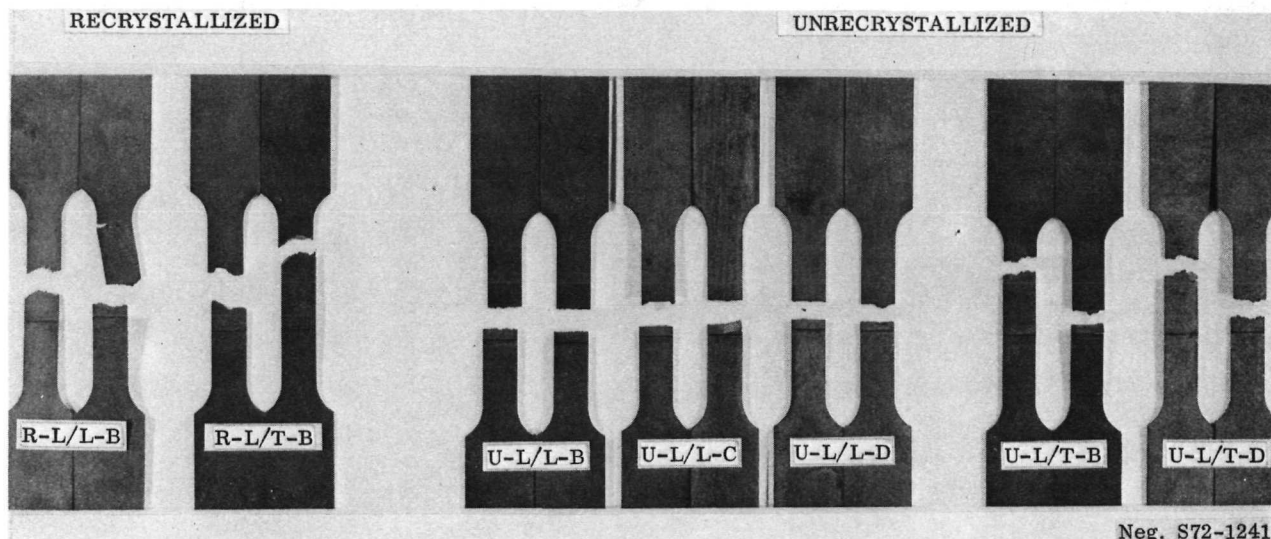
At the second tier of mechanical testing, eight specimen combinations were evaluated in duplicate by 1093C (2000F) tensile-shear tests. The eight combinations consisted of two materials (R and U), and two orientations (L/L and L/T) with one mechanical surface preparation (Condition B) and one electropolished preparation (Condition C and/or D). Typical specimens are shown after testing in Figure 90. The joint overlap, the uniaxial tensile stress in the parent material at fracture, and the level of shear stress attained in the joint are presented in the lower portion of Table 25.

Table 25. Tensile-Shear Test Data for Resistance Seam Welded (Solid-State) TD-NiCr Sheet

Test Temperature C (F)	Surface Preparation	Recrystallized (R)						Unrecrystallized (U)					
		L/L			L/T			L/L			L/T		
		Overlap cm (in)	Ultimate Tensile Strength MN/m ² (ksi)	Joint* Shear MN/m ² (ksi)	Overlap cm (in)	Ultimate Tensile Strength MN/m ² (ksi)	Joint* Shear MN/m ² (ksi)	Overlap cm (in)	Ultimate Tensile Strength MN/m ² (ksi)	Joint* Shear MN/m ² (ksi)	Overlap cm (in)	Ultimate Tensile Strength MN/m ² (ksi)	Joint* Shear MN/m ² (ksi)
Room	A	0.191 (0.075)	827 (120)	98.6 (14.3)	0.184 (0.073)	896 (130)	97.9 (14.2)	0.183 (0.072)	883 (128)	122.7 (17.8)	0.163 (0.064)	883 (128)	124.1 (18.0)
		0.188 (0.074)	869 (126)	99.3 (14.4)	0.188 (0.074)	855 (124)	92.4 (13.4)	0.183 (0.072)	855 (124)	117.9 (17.1)	0.168 (0.066)	862 (125)	122.7 (17.8)
	B	0.160 (0.063)	793 (115)	120.0 (17.4)	0.208 (0.082)	814 (118)	79.3 (11.5)	0.191 (0.075)	883 (128)	117.2 (17.0)	0.165 (0.065)	883 (128)	125.5 (18.2)
		0.160 (0.063)	779 (113)	111.0 (16.1)	0.208 (0.082)	724 (105)	71.0 (10.3)	0.191 (0.075)	827 (120)	110.3 (16.0)	0.165 (0.065)	883 (128)	125.5 (18.2)
	C	0.201 (0.079)	883 (128)	89.6 (13.0)		No Bond		0.170 (0.067)	841 (122)	113.1 (16.4)	0.175 (0.069)	896 (130)	116.5 (16.9)
		0.201 (0.079)	827 (120)	84.1 (12.2)		No Bond		0.170 (0.067)	876 (127)	117.2 (17.0)	0.191 (0.075)	876 (127)	107.6 (15.6)
	D	0.170 (0.067)	834 (121)	99.3 (14.4)		No Bond		0.165 (0.065)	903 (131)	130.3 (18.9)	0.170 (0.067)	862 (125)	116.5 (16.9)
		0.170 (0.067)	807 (117)	95.8 (13.9)		No Bond		0.165 (0.065)	869 (126)	124.1 (18.0)	0.170 (0.067)	848 (123)	114.5 (16.6)
1093 (2000)	B	0.183 (0.072)	114.5 (16.6)	15.2 (2.2)	0.173 (0.068)	123.4 (17.9)	14.5 (2.1)	0.198 (0.078)	114.5 (16.6)	15.2 (2.2)	0.193 (0.071)	133.1 (19.3)	17.9 (2.6)
		0.178 (0.070)	110.3 (16.0)	15.9 (2.3)	0.188 (0.074)	107.6 (15.6)	13.8 (2.0)	0.196 (0.077)	92.4 (13.4)	12.4 (1.8)	0.180 (0.071)	123.4 (17.9)	16.5 (2.4)
	C							-	98.6 (14.3)	14.7 (2.13)	-		
								-	112.4 (16.3)	15.6 (2.26)	-		
	D	0.165 (0.065)	135.1 (19.6)	16.5 (2.4)		No Bond		0.173 (0.068)	97.9 (14.2)	14.5 (2.1)	0.170 (0.067)	111.7 (16.2)	15.3 (2.22)
		0.165 (0.065)	104.1 (15.1)	13.1 (1.9)		No Bond		0.168 (0.066)	93.1 (13.5)	13.8 (2.0)	0.170 (0.067)	114.5 (16.6)	15.7 (2.28)
		0.165 (0.065)	106.9 (15.5)	13.1 (1.9)		No Bond							

Heat treated prior to test, 1177 C (2150 F) for 2 hours in dry hydrogen

* No joint failure.



Neg. S72-1241

Figure 90. TD-NiCr Tensile Shear Specimens After Testing at 1093C (2000F)

In all of the recrystallized specimens, fracture occurred either in the reduced section away from the joint or at the change of section adjacent to the joint. There was no evidence of joint delamination. Of the ten specimens made from unrecrystallized sheet, all failed in the parent material with just one showing minor delamination of the joint. In others that appear to show joint separation, fracture originated at the edge of the joint and propagated on a 45-degree plane through the sheet.

Analysis of the results of the tensile tests shows no significant differences. With the exception of weak welds for L/T oriented recrystallized sheet, neither sheet orientation nor surface preparation appeared to influence the final results, whether bonding originally employed recrystallized or unrecrystallized material. Although a rather large range of values has resulted, i.e., 92.4-135.1 MN/m² (13.4-19.6 ksi), this is not considered unusual for TD-NiCr, particularly at 1093C (2000F) and with varying sheet orientation.

Stress-Rupture Tests. - The third tier of mechanical testing is the 1204C (2200F) stress-rupture test. Test procedures and apparatus are described in Appendix E. A summary of stress-rupture tests performed at 1204C (2200F) is presented in Table 26. The primary purpose of these tests was to select the best surface preparation method (electro-polishing or mechanical abrasion) for use in Step B of the program. Based on stress level and time to failure, no correlation was found with the method used for surface preparation. However, as discussed in the next section, metallographic examination of failed stress-rupture specimens did appear to show a correlation of test results with surface preparation.

**Table 26. 1204C (2200F) Stress Rupture Tests of
Welded Lap Joint Specimens (Step A)⁽¹⁾**

Material Type ⁽²⁾	Surface Preparation ⁽³⁾	Joint Overlap cm (in)	Uniaxial Stress MN/m ² (ksi)	Joint Shear Stress MN/m ² (ksi)	Time to Failure (Hours)	Mode of Failure
Recrystallized	B	0.170 (0.067)	34.5 (5.0)	3.45 (0.50)	114.7+	No failure; test stopped
	B	0.165 (0.065)	37.9 (5.5)	5.17 (0.75)	30.7	PMAJ ⁽⁴⁾
	B	0.165 (0.065)	41.4 (6.0)	5.52 (0.80)	28.4	PMAJ
	B	0.124 (0.049)	51.7 (7.5)	9.52 (1.38)	2.9	PMAJ
	B	0.155 (0.061)	62.1 (9.0)	8.76 (1.27)	1.3	PMAJ
	D	0.165 (0.065)	48.3 (7.0)	6.69 (0.97)	67.7	PMAJ
	D	0.170 (0.067)	51.7 (7.5)	6.96 (1.01)	16.1	Failed PM 0.32 cm from joint
	D	0.163 (0.064)	58.6 (8.5)	8.07 (1.17)	31.6	Failed PM 0.32 cm from joint
	D	0.180 (0.071)	62.1 (9.0)	7.38 (1.07)	2.5	PMAJ
Unrecrystallized	B	0.196 (0.077)	34.5 (5.0)	4.48 (0.65)	95.0+	No failure; test stopped
	B	0.193 (0.076)	51.7 (7.5)	6.69 (0.97)	112.0+	No failure; test stopped
	B	0.196 (0.077)	62.1 (9.0)	7.86 (1.14)	0.1	PMAJ
	D	0.169 (0.066)	34.5 (5.0)	4.83 (0.70)	56.2	PMAJ
	D	0.165 (0.065)	37.9 (5.5)	5.79 (0.84)	17.0	PMAJ
	D	0.170 (0.067)	44.8 (6.5)	6.48 (0.94)	5.0	PMAJ
	D	0.155 (0.061)	55.2 (8.0)	9.45 (1.37)	0.85	PMAJ

(1) Specimens made from 0.025 cm (0.010 inch) sheet with longitudinal/longitudinal orientation. Weld parameters: 1379N (310 lb). Force: 60 amps; 20.3 cm (8 in) per minute. Recrystallized in dry H₂ for 2 hours at 1177 C (2150 F) after welding.

(2) Recrystallized Sheet Heat 3691 (Code L2). Unrecrystallized Sheet Heat 3689 (Code J2). These materials were welded in the "as-received" condition.

(3) Surface Preparation B: Hot alkaline degrease; tap water rinse; abrade through 600 grit emery paper; rinse deionized water/air blast; warm air dry.

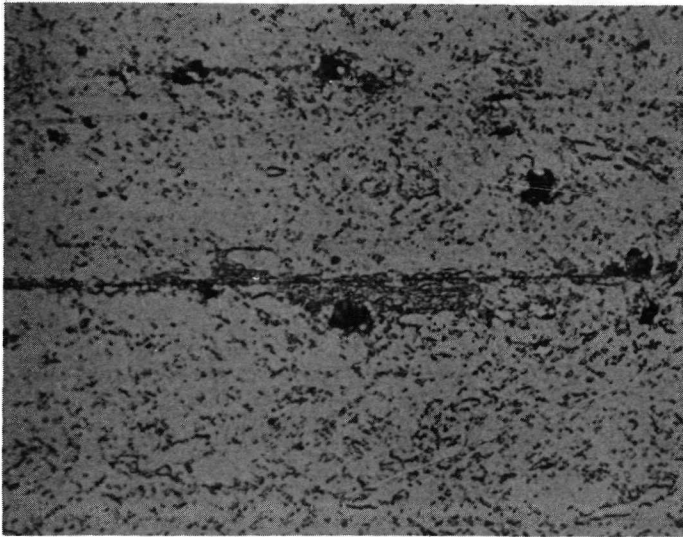
Surface Preparation D: Hot alkaline degrease; tap water rinse; electropolish in Summa solution (27 to 38 C (80 to 100 F) 8 volts, 1.5 minutes); rinse deionized water/air blast; warm air dry.

(4) PMAJ = Parent material failure at change of section of lap joint.

Metallographic Evaluation. - Metallographic evaluation was performed on a representative sample of each combination of material type, sheet orientation, and surface preparation.

Representative metallography of lap joints made from unrecrystallized sheet with L/L orientation is shown in Figure 91. The contrast in weld lines resulting from the B and D surface preparations (600 grit abrading versus electropolish) is evident and is equivalent to the effect previously observed for recrystallized material. From these observations it was concluded that surface preparations A and B result in fine recrystallized grains along the weld line regardless of material type or orientation. All four combinations, R-L/L, R-L/T, U-L/L and U-L/T reveal the same effect.

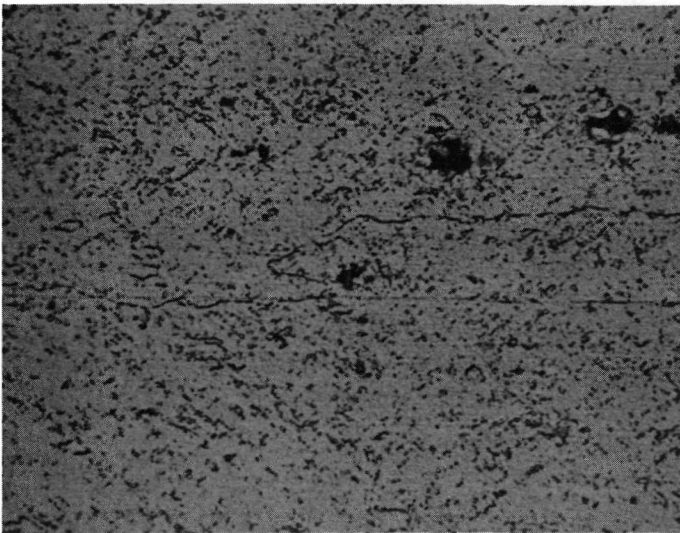
After short-time stress-rupture exposure at 1204C (2200F), the typical as-welded plus heat-treated structure is retained for the specimens shown in Figures 92 and 93.



(a) Surface Preparation B
(Abraded through 600 Grit Paper)

Magnification: 1000X

Log 4383



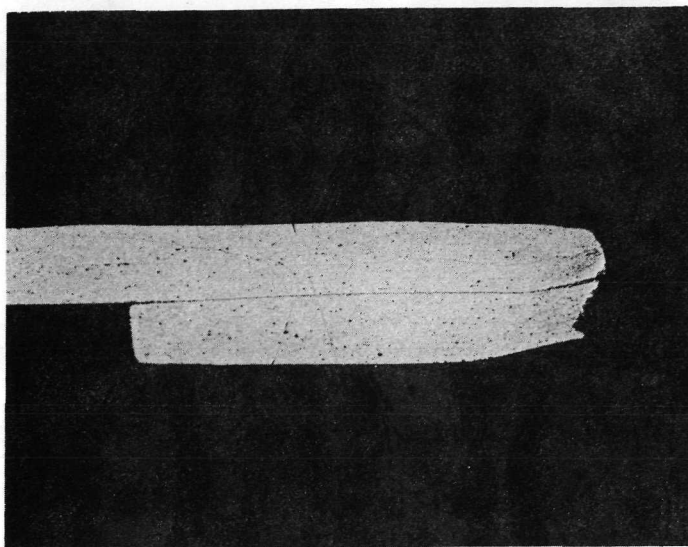
(b) Surface Preparation D
(Summa Electropolished)

Magnification: 1000X

Log 4384

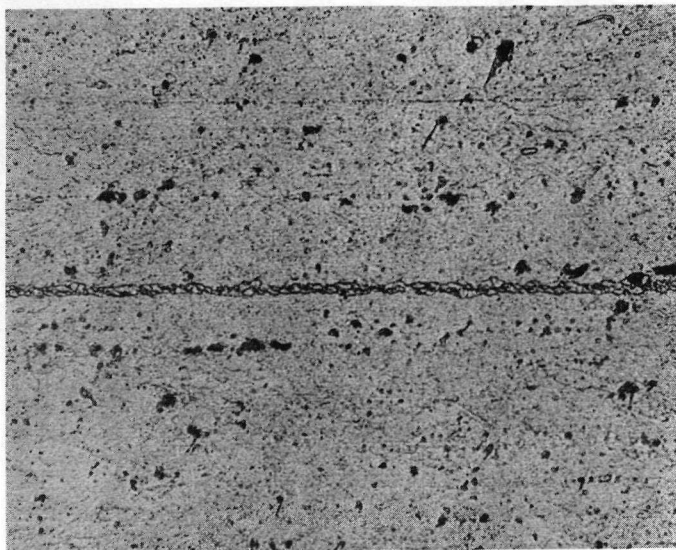
— Weld Interface

Figure 91. Transverse Section Through Lap Seam Weld in Unrecrystallized 0.25 mm (0.010 in.) TD-NiCr Sheet with L/L Orientation Showing Effect of Surface Preparation on Structure of Weld Line



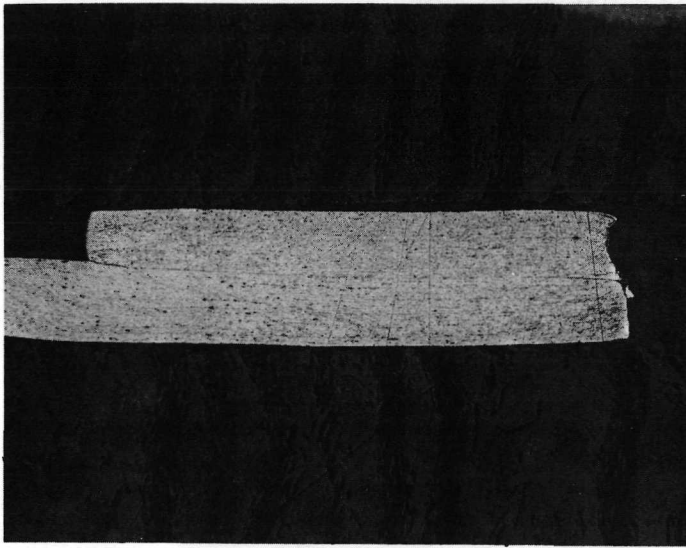
Magnification: 40X Log 5009A

10% Oxalic Acid
Electrolytic Etch



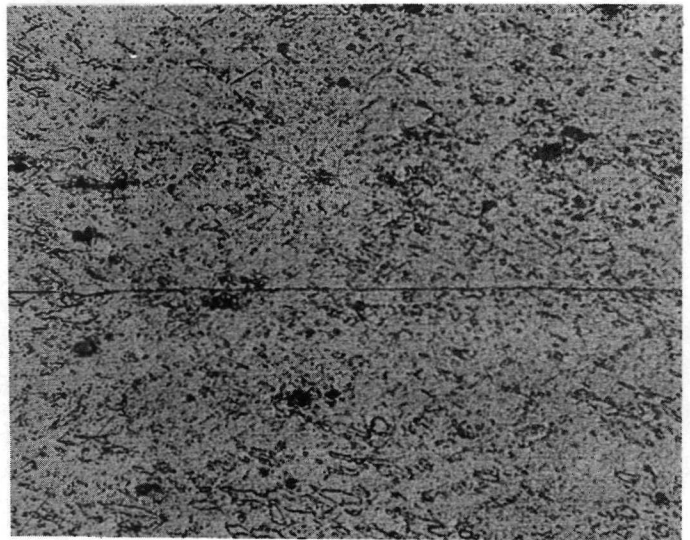
Magnification: 500X Log 5009B

Figure 92. Microstructure of Welded Lap Joint in 0.25 mm (0.010 in.) Recrystallized TD-NiCr After Stress Rupture Testing at 1204C (2200F). Uniaxial Stress of 62 MN/m^2 (9.00 ksi) for 1.3 Hours. Surface Preparation by Abrasion (Method B) with L/L Orientation



Magnification: 40X Log 5010A

10% Oxalic Acid
Electrolytic Etch



Magnification: 500X Log 5010B

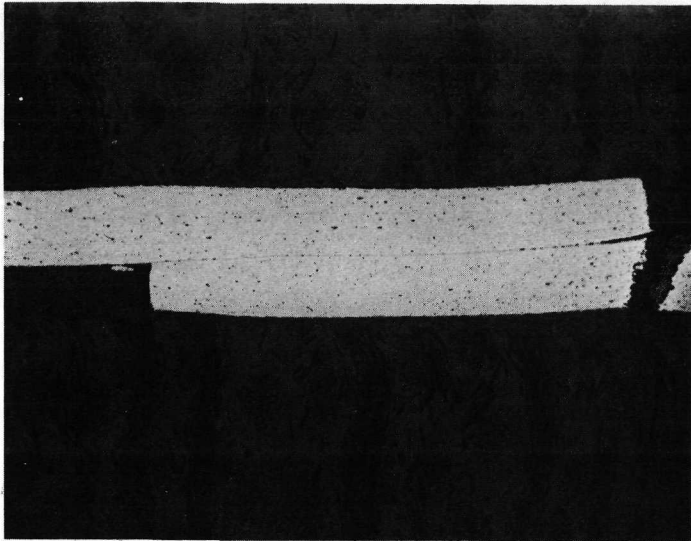
Figure 93. Microstructure of Welded Lap Joint in 0.25 mm (0.010 in.) Recrystallized TD-NiCr After Stress Rupture Testing at 1204C (2200F). Uniaxial Stress of 62 MN/m² (9.00 ksi) for 2.5 Hours. Electropolish Surface Preparation (D) with L/L Orientation

The specimen of Figure 93 was prepared for welding by electropolishing (Condition D) and shows a weld interface devoid of recrystallization, which is characteristic of this preparation method. The specimen of Figure 92 was prepared by abrasion (Condition B) and shows fine recrystallized grains typical of that preparation method. At the edges of the weld interface in each of these specimens, cavity formation and oxidation (believed to be stress induced) have penetrated to a depth of about 0.025 cm (0.010 in.). Figures 92, 94, and 95 show stress-rupture specimens, prepared by abrasion (Method B) after 1.3, 30.7 and 114.7 hours of testing at 1204C (2200F). The cavity formation and oxidation of the edge of the weld have increased slightly with increased exposure time, but more important is the remarkable stability of the recrystallized grains over the major portion of the weld interface, as shown in the high magnification photographs in each figure. A contrast to this apparent high-temperature stability can be seen in stress-rupture specimens shown in Figures 93 and 96. These specimens were prepared for welding by electropolishing (Condition D). After 67.7 hours of exposure at 48.3 MN/m² (7 ksi) and 1204C (2200F), cavity formation of the weld interface has occurred to an advanced stage (Figure 96).

The cavity formation with the recrystallized sheet is believed to be enhanced by the loss of substructure in the affected material. Figure 96 shows that the material affected by the cavity formation appears to have reduced substructure as shown by the reduced response to etching. It is hypothesized that grain boundary sliding of the single grain boundary shown in Figure 93 causes voids to form at offsets by the Chang and Grant mechanism. On the other hand, the fine grain recrystallized zone found for welds prepared by preparation B and shown in Figure 92, can accommodate grain boundary movement without void formation. As the grains in this recrystallized zone appear to contain the same degree of substructure as the parent material, as judged by etching rates, the shear process is limited principally to grain boundaries.

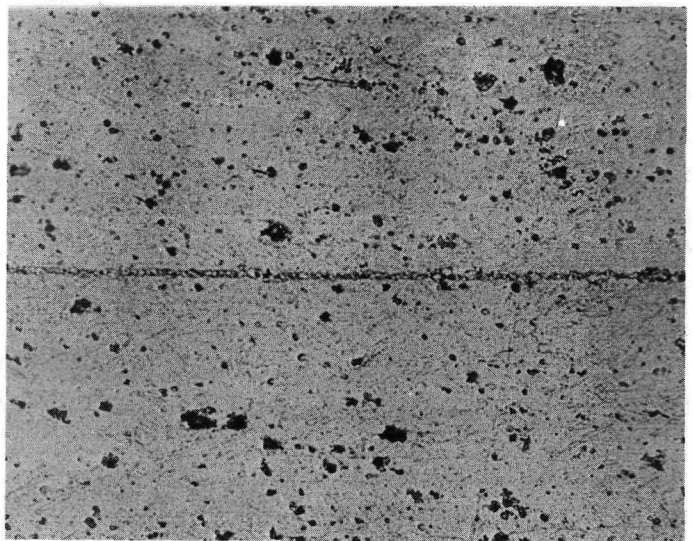
One observation was noted that distinguishes between recrystallized and unrecrystallized material. Figure 97 shows the cross section of a U-L/T-B type lap joint after being heat treated for 2 hours at 1177C (2150F) in dry hydrogen. At both edges of the joint are regions which, under greater magnification, are found to be areas of recrystallization. Although not confirmed, it is felt that this has resulted from what is termed a "back extrusion" effect. Initial contact at the edges of the joint, coupled with plastic flow in a lateral direction, right and left, at these areas during welding have caused critical deformation-temperature requirements to be exceeded for recrystallization. This effect was found to be independent of surface preparation with unrecrystallized material, but is not found with the recrystallized sheet in either L/T or L/L type lap joints.

The influence of the observed patches of recrystallization on the high-temperature properties of the joints is expected to be felt only in the long-time creep-rupture effects.



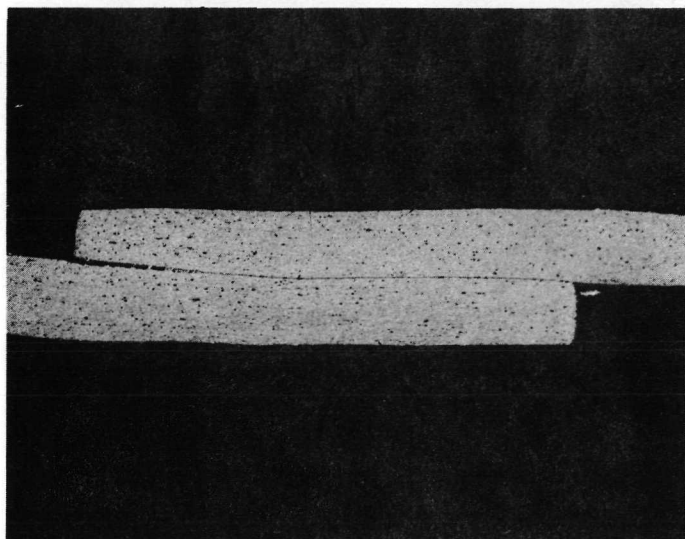
Magnification: 40X Log 5011B

10% Oxalic Acid
Electrolytic Etch



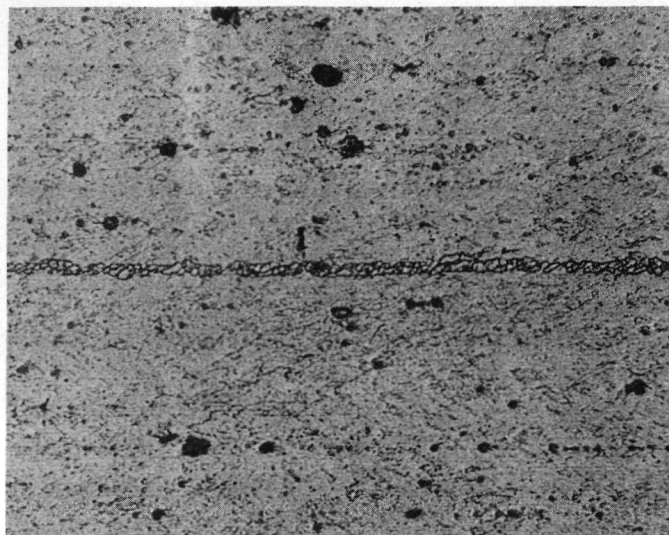
Magnification: 500X Log 5011B

Figure 94. Microstructure of Welded Lap Joint 0.25 mm (0.010 in.) Recrystallized TD-NiCr After Stress Rupture Testing at 1204 C (2200 F). Uniaxial Stress of 37.9 MN/m^2 (5.50 ksi) for 30.7 Hours. Surface Preparation by Abrasion (Method B) with L/L Orientation



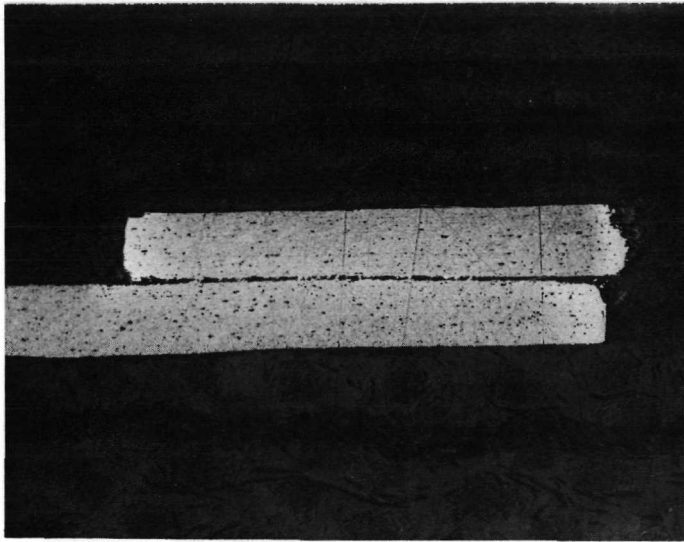
Magnification: 40X Log 5013A

10% Oxalic Acid
Electrolytic Etch



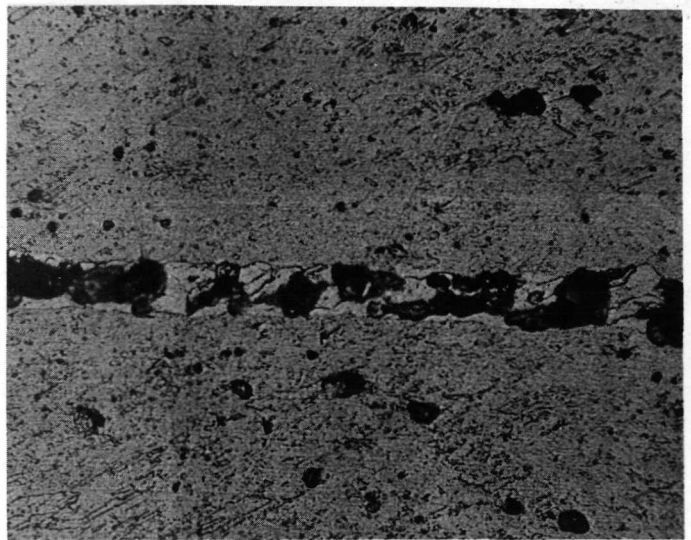
Magnification: 500X Log 5013B

Figure 95. Microstructure of Welded Lap Joint in 0.25 mm (0.010 in.) Recrystallized TD-NiCr After Stress Rupture Testing at 1204C (2200F). Uniaxial Preparation by Abrasion (Method B) with L/L Orientation



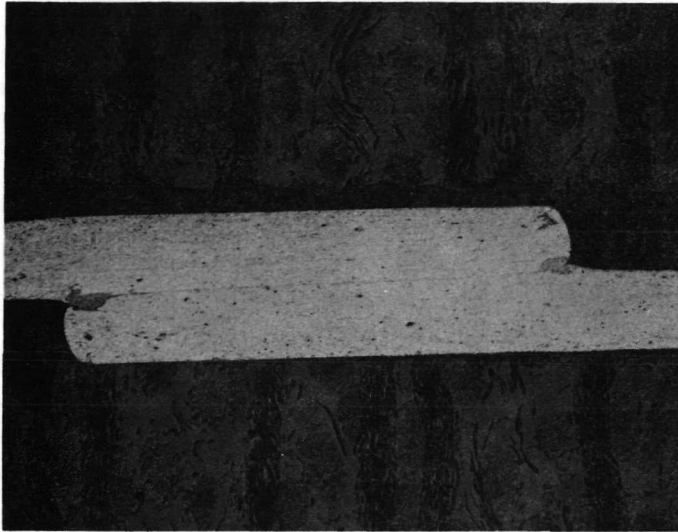
Magnification: 40X Log 5012A

10% Oxalic Acid
Electrolytic Etch



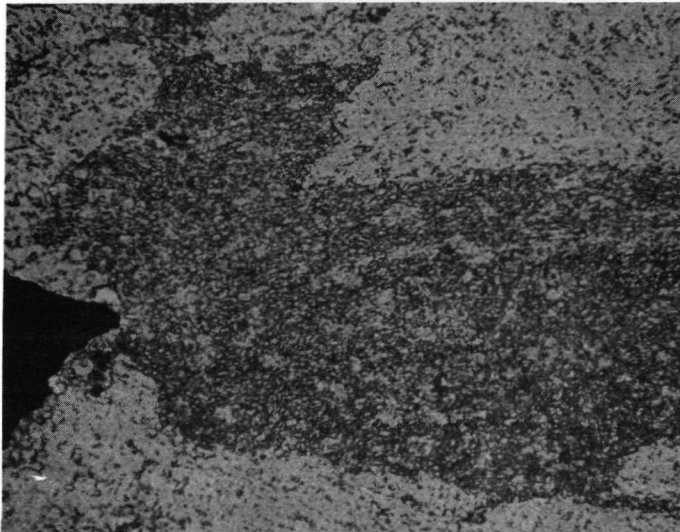
Magnification: 500X Log 5012B

Figure 96. Microstructure of Welded Lap Joint in 0.25 mm (0.010 in.) Recrystallized TD-NiCr After Stress-Rupture Testing at 1204 C (2200 F). Uniaxial Stress of 48.3 MN/m^2 (7.00 ksi) for 67.7 Hours. Electropolish Surface Preparation (D) with L/L Orientation



(a) Magnification: 40X

Log 4385A



(b) Magnification: 750X

Log 4385B

**Figure 97. Cross Section of U-L/T-B Type Lap Joints
Showing Recrystallization at Joint Edges**

This is because the processes operative in weakening the structure do not have sufficient time to become effective during the short-time tensile tests. In fact, the results of the 1093C (2000F) tensile-shear tests showed no essential difference between recrystallized and unrecrystallized material.

The size of the patches varies from one welded panel to the next and also along the length of the lap seam joint of any given panel. The size of the patches range from much less than 0.025 mm (0.001 in.) to about 0.38 mm (0.015 in.) across, as measured in transverse section. All stress-rupture failures occurred in the parent material; however, the origin of these failures appeared to be the recrystallization patches.

In an attempt to eliminate recrystallization patches from lap joints in unrecrystallized material, the weld parameters were varied on one weld panel to produce the following specimens:

Sheet Orientation	Surface Preparation	Squeeze Force N (lb)	Weld Speed cm/min (in./min)	Heating Current (amps)
L/T	D	1379 (310)	15.2 (6.0)	40
L/T	D	1379 (310)	15.2 (6.0)	50
L/T	D	1379 (310)	20.3 (8.0)	50
L/T	D	1379 (310)	20.3 (8.0)	60

For all parameter combinations, the weld interface was considered satisfactory; however, at the higher current for each speed, recrystallization patches were formed. There appears to be a threshold for recrystallization related to a product-type function of temperature and time. The strength of these joints has been evaluated only by simple room-temperature peel tests. All were found to be excellent.

A very interesting fracture phenomenon was observed when the first two unrecrystallized specimens of Table 26 were unloaded and removed from the furnace after 95 and 112 hours of testing. While cooling in still air without any external loading, both of these specimens fractured spontaneously and rather violently at both ends of the lap joint when the temperature of each had decreased to just below "red heat." It is hypothesized that this spontaneous fracturing may be the result of a four-step mechanism involving the patches of recrystallization at the edges of the joints. These steps are:

- (1) Cavity formation in recrystallized grains
- (2) Penetration of oxygen

(3) Growth of metal oxide

(4) Fracture on cooldown due to differential thermal expansion

The initial step, cavity formation, was believed to be stress induced.

To test this hypothesis, a specimen known to have recrystallization patches at the edges of the lap joint was exposed to 1204C (2200F) for 100 hours while unstressed. Subsequent metallographic examination of this specimen showed the structure of the recrystallization patches to be free of the cavities and oxide growth found in the specimens that had been similarly exposed while stressed, thus supporting the hypothesis.

Selection of Weld Parameters for Step B. - Selection of the weld parameters based on metallography and short-time tensile-shear and preliminary stress-rupture tests were the same for both recrystallized and unrecrystallized sheet. These conditions were:

Surface Preparation	D
Weld Force	1379 N (310 lb)
Weld Speed	20.3 cm (8 in.) per minute
Current	60 amperes (1316C (2400F) estimated)

The post-weld heat treatments recommended were 1177C (2150F) for 2 hours in dry hydrogen for both conditions of sheet. It was recognized that the actual welding conditions would vary from joint-to-joint. Experience has shown that the nominal joint overlap of 0.127 cm (0.050 in.) cannot be held closer than a range of 0.127 cm to 0.178 cm (0.050 to 0.070 in.).

Joint Efficiencies - Step B. - Using the selected weld parameters and surface preparation techniques, Step B was performed to evaluate the strength of resistance seam welded joints. Testing procedures used in Step B were unchanged from those previously used and are described in Appendix E. All specimens were heat treated at 1177C (2150F) for 2 hours in dry hydrogen prior to testing.

The tensile-shear data in Table 27 includes earlier data from Table 25, supplemented to provide further evaluation. The predominant mode of failure was PMAJ (parent metal adjacent to joint) caused by the high stress concentration at this change of section. Only one joint failure was found.

Tables 28, 29 and 30 present stress-rupture data at 982C (1800F), 1093C (2000F) and 1204C (2200F). In all of these tests, only one joint failure was found.

Table 27. Tensile-Shear Tests of Resistance Seam Welded Lap Joint Specimens⁽¹⁾

Test Temperature C (F)	Material Type	Joint Orientation	Joint Overlap cm (in)	Ultimate Stress		Mode of Failure		
				Parent Metal Uniaxial Stress MN/m ² (ksi)	Joint Shear Stress MN/m ² (ksi)			
Room	Unrecrystallized, Special processed, Sheet No. 637, Heat No. 3689 Code J3	L/L	0.165 (0.065)	903.2 (131)	130.3 (18.9)	PMAJ (2)		
		L/L	0.165 (0.065)	868.8 (126)	124.1 (18.0)	PMAJ		
		L/T	0.170 (0.067)	861.9 (125)	116.5 (16.9)	PMAJ		
		L/T	0.170 (0.067)	848.1 (123)	114.5 (16.6)	PMAJ		
	Recrystallized, Sheet No. 653, Heat No. 3691, Code L2	L/L	0.170 (0.067)	834.3 (121)	99.3 (14.4)	PMAJ		
		L/L	0.170 (0.067)	806.7 (117)	95.8 (13.9)	PMAJ		
L/L		0.170 (0.067)	758.5 (110)	89.6 (13.0)	PMAJ			
1093 (2000)	Unrecrystallized, Special Processed, Sheet No. 637, Heat No. 3689 Code J3	L/L	0.173 (0.068)	128.2 (18.59)	18.96 (2.75)	PMAJ		
		L/L	0.170 (0.067)	124.0 (17.98)	18.20 (2.64)	PMAJ		
		L/L	0.173 (0.068)	97.9 (14.2)	14.48 (2.1)	PMAJ		
		L/L	0.168 (0.066)	93.1 (13.5)	13.79 (2.0)	PMAJ		
		L/T	0.173 (0.068)	129.8 (18.83)	18.27 (2.65)	PM failure in transverse leg 0.635 cm (1/4") from joint		
		L/T	0.178 (0.070)	140.2 (20.33)	18.68 (2.71)	PMAJ in transverse leg		
		L/T	0.170 (0.067)	111.7 (16.2)	15.31 (2.22)	PM		
		L/T	0.170 (0.067)	114.6 (16.6)	15.72 (2.28)	PMAJ		
	Recrystallized, Sheet No. 653, Heat No. 3691, Code L2	L/L	0.165 (0.065)	94.32 (13.68)	13.45 (1.95)	Joint Separation		
		L/L	0.165 (0.065)	135.1 (19.6)	16.55 (2.4)	PMAJ		
		L/L	0.165 (0.065)	104.1 (15.1)	13.10 (1.9)	PMAJ		
		L/L	0.165 (0.065)	106.9 (15.5)	13.10 (1.9)	PMAJ		
		1316 (2400)	Unrecrystallized, Special processed, Sheet No. 637, Heat No. 3689, Code J3	L/L	0.175 (0.069)	59.37 (8.61)	8.14 (1.18)	PMAJ
				L/L	0.178 (0.070)	78.26 (11.35)	10.27 (1.49)	PMAJ
L/L	0.178 (0.070)			84.33 (12.23)	11.38 (1.65)	PM failure 0.48 cm (3/16") from joint		
L/T	0.193 (0.076)			83.43 (12.10)	10.48 (1.52)	PM failure in transverse leg 0.32 cm (1/4") from joint		
L/T	0.183 (0.072)			70.19 (10.18)	9.38 (1.36)	PM failure in transverse leg 0.64 cm (1/4") from joint		
Recrystallized, Sheet No. 653, Heat No. 3691, Code L2	L/L		0.168 (0.066)	56.4 (8.18)	7.86 (1.14)	PM failure at radius of reduced section		

(1) Conditions: 0.635 x 2.5 cm (0.25 x 1 in) reduced section specimen; 0.127 cm (0.050 in) per minute crosshead speed. (Specimens made from 0.25 mm (0.010 in) sheet using electropolishing surface preparation D. Weld parameters: 1379 N (310 lb) force; 60 amps; 20.3 cm (8 in) per minute. Heat treated in dry hydrogen for 2 hours at 1177 C (2150 F) after welding.

(2) PMAJ = parent metal adjacent to joint

**Table 28. 982C (1800F) Stress-Rupture Tests of Resistance
Seam Welded Lap Joint Specimens⁽¹⁾**

Material Type	Sheet Orientation	Joint Overlap cm (in)	Uniaxial Stress MN/m ² (ksi)	Joint Shear Stress MN/m ² (ksi)	Time to Rupture (hrs)	Mode of Rupture
Unrecrystallized, Special processed, Sheet No. 637, Heat No. 3689, Code J3	L/L(2)	0.175 (0.069)	113.7 (16.5)	14.48 (2.10)	95.1	PMAJ(3)
	L/L	0.178 (0.070)	117.2 (17.0)	14.89 (2.16)	85.9	PMAJ
	L/L	0.170 (0.067)	120.7 (17.5)	14.76 (2.14)	32.8	PMAJ
	L/L	0.178 (0.070)	124.1 (18.0)	13.45 (1.95)	33.9	PMAJ
	L/L	0.173 (0.068)	127.6 (18.5)	17.86 (2.59)	8.6	PMAJ
Recrystallized, Sheet No. 653, Heat No. 3691, Code L2	L/L	0.170 (0.067)	117.2 (17.0)	13.03 (1.89)	Test stopped at 118 hours	No rupture
	L/L	0.175 (0.069)	117.2 (17.0)	13.93 (2.02)	Test stopped at 100 hours	No rupture
	L/L	0.175 (0.069)	120.7 (17.5)	14.00 (2.03)	<0.1	PMAJ
	L/L	0.170 (0.067)	124.1 (18.0)	15.03 (2.18)	<0.1	PMAJ
	L/L	0.178 (0.070)	131.0 (19.0)	15.51 (2.25)	<0.1	Joint separation
<p>(1) Specimens made from 0.25 mm (0.010 in) sheet using electropolishing surface preparation D. Weld parameters: 1379 N (310 lb) force; 60 amps; 20.3 cm (8 in) per minute. Heat treated in dry hydrogen for 2 hours at 1177 C (2150 F) after welding.</p> <p>(2) L/L implies the final rolling direction of sheet in both members of lap joint at right angle to seam.</p> <p>(3) PMAJ = parent material failure at change of section of lap joint.</p>						

**Table 29. 1093C (2000F) Stress-Rupture Tests of Resistance
Seam Welded Lap Joint Specimens⁽¹⁾**

Material Type	Sheet Orientation	Joint Overlap (cm) (in)	Uniaxial Stress MN/m ² (ksi)	Joint Shear Stress MN/m ² (ksi)	Time to Rupture (Hours)	Mode of Rupture
Unrecrystallized Sheet No. 637 Heat No. 3689 Code J3	L/L ⁽²⁾	0.168 (0.066)	58.6 (8.5)	7.45 (1.08)	139.3+	No failure; test stopped
	L/L	0.170 (0.067)	62.1 (9.0)	8.21 (1.19)	47.6	PMAJ ⁽³⁾
	L/L	0.173 (0.068)	69.0 (10.0)	8.69 (1.26)	16.9	PMAJ
	L/L	0.170 (0.067)	75.8 (11.0)	9.86 (1.43)	14.6	PMAJ
	L/L	0.175 (0.069)	82.7 (12.0)	9.17 (1.33)	17.1	PMAJ
	L/L	0.178 (0.070)	89.6 (13.0)	10.27 (1.49)	2.7	PMAJ
	L/T ⁽⁴⁾	0.183 (0.072)	62.1 (9.0)	8.21 (1.19)	Test stopped at 118.1 hrs	No rupture
	L/T	0.178 (0.070)	69.0 (10.0)	9.24 (1.34)	113.8	Ruptured in transverse leg 0.32 cm (1/8") from joint
	L/T	0.180 (0.071)	75.8 (11.0)	10.00 (1.45)	49.9	PMAJ
	L/T	0.180 (0.071)	82.7 (12.0)	10.96 (1.59)	18.9	Ruptured in transverse leg 0.32 cm (1/8") from joint
Recrystallized Sheet No. 653 Heat No. 3691 Code L2	L/T	0.180 (0.071)	89.6 (13.0)	11.86 (1.72)	3.0	Ruptured in transverse leg 0.64 cm (1/4") from joint
	L/L	0.142 (0.056)	82.7 (12.0)	12.55 (1.82)	50.1	PMAJ
	L/L	0.175 (0.069)	89.6 (13.0)	10.55 (1.53)	19.9	PMAJ
<p>(1) Specimens made from 0.25 mm (0.010 in) sheet using electropolish surface Preparation D. Weld parameters: 1379N (310 lb) force; 60 amps; 20.3 cm (8 in) per minute. Heat treated in dry H₂ for 2 hours at 1177 C (2150 F) after welding.</p> <p>(2) L/L implies the final rolling direction of sheet in both members of lap joint at right angle to seam.</p> <p>(3) PMAJ = Parent material failure at change of section of lap joint.</p> <p>(4) L/T implies the final rolling direction of sheet in one member of the lap joint at right angle to the seam and that of the other member parallel to the seam.</p>						

**Table 30. 1204C (2200F) Stress-Rupture Tests of Resistance
Seam Welded Lap Joint Specimens⁽¹⁾**

Material Type	Sheet Orientation	Joint Overlap cm (in)	Uniaxial Stress MN/m ² (ksi)	Joint Shear Stress MN/m ² (ksi)	Time to Rupture hrs	Mode of Rupture
Unrecrystallized, Special processed, Sheet No. 637, Heat No. 3689, Code J3	L/L(2)	0.169 (0.066)	34.5 (5.0)	4.83 (0.70)	56.2	PMAJ (3)
	L/L	0.165 (0.065)	37.9 (5.5)	5.79 (0.84)	17.0	PMAJ
	L/L	0.170 (0.067)	44.8 (6.5)	6.48 (0.94)	5.0	PMAJ
	L/L	0.155 (0.061)	55.2 (8.0)	9.45 (1.37)	0.85	PMAJ
	L/L	0.180 (0.071)	34.48 (5.0)	4.41 (0.64)	Test stopped at 143.0 hrs	Unfailed when stopped but fractured in PMAJ while unloading from furnace
	L/T(4)	0.173 (0.068)	37.92 (5.5)	5.31 (0.77)	Test stopped at 100.2 hrs	Unfailed when stopped but fractured in longitudinal leg PMAJ while unloading from machine
	L/T	0.175 (0.069)	44.82 (6.5)	6.14 (0.89)	Test stopped at 113.3 hrs	Unfailed when stopped but fractured spontaneously in both legs PMAJ when unloaded and cooled
Recrystallized, Sheet No. 653, Heat No. 3691, Code L2	L/L	0.165 (0.065)	48.3 (7.0)	6.69 (0.97)	67.7	PMAJ
	L/L	0.170 (0.067)	51.7 (7.5)	6.96 (1.01)	16.1	Failed PM 0.32 cm from joint
	L/L	0.163 (0.064)	58.6 (8.5)	8.07 (1.17)	31.6	Failed PM 0.32 cm from joint
	L/L	0.180 (0.071)	62.1 (9.0)	7.38 (1.07)	2.5	PMAJ
<p>(1) Specimens made from 0.25 mm (0.010 in) sheet using electropolishing surface preparation D. Weld parameters: 1379 N (310 lb) force; 60 amps; 20.3 cm (8 in) per minute. Heat treated in dry hydrogen for 2 hours at 1177 C (2150 F) after welding.</p> <p>(2) L/L implies the final rolling direction of sheet in both members of lap joint at right angle to the seam.</p> <p>(3) PMAJ = parent material failure at change of section of lap joint.</p> <p>(4) L/T implies the final rolling direction of sheet in one member of the lap joint at right angle to the seam and that of the other member parallel to the seam</p>						

The stress-rupture results are plotted in Figures 98 through 105 and are compared with the best fit of parent metal data from Convair Aerospace tests. Figures 98 and 99 show that the joint strengths are above the parent metal values for both recrystallized and unrecrystallized sheet. Reasons for this were examined and included: measurement of thickness (Solar uses pin micrometers and measures the minimum thickness to determine the highest stress); variations in sheet thickness; surface preparation (electropolished); and edge preparation (electropolished). Electropolishing is known to be significant from earlier work, particularly where oxidation-assisted rupture occurs in low ductility metals. It is believed that electropolishing for surface and edge preparation is the major factor in obtaining higher strength in welded specimens than in parent material.

Figures 100 and 101 show the stress-rupture results at 1093C (2000F) for both orientations of the unrecrystallized sheet. Two of the longitudinal orientation data points were found to be low in stress-rupture strength based on the baseline data, but the failures occurred in the parent metal adjacent to the joint in both cases.

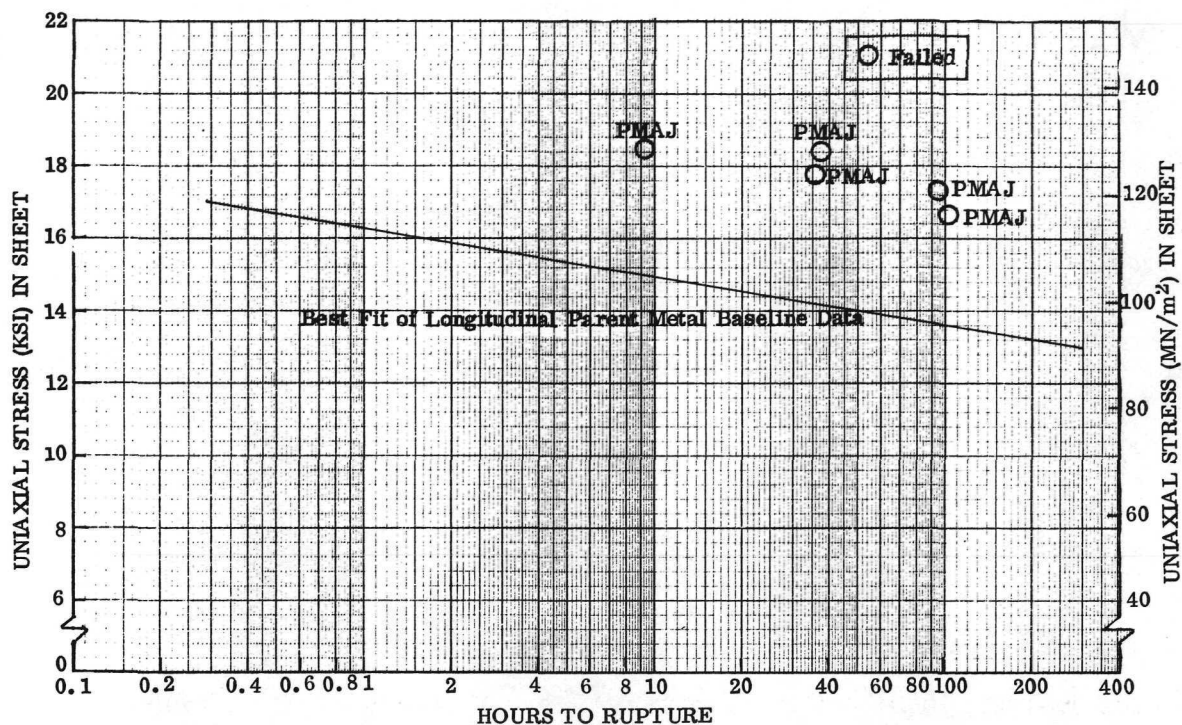


Figure 98. 982 C (1800 F) Stress-Rupture Properties of Longitudinal Resistance Seam Welded Joints of Unrecrystallized 0.25 mm (0.010 in.) TD-NiCr Sheet - Heat 3689. (5t Joint Overlap)

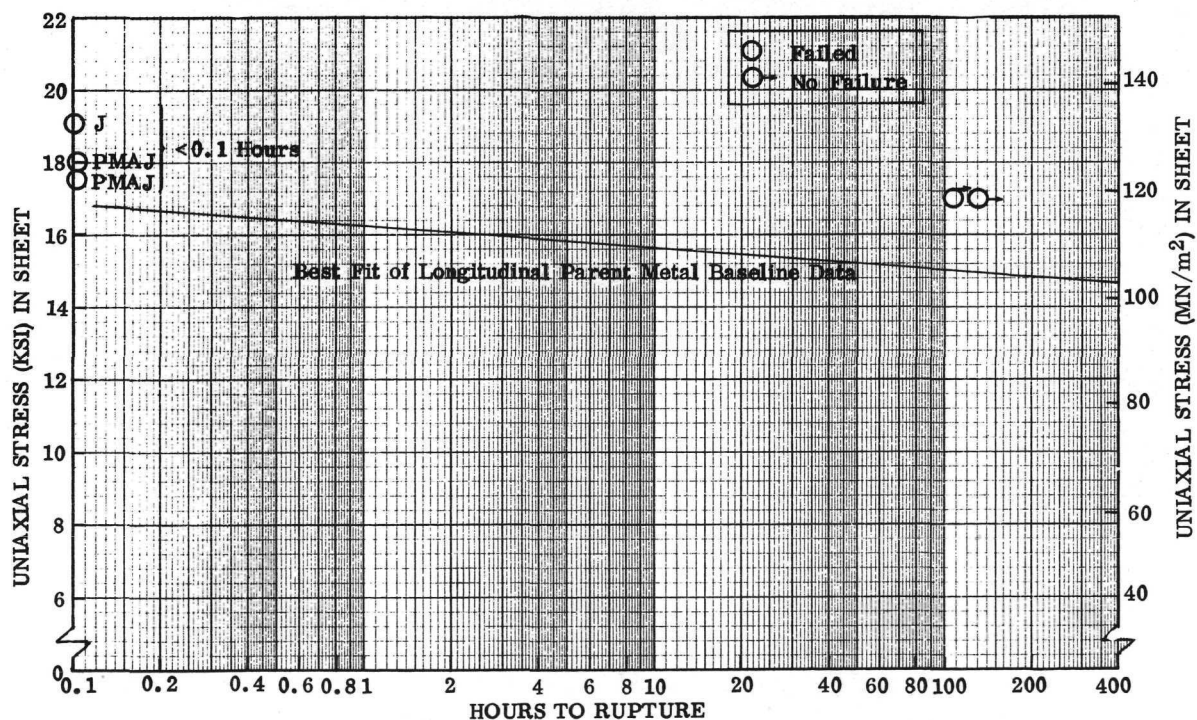


Figure 99. 982 C (1800 F) Stress-Rupture Properties of Longitudinal Resistance Seam Welded Joints of Unrecrystallized 0.25 mm (0.010 in.) TD-NiCr Sheet - Heat 3691. (5t Joint Overlap)

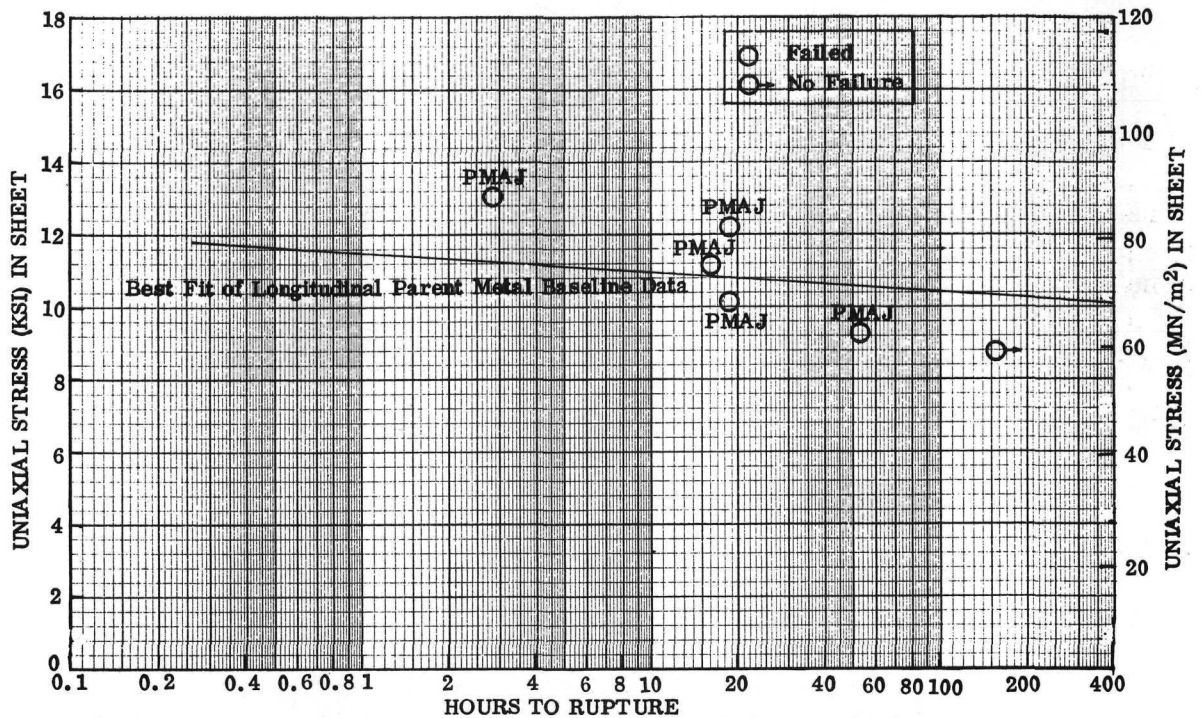


Figure 100. 1093 C (2000 F) Stress-Rupture Properties of Longitudinal Resistance Seam Welded Joints of Unrecrystallized 0.25 mm (0.010 in.) TD-NiCr Sheet - Heat 3689. (5t Joint Overlap)

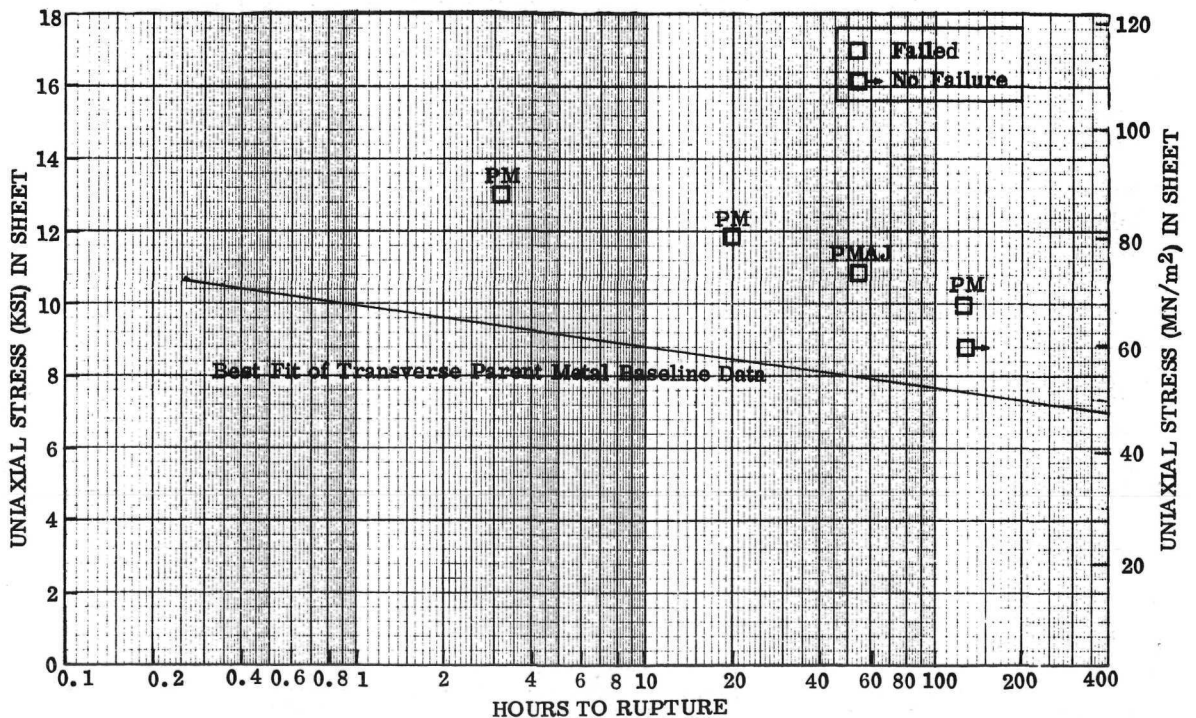


Figure 101. 1093 C (2000 F) Stress-Rupture Properties of Transverse Resistance Seam Welded Joints of Unrecrystallized 0.25 mm (0.010 in.) TD-NiCr Sheet - Heat 3689. (5t Joint Overlap)

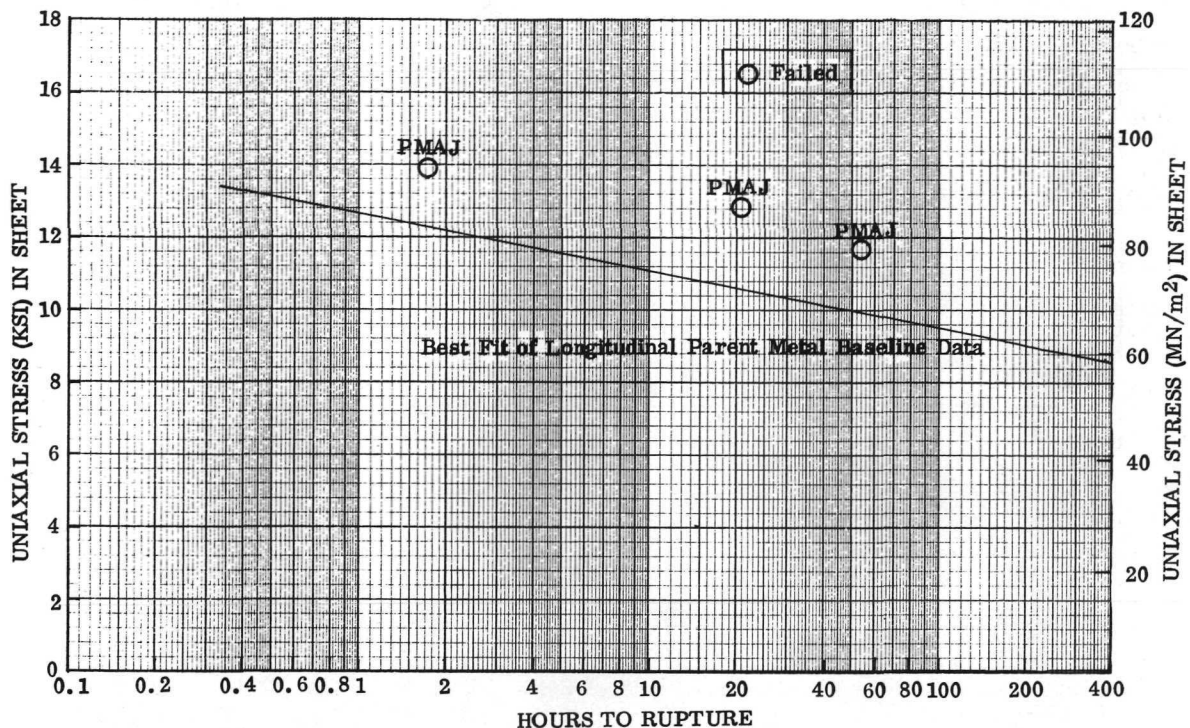


Figure 102. 1093 C (2000 F) Stress-Rupture Properties of Longitudinal Resistance Seam Welded Joints of Recrystallized 0.25 mm (0.010 in.) TD-NiCr Sheet - Heat 3691. (5t Joint Overlap)

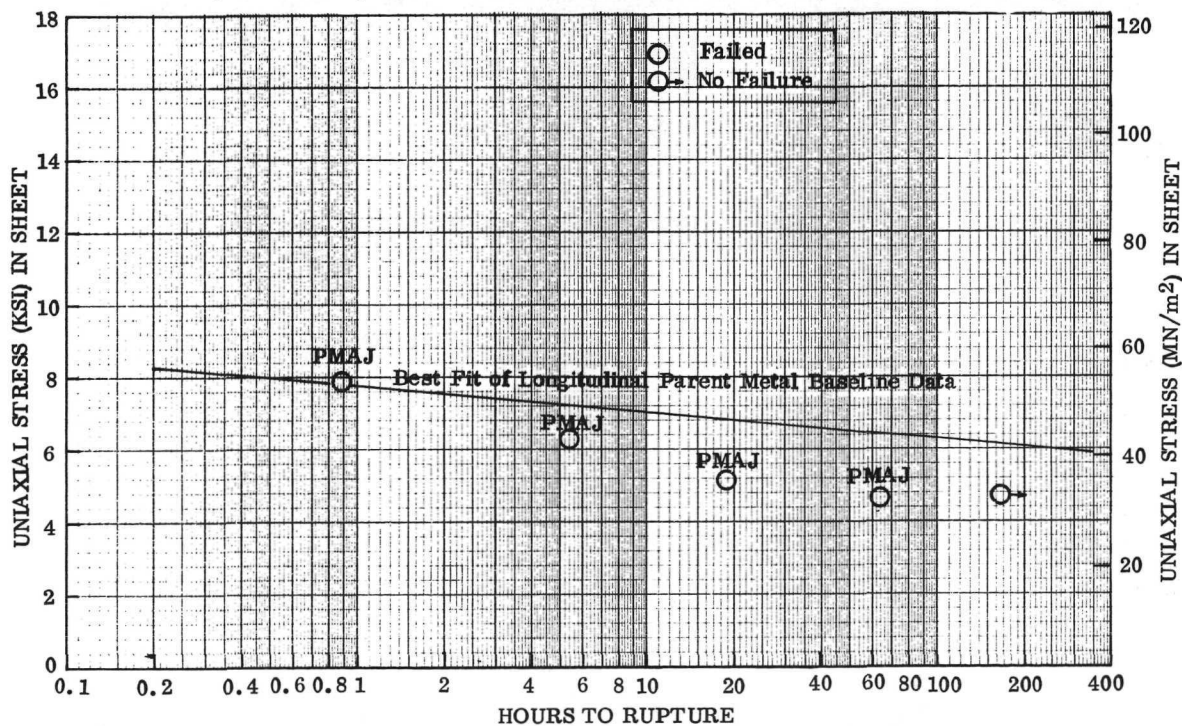


Figure 103. 1204 C (2200 F) Stress-Rupture Properties of Longitudinal Resistance Seam Welded Joints of Unrecrystallized 0.25 mm (0.010 in.) TD-NiCr - Heat 3689. (5t Joint Overlap)

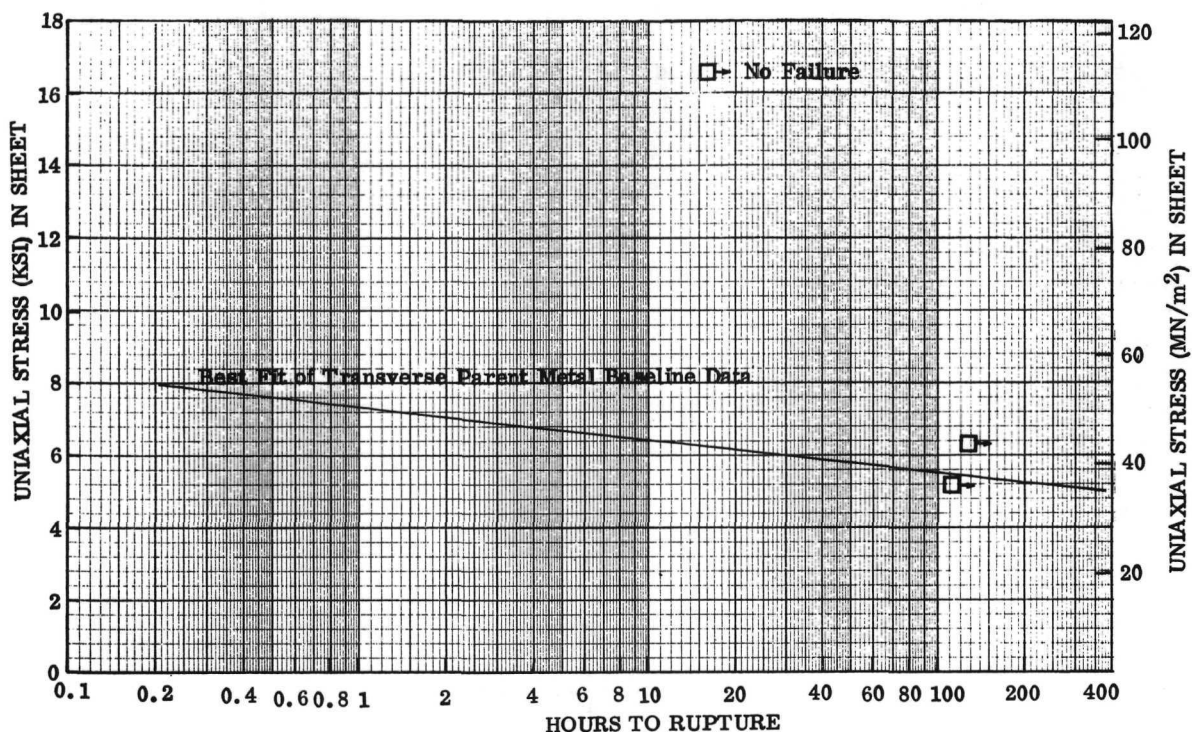


Figure 104. 1204 C (2200 F) Stress-Rupture Strength of Transverse Resistance Seam Welded Joints of Unrecrystallized 0.25 mm (0.010 in.) TD-NiCr Sheet - Heat 3689. (5t Joint Overlap)

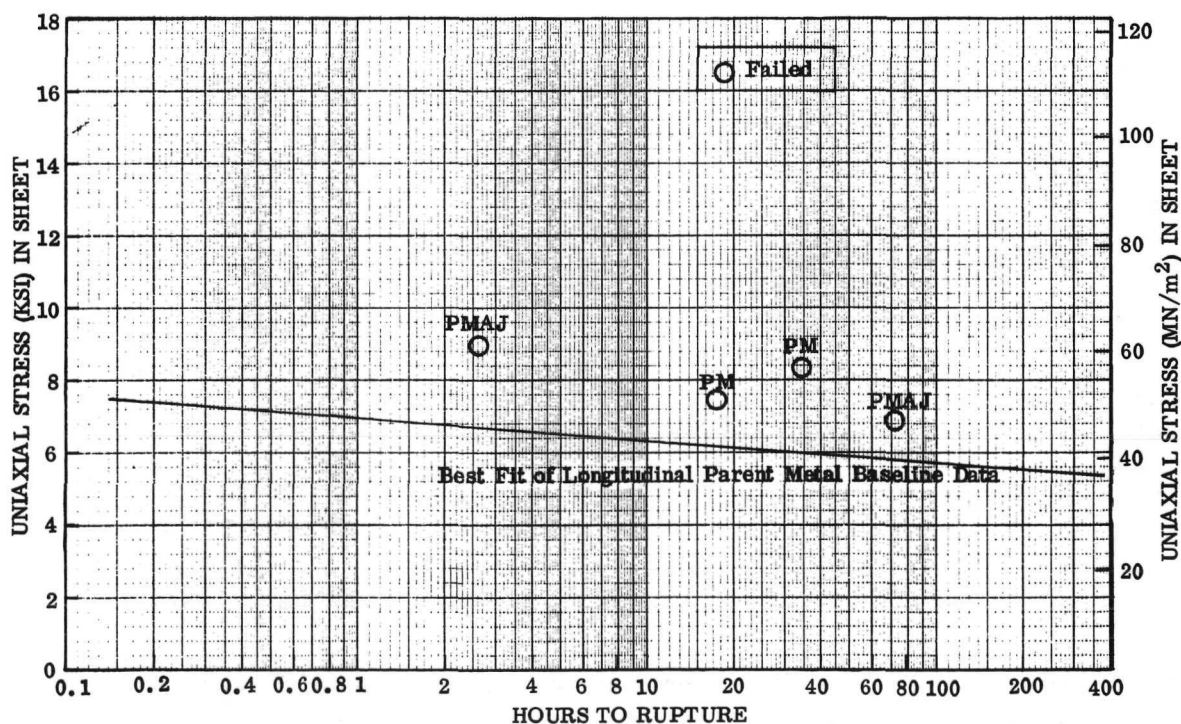


Figure 105. 1204 C (2200 F) Stress-Rupture Strength of Longitudinal Resistance Seam Welded Joints of Recrystallized 0.25 mm (0.010 in.) TD-NiCr Sheet - Heat 3691. (5t Joint Overlap)

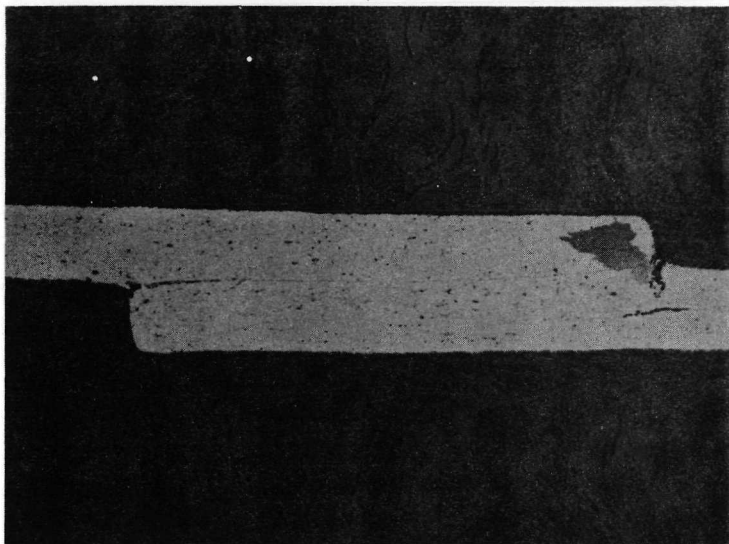
Figure 102 presents the stress-rupture values for joints in recrystallized sheet at 1093C (2000F). Again the joints failed at stresses in the parent metal higher than those found in separate tests conducted on sheet.

Figure 103 through 105 present the stress-rupture results for 1204C (2200F). The longitudinal and transverse orientations are compared in Figures 103 and 104 for unre-crystallized sheet. The joints for the longitudinal orientation show consistent strengths, but these are lower than for the parent metal. However, failures were in the parent metal, adjacent to the joint, so that the difference must be ascribed to one of the causes discussed earlier. All evidence suggests that the load-bearing capacity of these joints in stress-rupture testing equals or exceeds that of the parent metal. The data for joints in recrystallized sheet tested at 1204C (2200F) and presented in Figure 105 show excellent load-bearing capability with several failures in the parent metal at positions removed from the joint.

Post-Test Metallographic Examination. - Figure 106 shows the structure of an un-failed joint after testing for 118.1 hours under 62.1 MN/m^2 (9.0 ksi) stress at 1093C (2000F). Cracking of the parent metal can be seen with internal delamination under the peel component developed by joint rotation on loading. The failure is accelerated by oxidation and would undoubtedly have occurred on continuation of the test. A large patch of fine recrystallized grain does not appear to have affected failure. Cavity or hole formation on the bondline provides some evidence of slippage and generation of holes by the Chang and Grant mechanism. The lower view shows another magnification of movement on the bondline. The light areas are believed to represent recovery where the substructure has been swept out, and may be contrasted with the grain boundary where the major offsets have prevented slippage from occurring to the extent noted on the bondline. Failure of this specimen occurred in the parent metal as shown in Figure 107. It appears that an adverse combination of grain boundary orientations has contributed to this failure, with some contribution from oxidation.

Figure 108 shows a high stress test under 89.6 MN/m^2 (13.0 ksi) at 1093C (2000F) that failed in the parent metal in 3 hours. The joint showed areas of fine recrystallization, but these did not appear to affect failure. Noteworthy is the rapid formation of cavities along most of the bondline under the high shear stress (11.86 MN/m^2 or 1.72 ksi).

Figure 109 shows the results of a test at 1204C (2200F). The specimen was unfailed after 100.2 hours under 37.9 MN/m^2 (5.5 ksi) but failed on unloading. Oxidation appears to contribute to failure.



Magnification: 40X Log 6428A

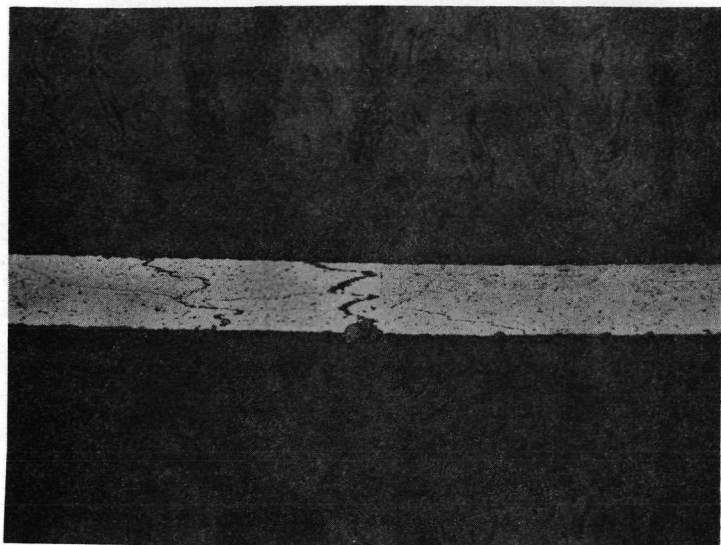
Weld Interface —



Magnification: 500X Log 6428B

10% Oxalic Acid - Electrolytic Etch

Figure 106. Microstructure of Welded Lap Joint in 0.25 mm (0.010 in.) Unrecrystallized TD-NiCr Sheet After Stress Rupture Testing at 1093 C (2000 F). Uniaxial Stress of 62.1 MN/m^2 (9.0 ksi) for 118.1 Hours. Specimen Was Unfailed. Surface Preparation by Electropolishing (Method D) with L/T Orientation



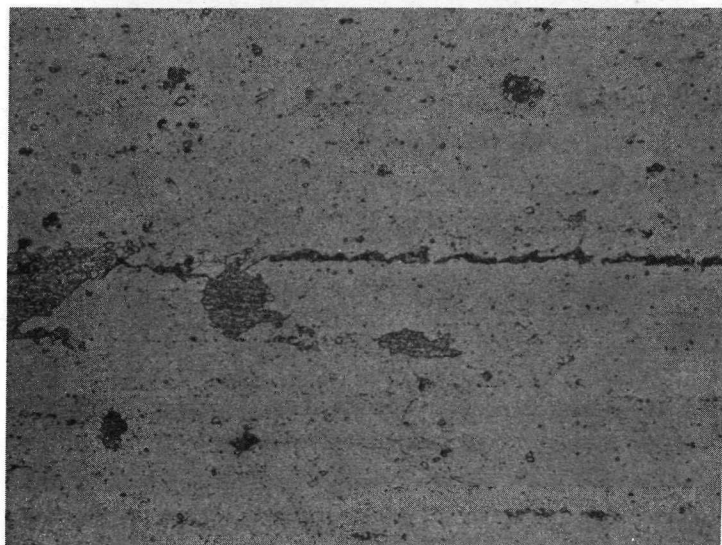
Log 6428C

10% Oxalic Acid

Electrolytic Etch

Magnification: 40X

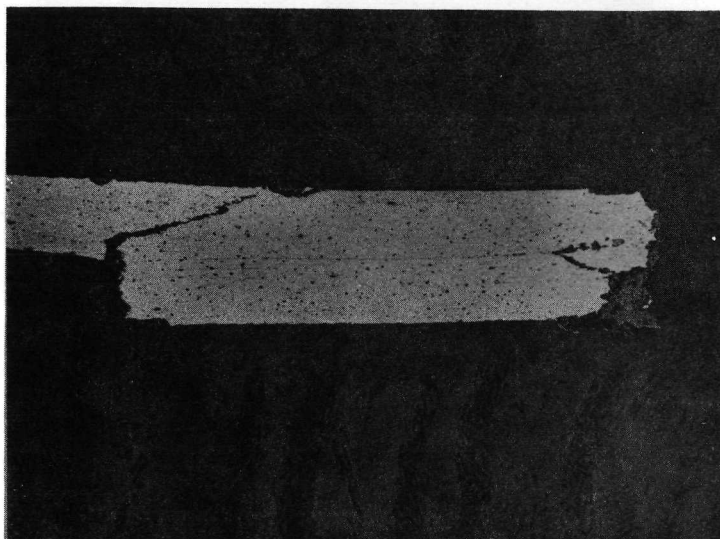
Figure 107. Grain Boundary Sliding in Transverse Leg of Stress Rupture Specimen of Figure 106, which was Exposed 118.1 Hours at 1093 C (2000 F) with a Uniaxial Stress of 62.1 MN/m^2 (9.0 ksi)



Magnification: 500X

Log 6427

Figure 108. Microstructure of Welded Lap Joint in 0.25 mm (0.010 in.) Unrecrystallized TD-NiCr Sheet After Stress Rupture Testing at 1093 C (2000 F). Uniaxial Stress of 89.6 MN/m^2 (13.0 ksi) for 3.0 Hours. Surface Preparation by Electropolishing (Method D) with L/T Orientation. Specimen Failed in Transverse Leg 0.63 cm (0.25 in.) from Joint



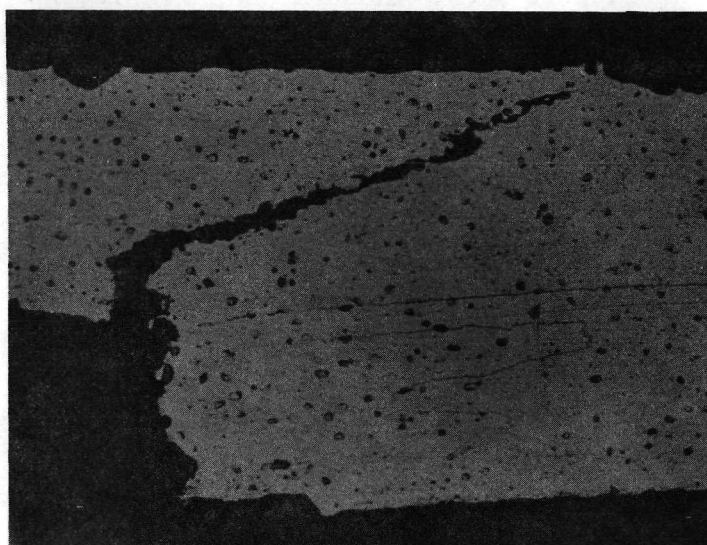
Magnification: 40X

Longitudinal orientation on right,
transverse orientation on left

Log 6429A

Magnification: 125X

Log 6429B



10% Oxalic Acid - Electrolytic Etch

Figure 109. Microstructure of Welded Lap Joint in 0.25 mm (0.010 in.) Unrecrystallized TD-NiCr Sheet After Stress Rupture Testing at 1204 C (2200 F). Uniaxial Stress of 37.9 MN/m² (5.5 ksi) for 100.2 Hours. L/T Orientation

Resistance Spot Welding (Solid-State)

The Convair Aerospace High-Power-Level (HPL) spot welding process (Ref. 21) was used for evaluation of solid-state spot welding of recrystallized and unrecrystallized TD-NiCr sheet. The proprietary HPL spot welding process employs an electronic control unit to modify a Federal 125 kVA, 3-phase spot welding machine for solid-state welding. The HPL process delivers most of the weld energy in a pulse length of 1 millisecond. The HPL spot welding unit is also equipped with a Convair Aerospace Weld Energy Monitor/Limiter, which provides digital readout of relative weld energy with low- or high-energy-level trip capabilities (Ref. 22). The energy level for each spot weld can be monitored for continuous control of process variations and recorded for comparative evaluations and correlation with test results.

The materials used for solid-state spot welding evaluation were as follows:

- (1) Recrystallized 0.25 mm (0.010 in.) sheet, Heat 3691 (Code L)
- (2) Unrecrystallized 0.25 mm (0.010 in.) sheet, Heat 3689 (Code J)

The welding variables investigated include electrode tip radii of 10.2 cm and 20.3 cm, (4 in. and 8 in.), electrode force of 1890 to 3558 N (200 to 800 lb), primary direct current (50 to 150 amperes), and four surface preparations. The surface preparation conditions were:

Surface Preparation A – Solvent clean (MEK)

Surface Preparation B – Abrasive polish through 600-grit, MEK wipe.

Surface Preparation C – Abrasive polish through 600-grit, electropolish in Summa solution, MEK wipe.

Surface Preparation D – Electropolish in Summa solution, MEK wipe.

The evaluation procedures used for weld schedule development were peel test, metallography, and room temperature tensile shear tests. Welds in the unrecrystallized material were given a recrystallization anneal at 1177°C (2150°F) for 2 hours prior to evaluation. No elevated temperature testing or joint efficiency evaluation of solid-state spot welds were performed under the present program.

Weld Schedules for Recrystallized Material. – Weld parameter studies resulted in the selection for further evaluation of three weld schedules for Surface Preparations A and B. These weld schedules and results of room temperature tensile shear tests are presented in Table 31. The microstructure of a typical solid-state spot weld made with Surface Preparation A (solvent cleaned) using 1334 N (300 lb) electrode force and 70 amperes welding current is shown in Figure 110. The microstructure of a solid-state spot weld for Surface Preparation B (abrasive polished) made with the same weld

Table 31. Tensile-Shear Tests of Solid-State Spotwelded Joints of 0.25 mm (0.010 in.) Recrystallized TD-NiCr Sheet - Heat 3691 (Code L4)

Weld Schedule	Surface Preparation	Grain Orientation	Weld ⁽¹⁾ Diameter cm (in.)	Tensile Shear Failure Load N (lb)	Failure Mode(2)
1 Current-70 amps Weld Force- 1334 N (300 lbs) Electrode R - 10.2 cm (4 in.)	A	L/L	0.23 (0.09)	787 (177)	NP
		T/T	↓	676 (152)	PP
		T/T	↓	1108 (249)	NP
		L/T	↓	903 (203)	↓
		L/T	↓	943 (212)	↓
	B	L/L	0.23 (0.09)	925 (208)	NP
		L/T	↓	1001 (225)	↓
		L/T	↓	1068 (240)	↓
		T/T	0.25 (0.10)	1179 (265)	↓
		T/T	0.25 (0.10)	1201 (270)	↓
2 Current-85 amps Weld Force- 1334 N (300 lbs) Electrode R - 10.2 cm (4 in.)	A	L/L	0.23 (0.09)	792 (178)	PP
		L/T	↓	1099 (247)	NP
		L/T	↓	1068 (240)	↓
		T/T	↓	1223 (275)	NTEW
		T/T	↓	952 (214)	↓
	B	L/L	0.23 (0.09)	774 (174)	NP
		L/T	0.25 (0.10)	1179 (265)	↓
		L/T	0.23 (0.09)	1005 (226)	↓
		T/T	0.25 (0.10)	1170 (263)	↓
		T/T	0.25 (0.10)	1223 (275)	↓
3 Current-65 amps Weld Force- 1334 N (300 lbs) Electrode R - 20.3 cm (8 in.)	A	L/L	0.23 (0.09)	774 (174)	PP
		L/T	0.25 (0.10)	965 (217)	NP
		L/T	0.25 (0.10)	1001 (225)	NP
	B	L/L	0.23 (0.09)	1068 (240)	NTEW
		L/T	0.23 (0.09)	854 (192)	NP
		L/T	0.25 (0.10)	1001 (225)	NTEW

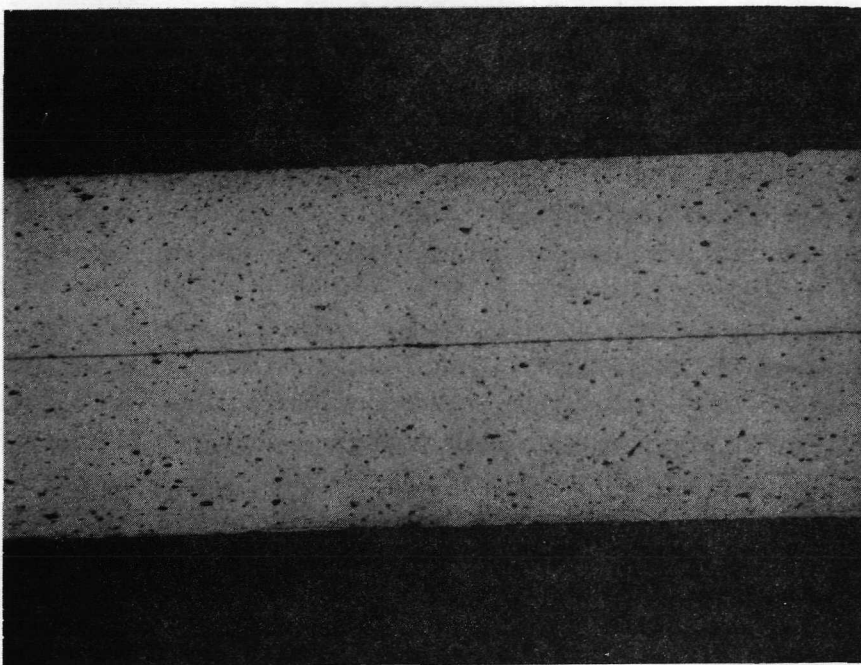
Annealed 2 hours at 1177C (2150F) in dry hydrogen after welding.

(1) Measured diameter of pulled nugget.

(2) PP = Partial nugget pullout; partial peel at interface.

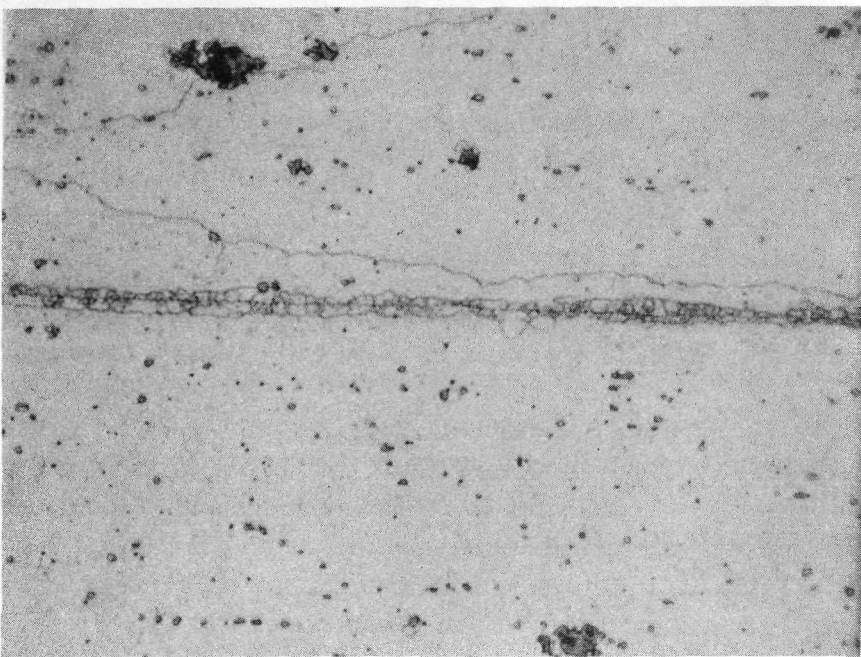
NP = Nugget pullout.

NTEW = Net tension edge of weld.



Neg. D2696

100X



Neg. D2692

1000X

Figure 110. Microstructure of Solid-State Spotweld of 0.25 mm (0.010 in.) Recrystallized TD-NiCr with Surface Preparation A – Weld Current 70 amps, Weld Force 1334 N (300 lb), Electrode Tip Radius 10.2 cm (4 in.)

schedule is shown in Figure 111. At 1000X magnification, the weld interface for both surface conditions contains a narrow band of fine recrystallized grains. The microstructure appears identical to that of resistance seam welds (solid-state) for the same type material and surface preparation (see Figure 87).

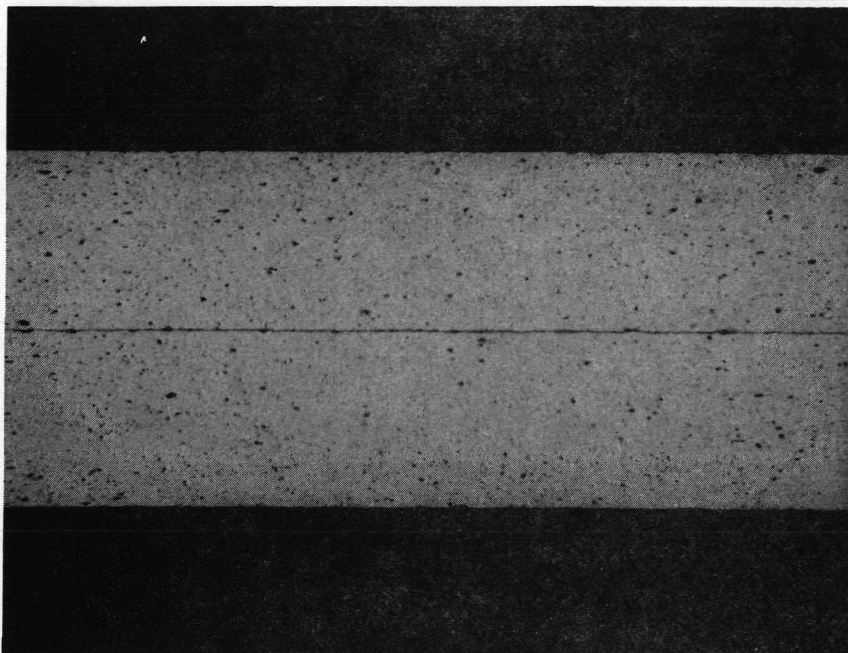
Satisfactory solid-state spot weld schedules could not be developed for Surface Preparations C (abrasive polished plus electropolished) or D (electropolished). Excellent fused nugget welds could be made with the electropolished surface, but the heat input range between no-weld and formation of a fused nugget was so narrow that consistent solid-state welds could not be obtained. It is believed that further refinement of weld schedules (see following section) would enable HPL spot welding of recrystallized TD-NiCr with electropolished surface preparation.

Observations from weld development studies on recrystallized sheet for Surface Preparation A and B are as follows:

- (1) Surface Preparation B (abrasive polished) gives slightly higher shear strength than Surface Preparation A (solvent cleaned)
- (2) No difference in shear strength was evident between the 20.3 cm (8 in.) and 10.2 cm (4 in.) electrode tip radii
- (3) L/T and T/T grain orientations give higher shear strength than L/L orientation
- (4) Solid-state spot welds had lower strength than fusion spot welds; i. e., 1001 N vs 1334 N (225 lb vs 300 lb). This is attributed primarily to the smaller diameter of the solid-state spot welds.
- (5) Further development effort should be directed toward obtaining larger weld diameters; i. e., 0.30 cm (0.12 in.) and evaluation of elevated temperature properties.

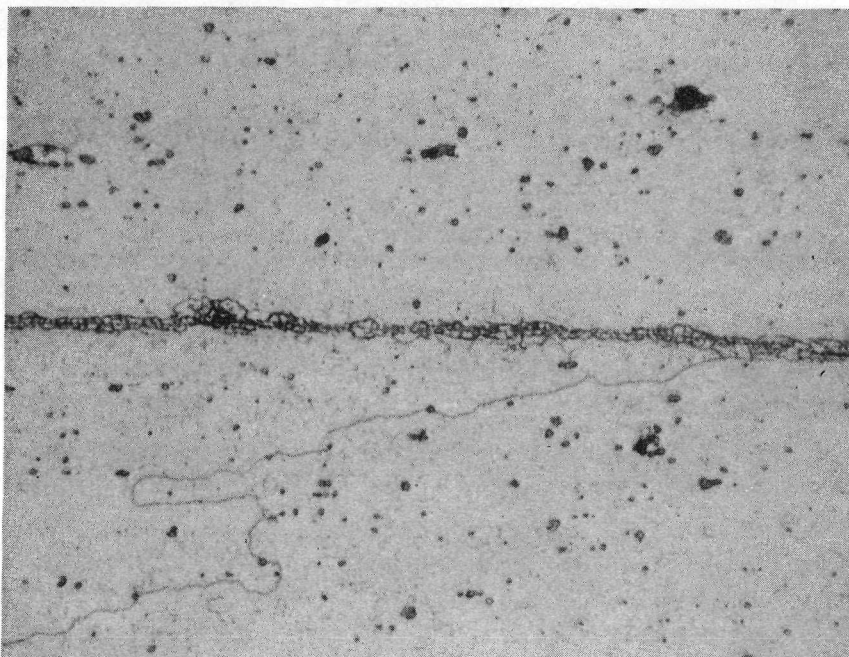
Weld Schedules for Unrecrystallized Material. - Weld parameter studies resulted in the selection of two weld schedules for further evaluation. These weld schedules and results of room temperature tensile-shear tests for all four surface preparations are presented in Table 32. Weld Schedule 5 (higher weld current and weld force) gave higher shear strength values than Weld Schedule 6, but this is attributed primarily to larger nugget diameter.

Subsequent metallographic studies revealed evidence of a heat-affected zone (nugget formation) for both weld schedules, which is undesirable microstructure for solid-state spot welds. Further investigation revealed that the energy input for these weld schedules was inadvertently selected too high. Refinement of the weld parameters resulted in Weld Schedule 7 as follows:



Neg. D2697

100X



Neg. D2693

1000X

Figure 111. Microstructure of Solid-State Spotweld of 0.25 mm (0.010 in.) Recrystallized TD-NiCr Sheet With Surface Preparation B — Weld Current 70 amps, Weld Force 1334 N (300 lb), Electrode Radius 10.2 cm (4 in.)

Table 32. Tensile-Shear Tests of Solid-State Spot Welded Joints of 0.25 mm (0.010 in.) Unrecrystallized TD-NiCr Sheet — Heat 3714 (Code J8)

Weld Schedule	Surface Preparation	Grain Orientation	Weld (1) Diameter cm (in.)	Tensile Shear Failure N (lbs)	Failure Mode
5 Current - 90 amps Weld Force - 2224 N (500 lbs) Electrode R - 10.2 cm (4 in.)	A	L/L L/T L/T	0.25 (0.10) ↓	1059 (238) 1063 (239) 1023 (230) Av. 1050 (236)	NTEW NP NP
	B	L/L L/T L/T	0.25 (0.10) ↓	1237 (278) 916 (206) 1272 (286) Av. 1143 (257)	NTEW NP NP
	C	L/L L/L L/L	0.25 (0.10) ↓	814 (183) 930 (209) 965 (217) Av. 903 (203)	NTEW NP NP
	D	L/L L/T L/T	0.25 (0.10) ↓	881 (198) 934 (210) 947 (213) Av. 921 (207)	NP NP NP
6 Current - 65 amps Weld Force - 1334 N (300 lbs) Electrode R - 10.2 cm (4 in.)	A	L/L L/T L/T	0.22 (0.085) ↓	876 (197) 890 (200) 894 (201) Av. 886 (199)	NTEW NP NTEW
	B	L/L L/T L/T	0.22 (0.085) ↓	1023 (230) 886 (199) 858 (193) Av. 920 (207)	NP NP NP
	C	L/L L/T L/T	0.22 (0.085) ↓	787 (177) 836 (188) 841 (189) Av. 823 (185)	NTEW NP NP
	D	L/L L/T L/T	0.22 (0.085) ↓	774 (174) 778 (175) 770 (173) Av. 774 (174)	NTEW NP NTEW

Annealed 2 hours at 2150 F in dry hydrogen after welding

(1) Measured diameter of pulled nugget

(2) NTEW = Net tension at edge of weld

NP = Nugget pullout

Weld Current — 92 amps

Weld Force — 3114 N (700 lb)

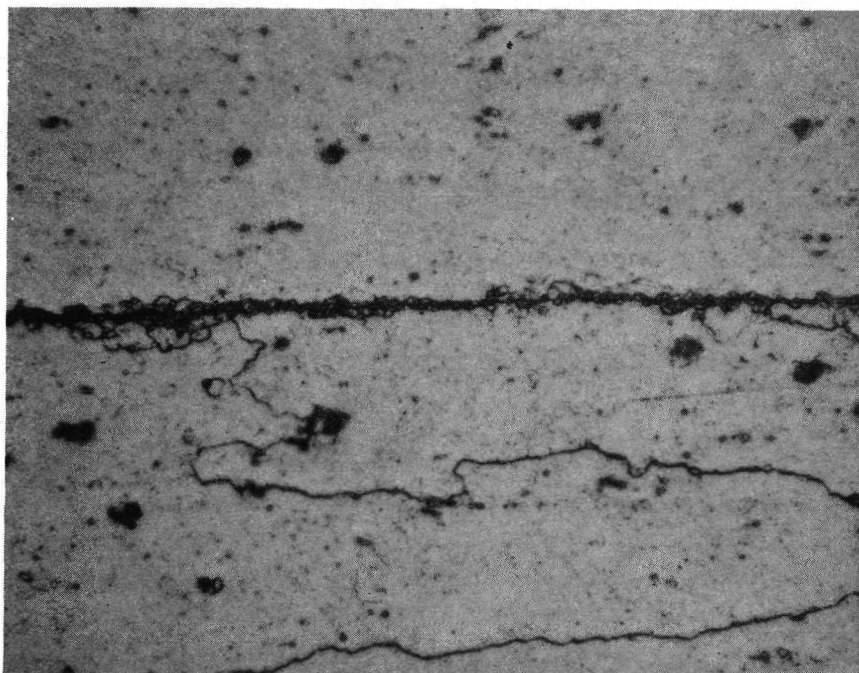
Electrode Radius — 25.4 cm (10 in.)

The most significant change is the use of a large electrode tip radius, which resulted in consistent welds of 0.25 cm (0.10 in.) diameter. Typical spot weld microstructure for Weld Schedule 7 and Surface Preparation B (abrasive polished) is shown in Figure 112. The narrow band of fine grain recrystallization at the weld line is almost identical to that of resistance seam weld joints of unrecrystallized material for the abrasive-polished preparation (see Figure 91a).

The scope of the present program did not permit optimization of weld schedules for electropolished surfaces or evaluation of elevated temperature properties of solid-state spot welds. However, the results for the improved weld schedules provide good indication that the HPL spot welding process can produce solid-state welded joints with equivalent microstructure to resistance seam welding for both recrystallized and unrecrystallized TD-NiCr sheet. Other work (Ref. 9) has shown that solid-state spotwelding of unrecrystallized material can be accomplished and the weld line completely eliminated by post-weld recrystallization heat treatment.

Corrugation-Stiffened Panel. - A corrugation-stiffened demonstration panel of unrecrystallized sheet was fabricated by HPL solid-state spot welding. The 15.2 by 22.9 cm (6 by 9 in.) panel consists of 60 degree corrugations and one face sheet, both of 0.25 mm (0.010 in.) material. The corrugation was hot formed at 760C (1400F) and then stress relieved for 2 hours at 816C (1500F) in hydrogen. The panel was solid-state spot welded using Weld Schedule 7 with abrasive polishing as the surface preparation method. Warpage was greater than anticipated, and use of a holding fixture during welding is necessary to ensure a flat panel. The panel was annealed for 2 hours at 1177C (2150F) in dry hydrogen. An attempt was made to flatten the panel during annealing, but no significant improvement was obtained. After annealing, a section of the panel was removed for metallographic examination. The spot weld microstructure (Figure 113) shows a slightly thicker band of fine grains at the weld-line than previous spot welds (Figure 112) for Weld Schedule 7. This may have resulted from the effects of hot forming or the 816C (1500F) stress relieving operation on the corrugation.

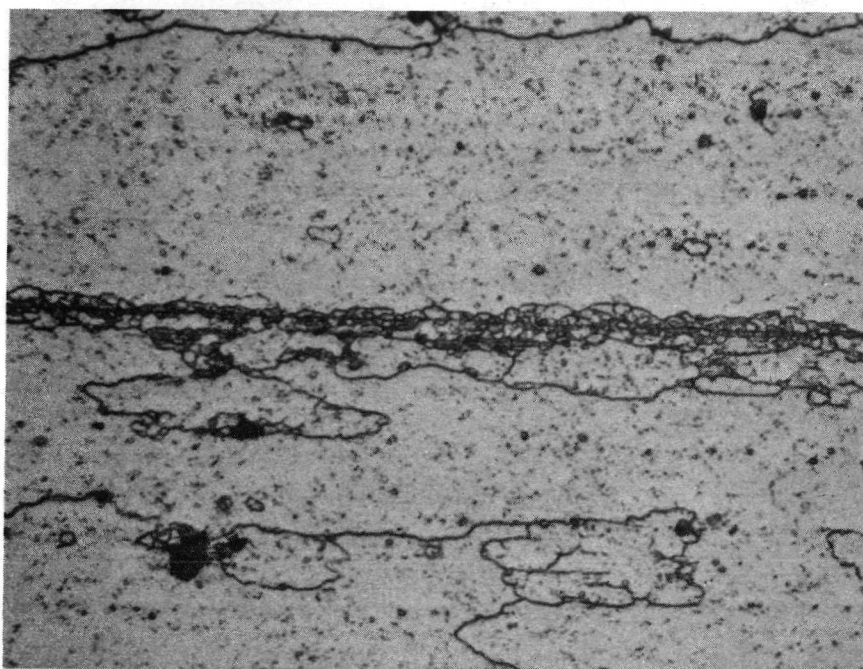
A second set of detail parts for a 15.2 by 22.9 cm (6 by 9 in.) corrugation-stiffened panel was prepared for evaluation of electropolished surface preparation to obtain a weldline free of small recrystallized grains. These parts have been delivered to NASA Lewis Research Center for surface preparation and welding.



Neg. D3787

1000X

Figure 112. Microstructure of Solid-State Spot Weld of 0.25 mm (0.010 in.) Unrecrystallized TD-NiCr with Surface Preparation A – Weld Current 92 amps, Weld Force 3114 N (700 lb), Electrode Radius 25.4 cm (10 in.) Recrystallized 2 Hours at 1177C (2150F)



Neg. D3788

1000X

Figure 113. Microstructure of Solid-State Spot Welded Joint in Corrugation Stiffened Panel Fabricated from 0.25 mm (0.010 in.) Unrecrystallized TD-NiCr Sheet – Recrystallized 2 Hours at 1177C (2150F)

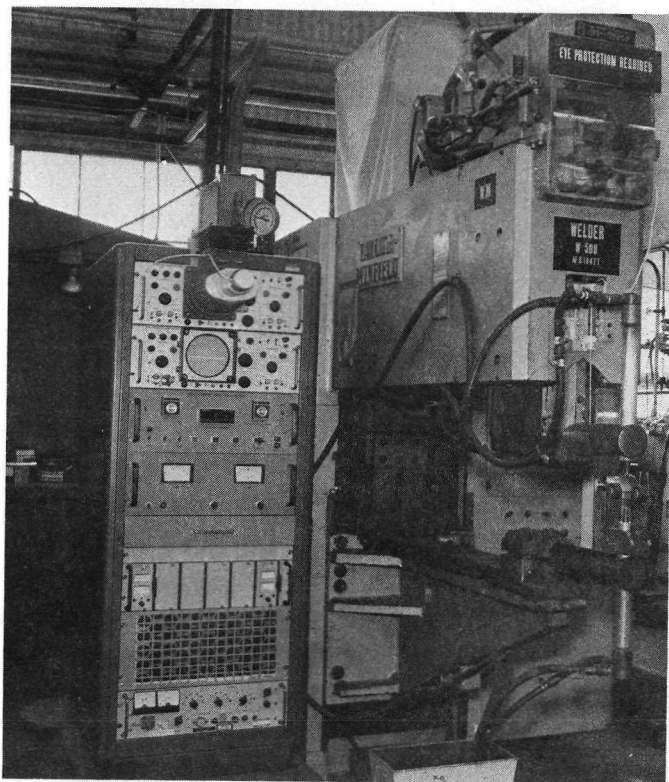
Resistance Spot Welding (Fusion)

Evaluation of conventional resistance spot welding of recrystallized TD-NiCr sheet was accomplished using the same Federal 125 kVA, 3-phase resistance welder used for solid-state spot welding except that the HPL control unit was disconnected. The characteristics of this welding machine are:

Make: Federal press-type seam/spot welder
Rating: 125 kVA, 3 phase
Maximum secondary current: 90,000 amps
Throat depth: 106.7 cm (42 in.)
Transformer: series/parallel
Polarity: Plus, minus, or neutral
Weld impulses: 1 to 100
Cool time: 1 to 10 cycles
Weld heat: 20 to 100% of transformer tap
Forge time: 1 to 100 cycles
Post heat impulses: 1 to 100
Squeeze and hold time: 1 to 100 cycles
Forge delay time: 1 to 100 cycles

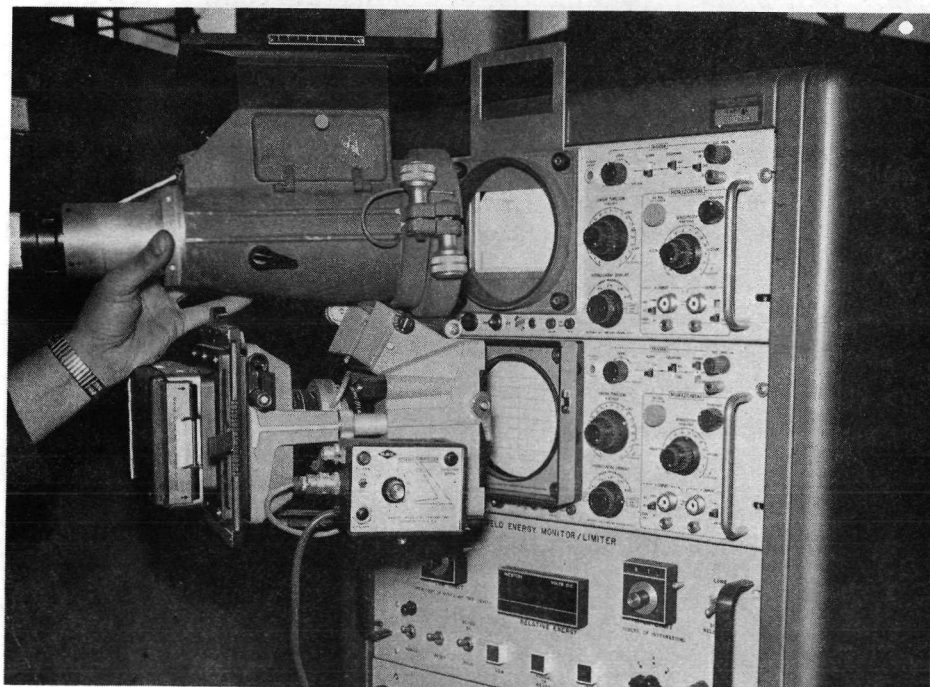
During weld schedule development and specimen fabrication, two proprietary Convair Aerospace-developed control devices were employed in conjunction with the resistance welding machine. The Convair Aerospace In-Process Control Unit (Refs. 22 to 25) was used to provide high-speed programming of welding current. This unit is shown in Figure 114. The Control uses a profile template that is followed by high-speed optical-electronic tracking during the heating cycle of each spot weld. The linear thermal expansion of the weld nugget, measured and controlled through electrode displacement, is caused to be an exact duplicate of the template profile. Preparation of a flat opaque template with the edge profile representing the desired thermal expansion as a function of time permits the optimum welding parameters to be maintained throughout a welding program.

The Convair Aerospace In-Process Control Unit provides the ability to vary the welding current continuously throughout the welding sequence. The time factor is $1/3$ cycle or 0.005 second (the resolution capability of the power source). The system is a fully automatic compensator from spot to spot. Significant changes in sheet fit-up, thickness, heat buildup, pressure variations, etc., cannot cause gross changes in the nugget, since the control parameter (sensing signal) is derived from the thermal characteristics of the nugget itself.



Electronics for the welder controls, feedback loop, dc stabilizer, and output display systems are housed in the cabinet to the left of the three-phase welder

Neg. 03418M

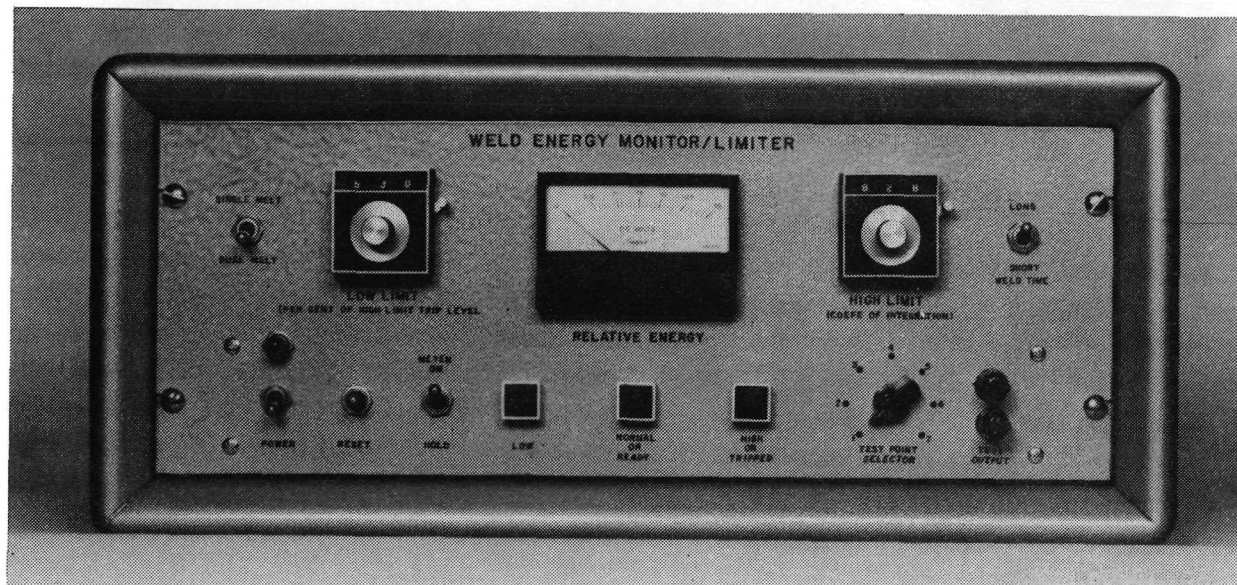


Optical-electronic portion. The oscilloscope displays the output of the welder transducer circuit. A photo-multiplier circuit transmits the cathode-ray tube trace location back to the welder control. Camera is attached to the enclosure housing to record the cathode ray tube trace during schedule development

Neg. 03417M

Figure 114. In-process Control Unit

A second proprietary Convair Aerospace device that was used throughout the resistance welding program is the Weld Energy Monitor/Limiter. Four of these units have been used for the past five years to monitor the consistency of electrical output of resistance welders in the final critical stages of Centaur spacecraft fabrication. These devices employ digital and analog circuitry to compute the total electrical energy (kilowatt-sec) delivered to each spot weld (Refs. 22 through 25). Electrical energy variations can be effected by changes in fit-up, force, electrode temperature, etc., in addition to machine malfunctions, misfiring, or instability of the power supply. In the event of an excessive drop or rise of energy, the welder is disabled until reset. Figure 115 shows the Weld Energy Monitor/Limiter Control panel, which has dual melt capability.



Neg. 102411B

The low-limit adjustment reads in an exact percentage of the high-limit trip energy. The meter switch holds the integrator on to permit convenient readings of the energy level in establishing limits. The single/dual melt switch provides efficient operation for weld sequences employing "temper" or "postheat" cycles.

Figure 115. Control Panel of Convair Weld Energy Monitor/Limiter

Materials. - Welding parameters were investigated for the following materials:

- (1) Recrystallized 0.25 mm (0.010 in.) sheet, Heat 3691 (Code L)
- (2) Recrystallized 0.08 mm (0.003 in.) sheet, Heat 3702 (Code M)

Since fused nugget spot welds are less sensitive to grain orientation than solid-state welds, all coupons were prepared for the L/L orientation only.

Test Plan for Weld Parameter Optimization. - The normal resistance welding parameters; i. e., current, cycles, pressures, electrode configuration, preheat, post-heat, multiple cycles, etc., were investigated for three surface preparation methods. The surface preparations were:

- (1) Method A: Solvent clean with Methyl Ethyl Ketone (MEK)
- (2) Method B: Abrasize polish with 600 grit paper, MEK solvent wipe before welding
- (3) Method C: Chemical clean, MEK solvent wipe before welding

The chemical cleaning procedures were:

- (1) Alkaline clean - Oakite 90(47-94 ml/l)at 77-88C (170-190F) for 5 minutes
- (2) Acid Etch - HCl(113-138 ml/l)plus CuCl_3 (20-23 ml/l)room temperature for 10 minutes
- (3) Brightener - H_2SO_4 (164-188 ml/l)plus Na_2CrO_4 (126-152 ml/l)room temperature for 10 minutes
- (4) Deionized water spray rinse
- (5) Air blast dry

Spotwelded joints were evaluated by peel tests, metallographic examination, and room temperature tensile-shear tests. Selected weld schedules were further evaluated by elevated temperature tensile-shear and stress-rupture tests.

Schedule Development for 0.25 mm (0.010 in.) Sheet. - Preliminary investigation resulted in the development of eight welding schedules for 0.25 mm (0.010 in.) recrystallized sheet. These schedules, listed in Table 33, show effect of variations in weld force, weld energy, weld time, electrode radius, and forge and post heat. Macro sections were used to optimize nugget diameters and weld penetration for each schedule. The formula $D = 2T + 0.15 \text{ cm}$ (0.06 in.) (where D is the nugget diameter and T is the material thickness) was used as an approximate guide to establish minimum nugget diameters. Preliminary weld schedules were developed with coupons cleaned by wiping with MEK solvent (Method A). A diagram illustrating the weld current, force, and time relationships for a typical weld schedule (Weld Schedule 3) is shown in Figure 116.

The best weld schedules developed with Surface Preparation A were then used to prepare evaluation specimens for the other two surface preparation methods. Results of tensile-shear tests and metallographic examination of single spot weld specimens

Table 33. Resistance Spotweld Schedules for 0.25 mm (0.010 in.) Recrystallized TD-NiCr Sheet

Weld Schedule	Variable (1)	Weld Force N (lb)	Heat %	Heat Time (cycles)	Phases	Weld Impulses	Electrode Radius cm (in.)	Relative Energy (volts) .	Macro Section Examination	
									Nugget Diameter cm (in.)	Nugget Penetration %
1	Low force	3114 (700)	51	2	2	1	15.2 (6)	4.98-5.08	0.25 (0.10)	40
2	High force	4448 (1000)	60	2	2	1	10.2 (4)	5.42-5.60	0.25 (0.10)	30
3	Electrode radius	4448 (1000)	65	2	2	1	15.2 (6)	5.92-6.28	0.28 (0.11)	50
4	Forge and post-heat ⁽²⁾	3114 (700)	53	2	2	1	15.2 (6)	5.10-5.42	0.25 (0.10)	40
5	Low weld energy	3114 (700)	90	1	1	1	10.2 (4)	2.17-2.27	0.23 (0.09)	35
6	High weld energy	4448 (1000)	63	3	2	1	15.2 (6)	8.43-8.72	0.28 (0.11)	30
7	Short weld time	2224 (500)	80	1	1	1	10.2 (4)	2.05-2.09	0.23 (0.09)	40
8	Long weld time	4448 (1000)	60	3	2	1	10.2 (4)	7.89-8.11	0.28 (0.11)	25

(1) Common Parameters

Squeeze time 35 cycles
Hold time 35 cycles
Transformer series

(2) Schedule 4 - Forge and Post-heat Parameters

Forge force 6672N (1500 lbs)
Quench 35 cycles
Forge delay end of weld cycle
Cool time 5 cycles
Post heat % 35
Post heat impulses 2
Forge time 55 cycles

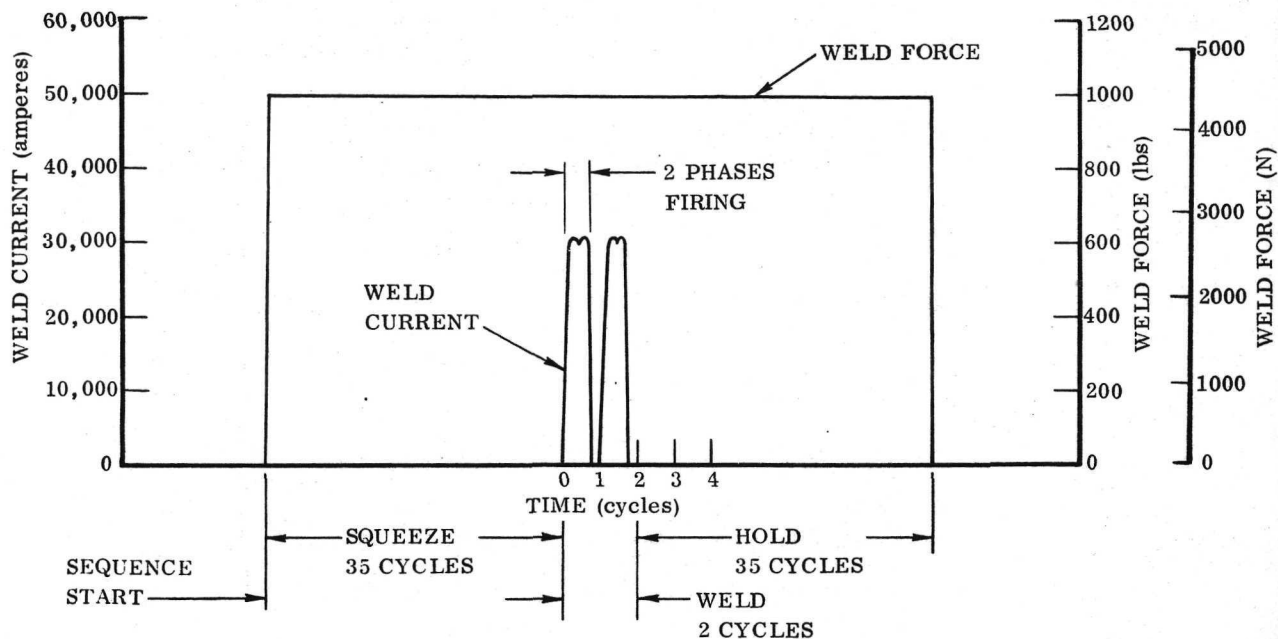


Figure 116. Diagram of Spotweld Schedule 3 for Resistance Spotwelding of 0.25 mm (0.010 in.) Recrystallized TD-NiCr

for the eight schedules and three surface preparations are listed in Table 34. Weld energy data obtained with the Convair Aerospace Weld Energy Monitor/Limiter is also listed in this table. Typical spot weld microstructure is shown in Figure 117.

Comparison of these data indicate the following:

- (1) Abrasive surface cleaning is slightly better than solvent cleaning and greatly superior to chemical cleaning.
- (2) The Convair Aerospace resistance weld monitor shows excellent correlation between relative weld energy and shear strength
- (3) Satisfactory resistance welds can be made for 0.25 mm (0.010 in.) recrystallized material without the use of forging pressure
- (4) Satisfactory resistance welds can be made using either 10.2 or 15.3 cm (4 or 6 in.) radius Class III copper welding electrodes. The large radius provides larger weld diameter

Weld schedules 1, 2 and 3 exhibited favorable combinations of tensile-shear, metallographic, and weld-energy data, and were selected for evaluation of elevated temperature properties.

Table 34. Results of Room Temperature Tensile Shear Tests and Metallographic Examination of Resistance Spotwelded 0.25 mm (0.010 in.) Recrystallized TD-NiCr Sheet – Heat 3691

Weld Schedule	Surface Preparation	Specimen Number ⁽¹⁾	Tensile Shear Failure Load N (lb)	Relative Energy (volts)	Failure Mode ⁽²⁾	Nugget Penetration (%)	Nugget ⁽³⁾ Diameter cm (in.)
1	A	1A-1	1197 (269)	5.04	NTEW	29-36	0.30 (0.12)
		1A-2	1197 (269)	5.03	NP		
		Avg.	1197 (269)	5.04			
	B	1B-1	1201 (270)	5.04	NTEW	39-43	0.30 (0.12)
		1B-2	1188 (267)	4.98	NTEW		
		Avg.	1192 (268)	5.01			
	C	1C-1	1192 (268)	4.99	NTEW	39-43	0.25 (0.10)
		1C-2	1232 (277)	5.04	NTEW		
		Avg.	1210 (272)	5.02			
2	A	2A-1	1312 (295)	5.37	NTEW	28-30	0.33 (0.13)
		2A-2	1383 (311)	5.60	NTEW		
		Avg.	1348 (303)	5.48			
	B	2B-1	1268 (285)	5.50	NTEW		
		2B-2	1441 (324)	5.42	NTEW		
		Avg.	1357 (305)	5.46			
	C	2C-1	1308 (294)	5.42	NTEW		
		2C-2	1308 (294)	5.42	NTEW		
		Avg.	1308 (294)	5.42			
3	A	3A-1	1294 (291)	6.25	NTEW	37-42	0.33 (0.13)
		3A-2	1370 (308)	6.28	NTEW		
		Avg.	1334 (300)	6.26			
	B	3B-1	1317 (296)	6.10	NP		
		3B-2	1272 (286)	6.18	NTEW		
		Avg.	1294 (291)	6.14			
	C	3C-1	1250 (281)	5.93	NTEW		
		3C-2	1259 (283)	5.92	NTEW		
		Avg.	1254 (282)	5.92			
4	A	4A-1	1268 (285)	5.42	NP	58	0.30 (0.12)
		4A-2	1343 (302)	5.10	NP		
		Avg.	1308 (294)	5.26			
	B	4B-1	1290 (290)	5.25	NP		
		4B-2	1272 (286)	5.27	NP		
		Avg.	1281 (288)	5.26			
	C	4C-1	1228 (276)	5.07	NP		
		4C-2	1223 (275)	5.08	NP		
		Avg.	1228 (276)	5.08			

Tabel 34. Results of Room Temperature Tensile Shear Tests and Metallographic Examination of Resistance Spotwelded 0.25 mm (0.010 in.) Recrystallized TD-NiCr Sheet — Heat 3691 (Contd)

Weld Schedule	Surface Preparation	Specimen Number ⁽¹⁾	Tensile Shear Failure Load N (lb)	Relative Energy (volts)	Failure Mode ⁽²⁾	Nugget Penetration (%)	Nugget (3) Diameter cm (in.)
5	A	5A-1	1112 (250)	2.18	NP	44	0.28 (0.11)
		5A-2	1099 (247)	2.19	NP		
		Avg.	1103 (248)	2.18			
	B	5B-1	1099 (247)	2.27	NP		
		5B-2	1103 (248)	2.19	NP		
		Avg.	1103 (248)	2.23			
	C	5C-1	1094 (246)	2.20	NP		
		5C-2	1099 (247)	2.17	NP		
		Avg.	1094 (246)	2.18			
6	A	6A-1	1285 (289)	8.72	NTEW	25-32	0.33 (0.13)
		6A-2	1334 (300)	8.70	NTEW		
		Avg.	1308 (294)	8.71			
	B	6B-1	1392 (313)	8.56	NTEW		
		6B-2	1366 (307)	8.67	NTEW		
		Avg.	1379 (310)	8.62			
	C	6C-1	1317 (295)	8.59	NTEW		
		6C-2	1348 (303)	8.49	NTEW		
		Avg.	1330 (299)	8.54			
7	A	7A-1	1019 (229)	2.06	NP	41	0.25 (0.10)
		7A-2	996 (224)	2.06	NP		
		Avg.	1005 (226)	2.06			
	B	7B-1	1041 (234)	2.07	NTEW		
		B-2	1005 (226)	2.07	NTEW		
		Avg.	1023 (230)	2.07			
	C	7C-1	1054 (237)	2.09	NP		
		7C-2	1005 (226)	2.06	NP		
		Avg.	1032 (232)	2.08			
8	A	8A-1	1366 (307)	7.90	NTEW	25-38	0.33 (0.13)
		8A-2	1317 (296)	7.91	NTEW		
		Avg.	1343 (302)	7.90			
	B	8B-1	1321 (297)	7.89	NTEW		
		8B-2	1406 (316)	8.11	NTEW		
		Avg.	1361 (306)	8.00			
	C	8C-1	1321 (297)	7.90	NTEW		
		8C-2	1299 (292)	7.98	NTEW		
		Avg.	1308 (294)	7.94			

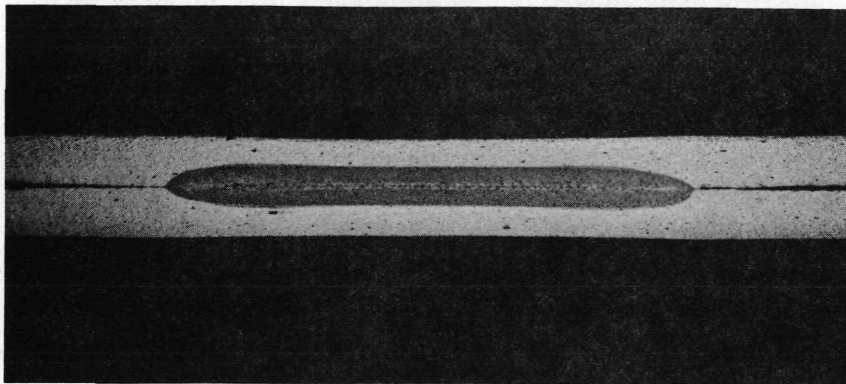
(1) 1st Number
1st Letter
Dash (-) Number

Schedule No.
Cleaning Method
Sample Number

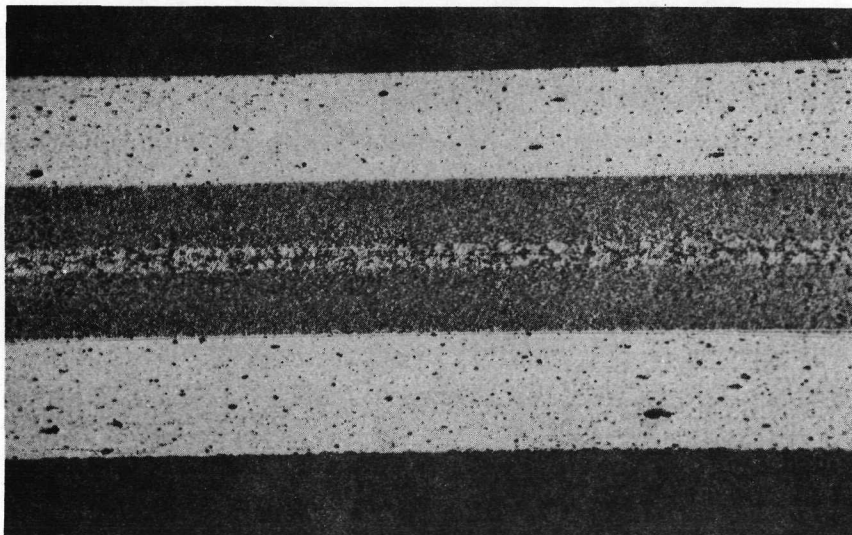
(2) NP
NTEW

Nugget Pull-out
Net Tension Edge of Weld

(3) Measured diameter of pulled nugget



Spec. 3A-3 Neg. D2019 25X



Spec. 3A-3 Neg. D2018 100X

Figure 117. Typical Resistance Spotweld Microstructure for 0.25 mm (0.010 in.) Recrystallized TD-NiCr – Weld Schedule 3

Evaluation of Elevated Temperature Spot Weld Properties. - Preliminary evaluation of elevated temperature tensile-shear and stress-rupture properties was conducted on spot welds of 0.25 mm (0.010 in.) recrystallized sheet using double spot specimens. Tensile shear tests were conducted at 1093C (2000F) for three weld schedules (Schedules 1, 2, and 3) and stress-rupture tests at 1204C (2200F) for two weld schedules (Schedules 2 and 3). The surface preparation was abrasive polishing with 600-grit silicon carbide paper (Method B). Test results are presented in Table 35. With the limited test data and large data scatter, it is difficult to discern which of the weld schedules provides the best spot weld properties. Influenced largely by the stress rupture test results, Schedule 3 with abrasive polished surface preparation was selected as most meriting further evaluation. However, the scope of the present program did not permit more comprehensive evaluation of elevated temperature spot weld properties and joint efficiencies.

Schedule Development for 0.08 mm (0.003 in.) Sheet. - Two weld schedules were developed for spot welding 0.08 mm (0.003 in.) recrystallized TD-NiCr sheet. A low electrode force of approximately 890N (200 lb) was necessary to obtain satisfactory welds using conventional three-phase resistance welding equipment. Typical nuggets are approximately 0.15 cm (0.06 in.) in diameter with 40 to 50% weld penetration.

Room temperature tensile-shear tests were conducted on single spot specimens for the two best weld schedules and two surface preparations. (Methods A and B). Results showed tensile shear failure loads from 26.7 to 29.8 N (60 to 67 lb). The data indicated no significant difference in tensile-shear strength for the two surface preparation methods. This was not unexpected, since abrasive polishing (Method B) provides no improvement in the excellent surface finish of the cold rolled sheet.

Table 35. Results of Tensile Shear and Stress Rupture Tests of Resistance Spotwelds (Fusion) of 0.25 mm (0.010 in.) Recrystallized TD-NiCr Sheet-Heat 3691

Weld Schedule ^(b)	Typical Nugget Diameter cm (in.)	1093C (2000F) Tensile-Shear Tests ^(a)				1204 (2200F) Stress-Rupture Tests ^(a)		
		Tensile Shear Failure Load N (lb)	Shear Stress MN/m ² (ksi) ^(c)	Net Tensile Stress MN/m ² (ksi) ^(d)	Failure Mode	Stress Rupture Load N (lb)	Rupture Life (hours)	Failure Mode
1	0.30 (0.12) Avg.	280 (63)	19.3 (2.8)	34.5 (5.0)	Joint shear with cracks. Joint shear with cracks and partial pullout.	No tests	-	-
		556 (125) 418 (94)	38.6 (5.6) 29.0 (4.2)	69.0 (10.0) 51.7 (7.5)				
2	0.33 (0.13) Avg.	448 (100)	26.2 (3.8)	55.2 (8.0)	Nugget pullout	222 (50)	25	Failed in grip.
		436 (98) 440 (99)	25.5 (3.7) 26.2 (3.7)	5.38 (7.8) 5.45 (7.9)	Nugget pullout	267 (60)	0.1	One nugget pullout, one joint shear.
3	0.33 (0.13) Avg.	423 (95)	24.8 (3.6)	5.24 (7.6)	Nugget pullout	167 (37.5)	150	Did not fail.
		387 (87) 405 (91)	22.8 (3.3) 23.4 (3.4)	4.76 (6.9) 5.03 (7.3)	Nugget pullout	267 (60)	8	Joint shear.

(a) Double spot specimen.

(b) Method B - Abrasive polish with 600-grit SiC paper; solvent wipe.

(c) Calculated for typical nugget diameter and two nuggets per specimen.

(d) Calculated for nominal thickness and width of 3.17 cm (1.25 in.) wide specimen.

Brazing

The plan through which alloys were developed and evaluated for brazing TD-NiCr sheet was a selective, three-part progression.* Satisfactory compliance with the selection criteria of each step was deemed a necessary prerequisite for progression to the next, and more advanced, phase of evaluation. Twenty candidate alloy compositions approved by NASA were considered in four groups (identified as the 1st through the 4th alloy series). TD-6 braze alloy was carried through all phases of the program as the baseline reference standard against which the characteristics of the candidate braze alloys were measured.

<u>Phase</u>	<u>Selection Criteria</u>
1. Alloy Preparation	Homogeneity Composition
2. Brazing Characteristics	Brazing Temperature Erosion Flow Residue Reaction Remelt Temperature
3. Brazement Properties	Tensile Strength, Ambient Temperature Tensile Strength, Elevated Temperature Stress-Rupture Properties

The principal TD-NiCr sheet material used for the brazing development work was unrecrystallized 0.25 mm (0.010 in.) sheet, Heat 3689, Sheet No. 638 (Code J4). In addition, a small quantity of recrystallized 1.0 mm (0.040 in.) sheet, Heat 3708, Sheet No. 547 (Code D1) was used for fabrication of the thicker leg of butt-joint braze specimens.

The original intention was to braze recrystallized TD-NiCr sheet. However this material was not available at the start of experimental work, therefore unrecrystallized sheet was used for all tests in preference to changing parameters by substituting recrystallized sheet midway through the program.

* The brazing development work was performed by the Solar Division of the International Harvester Company. The description of this subcontracted work was extracted from Solar Report RDR 1721-4 (Ref. 20).

Development of Braze Alloy Series No. 1. - The alloys were prepared with material from Solar stocks. The high-purity raw materials used are listed in Table 36. The bulk of nickel used in the alloys was the higher purity electrolytic material. A small amount of the Ni-200 foil was used to wrap the other elements preparatory to arc melting.

Table 36. Raw Material Sources

Alloy	Purity	Producer	Heat/Lot	Form
Cr	99.99	Material Research Corp.		Iochrome Crystallettes
W	99.9, low Fe	Rembar		0.0025 cm (1-mil) Foil
Al	99.99	Alcoa	R5784-4	Pig
Si	99.+	Keokuk Electro Metals	3667	Chunk
Mn	99.99	Foote Mineral Company		Electrolytic Flake
Fe	99.9, S 0.006%	Glidden		Electrolytic Flake
Mo	99.95	Atomergic Chemetals		Rondelles
Ni	99.95	Inco		Electrolytic
Ni	99.5	Rodney Metals	N22952A	Ni-200, 0.0125 cm (5-mil) Foil
Zr	99.95	Wah Chang	6810-222.9	Crystal Bar
Ti	99.95	Atomergic Chemetals	5838	Crystal Grade

The first series of braze alloys to be investigated contained Mn and in some cases Si as melting point depressants. The NASA approved compositions are given in Table 37. The TD-6 composition is included for comparison.

Alloy preparation was by arc melting. The alloy charges were arc melted to button form, using five meltings per sample to achieve homogeneity. Both 10-gram and 20-gram charges were evaluated, and the latter appeared to be more compatible with the capacity of the equipment, a 20 kW non-consumable tungsten arc melter with a water-cooled copper base plate.

Two problems encountered in the first attempts were resolved by use of pre-melted master alloys:

Table 37. Composition of TD-NiCr Braze Alloys

Test Series	Braze Alloy	Weight Percent									
		Ni	Cr	W	Mo	Al	Si	MN	Zr	Ti	Fe
1	NASA 1	Bal	16	20		8	2	3			
	NASA 2	Bal	16	20			2	3			
	NASA 3	Bal	16	20		8		5			
	NASA 4	Bal	16	20				5			
	NASA 5 ⁽¹⁾	Bal	16	20		0/8	2	5			
	NASA 6 ⁽¹⁾	Bal	16	20		0/8	0/2	3/5		2	
	TD-6	Bal	16	5	17		4				5
2	NASA 7	Bal	16	20		8			12		
	NASA 8	Bal	16	20		4			12		
	NASA 9	Bal	16	20					12		
	NASA 10	Bal	16	20					6		
	NASA 11	Bal	16	10					12		
	NASA 12	Bal	16	10					6		
3	NASA 13	Bal	16	6					6		
	NASA 14	Bal	16	2		3			6		
	NASA 15	Bal	16	20			2		6		
	NASA 16	Bal	16	5	15		2		4		
4	NASA 17	Bal	16			8	4				
	NASA 18	Bal	16		15	8	4				
	NASA 19	Bal	16		25	8	4				
	NASA 20	Bal	16			6	4			2	

(1) Composition not finalized; alloy deleted prior to melting button ingot.

1. Preparation of the alloys from elemental metals resulted in the incomplete solution of the higher melting fractions, principally tungsten, as evidenced by radiographic inspection. The problem was resolved by pre-melting a master alloy, 50 Wt. % W - 50 Wt. % Ni, near the 1500C (2732F) eutectic composition of these elements.

2. Violent outgassing of the manganese during arc melting (in 2/3 atmosphere of argon) resulted in unacceptable porosity and heterogeneity within the cast buttons. A 40 Wt. % Ni - 60 Wt. % Mn alloy, the 1018C (1863F) minimum, was prepared by plunging the manganese below the surface of induction-melted nickel under one atmosphere of argon. This master alloy was then used for manganese additions to the arc-melted braze alloys with negligible outgassing.

Subsequent to arc melting, the 20-gram buttons were submitted to radiographic and metallographic examination, both of which verified homogeneity and freedom from defects. Chemical analyses were not performed, but close control of composition was verified by accuracy of the button weights before and after melting.

Three of the buttons were crushed and graded to provide a uniform powder size of $-0.84/+0.15$ mm ($-20/+100$ U. S. S. mesh). NASA 2 and 4 alloys proved too malleable for this approach, and the buttons were therefore cold rolled to 0.025 cm (0.010 in.) gage foil, which was sheared to flakes of approximately the same dimension as the crushed alloy, or used as foil.

Three T joints of TD-NiCr were induction brazed with each of alloys NASA 1, 2, 3, and 4 and TD-6. Two of the T joints were 0.25 mm (0.010 in.) to 0.25 mm (0.010 in.) sheet. The third was 0.25 mm (0.010 in.) to 1.0 mm (0.040 in.) sheet, in the configuration of a butt joint, and was intended for remelt temperature testing.

Heating was provided by a 15 kW Lepel generator and tantalum induction susceptor. A vacuum of 6.5×10^{-3} N/m² (5×10^{-5} Torr) or better was maintained as the brazing atmosphere within a Vycor cylinder. Temperature was measured by a micro-optical pyrometer (Optical Pyrometer Co., Inc., Model No. 95), calibrated against an NBS calibrated tungsten strip lamp (Optical Pyrometer Co. Model No. 170). Approximately 20 mg of each braze alloy was held in place at the joints with high-purity polybutene binder. Heating proceeded slowly to about 538C (1000F) for evolution of the binder, and then more rapidly, reaching maximum temperature in 3 to 5 minutes.

Alloys NASA 3 and 4 did not melt up to 1399C (2550F). Approximately 10 percent of alloy NASA 1 began melting at 1343C (2450F), flowing away from the 90 percent residue by liquation and forming a small fillet. Alloy NASA 2 flowed well at 1399C (2550F), forming a satisfactory fillet and leaving no residue. The sample of TD-6 prepared by Solar brazed satisfactorily at 1316C (2400F) in agreement with published data for this alloy. A second sample of this alloy, commercially prepared as AMI Lot 120 (Alloy Metals Inc., Troy, Michigan) was tested for confirmation of Solar alloy preparation techniques and temperature measurement. These T joint samples melted and flowed at the identical temperature of the Solar-prepared TD-6, 1316C (2400F).

It was concluded that the Series 1 braze alloys were unsatisfactory because of too high brazing temperatures. The manganese addition did not have the desired effect in depressing the melting point. No attempt was made to evaluate braze alloys NASA 5 and 6.

Development of Braze Alloy Series No. 2. - The braze alloys selected for the second test series contained no Mn or Si as melting point depressants. Compositions of the

new alloys listed in Table 37 were predicated on the ability of Zr in Ni-base alloys to depress melting points.

Twenty-gram buttons of each alloy were prepared. The tungsten was added as a pre-melted master alloy of 50W-50Ni. Radiographic examinations of the buttons after arc melting five times, and again after an additional three melts, disclosed macro segregation in all but NASA 10 and 12. A second melting procedure was employed in which the zirconium also was added as a pre-melted master alloy of 18Cr-82Zr. Radiographic inspection results were essentially the same: only NASA 10 and 12 were homogeneous alloys. It is noted that those compositions contain only 6 percent zirconium, as opposed to the remainder of compositions, which contain 12 percent zirconium and which possibly have exceeded the limits of solubility which can be achieved by arc melting. Metallographic examination of the NASA 10 button revealed that there was, in fact, relatively large amounts of an undissolved heavy phase. The NASA 12 button microstructure appeared homogeneous although flawed by small shrinkage cracks.

Buttons of four alloys, NASA 8, 9, 10 and 12, were crushed to powder with a tool-steel mortar and pestle as before, and were graded to $-0.84/+0.15$ mm ($-20/+100$ U.S.S. mesh) size. NASA 7 and 11 buttons were not considered suitable for further evaluation.

Duplicate T-joint brazements were made with alloys NASA 8, 9, 10 and 12, brazing in vacuum by induction heating as before. Braze temperatures, again measured by a micro optical pyrometer, were:

NASA 8	over 1260C (2300F)*
NASA 9	over 1260C (2300F)*
NASA 10	1316C (2400F)
NASA 12	1343C (2450F)

No alloy melted completely; only about 10 to 30 percent of the charge melted and flowed by liquation, leaving a large residue. Metallographic examinations and electron microprobe analyses were performed on T joint brazements of alloy NASA 8, 9, 10 and 12 to determine the composition of the low melting faction.

The following summarizes the data derived from the microprobe analyses.

The quantitative electron microprobe analyses determinations on the low melting fraction of the four braze alloys have several points in common to establish a trend for further modification:

* Heavy deposition of vaporized chromium on the Vycor vacuum cylinder prevented measurement of higher temperatures.

- (1) Nickel content was appreciably increased beyond that of the arc-melted alloy buttons
- (2) The W/Zr ratio was diminished to less than 1/1, in all but alloy NASA 10, results of which were discounted due to the large differential between the analyses and 100 percent
- (3) Chromium was less than the 16 percent of the arc-melted buttons (probably due to evaporation)
- (4) Tungsten in liquated NASA 8 (which contained 4 percent Al) was much less than that in the other three liquated alloys, but there was 3 percent Al in the flowed alloy

Development of Braze Alloy Test Series No. 3. - Four new alloys, NASA 13 through 16, were selected for the third test series. Compositions of these alloys are shown in Table 37. NASA 13 and 14 were generally based upon the microprobe analyses of liquated portions of brazements of NASA 9 and 8 respectively. NASA 15 is a 2 percent silicon modification of NASA 9. NASA 16 is a modification of TD-6, substituting 4 percent zirconium for a reduction in silicon from 4 to 2 percent and eliminating iron.

As with previous series, the alloys were arc melted, five times each, in partial pressure of gettered argon. The button ingots were radiographically inspected without evidence of heterogeneity. Alloy NASA 13A, which was included to evaluate the benefit of adding zirconium as 82Zr-18Cr eutectic, appeared identical in this inspection and in subsequent metallographic examination and brazing tests.

Metallographic examination showed the button ingots of NASA 13 through 16 to be homogeneous with the exception of NASA 15. All were two-phase, containing large, primary dendrites. In the case of NASA 15 segregation of a heavy phase was noted. Similar results were observed in the second series of alloys, which exhibited gross macro-segregation of a heavy phase in radiographic examination of NASA 7, 8 and 9 and in metallographic examination of NASA 10. All of these alloys have 20 percent tungsten which, as previously noted, may exceed the limit of solubility.

Button ingots of NASA 13 and 13A were cold rolled to approximately 0.18 cm (0.070 in.) sheet, sheared to small 0.3 cm (0.12 in.) chips, and powdered with mortar and pestle. The other braze alloy button ingots were crushed directly to powder with the tool-steel mortar and pestle.

Braze tests were conducted in vacuum of better than 6.5×10^{-3} N/m² (5×10^{-5} Torr) by induction heating, as with previous test series. Approximately 20 milligrams of each alloy was loaded with high purity polybutene binder on TD-NiCr T joints. Heating was conducted rapidly after outgassing the binder at 538C (1000F), reaching maximum

temperature in less than 3 minutes. Each alloy was brazed both as approximately 2 mm (10 U.S.S. mesh) chunks and as 0.3 mm (48 U.S.S. mesh) powder. The temperature of visible melting was measured with an optical pyrometer and the T joint held at this temperature for about 30 seconds to permit flow. In some cases a second run was made at a slightly higher temperature, again holding for about 30 seconds. Very little difference could be noted between the two runs.

A sample of TD-6 braze alloy, produced by Solar in identical fashion to the experimental NASA alloys, was also brazed in the same manner. The excellent brazement confirmed the production and brazing techniques. Results are shown in Table 38.

All powder brazements of the experimental alloys were left with a cinder-like residue on the side where the alloy had been loaded and with minimal filleting on the opposite side. Brazements made from the chunk form exhibited partial melting in all four experimental alloys.

In contrast to these results are the good flowability and filleting of the TD-6 brazement. This alloy was prepared at Solar in the same manner as experimental alloys NASA 13 through 16, and the T joint brazed under identical conditions.

Table 38. Test Results for Series 3 Braze Alloys

Alloy	Brazing Characteristics				Metallographic Examinations Conducted			
	Approximate Size mm (U.S.S. Mesh)	Visual Melt Point C (F)	Maximum Brazing Temperature (Second Test) C (F)	Comments	Button- Ingots	Macrographs of T-Joints	Micrographs of T-Joints	
							Joint Configuration	Structure
NASA 13	2.0 (10)	1343 (2450)	-- --	Good flow and filleting. Large residue.	X			
	0.3 (48)	1316 (2400)*	1343 (2450)	Negligible flow. Cindery residue. Slightly better at 1343 C (2450 F).		X	X	X
NASA 13A	2.0 (10)	1371 (2500)	-- --	Same as NASA 13.				
NASA 14	2.0 (10)	1316 (2400)*	-- --	Small fillets. Large residue.	X	X	X	X
	0.3 (48)	1288 (2350)	1343 (2450)*	Negligible flow or fillets. Cindery residue.			X	X
NASA 15	2.0 (10)	1316 (2400)	-- --	No braze.	X			
	0.3 (48)	1280 (2335)*	1343 (2450)*	Marginal filleting. Much cindery residue. Slightly better at 1343 C (2450 F).		X	X	X
NASA 16	2.0 (10)	1338 (2440)	1288 (2450)*	Good flow and filleting. Large residue	X	X	X	X
	0.3 (48)	1282 (2340)	1288 (2450)*	Very small fillets. Much cindery residue.		X	X	X
TD-6	0.3 (48)	1316 (2400)*	-- --	Excellent braze. No residue.		X	X	X

* Examined brazement.

Metallographic cross sections were taken through several of the T joints, as indicated in Table 38. All four experimental alloys and TD-6 were examined as brazed from powder. Results confirmed incomplete melting and inadequate filleting of NASA 13 to 16 in marked contrast to TD-6. Sections through the large, unmelted residue chunk and through the liquated alloy flow of NASA 14 and 16 T-joints again showed evidence of incomplete melting and marginal filleting.

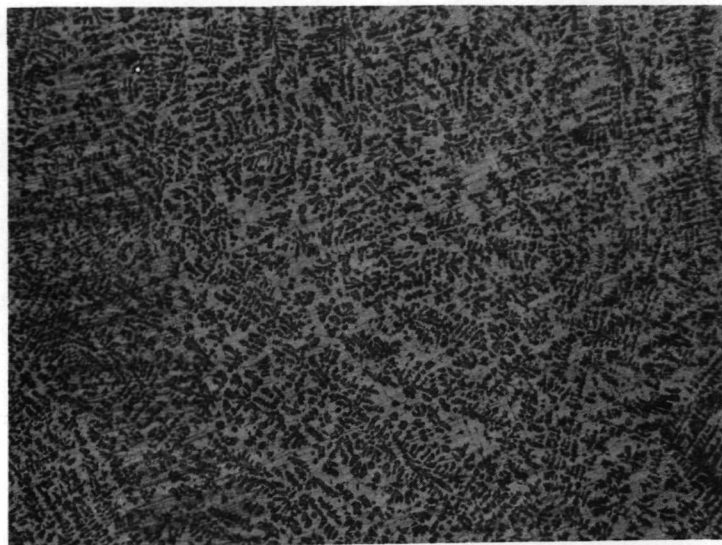
Examination of the partially melted experimental braze alloy powders revealed large amounts of primary phase surrounded by lesser amounts of eutectic. In contrast, TD-6 showed a predominantly eutectic structure with lesser amounts of dendrites.

Conclusions from the Series 3 braze alloys are summarized as follows:

- (1) Initial flow temperature is in the desired temperature range, but flow range remains excessive so that residue remains at 28-56C (50-100F) above the initial flow point
- (2) Twenty percent tungsten is excessive even with 2 percent silicon (NASA 15)
- (3) Substitution of 15 percent Mo for tungsten gives no improvement (NASA 16)
- (4) NASA 14 with 3 percent Al flows better from chunk than fine powders (characteristic of Al-containing braze alloys)
- (5) Section through residue for NASA 14 shows it to be entirely metallic, although it appeared to be a nonmetallic cinder on braze specimens

Development of Braze Alloy Series No. 4. - Four new alloys, NASA 17 through NASA 20, were selected for the fourth test series, as listed in Table 37. These compositions represent a departure from the previous concept of major tungsten and zirconium additions. The fourth series contains 6 to 8 percent aluminum, presumably sufficient to develop gamma prime strengthening, plus molybdenum or titanium in three of the alloys. Melting point depression is provided by 4 percent silicon.

Button ingots of NASA 17-20 alloys were prepared by arc melting and examined by radiography. No evidence of heterogeneity was noted. Subsequent metallographic examination (Figures 118 through 121) showed evenly distributed, large, primary dendrites in NASA 17 and 20. NASA 19 was of duplex structure, however, containing both very fine and coarse regions, separated by distinct, linear boundaries. The coarser structure appears similar to that of NASA 18, which has a similar composition but less (15% vs 25%) molybdenum. It was further noted in arc melting of NASA 19 that one of three button ingots suffered explosive cracking as it was struck with the arc in multiple melting, suggesting severe, locked-in, solidification stresses. (This button-ingot was subsequently discarded.) Brazing tests with NASA 19 evidenced a wide spread

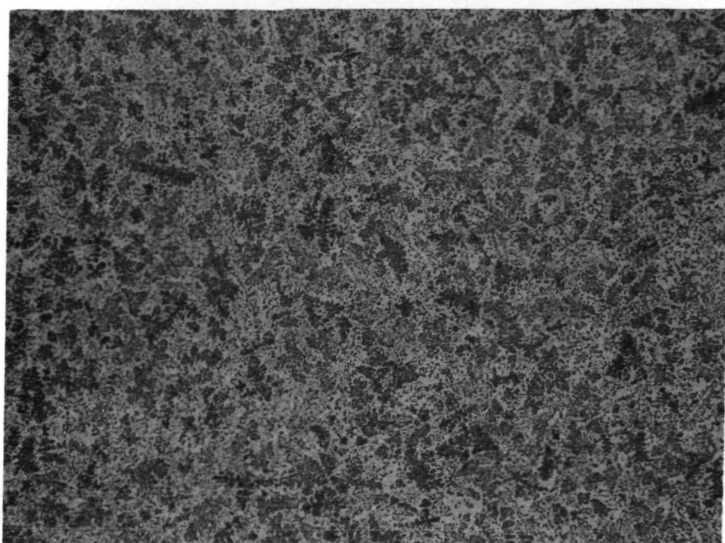


Log. No. 6250

Etchant: Kallings

Magnification: 75X

Figure 118. Alloy NASA 17 - Button Ingot

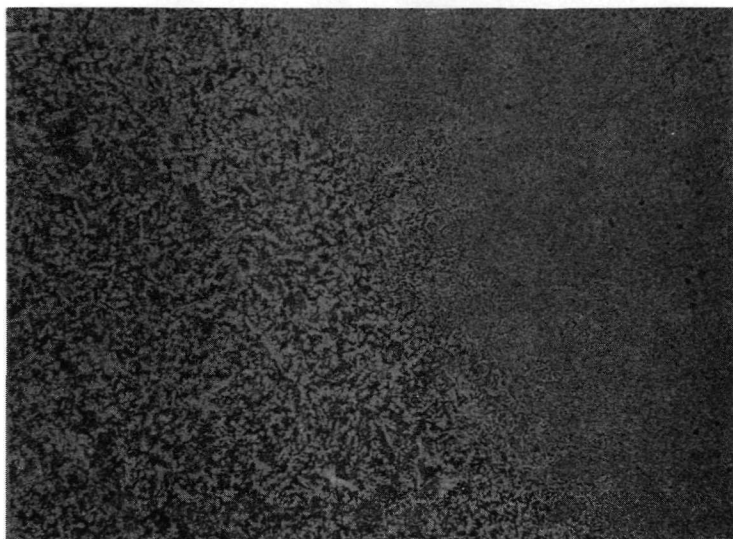


Log. No. 6251

Etchant: Kallings

Magnification: 75X

Figure 119. Alloy NASA 18 - Button Ingot

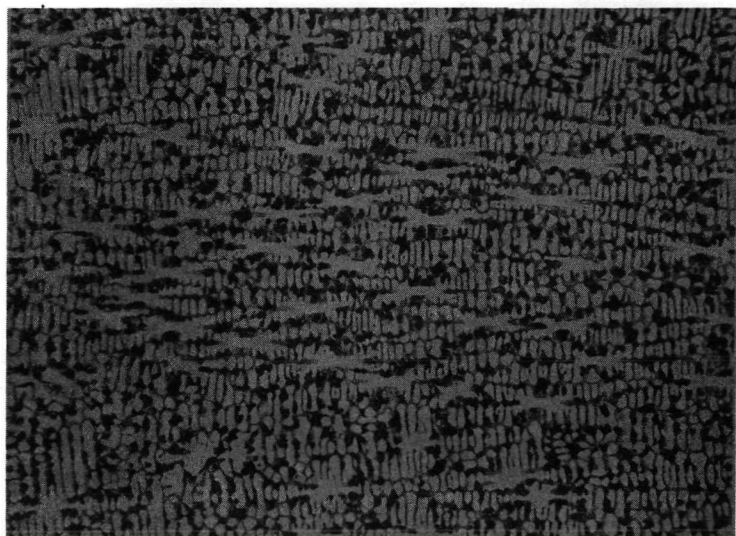


Log. No. 6252

Etchant: Kallings

Magnification: 75X

Figure 120. Alloy NASA 19 - Button Ingot



Log. No. 6253

Etchant: Kallings

Magnification: 75X

Figure 121. Alloy NASA 20 - Button Ingot

between the braze temperatures of fine and coarse particles. It was hypothesized from these several facts that solidification of NASA 19 arc-melted button ingots resulted in two compositions – perhaps binary and ternary eutectics – and that the more friable (smaller particle fraction) has a lower melting point.

Three additional button-ingots were prepared in which the molybdenum was added as a premelted Ni-45 Mo eutectic master composition. This alloy is designated NASA 19M. One of these buttons also split in multiple arc melting. Radiographs of the remaining two were homogeneous, but metallographic examination revealed the same structure is concentrated at the bottom of the ingot (initial solidification area) and comprises about 20 to 30 percent of the volume. The buttons were crushed to small chunks and powder with a tool steel mortar and pestle.

T joints of 0.25 mm (0.010 in.) TD-NiCr sheet were induction brazed with each of the Series 4 braze alloys. Results are summarized in Table 39. All alloys could be brazed with slight or moderate residue. Braze temperatures for all but NASA 19 were near the 1288C (2350F) selection parameter.

Table 39. Test Results for Series 4 Braze Alloys

Alloy	Approximate Particle Size mm (U.S.S. Mesh)	Brazing Temperature		Residue
		Pyrometer C (F)	Thermocouple C (F)	
NASA 17	2.0	10	1299 (2370)	Moderate
	2.0	10	1343 (2450)	Slight
	0.3	48	1302 (2375)	Moderate
NASA 18	2.0	10	1310 (2390)	Very slight
	2.0	10	1321 (2410)	Negligible
	0.3	48	1299 (2370)	Slight
NASA 19	2.0	10	1371 (2500)	Very slight
	2.0	10	1382 (2520)	Slight
	0.3	48	1310 (2390)	Heavy
NASA 20	2.0	10	1293 (2360)	Moderate
	2.0	10	1299 (2370)	Moderate
	0.3	48	1310 (2390)	Moderate

Each alloy was brazed both in chunk [2.0 mm (10 U.S.S. mesh)] and powder [0.3 mm (48 U.S.S. mesh)]. It appeared that braze temperatures were slightly deficient for the powders which, containing aluminum, tended to leave proportionately more residue than did the chunk form. The T joints brazed with chunk are shown in Figures 122 through 125. A brazed T joint for TD-6 alloy is shown in Figure 126.

The powder brazing tests were monitored by both the micro-optical pyrometer and Type R thermocouple. Pyrometer readings were 5 to 28C (10 to 50F) in excess of the thermocouple readings.

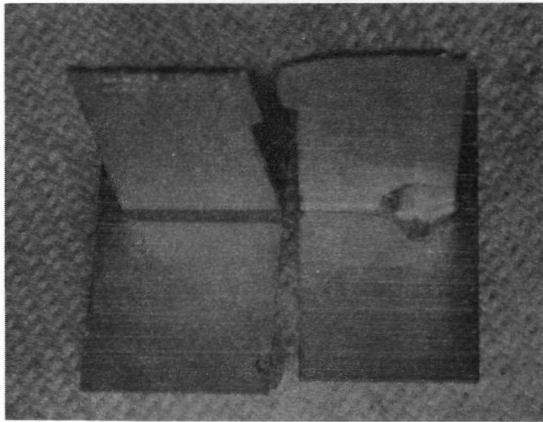
The brazements were subjected to a diffusion anneal, 1204C (2200F) for 1 hour in dry hydrogen followed by metallographic examination. Photomicrographs are shown in Figures 127 through 134. Typical brazed T joints of TD-6 alloy are shown in Figures 135 and 136

It was noted during metallographic examination that both NASA 17 and NASA 20 appeared to have partially remelted during the 1204C (2200F) anneal (Figures 131 and 134). Alloys NASA 18 and 19 showed only eutectic spheroidization (Figures 132 and 133).

Remelt Temperature Tests. - Following a review of brazing results for alloys NASA 17 through 20, it was decided to proceed with NASA 18, 19 and baseline alloy TD-6 into remelt testing and, depending upon results, to limited creep-rupture and tensile testing in the advanced phases of the program. Several specimens were brazed with each of alloys NASA 18, 19 and AMI-produced TD-6. The specimen configuration was a braze filleted T joint formed by butting the end of an 0.25 mm (0.010 in.) thick leg to the end of an 1.0 mm (0.040 in.) thick leg. Two gap configurations were employed: no-gap in which the pieces were butted directly together, and 0.05 mm (0.002 in.) gap in which a 0.05 mm (0.002 in.) step was ground in the end of the 1.0 mm (0.040 in.) stock to separate all but the very edges of the sheets. Brazing was conducted in 6.5×10^{-3} N/m² (5×10^{-5} Torr) or lower indicated pressure, by induction heating within a columbium susceptor.

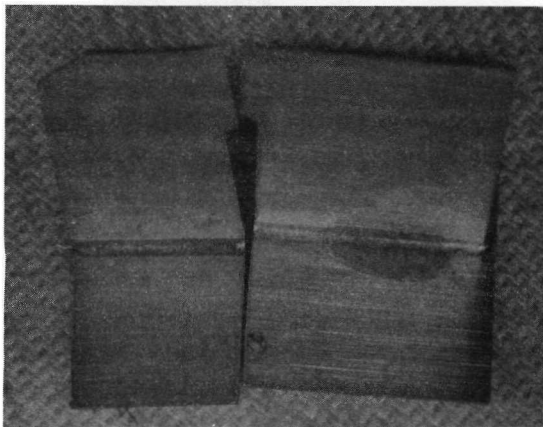
The specimens were annealed, 1204C (2200F) for 15 hours in argon prior to testing. This procedure provided more complete diffusion in wide gap areas than the 1 hour treatment used in the initial tests.

Remelt tests were conducted in argon, heating by induction with a columbium susceptor. Deadweight loading of 0.69 MN/m² (100 psi) was applied to the joint area and the temperature increased at 56C (100F) per minute from 1093C (2000F) upward. Braze and failure temperatures were monitored by a Type R thermocouple attached to the 0.25 mm (0.010-in.) sheet approximately 0.16 cm (0.06 in.) from the braze fillet. Table 40 is a summary of the remelt test program.



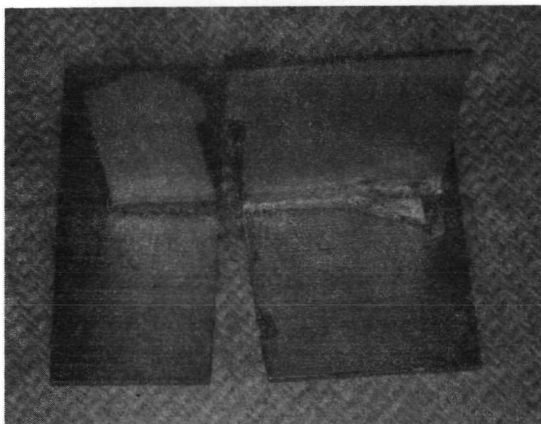
Log. No. 6208A
Magnification: 4X

Figure 122. T-Joint Brazement - NASA 17 Loaded Side - 2 mm
(10 U.S.S. Mesh) Chunk



Log. No. 6209A
Magnification: 4X

Figure 123. T-Joint Brazement - NASA 18 Loaded Side - 2 mm
(10 U.S.S. Mesh) Chunk



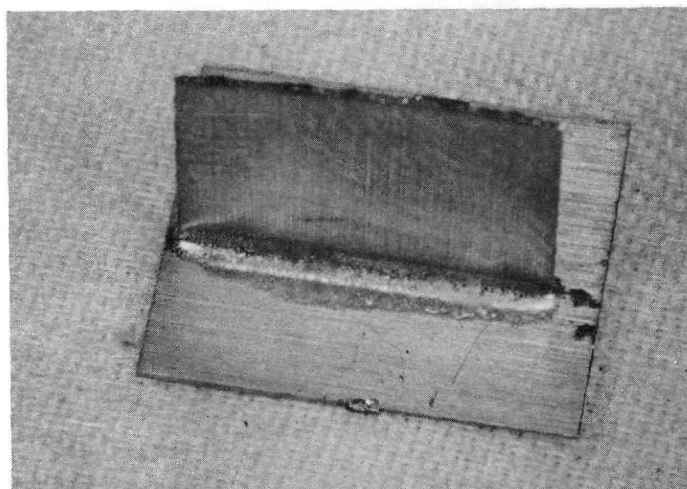
Log. No. 6210A
Magnification: 4X

Figure 124. T-Joint Brazement - NASA 19 Loaded Side - 2 mm
(10 U.S.S. Mesh) Chunk



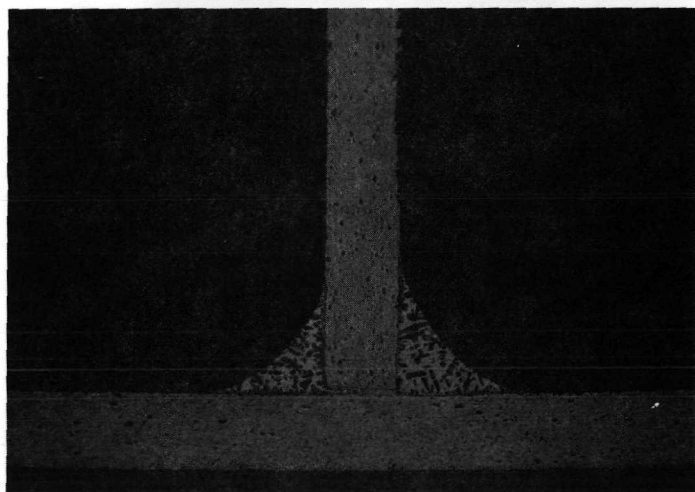
Log. No. 6211A
Magnification: 4X

Figure 125. T-Joint Brazement - NASA 20 Loaded Side - 2 mm
(10 U.S.S. Mesh) Chunk



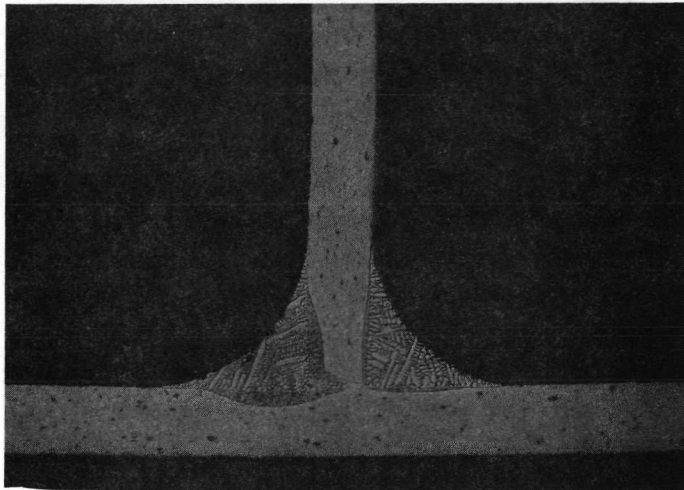
Log. No. 4945A
Magnification: 4X

Figure 126. T-Joint Brazement, TD-6 Powder, Loaded Side



Log. No. 6208B
Etchant: 10% Oxalic - Electrolytic
Magnification: 40X

Figure 127. NASA 17 Alloy Brazement - As-Brazed

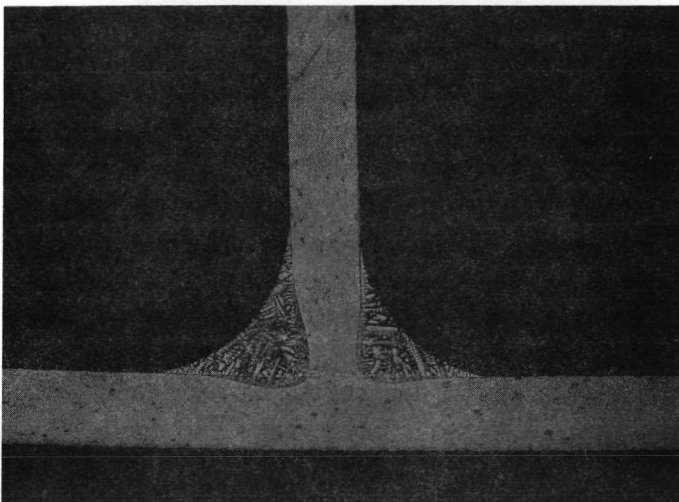


Log. No. 6209B

Etchant: 10% Oxalic - Electrolytic

Magnification: 40X

Figure 128. NASA 18 Alloy Brazement - As-Brazed

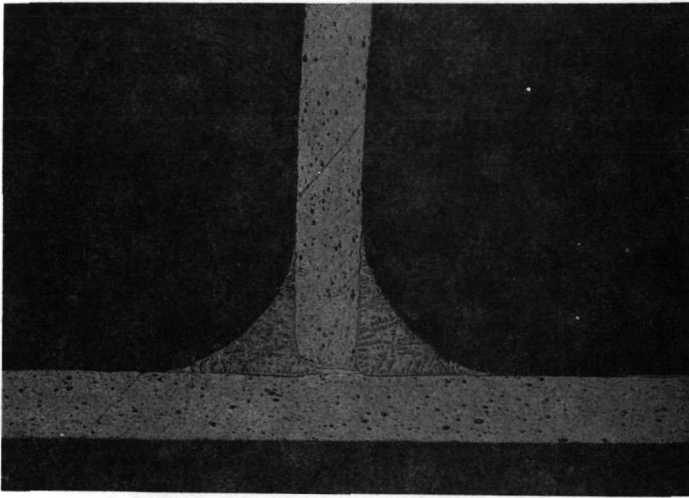


Log. No. 6210B

Etchant: 10% Oxalic - Electrolytic

Magnification: 40X

Figure 129. NASA 19 Alloy Brazement - As-Brazed



Log. No. 6211B

Etchant: 10% Oxalic - Electrolytic

Magnification: 40X

Figure 130. NASA 20 Alloy Brazement - As-Brazed

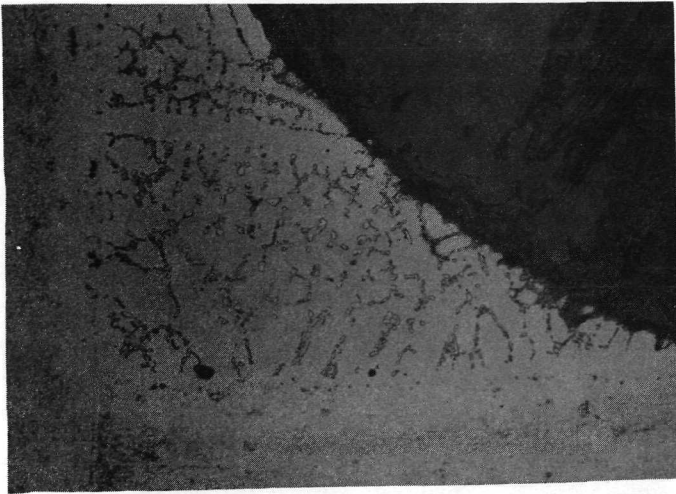


Log. No. 6208C

Etchant: 10% Oxalic - Electrolytic

Magnification: 200X

Figure 131. NASA 17 Alloy Brazement - Diffusion Annealed

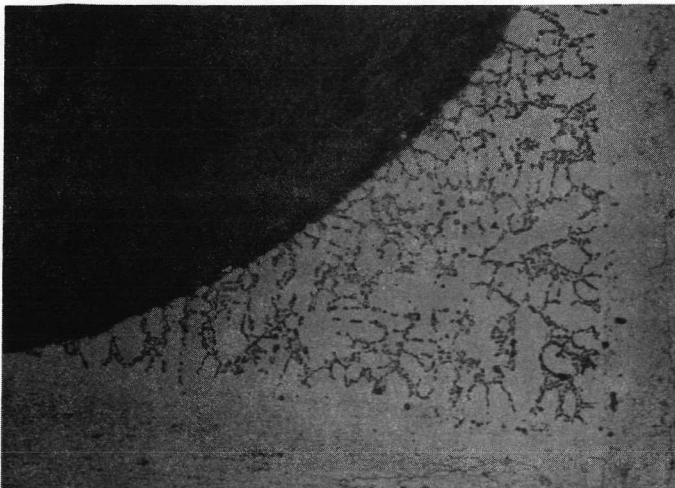


Log. No. 6209C

Etchant: 10% Oxalic – Electrolytic

Magnification: 200X

Figure 132. NASA 18 Alloy Brazement - Diffusion Annealed

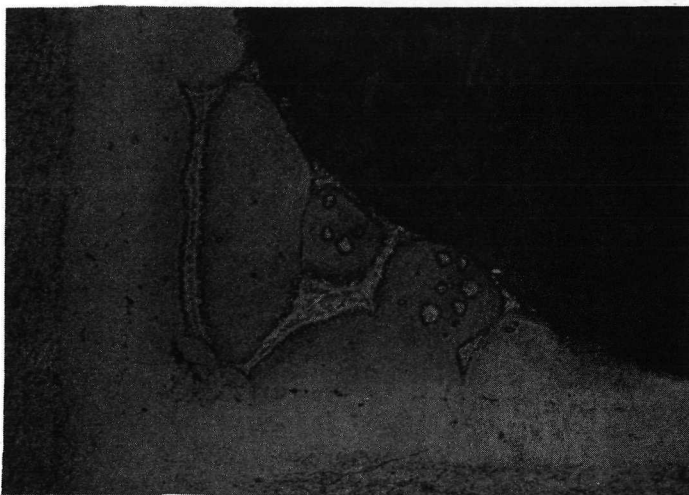


Log. No. 6210C

Etchant: 10% Oxalic – Electrolytic

Magnification: 200X

Figure 133. NASA 19 Alloy Brazement - Diffusion Annealed

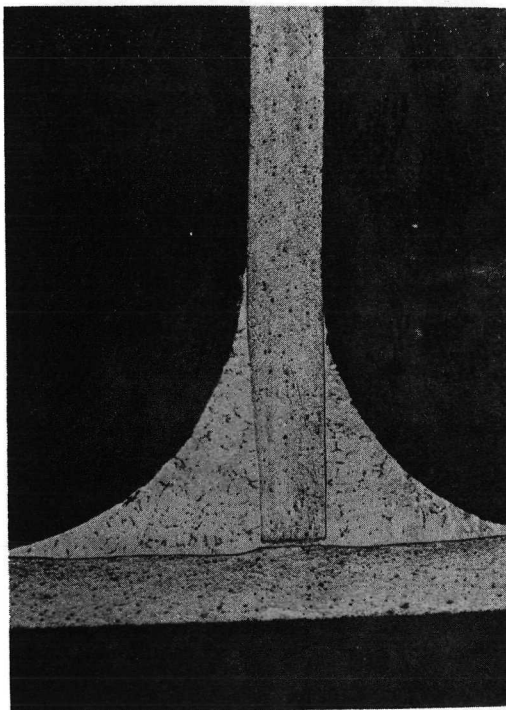


Log. No. 6211C

Etchant: 10% Oxalic – Electrolytic

Magnification: 200X

Figure 134. NASA 20 Alloy Brazement - Diffusion Annealed

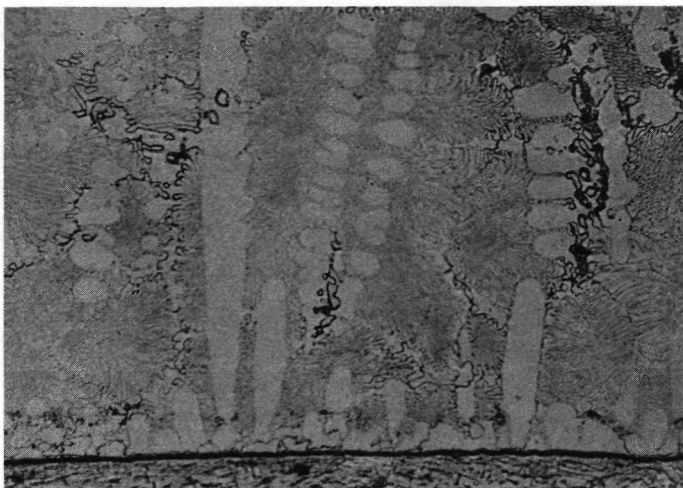


Log. No. 4945B

Etchant: Kallings

Magnification: 40X

Figure 135. TD-6 Alloy T-Joint Brazement



Log No. 4945C

Etchant: Kallings

Magnification: 40X

Figure 136. Microstructure of TD-6 Brazement

Table 40. Braze Alloy Remelt Temperature Tests – Tensile Loaded T-Joints.

Alloy	Form	Braze Temp. (2)		Separation Temperature at 0.69 MN/m ² (1) (100 psi) Tensile Load			
				No Gap		0.005 cm (0.002-in.) Gap	
		C	(F)	C	(F)	C	(F)
NASA 18	2.0 mm (10 U.S.S. mesh) chunk	1304	(2380)	1299 1304 1310	(2370) (2380) (2390)		
NASA 19	2.0 mm (10 U.S.S. mesh) chunk	1343	(2450)	1354 1396	(2470) (2545)		
NASA 19M	2.0 mm (10 U.S.S. mesh) chunk	1343	(2450)	1327 1349	(2420) (2460)	1332 1332	(2430) (2430)
NASA 19M	0.3 mm (48 U.S.S. mesh) powder	1288	(2350)	1277 1310	(2330) (2390)		
TD-6	0.149 mm (100 U.S.S. mesh) powder	1304	(2380)	1349 1377	(>2460) ⁽³⁾ (2510)	1293 1310	(2360) (2390)
Weight Percent →	Ni	Cr	Mo	Al	Si	W	Fe
NASA 18	57	16	15	8	4	-	-
NASA 19	47	16	25	8	4	-	-
NASA 19M	Same as NASA 19 but prepared with pre-melted Ni-45 w/o Mo master						
TD-6	53	16	17		4	5	5
(1) Heated at 38C (100F)/minute from 1090C (2000F) upward. (2) All temperatures monitored by Type R thermocouple (Pt/Pt-13% Rh). (3) No separation. Diffusion annealed at 1204C (2200F) for 15 hours in argon prior to test.							

Although NASA 19 showed good remelt temperature (Table 40) with the 2.0 mm (10 U. S. S. mesh) chunk, the low values for the finer material suggested segregation was occurring with this high molybdenum alloy. Heterogeneity precluded continuation of NASA 19 alloy into the brazement evaluation portion of the program. The preliminary data suggest, however, that the alloy made by a different process, e. g., inert gas atomization, might exhibit superior properties. This is recommended for further consideration.

Brazement Properties Evaluation. - Two experimental braze alloys, NASA 18 and B-2, and the baseline braze alloy TD-6 were approved by NASA for further evaluation. Table 41 is the schedule established for testing these alloy brazements.

Table 41. Schedule of Testing - Brazement Evaluation

	0.25 mm (0.010 in.) Sheet T-Joints Metallography A.B. (1) D.A. (2)		0.25/1.0 mm (0.010/0.040 in.) Sheet T-Joints Approximately 20 mg of Braze Alloy			
			Remelt	Tensile		Stress Rupture
			Argon 0.69 MN/m ² (100 psi) No Gap D.A.	Air 1093C (2000F) No Gap D.A.	Air Ambient No Gap D.A.	Air 1093C (2000F) No Gap D.A.
NASA 18	1	1	2	2	2	5
TD-6	1	1	2	2	2	5
NASA B-2	1	1	2	2	2	5
(1) A.B. = As Brazed (2) D. A. = Diffusion Annealed at 1204C (2200F) for 15 hours in Argon						

The B-2 alloy is a promising composition resulting from a TD-NiCr brazing research program at NASA-Lewis Research Center. The nominal composition of B-2 alloy and analysis for AMI Lot 1964 powder are as follows:

	Weight Percent						
	Ni	Cr	Mo	Al	Si	B	C
Nominal	49.5	16	30	4	0.5	-	-
AMI Analysis	Bal	19.83	30.11	4.20	0.59	0.0009	0.018

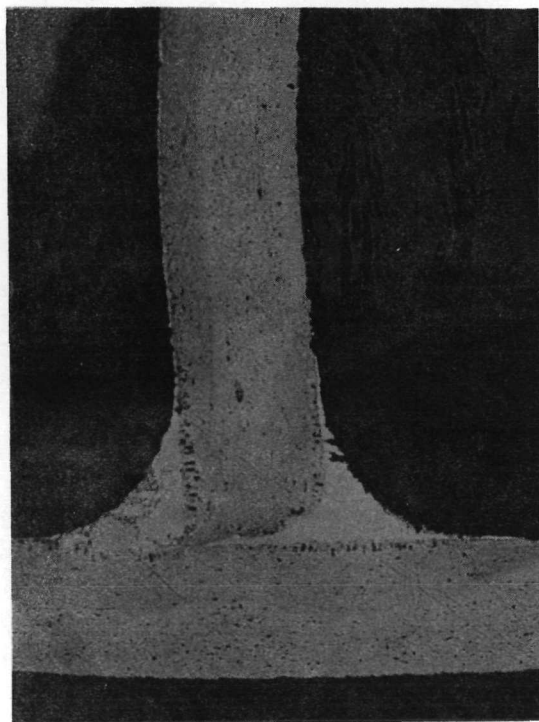
Duplicate T joint brazements were prepared with the B-2 and TD-6 alloys. One of each was metallographically examined as-brazed. The second was diffusion annealed for 15 hours at 1204C (2200F), in argon, before examination. Microstructure of NASA B-2 is shown in Figure 137. Voids have formed in the TD-NiCr substrate after annealing. Figures 138 and 139 show the TD-6 alloy as-brazed and after diffusion annealing. Extensive erosion is noted in both and is especially evident in the as-brazed specimen. Microstructure of the NASA 18 alloy, diffusion annealed for only one rather than 15 hours, is shown in Figure 132.

Table 42. Braze Alloy Remelt Temperature Tests of Tensile Load T-Joints

	Braze Temperature C (F)	Remelt Temperature C (F)
NASA 18	1304 (2380)	1346 & 1366 (2455 & 2490)
B-2	1291 (2355)	1346 & 1346 (2455 & 2455)
TD-6	1304 (2380)	1338 & 1380 (2440 & 2515)
* Temperature of separation at 0.69 MN/m ² (100 psi) tensile load. Diffusion annealed at 1204C (2200F) for 15 hours in argon prior to test.		

Duplicate remelt temperature tests were conducted in the same manner as previously described, except the brazements were diffusion annealed in argon at 1204C (2200F) for 15 hours. Results are presented in Table 42.

Some variation in remelt temperature was evident in comparing these data with previous results given in Table 39. This variation may be attributed to differences in gap dimensions. The manner



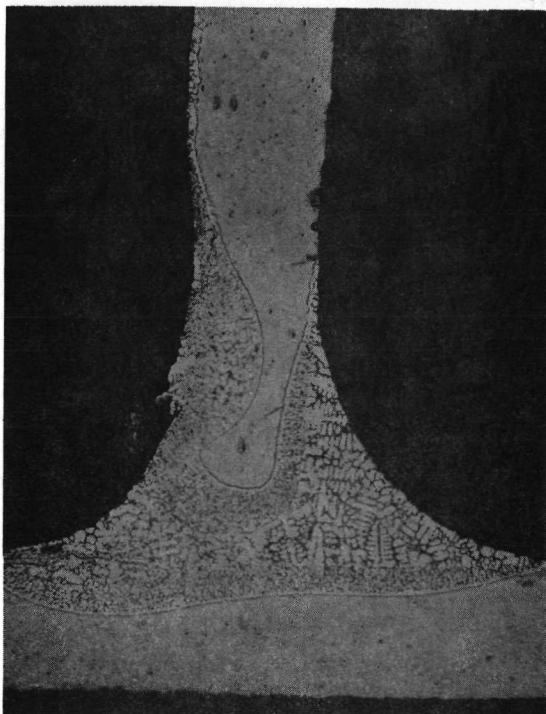
Log. No. 6546

Etchant: 10% Oxalic - Electrolytic

Magnification: 75X

Note: Diffusion induced voids in TD-NiCr substrate

Figure 137. Microstructure of B-2 Alloy Brazement - Diffusion Annealed



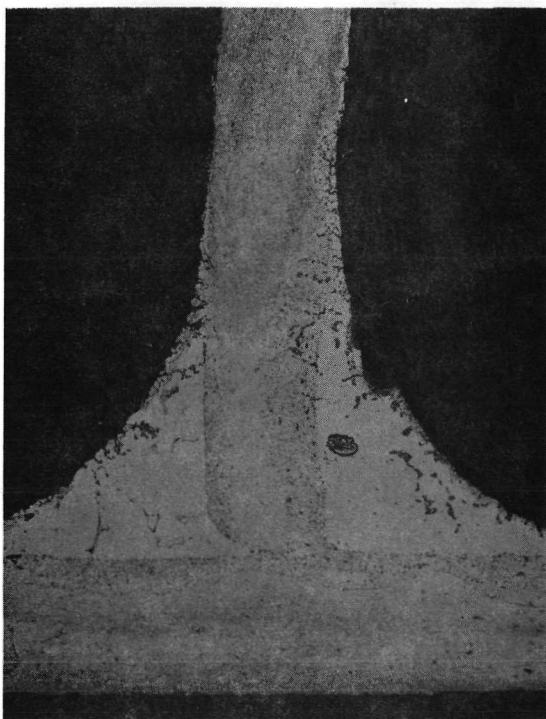
Log. No. 6547

Etchant: 10% Oxalic

Magnification: 75X

Note: Erosion of substrate TD-NiCr

Figure 138. TD-6 Alloy Brazement - As-Brazed



Log. No. 6445

Etchant: Oxalic

Magnification: 75X

Figure 139. TD-6 Alloy Brazement - Diffusion Annealed

of fixturing the specimens for brazing, with refractory alloy (low expansion) straps to hold the thinner to thicker sheets in a butt joint configuration, was less than entirely reliable and probably resulted in larger than anticipated gaps in some instances. Larger gaps result in lower remelt temperature. The NASA 18 brazement remelt temperatures were 52C (93F) higher, on the average, than those recorded for the first series of tests.

Tensile test specimens of the three alloys (NASA 18, B-2 and TD-6) were prepared in an identical manner to the remelt specimens, and were also diffusion annealed at 1204C (2200F) for 15 hours in argon, prior to testing. An attempt was made to load each specimen with an equivalent amount (20 mg) of braze alloy powder. Those that suffered the most obvious loss of part of the alloy during volatilization of the polybutene binder were discarded. Results are given in Table 43.

Table 43. Tensile Strength of Brazements⁽¹⁾

Braze Alloy	Spec. No.	Test Temperature C (F)	Tensile Stress in 0.25 mm (0.010 in.) Sheet at Failure MN/m ² (ksi)	Location of Failure
NASA 18	1	21 (70)	667.4 (96.8)	Braze affected zone
NASA 18	2	↓	541.9 (78.6)	Tack weld in parent metal
NASA B-2	1	↓	667.4 (96.8)	Tack weld in parent metal
NASA B-2	2	↓	483.3 (70.1)	Braze affected zone
TD-6	1	↓	664.7 (96.4)	Tack weld in parent metal
TD-6	2	↓	650.2 (94.3)	Braze affected zone
NASA 18	3	1093 (2000)	122.7 (17.8)	Parent metal
NASA 18	4	↓	109.6 (15.9)	Parent metal
NASA B-2	3	↓	113.8 (16.5)	Braze joint
NASA B-2	4	↓	118.6 (17.2)	Braze affected zone
TD-6	3	↓	113.8 (16.5)	Parent metal
TD-6	4	↓	120.7 (17.5)	Braze affected zone
(1) Joining 0.25 mm (0.010 in.) TD-NiCr sheet, unrecrystallized, Heat No. 3689, Diffusion annealed 1204°C (2200°F) for 15 hours in argon.				

Interpretation of the data is complicated by failure of several specimens in the parent metal due to tack-welding attachments of fixturing straps and thermocouples. All three alloy brazements sustained similar stresses 664.7-667.4 MN/m² (96.4-96.8 ksi) in at least one of the tests at ambient temperature. The low stress failure in the parent metal of NASA 18 brazement, Specimen No. 2, can be discounted as premature. However, B-2, Specimen No. 2 appears to have suffered a valid (braze affected zone) failure at 483.3 MN/m² (70.1 ksi).

Oxidation of the elevated temperature specimens in test precluded determination of whether parent metal failures in alloys NASA 18 and TD-6 brazements had occurred at tackwelds, as was the case with the ambient temperature tests. Maximum stresses sustained by brazements of the three alloys at 1093C (2000F) were similar. Both specimens of NASA 18 failed in the parent metal, and the possibility remains that higher strength could have been attained with this alloy if tack welds had not been used near the joint in the 0.25 mm (0.010 in.) leg.

Parent metal strength of TD-NiCr, tested in tension at ambient temperature and 1093C (2000F), as determined by Metcut Research Associates (Ref. 4) are presented in Table 44.

Table 44. Parent-Material Tensile Properties of 0.25 mm (0.010 in.) TD-NiCr Sheet*

Test Temperature C (F)	Ultimate Tensile Strength	
	Longitudinal MN/m ² (ksi)	Transverse MN/m ² (ksi)
Room	846.7 (122.8)	766.0 (111.1)
982 (1800)	122.0 (17.7)	113.8 (16.5)
1093 (2000)	95.2 (13.8)	94.5 (13.7)
1204 (2200)	78.6 (11.4)	66.2 (9.6)
1316 (2400)	68.3 (9.9)	46.9 (6.8)

* Tests conducted by Metcut Research Associates on Heats 3637 and 3697 commercial (recrystallized) material

conducted using the same procedures described for solid-state seam welding (Appendix E). Results are shown in Table 45.

Strength of the diffusion annealed brazements at room temperature is below that of the parent metal; at 1093C (2000F) brazement strength exceeds parent metal properties data. However, it should be noted that these tests were performed on different heats of 0.25 mm (0.010 in.) TD-NiCr sheet and the effects of diffusion annealing on parent metal properties has not been evaluated.

Configuration and preparation of stress-rupture test specimens was identical to the remelt and tensile test specimens. All were diffusion annealed at 1204C (2200F) for 15 hours in argon prior to tests. Testing was

The stress-rupture data are plotted against parent metal data in Figures 140 through 142. The baseline data are for the same heat of material and are represented by a single line taken from Figure 79. The butt-joint configuration of the brazements precludes comparison of these data to lap joint strength data available from other programs. It is apparent that results for brazements of alloys B-2 and NASA 18 are

Table 45. Stress-Rupture Properties of Brazements at 1093C (2000F)⁽¹⁾

Braze Alloy	Specimen Number	Applied Stress in 0.25 mm (0.010 in.) Foil MN/m ² (ksi)	Failure Time (Hours)	Location of Failures (3)
NASA 18	1	34.5 (5.0)	53.2	BJ
	2	69.0 (10.0)	0.7	BAZ
	3	48.3 (7.0)	1.9	BJ
	4	34.5 (5.0+) ⁽²⁾	187.1	
		48.3 (7.0+)	49.5	
		62.1 (9.0)	5.1	BJ & BAZ
	5	41.4 (6.0)	0.2	BJ
NASA B-2	1	34.5 (5.0+)	142.7	
		48.3 (7.0+)	46.4	
		62.1 (9.0)	0.003	BAZ
	2	55.2 (8.0)	0.3	BJ & BAZ
	3	55.2 (8.0)	0.1	BJ & BAZ
	4	48.3 (7.0)	2.3	BJ
	5	41.4 (6.0)	0.25	BJ
TD-6	1	69.0 (10.0)	0.4	BJ
	2	48.3 (7.0)	0.0	BJ & BAZ
	3	48.3 (7.0)	1.8	BJ
	4	34.5 (5.0)	0.05	BJ
	5	34.5 (5.0)	0.1	BJ
	6	34.5 (5.0)	0.05	BJ & BAZ
	7	34.5 (5.0)	0.2	BJ

(1) Joining 0.25 mm (0.010 in) TD-NiCr sheet unrecrystallized, Heat No. 3689, diffusion annealed 1204 C (2200 F) for 15 hours in argon.

(2) + Indicates that the specimen did not fail but was continued in test at a higher stress.

(3) BJ = Braze joint

BAZ = Braze affected zone

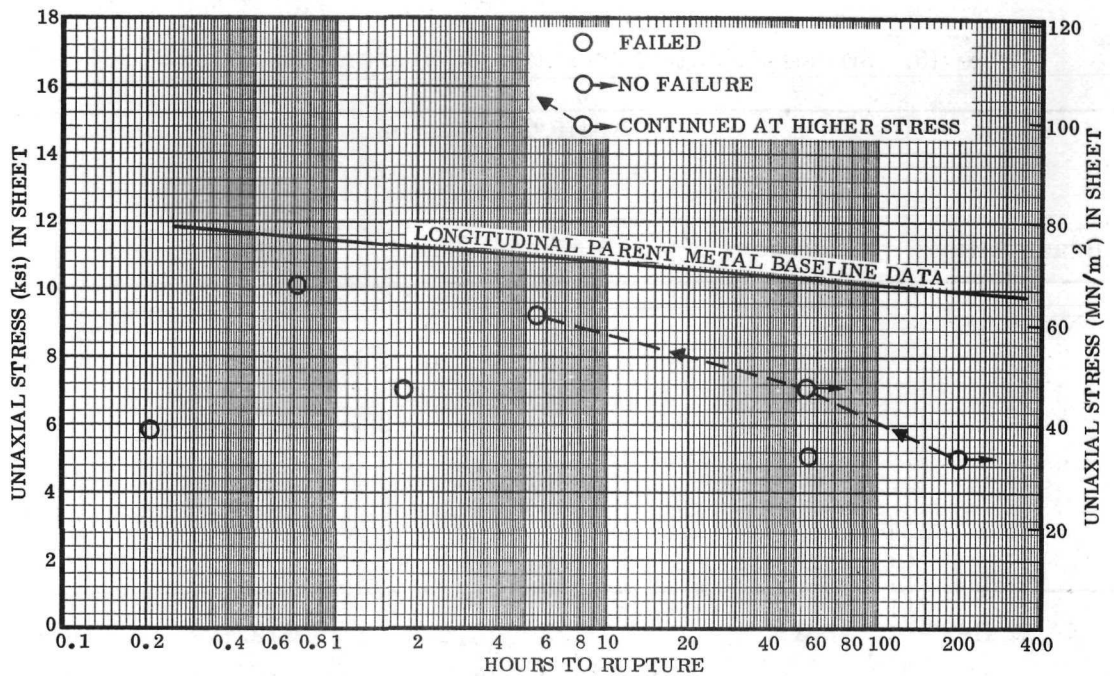


Figure 140. 1093C (2000F) Stress-Rupture Properties of NASA 18 Alloy Brazements; (Joining Longitudinal 0.25 mm (0.010 in.) TD-NiCr Sheet, Heat 3689 , Diffusion Annealed, 1204C (2200F) for 15 Hours)

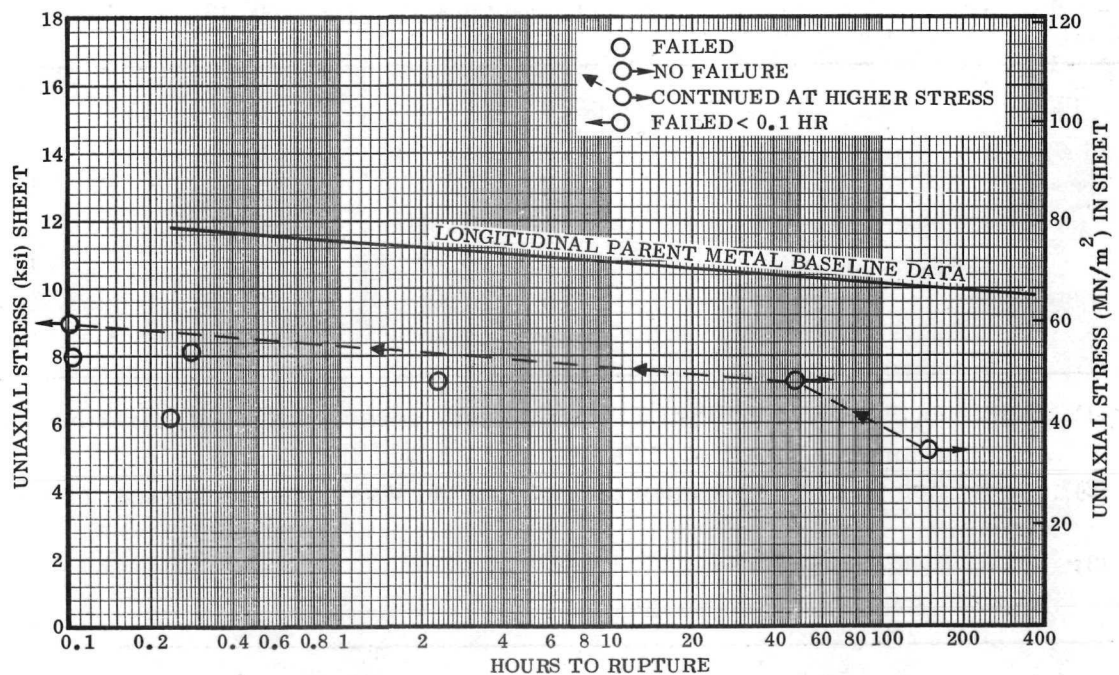


Figure 141. 1093C (2000F) Stress-Rupture Properties of NASA B-2 Alloy Brazements; (Joining Longitudinal 0.25 mm (0.010 in.) TD-NiCr Sheet, Heat 3689 , Diffusion Annealed, 1204C (2200F) for 15 Hours)

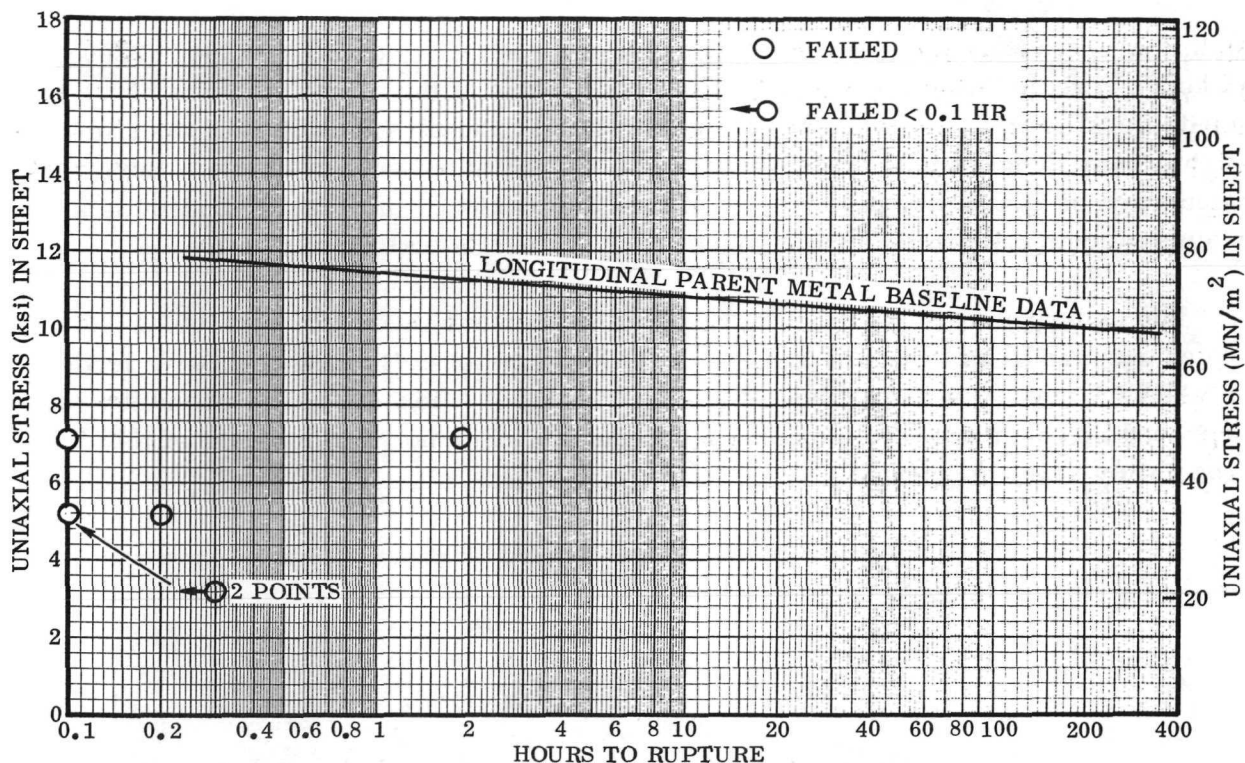


Figure 142. 1093C (2000F) Stress-Rupture Properties of TD-6 Alloy Brazements; (Joining Longitudinal 0.25 mm (0.010 in.) TD-NiCr Sheet, Heat 3689), Diffusion Annealed, 1204C (2200F) for 15 Hours

similar; those for TD-6 brazements are erratic and much lower. The explanation may be the extensive erosion noted for alloy TD-6 in Figures 138 and 139.

It is evident that NASA 18 alloy shows promise for brazing TD-NiCr sheet. NASA 18 brazed satisfactorily at 1288-1304C (2350-2380F) and exhibited remelt temperature in excess of 1343C (2450F) with no gap clearance at the joint. The evidence suggests that remelt temperature of the brazements may be less with greater joint clearance, but this point was not confirmed and should be investigated further.

Strengths of NASA 18 brazements equalled or exceeded those of the reference TD-6 alloy brazements at ambient temperature and 1093C (2000F) in tensile and stress-rupture tests. Data were insufficient to calculate joint efficiency on the basis of parent metal strength. Although test data scatter is severe, it is possible to recognize that the rupture strength for NASA 18 is greater — perhaps 50 percent — than that of TD-6 at 1093C (2000F).

B-2 Alloy, developed in research at NASA, was included only in the final brazement evaluation portion of this program. Brazing temperature of B-2 was slightly less than that of NASA 18, and the remelt temperature slightly lower or equal.

Metallographic examination of the B-2 brazements after annealing at 1204C (2200F) for 15 hours revealed what appear to be Kirkendall voids at the interface of the braze and substrate TD-NiCr parent metal. Tensile strength and stress-rupture properties were slightly less than those of NASA 18, at least in the limited data available. Here again, calculation of joint efficiency is precluded by insufficiency of data. B-2 alloy is a promising composition for brazing TD-NiCr and merits further evaluation.

The comparative superiority of NASA 18 brazements over TD-6 in 1093C (2000F) stress-rupture tests is felt to be the result of two factors: (1) lack of erosive tendencies of NASA 18, and (2) the 8 percent aluminum content of NASA 18, which promotes both improved strength and better oxidation resistance. Further development of NASA 18 braze alloy is recommended.

7. CONCLUSIONS

Forming and joining techniques and joint properties data have been developed for thin-gage TD-NiCr sheet in the recrystallized and unrecrystallized conditions. This technology can be used for design and fabrication of improved hot structures for applications such as thermal protection systems for space shuttle vehicles. The specific conclusions are as follows:

Forming of Recrystallized Sheet

Theoretical and actual forming limits have been established for four gages of recrystallized TD-NiCr sheet using five basic forming processes. Tensile elongation transverse to the rolling direction is not a valid criterion for predicting the formability of TD-NiCr sheet. Satisfactory formability in the longitudinal direction was demonstrated for brake forming, corrugation forming, joggling, and beading. Formability for the transverse orientation is poor. Forming in this direction should be avoided or the degree of strain minimized. The poor transverse formability is attributed to thermal-mechanical processing that is designed for optimum strength at high temperature. Formability is further degraded by poor surface finish. Improvement in surface finishing procedures would improve formability. Forming to the established forming limits results in no apparent detrimental effects on microstructure, but causes some reduction in tensile ductility of formed parts. A stress relief annealing temperature of 982 to 1093 C (1800 to 2000 F) is satisfactory for formed parts, but the loss of tensile ductility cannot be fully recovered by annealing.

Dimpling involves severe deformation in both the longitudinal and transverse direction and for this reason was unsuccessful for recrystallized sheet using standard dimpling tools and techniques. Modified dimpling dies gave greatly improved results and show the way for development of useful dimpling procedures.

Forming of Unrecrystallized Sheet

An optimum forming temperature of 760 C (1400 F) was established for unrecrystallized TD-NiCr sheet based on tensile ductility and theoretical forming data. Theoretical and actual forming limits at the optimum forming temperature were developed for two gages of unrecrystallized sheet with three forming processes. Transverse tensile elongation is not a valid

criterion for predicting the formability of unrecrystallized sheet. Material in the unrecrystallized condition can be satisfactorily hot formed by the brake and corrugation forming processes. Subsequent recrystallization annealing of hot formed parts results in no significant degradation in microstructure or room-temperature tensile properties. Regions of severe plastic deformation have somewhat smaller grain size after recrystallization annealing. It is believed that forming within the established limits will not cause a significant reduction in elevated temperature strength. Formability is better for the longitudinal than for the transverse direction. Forming with strain transverse to the rolling direction should be avoided or the degree of strain minimized.

Hot dimpling of unrecrystallized sheet was not successful using the currently available dimpling techniques because of heating limitations and poor transverse formability. The most promising results were obtained with the Convair Aerospace-developed resistance heating dimpling process, but further development is required to control temperature uniformity. Radial and circumferential cracking could not be avoided without localized overheating and degradation of microstructure by fine-grain recrystallization.

The greater complexity of tooling and procedures for hot forming of unrecrystallized sheet are major disadvantages to fabrication of TD-NiCr hardware by this process.

Resistance Seam Welding (Solid-State)

A resistance seam welding process was successfully applied to solid-state welding of recrystallized and unrecrystallized 0.25 mm (0.010 in.) sheet. Welding parameters and surface preparation techniques were developed that eliminated or minimized fine-grain recrystallization in the welded joints. The optimum surface preparation method was electropolishing, which served the dual purpose of reducing surface roughness and removing residual deformed metal introduced by sheet finishing operations.

The load-bearing capability of joints with 5t overlap was adequate to force failure into the parent metal for tensile-shear tests at room temperature, 1093 and 1316 C (2000 and 2400 F). Failure also occurred in parent material during stress-rupture tests at 982, 1093, and 1204 C (1800, 2000, and 2200 F) for time up to 100 hours. The 5t overlap and resultant test failures in the parent metal prevented comparison of joint efficiency between material in the recrystallized and unrecrystallized conditions.

Resistance Spot Welding (Solid-State)

The Convair Aerospace-developed High Power Level (HPL) resistance welding process was applied to solid-state spot welding of recrystallized and unrecrystallized 0.25 mm (0.010 in.) sheet. The most successful surface preparation method was abrasive polishing, based on microstructure and room temperature tensile-shear tests. Further development effort is required to fully evaluate the effects of electropolish surface preparation on spot weld properties. A 15.2 by 22.9 cm (6 by 9 in.) corrugation-stiffened panel of unrecrystallized sheet was fabricated by hot forming and solid-state spot welding to demonstrate the feasibility of this processing technique.

Resistance Spot Welding (Fusion)

Weld parameters and surface preparation methods were evaluated for conventional resistance spot welding of 0.08 mm (0.003 in.) and 0.25 mm (0.010 in.) recrystallized sheet. Abrasive polishing was a better surface preparation method than solvent or chemical cleaning for 0.25 mm (0.010 in.) sheet, based on microstructure and tensile-shear tests. There was no difference in weld properties for solvent cleaning and abrasive cleaning methods for cold rolled 0.08 mm (0.003 in.) sheet.

Brazing

The experimental brazing alloy NASA 18 (Ni-16Cr-15Mo-8Al-4Si) has several areas of superiority compared to commercially available alloys for brazing thin-gage TD-NiCr sheet. NASA 18 brazements of thin-gage TD-NiCr sheet have higher strength, reduced reaction with substrate, and lower brazing temperature than the baseline TD-6 braze alloy. The brazing temperature for NASA 18 is 1288 C (2350 F), and the remelt temperature of brazed joints is in excess of 1343 C (2450 F). Braze joints of NASA 18 show no evidence of thoria depletion, diffusion porosity, or excessive erosion, which have been experienced with TD-6 alloy. The stress-rupture properties at 1093 C (2000 F) are probably 50 percent higher than TD-6 brazements. NASA 18 braze alloy has the potential for correcting several of the deficiencies of TD-6 alloy and further evaluation is recommended.

APPENDIX A

COMPUTER PROGRAM FOR CALCULATION OF THEORETICAL FORMABILITY EQUATIONS

(Written in FORTRAN IV Language for CDC 6400 Computer)

```

PROGRAM MAIN(INPUT,OUTPUT,TAPE5=INPUT, TAPE6=OUTPUT)

DIMENSION ALPH(5),F(5),ARAD(5),ROT(5),F1(5),F2(5),F3(5),F4(5)
NAMelist/DATA/ NALPH,ALPH,EL,EW,IOPT,E,EC,SCY,NROT,ROT,STY,SU
RDEG=57.295779513082
2 READ(5,DATA)
GO TO (100,200,300,400,500) IOPT
C PRESS BRAKE FORMING
100 CONTINUE
PRINT 101
101 FORMAT(* OUTPUT FOR PRESS BRAKE FORMING DATA *)
ELR= ALOG( 1.0 +EL)
EWR= ALOG(1.0+EW)
ECORR= ELR-EWR**2/ELR
ETEM= EXP(2.0*ECORR) -1.0
RTMAX=1.0/ETEM
PHI= (11.4-RTMAX)/ .0845
DO 120 I=1,NALPH
DEG=15.21*ALPH(I)/(11.4-1.0/ETEM)-90.0
F(I)=0.5*RTMAX *(1.0+SIN(DEG/RDEG))
120 CONTINUE
PRINT 123,ECORR,RTMAX,PHI,(F(I),I=1,NALPH)
123 FORMAT(* E .25(CORR)= * E13.3 / * R/T MAX= * E13.3/
1* PHI = * E13.3/
2* R/T = *5E13.3 )
GO TO 2
C JOGGLE FORMING
200 CONTINUE
PRINT 201
201 FORMAT(* OUTPUT FOR JOGGLE FORMING DATA * )
DL1=SQRT(E*(1.44*E+2.4))
DT=(.0118*EC/SCY)**0.4
DL2=0.43*DT**0.5
DL3=EC/SCY*1.0E-3
PRINT 205,DL1,DT,DL2,DL3
205 FORMAT(* D/L 1 = * E13.3 / * D/T= * E13.3 /
1* D/L 2 = * E13.3/ * D/L 3 = * E13.3 )
GO TO 2

```

1

2

4

APPENDIX A (cont'd)

```

C      DIMPLe FORMING
300  CONTINUE
      PRINT 301
301  FORMAT(* OUTPUT FOR DIMPLe FORMING DATA *)
      DO 310 I=1,NALPH
        F(I)= 0.444*E**0.253/(1.0-COS(ALPH(I)/RDEG))
310  CONTINUE
      PRINT 315,F,(F(I),I=1,NALPH)
315  FORMAT(* E 2.0= * E13.3 /           * H/R = * 5E13.3 )
      GO TO 2

C      RUBBER PRESS READ FORMING
400  CONTINUE
      PRINT 401
401  FORMAT(* OUTPUT FOR RUBBER PRESS READ FORMING DATA *)
      DO 450 I=1,NROT
        F1(I)=.065*(1.E4/STY/.065)**.216 *ROT(I)**.29
        F2(I)=6.0E-21*(F*SU)**9.3*(ROT(I)**(-12.4))
        F3(I)=.065*ROT(I)**.37
        F4(I)=6.84E-4*ROT(I)**1.5
450  CONTINUE
      PRINT 452,(F1(I),I=1,NROT)
452  FORMAT(* R/L 1= */(5E13.3))
      PRINT 453,(F2(I),I=1,NROT)
453  FORMAT(* R/L 2= */(5E13.3))
      PRINT 454,(F3(I),I=1,NROT)
454  FORMAT(* R/L 3= */(5E13.3))
      PRINT 455,(F4(I),I=1,NROT)
455  FORMAT(* R/L 4= */(5E13.3))
      GO TO 2

C      DROP HAMMER
500  CONTINUE
      PRINT 501
501  FORMAT(* OUTPUT FOR DROP HAMMER READ FORMING DATA *)
      ELB= ALOG(1.0+EL)
      EWB= ALOG(1.0+EW)
      ECORR=ELB-EWB**2/ELB
      ECORR= EXP(ECORR) -1.0
      DO 510 I=1,NROT
        F1(I)=ECORR**2 *60.6/ROT(I)
        F2(I)=60.6*F1(I)
510  CONTINUE
      PRINT 530,(F1(I),I=1,NROT)
530  FORMAT(* R/L 1=* */(5E13.3))
      PRINT 540,(F2(I),I=1,NROT)
540  FORMAT(* R/T 2=* */(5E13.3))
      GO TO 2
      END

```

APPENDIX B

TENSILE PROPERTIES OF RECRYSTALLIZED TD-NiCr SHEET

Table B-1. Tensile Properties of 0.25 cm (0.010 in.) Recrystallized TD-NiCr Sheet

Heat No.	Grain Direction	Specimen No.	Ultimate Tensile Strength MN/m ² (ksi)	Tensile Yield Strength MN/m ² (ksi)	Elongation or Strain, Percent							Indicated Modulus GN/m ² (10 ⁶ psi)
					ε _{2.0}	ε _{1.0}	(ε _L)0.5	(ε _W) 0.5	(ε _L) 0.25	(ε _W) 0.25	ε _{0.02}	
3537	L	F1L-1	866 (128.5)	648 (93.9)	9.5	10.0	12.5	-5	15	-4	-	164 (23.8)
		-2	870 (126.2)	632 (91.6)	9.5	10.0	11.5	-4	14	-4	-	168 (24.4)
		-3	900 (130.6)	662 (96.0)	9.5	11.0	14	-4	16.5	-4	-	172 (24.9)
		Average	866 (128.5)	647 (93.8)	9.5	10.5	12.5	-4.5	15	-4	-	168 (24.4)
	T	F1T-1	834 (121.0)	607 (88.1)	16.5	19	24.5	-16	29	-15	-	177 (25.7)
		-2	841 (121.9)	596 (86.5)	16.5	20	23	-15	29	-12.5	-	178 (25.8)
		-3	802 (116.3)	577 (83.7)	13	14	16	-10	23.5	-9	-	175 (25.4)
		Average	825 (119.7)	594 (86.1)	15.5	17.5	21	-13.5	27	-12	-	177 (25.6)
3700	L	H1L-4	857 (124.3)	637 (92.4)	9	10	12	-3	15	-2.5	20.5	141 (20.5)
		-5	845 (122.5)	641 (92.9)	9	10	11.5	-3	14.5	-2.5	16.5	138 (20.0)
		-6	838 (121.6)	642 (93.1)	8.5	9.5	10.5	-2.5	12.5	-2.5	21	146 (21.2)
		Average	847 (122.8)	640 (92.8)	9	10	11.5	-3	14	-2.5	19.5	141 (20.5)
	T	H1T-1	736 (106.8)	558 (80.9)	21	22	26	-17	28	-17	30.5	171 (24.7)
		-2	719 (104.3)	551 (79.9)	17.5	20	24.5	-15.5	27	-16	35	172 (24.9)
		-3	730 (105.9)	556 (80.7)	19	22	26.5	-15	31.5	-15.5	34	168 (24.4)
		Average	729 (105.7)	555 (80.5)	19	21	25.5	-16	29	-16	33	170 (24.6)

Elongation and (ϵ_L) strain measurements made across fracture except (ϵ_L) 0.02, which were made adjacent to fracture

$\epsilon_{2.0}$ = Elongation (strain) for 5.08 cm (2.0 in.) gage length

$\epsilon_{1.0}$ = Elongation (strain) for 2.54 cm (1.0 in.) gage length

APPENDIX B, Continued

TENSILE PROPERTIES OF RECRYSTALLIZED TD-NiCr SHEET

Table B-2. Tensile Properties of 0.5 mm (0.020 in.) Recrystallized TD-NiCr Sheet

Heat No.	Grain Direction	Specimen No.	Ultimate Tensile Strength MN/m ² (ksi)	Tensile Yield Strength MN/m ² (ksi)	Elongation or Strain, Percent						Indicated Modulus GN/m ² (10 ⁶ psi)
					ϵ_1 0	ϵ_1 0.5	ϵ_1 0.5	ϵ_1 0.25	ϵ_1 0.25	ϵ_1 0.02	
3629	L	A4L-1	883	(128.0)	16	18	*	*	*	-	145 (21.1)
		-2	889	(129.0)	16.5	18	-13.5	24.5	-5.5	-	144 (20.9)
		-3	892	(130.5)	17.5	18	-6.5	27	-5.5	-	142 (20.6)
		Average	891	(129.2)	16.5	18	-10	26	-5.5	-	144 (20.9)
	T	A4T-1	838	(121.6)	18	22	-17.5	31.5	-16.5	-	169 (24.5)
		-2	837	(121.4)	17	21	-13.5	28	-13	-	164 (23.8)
		-3	845	(122.6)	19	23	-18.5	36	-19	-	165 (24.0)
		Average	843	(123.8)	18.5	21	-14	30	-13.5	-	182 (26.4)
3640	L	B2L-1	867	(125.8)	16.5	20	-7.5	28	-5	21.5	142 (20.6)
		-2	884	(128.1)	15	16.5	-6	18	-4.5	24	139 (20.2)
		-3	893	(128.1)	15.5	17.5	-8	25	-6	26.5	146 (21.2)
		Average	889	(129.0)	16	18	-7.5	24	-7	24	168 (24.4)
	T	B2T-1	834	(120.9)	18	21	-14.5	29	-14	28	167 (24.3)
		-2	849	(123.2)	19	20	-13.5	25.5	-11.5	23.5	163 (23.7)
		-3	827	(120.0)	20.5	23	-14	29	-14.5	24	163 (23.7)
		Average	837	(121.4)	19	21	-14	28	-13.5	25	165 (23.9)

Elongation and (ϵ_1) strain measurements made across fracture except ϵ_1 0.02, which were made adjacent to fracture

* Fractured outside 2-inch gage length; elongation values not valid

APPENDIX B, Continued

TENSILE PROPERTIES OF RECRYSTALLIZED

TD-NiCr SHEET

Table B-3. Tensile Properties of 1.0 mm (0.040 in.) Recrystallized TD-NiCr Sheet

Heat No.	Grain Direction	Specimen No.	Ultimate Tensile Strength MN/m ² (ksi)	Tensile Yield Strength MN/m ² (ksi)	Elongation or Strain, Percent							Indicated Modulus GN/m ² (10 ⁶ psi)
					ε _{2.0}	ε _{1.0}	(ε _L) 0.5	(ε _W) 0.5	(ε _L) 0.25	(ε _W) 0.25	ε _{0.02}	
3708	L	D2L-1	873 (126.6)	571 (82.8)	16.5	20	25.5	-8	31.5	-9.5	-	143 (20.7)
		-2	875 (126.8)	568 (82.4)	19	20	28	-10.5	35	-10	-	148 (21.4)
		-3	872 (126.5)	571 (82.8)	16	19	25	-10	31.5	-9	-	143 (20.7)
		Average	873 (126.6)	570 (82.7)	17	20	26	-9.5	32.5	-9.5	-	144 (20.9)
	T	D2T-1	812 (117.7)	544 (78.9)	21.5	26	34	-19	36.5	-17.5	-	167 (24.3)
		-2	820 (118.9)	545 (79.1)	21.5	26	34	-22	42.5	-21	-	166 (24.2)
		-3	821 (119.1)	550 (79.8)	20.5	24	30.5	-19	40.5	-18	-	170 (24.7)
		Average	818 (118.6)	547 (79.3)	21	25.5	33	-20	40	-19	-	168 (24.4)
3715	L	E2L-1	683 (125.1)	605 (87.7)	17.5	20	26	-10	35.5	-9	48	140 (20.4)
		-2	870 (126.2)	611 (88.6)	16.5	19	27.5	-11	37	-10	48.5	136 (20.1)
		-3	872 (126.4)	714 (88.2)	16.5	19	25	-10.5	33.5	-10	50	145 (21.0)
		Average	868 (125.9)	714 (88.2)	17	19.5	26	-10.5	35.5	-9.5	49	141 (20.5)
	T	E2T-1	797 (115.6)	542 (78.6)	21	26	33.5	-20	43.5	-18	46.5	164 (23.8)
		-2	804 (116.6)	538 (78.1)	22	27	34.5	-21.5	45	-21.5	50	163 (23.7)
		-3	803 (116.5)	531 (77.0)	21.5	26.5	33	-20.5	41	-19.5	47.5	166 (24.1)
		Average	801 (116.2)	537 (77.9)	21.5	26.5	33.5	-20.5	43	-19.5	48	164 (23.8)

Elongation and (ϵ_L) strain measurements made across fracture except $\epsilon_{0.02}$, which were made adjacent to fracture

APPENDIX B, Concluded

TENSILE PROPERTIES OF RECRYSTALLIZED

TD-NiCr SHEET

Table B-4. Tensile Properties of 0.08 mm (0.003 in.) Recrystallized TD-NiCr Sheet

Heat Number	Grain Direction	Specimen Number	Ultimate Tensile Strength MN/m ² (ksi)	Tensile Yield Strength MN/m ² (ksi)	Elongation or Strain, Percent				Indicated Modulus GN/m ² (10 ⁶ psi)
					ε _{2.0}	ε _{1.0}	(ε _L) 0.25	(ε _W) 0.25	
3702	L	ML-1	886 (128.5)	677 (98.2)	11.5	12	14	-4.5	271 (39.3)
		ML-2	893 (129.4)	679 (98.5)	16	18.5	29	-9	205 (29.8)
		ML-3	905 (131.2)	702 (101.8)	16.5	19	22.5	-9	206 (29.9)
		Average	894 (129.7)	686 (99.5)	14.5	16.5	22	-7.5	228 (33.0)
3523	T	MT-1	*	-	-	-	-	-	-
		MT-2	916 (132.9)	718 (104.1)	15.5	18	22.5	-10	319 (46.3)
		MT-3	887 (128.6)	713 (103.4)	15.5	17.5	22.5	-8	226 (32.8)
		Average	901 (130.7)	716 (103.8)	15.5	17.5	22.5	-9	272 (39.5)
	L	PL-3	883 (128.0)	731 (106.0)	6	6.5	9	-3	193 (28.0)
		PL-4	819 (118.7)	754 (109.3)	2.5	3.5	5	-1	193 (28.0)
		PL-5	946 (137.2)	761 (110.3)	9	9.5	13.5	-3.5	208 (30.2)
		Average	883 (128.0)	748 (108.5)	6	6.5	9	2.5	198 (28.7)
	T	PT-3	846 (122.7)	758 (110.0)	3	4	4	-2.5	257 (37.3)
		PT-4	927 (134.5)	747 (108.3)	6	7.5	7.5	-2	207 (30.0)
		PT-5	814 (118.1)	747 (108.4)	3	3.5	12.5	-4	202 (29.3)
		Average	863 (125.1)	751 (108.9)	4	5	8	-3.5	222 (32.2)

Elongation and (ε_L) strain measurements made across fracture.

* Failed at extensometer contact, results invalid.

APPENDIX C

TENSILE PROPERTIES OF UNRECRYSTALLIZED TD-NiCr SHEET

Table C-1. Tensile Properties of 0.25 mm (0.010 in.) Unrecrystallized
TD-NiCr Sheet - Heat 3714 (Code K5)

Test Temp. C (F)	Grain Direc- tion	Specimen No.	Ultimate Tensile, Strength		Tensile Yield Strength,		Elongation (strain), Percent		Indicated Modulus	
			MN/m ²	(ksi)	MN/m ²	(ksi)	ε _{2.0}	ε _{1.0}	GN/m ²	(10 ⁶ psi)
RT	L	K5L-1	1116	(161.8)	1071	(155.4)	2	3.5	191	(27.7)
		-2	1133	(164.3)	1091	(158.2)	3	5	199	(28.8)
		-3	1120	(162.5)	1066	(154.6)	3	6	196	(28.4)
		Average	1123	(162.9)	1076	(156.1)	2.5	5	195	(28.3)
	T	K5T-1	1267	(183.8)	1220	(176.9)	1	2	230	(33.4)
		-2	1258	(182.4)	1229	(178.2)	1.5	3	232	(33.6)
		-3	1128	(163.6)	1220	(176.9)	1.5	2.5	239	(34.7)
		Average	1264	(183.3)	1222	(177.3)	1.5	2.5	234	(33.9)
649(1200)	L	K5L-6	337	(48.9)	228	(33.0)	10	13	59	(8.5)
		-7	382	(55.4)	265	(38.5)	7.5	9.5	69	(10.0)
		-8	394	(57.1)	248	(36.0)	8	10.5	84	(12.2)
		Average	371	(53.8)	247	(35.8)	8.5	11	70	(10.2)
	T	K5T-6	345	(50.1)	161	(23.4)	6	7.5	65	(9.4)
		-7	270	(39.1)	122	(17.7)	8.5	9.5	36	(5.2)
		-8	249	(36.1)	116	(16.8)	10	11.5	83	(12.0)
		Average	288	(41.8)	133	(19.3)	8	9.5	61	(8.9)
704(1300)	L	K5L-9	279	(40.4)	185	(26.8)	9	11.5	74	(10.7)
		-10	283	(41.1)	186	(27.0)	10	12	77	(11.2)
		-11	292	(42.4)	195	(28.3)	8.5	10.5	64	(9.3)
		Average	285	(41.3)	189	(27.4)	9	11.5	72	(10.4)
	T	K5T-9	214	(31.1)	97	(14.1)	11.5	14	129	(18.7)
		-10	242	(35.1)	124	(18.0)	8.5	11	50	(7.3)
		-11	222	(32.2)	104	(15.1)	11.5	15.5	99	(14.4)
		Average	226	(32.8)	108	(15.7)	10.5	13.5	93	(13.5)
760(1400)	L	K5L-12	201	(29.1)	-	-	11.5	14	-	-
		-13	228	(33.0)	-	-	13	16	-	-
		-14	234	(34.0)	156	(22.6)	10	12	61	(8.9)
		Average	221	(32.0)	156	(22.6)	11.5	14	61	(8.9)
	T	K5T-12	121	(17.6)	63	(9.1)	24	29	41	(6.0)
		-13	124	(18.0)	68	(9.8)	20	23.5	103	(15.0)
		-14	136	(19.8)	70	(10.2)	15	17.5	35	(5.1)
		Average	128	(18.5)	67	(9.7)	20	23.5	60	(8.7)
816(1500)	L	K5L-15	164	(23.8)	113	(16.4)	11.5	14.5	67	(9.6)
		-16	147	(21.3)	108	(15.6)	11.5	16.5	86	(12.5)
		-17	168	(24.4)	123	(17.9)	11.5	17.5	56	(8.1)
		Average	160	(23.2)	114	(16.6)	11.5	16	69	(10.1)
	T	K5T-15	100	(14.5)	53	(7.7)	25	28	46	(6.6)
		-16	88	(12.8)	50	(7.3)	27	31.5	63	(9.1)
		-17	118	(17.1)	66	(9.5)	27.5	34	27	(3.9)
		Average	102	(14.8)	57	(8.2)	26.5	31	45	(6.5)
871(1600)	L	K5L-18	135	(19.6)	122	(17.8)	6.5	8	-	-
		-19	126	(18.3)	107	(15.7)	3	4	-	-
		-20	133	(19.4)	-	(13.9)	8	11	74	(10.7)
		Average	132	(19.1)	109	(15.8)	6	7.5	74	(10.7)
	T	K5T-18	66	(9.5)	44	(6.4)	13	15	66	(10.6)
		-19	68	(9.9)	-	-	25	29.5	-	-
		-20	69	(10.0)	54	(7.9)	-	-	34	(4.9)
		Average	68	(9.8)	49	(7.1)	19	22.5	54	(7.8)

ε_{2.0} = Elongation (strain) for 5.08 cm (2.0 in.) gage length

ε_{1.0} = Elongation (strain) for 2.54 cm (1.0 in.) gage length

APPENDIX C, Continued

TENSILE PROPERTIES OF UNRECRYSTALLIZED

TD-NiCr SHEET

Table C-2. Tensile Strain Measurements for 0.25 mm (0.010 in.)
Unrecrystallized TD-NiCr Tensile Specimens -
Heat 3714 (Code K5)

Test Temperature C (F)	Grain Direction	Specimen Number	Strain, Percent			
			(ϵ_L) _{0.5}	(ϵ_L) _{0.5}	(ϵ_L) _{0.25}	(ϵ_L) _{0.25}
760 (1400)	L	K5L-12	18	4	20.5	2.5
		13	21	5	19.5	4.5
		14	17	5	22	3.5
		Average	18.5	4.5	20.5	3.5
	T	K5T-12	25.5	2	26	2.5
		13	26	2	27	2.5
		14	19	1	22	1.5
		Average	23.5	1.5	25	2
816 (1500)	L	K5L-15	18.5	6	24.5	4
		16	21	6	23.5	5.5
		17	20	4.5	22.5	4.5
		Average	20	5	23.5	4.5
	T	K5T-15	28	4	33.5	2
		16	35	2.5	36.5	2.5
		17	39	4	40	4
		Average	34	3.5	36.5	3

(ϵ_L)_{0.5} = Elongation (strain) for 1.27 (0.5 in.) gage length

(ϵ_W)_{0.5} = Elongation (strain) for 1.27 (0.5 in.) gage width

(ϵ_L)_{0.25} = Elongation (strain) for 0.63 (0.25 in.) gage length

(ϵ_W)_{0.25} = Elongation (strain) for 0.63 (0.25 in.) gage width

APPENDIX C, Continued

TENSILE PROPERTIES OF UNRECRYSTALLIZED TD-NiCr SHEET

Table C-3. Tensile Properties of 0.5 mm (0.020 in.) Unrecrystallized TD-NiCr Sheet - Heat 3709 (Code G1)

Test Temp. C (F)	Grain Direc- tion	Specimen No.	Ultimate Tensile Strength		Tensile Yield Strength		Elongation (strain), Percent		Indicated Modulus GN/m ² (10 ⁶ psi)
			MN/m ²	(psi)	MN/m ²	(ksi)	ε _{2.0}	ε _{1.0}	
RT	L	G1L-1	1165	(169.0)	1108	(160.7)	3	5	199 (28.9)
		-2	1169	(169.6)	1124	(163.1)	3.5	6	194 (28.1)
		-3	1167	(169.3)	1111	(161.2)	2.5	4	198 (29.8)
		Average	1167	(169.3)	1122	(162.7)	3	5	199 (28.9)
	T	G1T-1	1300	(188.5)	1229	(178.2)	2	2.5	245 (35.6)
		-2	1313	(190.4)	1236	(179.3)	1.5	2.5	248 (36.0)
		-3	1314	(190.5)	1262	(183.1)	2.5	3.5	248 (35.9)
		Average	1309	(189.8)	1242	(180.2)	2	3	247 (35.8)
649(1200)	L	G1L-4	339	(49.1)	210	(30.5)	11	11.5	114 (16.5)
		-5	341	(49.5)	237	(34.4)	12	16	97 (14)
		-6	345	(50.1)	234	(33.9)	10.5	12	139 (20.2)
		Average	342	(49.6)	227	(32.9)	11	13	117 (16.9)
	T	G1T-4	265	(38.4)	134	(19.5)	11	13	57 (8.2)
		-5	277	(40.2)	143	(20.8)	12	13	67 (9.7)
		-6	250	(36.3)	129	(18.7)	9	10.5	89 (12.9)
		Average	264	(38.3)	136	(19.7)	10.5	12	70 (10.2)
704(1300)	L	G1L-7	259	(37.6)	185	(26.9)	9	12.5	84 (12.2)
		-8	265	(38.4)	-	-	12	16.5	-
		-9	258	(37.4)	194	(28.2)	8.5	11	52 (7.6)
		Average	261	(37.8)	190	(27.5)	10	13	68 (9.9)
	T	G1T-7	170	(24.6)	94	(13.7)	19.5	22.5	50 (7.2)
		-8	177	(25.7)	101	(14.6)	19	24	57 (8.3)
		-9	173	(25.1)	91	(13.2)	20	24	79 (11.5)
		Average	173	(25.1)	95	(13.8)	19.5	23.5	62 (9.0)
760(1400)	L	G1L-10	206	(29.9)	160	(23.5)	14.5	19	81 (11.8)
		-11	241	(31.0)	156	(22.6)	14	18	63 (9.1)
		-12	206	(29.9)	158	(22.9)	12.5	17	105 (15.2)
		Average	209	(30.3)	159	(23.0)	13.5	18	83 (12.0)
	T	G1T-10	113	(16.4)	65	(9.4)	27	30	107 (15.6)
		-11	108	(15.7)	59	(8.5)	25.5	28	76 (11.0)
		-12	110	(15.9)	64	(9.3)	29	36	106 (15.5)
		Average	110	(16)	63	(9.1)	27	31.5	97 (14.0)
816(1500)	L	G1L-13	159	(23.1)	126	(18.3)	13	19	50 (7.3)
		-14	175	(25.4)	135	(19.6)	15.5	21	68 (9.8)
		-15	174	(25.3)	154	(22.4)	12.5	16	72 (10.4)
		Average	170	(24.6)	139	(20.1)	13.5	18.5	63 (9.1)
	T	G1T-13	67	(9.6)	52	(7.6)	29	36	67 (9.6)
		-14	82	(11.9)	51	(7.5)	28	32	86 (12.5)
		-15	85	(12.3)	53	(7.7)	28.5	33	50 (7.3)
		-19	78	(11.3)	50	(7.3)	25	31	51 (7.5)
		Average	81	(11.8)	50	(7.5)	27	33	85 (12.3)
871(1600)	L	G1L-16	132	(19.1)	108	(15.7)	11	14	47 (6.8)
		-17	131	(19.0)	106	(15.4)	11.5	15	59 (8.5)
		-18	123	(17.8)	106	(15.4)	10	14	32 (4.7)
		Average	128	(18.6)	108	(15.5)	11	14.5	46 (6.6)
	T	G1T-16	64	(9.3)	46	(6.7)	27	34	67 (9.6)
		-17	63	(9.2)	47	(6.8)	26	32	37 (5.4)
		-18	59	(8.5)	43	(6.2)	28	35	-
		Average	62	(9.0)	46	(6.6)	27	33.5	34 (5.0)

ε_{2.0} = Elongation (strain) for 5.08 cm (2.0 in.) gage length

ε_{1.0} = Elongation (strain) for 2.54 cm (1.0 in.) gage length

APPENDIX C, Concluded

TENSILE PROPERTIES OF UNRECRYSTALLIZED

TD-NiCr SHEET

Table C-4. Tensile Strain Measurements for 0.5 mm (0.020 in.)
Unrecrystallized TD-NiCr Tensile Specimens -
Heat 3709 (Code G1)

Test Temperature C (F)	Grain Direction	Specimen Number	Strain, Percent			
			(ϵ_L) _{0.5}	(ϵ_L) _{0.5}	(ϵ_L) _{0.25}	(ϵ_L) _{0.25}
704 (1300)	L	G1L-7	15.5	3.5	16.5	3
		-8	16.5	3	16.5	3
		-9	15.5	3	14.5	3
		Average	16	3	16	3
	T	G1T-7	24	1.5	26	2
		-8	25	2	26	2
		-9	26	2	29	2
		Average	25	2	27	2
760 (1400)	L	G1L-10	24	4.5	26.5	4.5
		-11	22.5	5	25	5
		-12	21	5	20.5	4
		Average	22.5	5	23	4.5
	T	G1T-10	28	2	30.5	1.5
		-11	36.5	3	39.5	3
		-12	31	2	34.5	2
		Average	32	2.5	35	2
816 (1500)	L	G1L-13	22	5	22.5	4
		-14	23.5	6.5	27.5	6
		-15	19.5	4	23.5	3.5
		Average	21.5	5	24.5	4.5
	T	G1T-13	44	4	49.5	3
		-14	42	3.5	43.5	3
		-15	37.5	4.5	42.5	4
		Average	41	4	45	3.5

APPENDIX D
PARENT MATERIAL PROPERTIES OF RECRYSTALLIZED
TD-NiCr SHEET

Table D-1. Tensile-Shear Test Results for Recrystallized TD-NiCr Sheet

Test Temp C (F)	Shear Direc- tion (a)	0.25 mm (0.010 in.) Heat 3691 (Code L6)		0.025 mm (0.010 in.) Heat 3689 (Code J1)		0.008 mm (0.003 in.) Heat 3702 (Code M)	
		Specimen Number	Tensile Shear Strength MN/m ² (ksi)	Specimen Number	Tensile Shear Strength MN/m ² (ksi)	Specimen Number	Tensile Shear Strength MN/m ² (ksi)
R. T.	L	L6L-19	525 (76.2)	J1L-21	469 (68.0)	ML-16	387 (56.1)
		-22	541 (78.5)	-22	449 (65.1)	-17	409 (59.3)
		-23	539 (78.2)	-23	464 (67.3)	-22	Invalid
		Average	535 (77.6)		461 (66.8)		398 (57.7)
	T	-19	538 (78.0)	J1T-21	461 (66.9)	MT-16	424 (61.5)
		-21	543 (78.7)	-22	476 (69.0)	-17	415 (60.2)
		-22	525 (76.2)	-23	503 (73.0)	-18	410 (59.5)
		Average	535 (77.6)		480 (69.6)		416 (60.4)
1093(2000)	L	L6L-20	88 (12.8)	J1L-24	90 (13.0)	ML-19	54 (7.9)
		-21	88 (12.7)	-25	94 (13.7)	-16A	50 (7.2)
		-27	81 (11.8)	-26	99 (14.3)	-16B	52 (7.5)
		Average	86 (12.5)		94 (13.7)		52 (7.5)
	T	L6T-26	104 (15.1)	J1T-24	97 (14.1)	MT-19	600 (8.7)
		-27	95 (13.8)	-25	91 (13.2)	-20	57 (8.3)
		-29	101 (14.7)	-26	93 (13.5)	-21	47 (6.8)
		Average	100 (14.5)		94 (13.6)		54 (7.9)
1316(2400)	L	L6L-24	79 (11.5)	J1L-27	64 (9.3)	ML-21	37 (5.4)
		-25	68 (9.9)	-28	64 (9.3)	-23	44 (6.4)
		-26	63 (9.1)	-29	57 (8.2)	-24	47 (6.8)
		Average	70 (10.2)		61 (8.9)		43 (6.2)
	T	L6T-24	77 (11.2)	J1T-27	54 (7.9)	MT-23	38 (5.5)
		-25	Invalid	-28	57 (8.3)	-24	35 (5.1)
		-28	69 (10.0)	-29	59 (8.6)	-25	36 (5.2)
		Average	73 (10.6)		57 (8.3)		37 (5.3)

(a) L = Shear direction parallel to rolling direction. T = Shear direction normal to rolling direction.

(b) Unrecrystallized sheet annealed 2 hours at 1177C (2150F) prior to test.

APPENDIX D, Concluded

PARENT MATERIAL PROPERTIES OF RECRYSTALLIZED

TD-NiCr SHEET

Table D-2. Stress-Rupture Tests of Recrystallized
TD-NiCr Sheet

Test Temperature C (F)	Grain Direction	0.25 mm (0.010 in.) Heat 3691 (Code L6)		0.25 mm (0.010 in.) Heat 3689 (Code J1) ^(b)		0.08 mm (0.003 in.) Heat 3702 (Code M)	
		Stress Level MN/m ² (ksi)	Test Duration (hours) ^(a)	Stress Level MN/m ² (ksi)	Test Duration (hours)	Stress Level MN/m ² (ksi)	Test Duration (hours)
982 (1800)	L	69 (10)	219 NF	90 (13)	47.5	62 (9)	340 NF
		83 (12)	249 NF	97 (14)	29	66 (9.5)	28
		97 (14)	22.4 **	97 (14)	48	69 (10)	0.1
		97 (14)	212	103 (15)	7	69 (10)	0.1
		103 (15)	211.6	103 (15)	29.6		
		110 (16)	59.2	110 (16)	4		
		117 (17)	*	110 (16)	2		
	T	69 (10)	332.6 NF	69 (10)	234 NF	55 (8)	280 NF
		69 (10)	167 NF	69 (10)	238 NF	62 (9)	6.5
		76 (11)	*	76 (11)	48.5	69 (10)	0.1
		76 (11)	*	76 (11)	233 NF	76 (11)	<0.1
		76 (11)	*	83 (12)	61.3		
		83 (12)	*	83 (12)	48.5		
				90 (13)	1		
1093 (2000)	L	62 (9)	290 NF	48 (7)	239 NF	41 (6)	203
		62 (9)	259 NF	55 (8)	233 NF	45 (6.5)	149
		69 (10)	22	69 (10)	210 NF	48 (7)	27
		69 (10)	79	69 (10)	75	55 (8)	0.5
		76 (11)	25	76 (11)	7		
		76 (11)	16.5				
		83 (12)	29				
	T	48 (7)	233	48 (7)	221	28 (4)	92
		48 (7)	2	52 (7.5)	208	28 (4)	216
		55 (8)	155	55 (8)	72	34 (5)	37
		55 (8)	*	55 (8)	144	41 (6)	1.5
		55 (8)	33.1	62 (9)	11		
		62 (9)	4	62 (9)	8		
		62 (9)	*				
		62 (9)	*				
1204 (2200)	L	41 (6)	101	41 (6)	74 NF	28 (4)	99.5 NF
		41 (6)	51.5	41 (6)	4 **	34 (5)	41
		45 (6.5)	6.9	48 (7)	93.3 NF		
		45 (6.5)	16	48 (7)	3.5		
		48 (7)	11	55 (8)	1		
		48 (7)	3.5	55 (8)	2		
	T	34 (5)	262 NF	34 (5)	162	21 (3)	111 NF
		38 (5.5)	4.7	34 (5)	145	24 (3.5)	31 NF
		38 (5.5)	95	41 (6)	121	28 (4)	2.5
		41 (6)	*	41 (6)	41	34 (5)	0.2
				48 (7)	7		
				48 (7)	2.5		

(a) NF denotes no failure; test discontinued

(b) Unrecrystallized sheet annealed 2 hours at 1177C (2150F) in hydrogen prior to test

* Specimen failed during or immediately after loading

** Grip failure; test not valid

APPENDIX E

TEST PROCEDURES FOR DETERMINING MECHANICAL PROPERTIES OF RESISTANCE SEAM WELDED AND BRAZED JOINTS

Tensile and Tensile-Shear Tests. - Room temperature, 1093C (2000F), and 1316C (2400F) tests were performed on an Instron machine (Model TTD) at a cross head speed of 0.125 cm (0.05 in.) per minute.

The 1093C (2000F) tests were conducted in air using a three-zone Kanthal-element furnace (Satec SF-15). Five chromel-alumel (Type K) thermocouples were used in the furnace, one master and two master-slave pairs, controlling the three furnace zones independently. An additional five monitoring thermocouples contacted the specimen, three on the reduced section and the fourth and fifth 2.5 cm (1 in.) above and below the reduced section. The specimens were loaded to failure when all five of the monitoring thermocouples registered $1093 \pm 1.7^\circ\text{C}$ ($2000 \pm 3^\circ\text{F}$). A soak of about 15 minutes was typically required to achieve this uniformity.

The 1316C (2400F) tests were conducted in air using a platinum alloy wire resistance furnace. Load was monitored by a Transducers Inc. load cell, Model ML 2-251, 444.8 N (100 pound) capacity, and recorded against a time base on a Mosely Autograf, Model 7000A, X-Y recorder. Temperature calibrations were determined by attaching three Pt/Pt-13%Rh (Type R) thermocouples across the gage section of specimens. A plot of actual specimen temperature versus furnace control thermocouple temperature was made, and the resultant calibration curve was used throughout the test program. Recorded temperature gradients were less than 8.3°C (15°F) in an area 1.27 cm (0.5 in.) above and below the joint.

Stress-Rupture Tests. - Stress-rupture tests were conducted in air with a platinum alloy wire resistance furnace, identical to that used for 1316 C (2400 F) tensile-shear tests. Load was applied by dead weights with no multiplying linkage.

Two furnace calibrations were performed for the furnace used in stress-rupture of welded and brazed TD-NiCr specimens. For these calibrations, junctions of three 0.025 cm (0.010 in.) diameter wire Type R thermocouples were spot welded to a 0.25 mm (0.010 in.) TD-NiCr lap joint specimen. One junction was welded to the joint, and the others were welded 1.27 cm (0.5 in.) above the joint. A Leeds and Northrop precision potentiometer was used to measure the thermal EMF. Both calibrations showed close conformity to specified temperatures and were in excellent agreement with one another.

REFERENCES

1. Blankenship, C. P. and Saunders, N. T., "Development of Dispersion Strengthened Ni-Cr-ThO₂ Alloys for the Space Shuttle Thermal Protection System," NASA TM X-68024, March 1972.
2. Saunders, N. T., "Dispersion-Strengthened Alloys for Space Shuttle Heat Shields," Proceedings of Space Transportation System Technical Conference," NASA TMX 52876, Vol. 3, 1970.
3. Klinger, L. J., et al., "Development of Dispersion Strengthened Nickel Chromium Alloy (Ni-Cr-ThO₂) Sheet for Space Shuttles," NASA CR-120796, NASA Contract 3-13490, Fansteel, Inc., December 1971.
4. NASA Contract NAS3-15558, "Characterization of the Mechanical and Physical Properties of TD-NiCr (Ni-20Cr-2ThO₂) Alloy," Metcut Research Associates.
5. Holko, K. H., "TD-NiCr Sheet Mechanical and Physical Properties, Welding and Forming — State of Technology Report," NASA TMX-52952, January 1971.
6. Black, W. E., "Radiative Thermal Protection System Development for Maneuverable Re-Entry Spacecraft," Convair Aerospace Report GDC-ERR-1272, February 1969.
7. Black, W. E., "Space Shuttle Vehicle Radiative Thermal Protection Systems," Convair Aerospace Report GDC-ERR-1458, December, 1969.
8. Holko, K. H., and Moore, T. J., "Enhanced Diffusion Welding of TD-NiCr Sheet", NASA TN D-6493, September 1971.
9. Holko, K. H., Moore, T. J. and Gyorgak, C. A., "State of the Art Technology for Joining TD-NiCr Sheet," NASA TMX-68070, September 1972.
10. Wood, W. W., et al., "Theoretical Formability," AFML-TR-61-191, Vol. I & II, August 1961.
11. Wood, W. W., et al., "Final Report on Sheet Metal Forming Manufacturing Technology," AFML-TR-63-7-871, Vol. I & II, March 1964.

REFERENCES, Contd

12. Wood, W. W., et al., "Final Report on Advanced Theoretical Formability Manufacturing Technology," AFML-TR-64-411, Vol. I & II, January 1965.
13. Webster, D., "Strengthening Mechanisms in Dispersion Hardened Nichrome," Trans. ASM, Vol. 62, 1969.
14. Webster, D., "Grain Growth and Recrystallization in Thoria-Dispersed Nickel and Nichrome," Trans. Met. Society of AIME, Vol. 242, April 1968.
15. Carpenter, S. R., "Forming and Joining of Ni-20Cr-2ThO₂ TD-NiCr Alloy Sheet," Convair Aerospace Report GDC-ERR-AN-1215, December 1967.
16. Carpenter, S. R., "Forming and Joining Developments for Columbium and TD-NiCr Radiative Heat Shields," Convair Aerospace Report GDC-ERR-1344, December 1968.
17. Carpenter, S. R., "Fabrication Developments of High-Temperature Materials - Columbium and TDNiCr," Convair Aerospace Report GDC-ERR-1458, December 1969.
18. "Standard Elevated Temperature Testing Procedures for Metallic Materials," ATC Report ARTC-13, Aerospace Research & Testing Committee, Aerospace Industries Association of America, Inc., Washington, D.C., July 1964.
19. Langloes, A. P., et al., "Titanium Development Program May 1961," ASD Technical Report 61-7-576, Convair Aerospace Division of General Dynamics.
20. Rose, F. K., Hammer, A. N. and Metcalfe, A. G., "Development of Joining Technology for TD-NiCr Sheet," Solar Report RDR 1721-4, November, 1972.
21. Roden, W. A., "Titanium Spot Welding Development Including Stored Electromagnetic Energy Welding," Convair Aerospace Report GDC-AKM70-001, December 1969.
22. Roden, W. A., "Resistance Weld Monitors and In-Process Control," Convair Aerospace Report GDC-ERR-AN-1178, December 1967.
23. Roden, W. A., "In-Process Control Resistance Welding," Convair Aerospace Report GDC-ERR-1387, December 1969.

REFERENCES, Contd

24. Roden, W. A., "Resistance Welding In-Process and Quality Assurance Controls," Convair Aerospace Report GDC-ERR-1295, December 1968.
25. Roden, W. A., "Evaluation of Resistance Welding In-Process Monitors," Welding Journal, pp. 515-5 to 522-5, November 1968.

Page Intentionally Left Blank

DISTRIBUTION LIST

Dr. R. L. Ashbrook
MS 49-1
NASA Lewis Research Center
21000 Brookpark Road
Cleveland, Ohio 44135

Mr. C. P. Blankenship (10)*
MS 105-1
NASA Lewis Research Center
21000 Brookpark Road
Cleveland, Ohio 44135

Miss T. D. Gulko
MS 49-3
NASA Lewis Research Center
21000 Brookpark Road
Cleveland, Ohio 44135

Dr. H. B. Probst
MS 49-3
NASA Lewis Research Center
21000 Brookpark Road
Cleveland, Ohio 44135

Mr. N. T. Saunders
MS 105-1
NASA Lewis Research Center
21000 Brookpark Road
Cleveland, Ohio 44135

Mr. J. W. Weeton
MS 49-3
NASA Lewis Research Center
21000 Brookpark Road
Cleveland, Ohio 44135

Contracts Section B
MS 500-313
NASA Lewis Research Center
21000 Brookpark Road
Cleveland, Ohio 44135

*Number of Copies

Mr. S. J. Grisaffe
MS 49-3
NASA Lewis Research Center
21000 Brookpark Road
Cleveland, Ohio 44135

Mr. J. C. Freche
MS 49-1
NASA Lewis Research Center
21000 Brookpark Road
Cleveland, Ohio 44135

Mr. R. W. Hall
MS 105-1
NASA Lewis Research Center
21000 Brookpark Road
Cleveland, Ohio 44135

Mr. M. Quatinetz
MS 49-3
NASA Lewis Research Center
21000 Brookpark Road
Cleveland, Ohio 44135

Mr. P. F. Sikora
MS 49-3
NASA Lewis Research Center
21000 Brookpark Road
Cleveland, Ohio 44135

Dr. J. D. Whittenberger
MS 105-1
NASA Lewis Research Center
21000 Brookpark Road
Cleveland, Ohio 44135

Library (2)
MS 60-3
NASA Lewis Research Center
21000 Brookpark Road
Cleveland, Ohio 44135

Patent Counsel
MS 500-311
NASA Lewis Research Center
21000 Brookpark Road
Cleveland, Ohio 44135

Technology Utilization
MS 3-19
NASA Lewis Research Center
21000 Brookpark Road
Cleveland, Ohio 44135

Mr. G. C. Deutsch
RW
NASA Headquarters
Washington, DC 20546

Mr. J. Maltz
RWM
NASA Headquarters
Washington, DC 20546

Mr. H. K. Larson
MS 234-1
NASA Ames Research Center
Moffett Field, California 94035

Library
NASA Flight Research Center
P.O. Box 273
Edwards, California 93523

Library - Acquisitions
Jet Propulsion Lab.
4800 Oak Grove Drive
Pasadena, California 921102

Mr. B. A. Stein
MS 188A
NASA
Langley Research Center
Langley Field, Virginia 23365

Report Control Office
MS 5-5
NASA Lewis Research Center
21000 Brookpark Road
Cleveland, Ohio 44135

Mr. F. J. Demeritte
RV
NASA Headquarters
Washington, DC 20546

Mr. J. Gangler
RWM
NASA Headquarters
Washington, DC 20546

Dr. A. O. Tischler
RP
NASA Headquarters
Washington, DC 20546

Library - Reports
MS 202-3
NASA Ames Research Center
Moffett Field, California 94035

Library
NASA
Goddard Space Flight Center
Greenbelt, Maryland 20771

Dr. R. A. Anderson
MS 188
NASA
Langley Research Center
Langley Field, Virginia 23365

Library
MS 185
NASA
Langley Research Center
Langley Field, Virginia 23365

Mr. D. Cole
EJ
NASA
Johnson Space Center
Houston, Texas 77058

Mr. M. A. Silveira
NASA
Johnson Space Center
Houston, Texas 77058

Technical Library
JM6
NASA
Johnson Space Center
Houston, Texas 77058

Library
NASA
Marshall Space Flight Center
Huntsville, Alabama 35812

NASA Representative (2)
Scientific and Technical Information
Facility
Box 33
College Park, Maryland 20740

Mr. N. Geyer
AFML/LLP
Headquarters
Wright Patterson AFB, Ohio 45433

Mr. W. L. Goesch
AFDL/FDTS
Headquarters
Wright Patterson AFB, Ohio 45433

Dr. I. Perlmutter
AFML/LLP
Headquarters
Wright Patterson AFB, Ohio 45433

Mr. R. E. Johnson
ES5
NASA
Johnson Space Center
Houston, Texas 77058

Mr. R. E. Vale
ES
NASA
Johnson Space Center
Houston, Texas 77058

Mr. C. E. Cataldo
S+E ASTN
NASA
Marshall Space Flight Center
Huntsville, Alabama 35812

National Technical (40)
Information Service
Springfield, Virginia 22151

Defence Documentation Center
Cameron Station
5010 Duke Street
Alexandria, Virginia 22314

Mr. G. Glenn
AFML/LTP
Headquarters
Wright Patterson AFB, Ohio 45433

Mr. W. O'Hare
AFML/LLP
Headquarters
Wright Patterson AFB, Ohio 45433

Mr. S. V. Arnold
AMXMR-XW
Army Materials and
Mechanics Research Center
Watertown, Maryland 02172

Mr. I. Machlin
AIR-52031B
Naval Air Systems Command
Navy Department
Washington, DC 20360

MCIC
Battelle Memorial Inst.
505 King Avenue
Columbus, Ohio 43201

Library
Denver Research Institute
University Park
Denver, Colorado 80210

Prof. O. Sherby
Dept. of Materials Sci.
Stanford University
Palo Alto, California 94305

Mr. R. A. Lula
Allegheny Ludlum Steel Corp.
Brackenridge, Pennsylvania 15014

Mr. E. F. Styer
MS/8K-93
Boeing Company
P.O. Box 3999
Seattle, Washington 98124

Dr. S. T. Wlodek
Stellite Division
Cabot Corporation
1020 W. Park Avenue
Kokomo, Indiana 46901

Dr. D. R. Muzyka
Carpenter Technology Corp.
Res. & Dev. Center
P.O. Box 662
Reading, Pennsylvania 19603

Mr. N. S. Spence
Department of Defence
DEMR
Ottawa, Ontario
Canada

Dr. B. Wilcox
Battelle Memorial Inst.
505 King Avenue
Columbus, Ohio 43201

Dr. N. M. Parikh
IIT Research Institute
10 West 35th Street
Chicago, Illinois 60616

Dr. J. Colwell
Aerospace Corporation
P.O. Box 95085
Los Angeles, California 90045

Mr. A. E. Leach
Bell Aerosystems Company
Buffalo, New York 14240

Dr. R. Grierson
Stellite Division
Cabot Corporation
1020 W. Park Avenue
Kokomo, Indiana 46901

Library
Cabot Corporation
Stellite Division
P.O. Box 746
Kokomo, Indiana 46901

Mr. C. E. Tharratt
Space Division
Chrysler Corporation
P.O. Box 29200
New Orleans, Louisiana 70129

Dr. M. Ashby
Fordon McKay Laboratory
6 Oxford Street
Cambridge, Maryland 02138

Mr. R. T. Torgerson
Convair Aerospace Division
General Dynamics Corporation
P.O. Box 80847
San Diego, California 92138

Dr. R. E. Allen
MPTL
AETD
General Electric Company
Cincinnati, Ohio 45215

Mr. L. P. Jahnke
MPTL
AETD
General Electric Company
Cincinnati, Ohio 45215

Mr. L. A. Mead
Grumman Aerospace Corp
Plant 25
Bethpage, New York 11714

Mr. J. V. Long
Director of Research
Solar, Int. Harvester
2200 Pacific Highway
San Diego, California 92112

Mr. J. Debord
Huntington Alloys Div.
International Nickel Co.
Huntington, West Virginia 25720

Technical Information Center
Materials & Science Laboratory
Lockheed Research Labs
3251 Hanover Street
Palo Alto, California 94304

Mr. R. A. Nau
Convair Aerospace Division
General Dynamics Corporation
P.O. Box 80847
San Diego, California 92138

Library
Advanced Technology Lab
General Electric Company
Schenectady, New York 12305

Mr. D. B. Arnold
MPTL
AETD
General Electric Company
Cincinnati, Ohio 45215

Mr. D. Hanink
Engineering Operations
Detroit Diesel Allison
General Motors Corp.
Indianapolis, Indiana 46206

Mr. R. J. Nylan
Homogenous Metals Inc.
West Canada Blvd.
Herkimer, New York 13350

Dr. F. Decker
International Nickel Co.
Merica Research Lab
Sterling Forest
Suffern, New York 10901

Mr. R. Perkins
Lockheed Palo Alto R. Lab.
3251 Hanover Street
Palo Alto, California 94304

Mr. P. P. Plank
Martin-Marietta Corp.
Denver Divisions
Denver, Colorado 80201

Mr. S. Kessler
Materials and Process
Research Associates, Inc
P.O. Box 527
Canoga Park, California 91305

Dr. D. H. Killpatrick
McDonnell Douglas Corp.
5301 Bolsa Avenue
Huntington Beach, California 92647

Mr. B. Fitzgerald
McDonnell Douglas Corp.
P.O. Box 516
St. Louis, Missouri 63166

Mr. G. G. Shurr
Space Division
North American Rockwell
12214 Lakewood Blvd.
Downey, California 90241

Mr. G. J. Wile
Polymet Corporation
10597 Chester Road
Cincinnati, Ohio 42515

Mr. E. D. Weisert
Special Metals Corporation
New Hartford, New York 13413

Dr. H. E. Collins
Materials Technology
TRW Equipment Group
23555 Euclid Avenue
Cleveland, Ohio 44117

Mr. S. S. Blecherman
Pratt & Whitney Aircraft
United Aircraft Corporation
400 Main Street
East Hartford, Connecticut 06108

Mr. R. Johnson
McDonnell Douglas Corporation
A3-833 MS 9
Huntington Beach, California 92647

Mr. J. W. Davis
MS5101
McDonnell Douglas Corporation
P.O. Box 516
St. Louis, Missouri 63166

Mr. L. K. Crockett
Space Division
North American Rockwell
12214 Lakewood Blvd.
Downey, California 90241

Mr. R. A. Harlow
Aeronutronic Division
Philco-Ford Corporation
Ford Road
Newport Beach, California 92663

Mr. R. W. Fraser
Sherritt-Gordon Mines
Fort Saskatchewan
Alberta, Canada

Dr. J. S. Smith
Chem & Met Division
Sylvania Electric Prod.
Towanda, Pennsylvania 18848

Library
Materials Technology
TRW Equipment Group
2355 Euclid Avenue
Cleveland, Ohio 44117

Mr. Allen Hauser
Pratt & Whitney Aircraft
United Aircraft Corporation
400 Main Street
East Hartford, Connecticut 06108

Library
Pratt & Whitney Aircraft
United Aircraft Corporation
West Palm Beach, Florida 33402

Mr. D. Goldberg
Westinghouse Electric
P.O. Box 10864
Pittsburgh, Pennsylvania 15236

Mr. R. W. Strusrud
Dept. 5827
Detroit Diesel Allison
P.O. Box 894
Indianapolis, Indiana 46206